Modelling and Control Design of River Systems

Mathias Fui Lin FOO

M.Eng.Sc., B.Eng. (Hons)

Submitted in total fulfilment of the requirements of the degree of Doctor of Philosophy

National ICT Australia, NICTA

Department of Electrical and Electronic Engineering

The University of Melbourne

Australia

February 2012

Produced on archival quality paper

To my wife and parents

Abstract

Farming consumes a large amount of water usage and it is reported that large portion of this water is wasted through inefficient water distribution from river to farms. More efficient water distribution and preservation of environmental demands can be achieved through better control and decision support systems. In order to design better control and decision support systems, a river model is required. This model needs to be able to capture the relevant river dynamics and easy to be used for control design.

Traditionally, the Saint Venant equations have been used to model river systems. These equations are nonlinear hyperbolic partial differential equation (PDE) and are solved numerically using Preissmann scheme. The simulated Saint Venant equations are compared against operational data from the Broken River, and it is found that the Saint Venant equations are accurate in representing the river systems. Through further study, it is found that a single segmentation, i.e. treating the river as one long stretch with uniform geometry is sufficiently accurate for representation of the river for the purpose of control design. For the representation of meandering river, the Saint Venant equations are as accurate a two-dimensional flow model. The nonlinearities in the Saint Venant equations are also investigated. From the nonlinearity test, it is found that the Saint Venant equations are approximately linear within an operating region.

The Saint Venant equations are difficult to use for control design. An alternative model is therefore sought. Based on the operational data from the Broken River, simple time delay model (TDM) and integrator delay model (IDM) are proposed and estimated using system identification procedures. These models are found to be accurate in capturing the relevant dynamics of the river system. Furthermore, they are easy to use for control design. It is found that the time delay varies with the flow and hence controllers must be robust to variations in the time delay. A comparison between both TDM and IDM and the Saint Venant equations shows that they are as accurate as the Saint Venant equations

within the operating range. The TDM and IDM are desirable as they are easier to be used for control design and decision support system.

The TDM and IDM are used to design Model Predictive Control (MPC) to control the river system. The choice of using MPC is motivated by the fact that MPC handles constraints very well. Despite that, tuning the weights in the MPC cost function is not trivial. The methods of reverse engineering are used to obtain these weights. Building on the results of existing method of reverse engineering used in the literatures, two additional methods are developed. In addition, the design of MPC from scratch is also considered. A realistic year long simulations using both MPCs on the Broken River is carried out. The MPCs are compared with the current manual operation and a decentralised control configuration. The results show that with MPCs, significant water savings, improvement of water delivery service to the irrigators and the environmental demands satisfaction are achieved.

Declaration

This is to certify that

(i) the thesis comprises only my original work towards the PhD except where indicated in the Preface,

(ii) due acknowledgement has been made in the text to all other material used.

(iii) the thesis is fewer than 100,000 words in length, exclusive of tables, maps, bibliographies and appendices.

Mathias Fui Lin FOO

February 2012

Preface

Unless otherwise stated, this thesis comprises of materials, which are results of the collaboration between my supervisor and myself during my postgraduate study undertaken at the University of Melbourne, Australia.

The program used to solve the Saint Venant equations numerically using the Preissmann scheme is developed based on the program written by M.P.M Krutzen (Krutzen, 2000).

The quadratic programming in the simulation of Model Predictive Control (MPC) is formulated using YALMIP in MATLAB®, which is developed by J. Löfberg (Löfberg, 2004) and solved using commercial package CPLEX 12.2 (IBM, 2009).

The simulation of the decentralised controller is done by S.K. Ooi and the results of the simulation from the decentralised controller, which are used in this thesis (with permission) for comparison with the MPC are generated by S.K. Ooi in (Ooi *et al.*, 2010).

The list of publications during the course of the research are listed below.

Book Chapter

1. M. Foo, S.K. Ooi and E. Weyer, "Modelling of rivers for control design", in System Identification, Environmental Modelling and Control, Eds. L. Wang and H. Garnier, Springer, pp. 423-448, 2011.

Conference Publications

1. M. Foo, S.K. Ooi and E. Weyer, "Modelling of river for control design", Proceedings of IEEE International Conference on Control Applications, Yokohama, Japan, 2010.

2. M. Foo, N. Bedjaoui and E. Weyer, "Segmentation of a river using the Saint Venant equations", Proceedings of IEEE International Conference on Control Applications, Yokohama, Japan, 2010.

3. S.K. Ooi, M. Foo, and E. Weyer, "Control of the Broken River", Proceedings of the 18th IFAC World Congress, Milan, Italy, 2011.

4. M. Foo, and E. Weyer, "On reproducing existing controllers for Model Predictive Controllers", Proceedings of Australian Control Conference, Melbourne, Australia, 2011.

Acknowledgements

First and foremost, all glory, honor, praise and thanksgiving are given to Lord God Almighty for this PhD thesis is made possible through Him.

I would like express my gratitude to my supervisor Assoc. Prof. Erik Weyer for his continuous help, support and encouragement. I have learnt a lot from him not only the technical side of the research, but also how to develop myself as a researcher for my future undertaking. It has been a great honor and pleasure working with him. There are a lot of ups and downs but all those experiences are priceless and I truly appreciate it. I also truly enjoy our fun conversations about English soccer throughout these years.

I would also like to thank my collaborators cum co-supervisors, Dr. Su Ki Ooi and Dr. Nadia Bedjaoui for their endless help, support and encouragement. It has been a great pleasure working with them especially through all the stimulating discussion sessions. More importantly, the friendship we have developed over the years is deeply appreciated.

Special mention also to Dr. Li Li, Dr. Yuping Li and Dr. Michael Kearney for their help particularly on the control design part of this thesis. In addition, Dr. Michael Kearney's help pertaining to the setup of MPC and proof reading the materials related to MPC was gratefully acknowledged. Thanks also to Assoc. Prof. Michael Cantoni and Dr. Peter Dower for their advices and comments in areas, which I can improve on for my presentations.

Thanks also to National ICT of Australia (NICTA) and The University of Melbourne for funding my postgraduate studies and providing me with the opportunity to attend conferences, workshops and seminars. Thanks also extended to the Farms, Rivers and Markets (FRM) project for the opportunity to be involved in the project and the field trip to the Broken River, Victoria, Australia.

I would also like to thank all the administrative staffs in the Department of Electrical and Electronics Engineering and National ICT of Australia (NICTA) for all the effort they put in to make my experiences here enjoyable, in particular David Strover, Jackie Brissonnette, Nasrin Hashemi, Natasha Baxter, Domenic Santilli-Centofanti and Fang Chen. Thanks also to Dr. Isaac Kao, Assoc. Prof. Mohammad Aldeen, Assoc. Prof. Michael Cantoni and my supervisor for giving me the opportunity to do lab demonstrations.

Special thanks and love to my wife, Flora for her endless support and love throughout this whole journey. Also deep gratitude for my family for their prayer, love and encouragement throughout.

Last but not least, to all my friends, in particular Dr. David Ng, Dr. Khusro Saleem, Sei Zhen Khong, Shun Bai, Mohd Asyraf Zulkifley, Tuyet Vu, Michelle Chong, Chih Feng Lee, Sajeeb Saha, Kelvin Layton, Huynh Trong Anh, Senaka Samarasekera, Sachinta Karunaratne, Juan Lu, Adel Ali, Amir Neshasteriz, Laven Soltanian and Bahman Tahayori for their friendship and fruitful discussions on matters related or non-related to the research.

Contents

List of Figures

List of Tables

Chapter 1

Introduction

The main motivation behind the research in this thesis is to improve the sustainability of water resources. This is in line with the recent effort by the Australian government to promote prudent use of water for future generations. One way of improving the sustainability is to achieve better efficiency in water distribution in the river system such that not only water wastage is minimised, the water delivery services to the irrigators can be improved and the environment benefits can be achieved. To achieve better efficiency in water distribution, proper control and management of the river system are needed. To facilitate proper control and management, we need a river model. The river model must be able to capture the relevant dynamics for control, and it should be easy to use for control design. This forms one of the two main objectives considered in this thesis, i.e. modelling of river systems with the focus on the following areas:

(i) Develop models of river systems useful for control design.

(ii) Develop models of river systems useful for simulation.

The idea behind the modelling approach of using system identification techniques considered in this thesis comes from its successful use in the modelling of irrigation channels through the works of (Weyer, 2001) and (Ooi, 2003). Moreover, the implementation of the controllers (see e.g. (Cantoni *et al.*, 2007) and (Weyer, 2008)) designed using those models has shown improvement in water distribution efficiency from 70% to 90% (Mareels *et al.*, 2005). The substantial improvement motivates the second main objectives considered in this thesis, i.e. controller design of river system, where the focus is on the following

areas:

(i) Design the controller using the developed river model.

(ii) Assess the performance of the controllers through simulations study as the actual implementation on the river itself is not feasible.

The Broken River in Victoria, Australia is used as a case study.

1.1 Main water issues and potential key solutions

Water is one of the most important natural elements in the world. The world population relies on water not only for consumption but also for production of daily needs such as food, clothing, etc. The increase in world population coupled with the growth of agricultural sectors, create a surge in the demand for water worldwide, making water a scarce resource. Recent reports from the United Nation indicate that the world will be running out of clean water by the year 2020 ((IRIN, 2006) and (UNESCO, 2006)). As things stand, the world will be facing serious water shortages if no action is taken to address this problem.

One of the main water users is the agricultural sector. It is estimated that 70% of all water resources are used in the agricultural sector (UNESCO, 2006). The agricultural sector in Australia is one of the major economic contributions to the nation. This coupled with the fact that Australia is a dry continent, makes water a very precious resource.

Fortunately, in Australia, the supply of water to consumer has not been an issue yet. The main issue of concern however, is the ability to utilise the available water supply in the most efficient way, thus ensuring minimal water losses. As reported in (NRW, 2001), the current water losses through inefficient water distribution (in Australia) are large, and they are estimated to be about 30% of the supplied water. The bulk of losses are due to oversupply in distribution of water in the agricultural sector. Other losses include leakage and seepage.

With the expectation that the drought in Australia will continue to worsen rather than improving, it has becoming increasingly important to explore new farming practices and strategies for water management in preparation for a drier future. To deliver those strategies, interdisciplinary approach, which includes agricultural science, engineering, ecology, hydrology, etc is required. The above mentioned interdisciplinary approach is utilised

in the Farms, Rivers and Markets (FRM) project, where this research is part of. The FRM project was initiated by Uniwater, a joint research initiative by The University of Melbourne and Monash University, Australia as a response to tackle the above challenges (FRM, 2009). As the name suggests, the project comprises of a Farms, a Rivers and a Markets component. The Farms component is looking at ways of using several sources of water to make farming more robust to drier condition. The Rivers component is looking at the development of systems to make the distribution of water between different users in the most cooperative way. Lastly, the Markets component aims to create new water products and services that are more suited to future demands. The research undertaken in this thesis is part of the Rivers component, and the focus is on the development of good control and management systems for managing water cooperatively between different end users.

The control and management of a river system is a big challenge. The river is often the source of water supply for farming, urban and industrial usages. The challenge comes when the preservation of the environment is becoming more important, where a certain amount of water need to be left in the river for habitat preservation while at the same time ensuring adequate water supply to the designated users mentioned above. Modelling and control system have vital roles to play in the Rivers component as a well designed control system for rivers allows for a more efficient distribution of water to reduce operational water losses, timely water delivery to the irrigators, improved water delivery services to the irrigators and meeting the environmental demands. There is also a question on what infrastructures, which are currently or potentially available that can be used to further improve the efficiency of water distribution.

Broadly speaking, the aim of the control system is to improve water resource management and operation for the benefit of the consumptive users and the environment. However, what specific control objectives should be is not fully understood as most likely there will be a change in farming practices due to less available water in the future, which would change the demand patterns for water from the irrigators. On the legislative side, higher priorities have been given to environment in the Water Act 2007 (Water In Our Environment, 2010) in order to ensure a sustainable water supply to protect and restore environmental assets such as wetlands and streams. Part of the research in the Rivers component is to investigate what constitute desirable flows and water levels from an environmental and ecological point of view, and how this will have an impact on the control objectives. As an example, instead of keeping the water levels at the desired level, the

control system may in the future aim to recreate more natural water level fluctuations. There will also be a number of constraints on the operation of the river that the control system must make sure are satisfied. This includes maximum and minimum allowable flow rates, maximum allowable rates of change in flows at key areas in the river, rules and water quality issues associated with "re-starting the river" after periods of low or no flow, maintenance of slack water in specific reaches at defined times, etc.

1.2 The Broken River

This research uses Broken River in Victoria, Australia as a case study. In this section, a description of the Broken River is given. Figure 1.1 shows a top view of the Broken River.

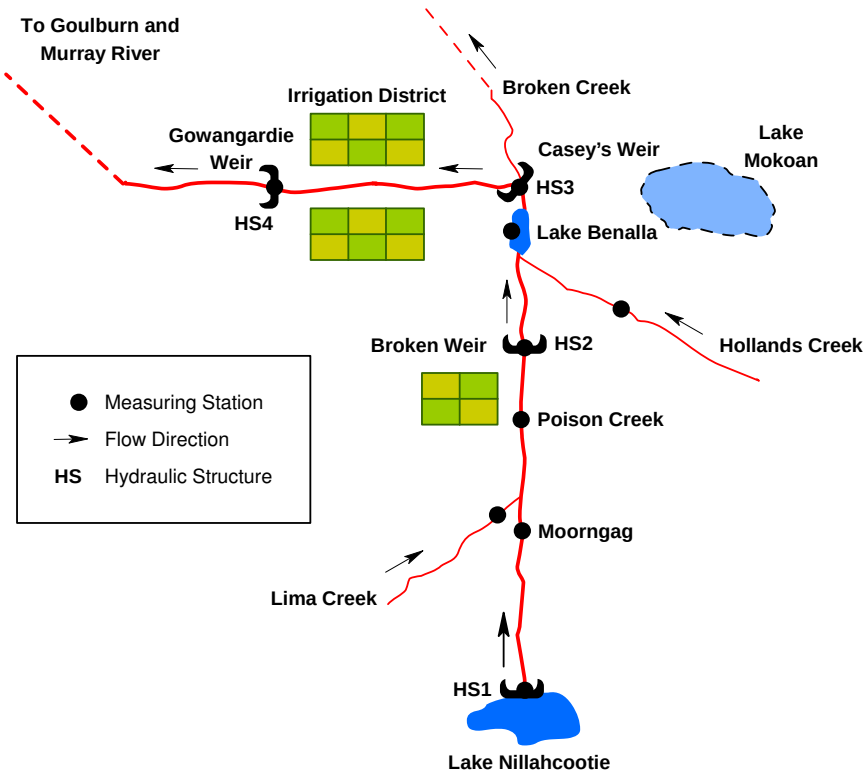

Figure 1.1: Top view of Broken River. Note: Figure is not to scale.

The Broken basin covers 7,724km^2 of catchment area, and rainfall varies from 1,000mm per year in the upper catchment to less than 500mm per year in the lower catchment (Victorian Water Resources, 2009). The primary entitlements for water shares, licences and associated commitments in the Broken system are 17,929.8ML high-reliability water shares and 3,338.3ML low-reliability water shares. The environment is protected with minimum flow requirements ranging from the natural flow to 0.2894m^3/s (25ML/day) (Bulk Entitlements, 2010).

The river originates from Lake Nillahcootie, which stores 40GL of water. Typical historical releases into the Broken River is about 0.1736m^3/s (15ML/day) during winter and in the range of 0.5787m^3/s (50ML/day) to 0.6944m^3/s (60ML/day) during summer. These releases are expected to increase due to the decommissioning of an artificial lake, Lake Mokoan, which also contributed to the flow in the lower parts of the river. The length of the river from Lake Nillahcootie to Gowangardie Weir (HS4) is about 76km.[1]. The two major streams that contribute flow into the Broken River are Lima and Hollands Creeks as shown in Figure 1.1.

The Broken River is the main water supply for the irrigation activities and most of the irrigation activities are concentrated in between Casey's Weir and Gowangardie Weir. The irrigators normally draw water from the river using pumps. An example of the pump used to draw the water is shown in Figure 1.2.

Water is released from Lake Nillahcootie and flows through Lake Benalla, turning west and eventually joined with Goulburn and Murray Rivers before ended up in the sea. Along the river, there are three hydraulic structures labelled HS2 to HS4 in Figure 1.1. At Lake Nillahcootie, the flow into Broken River is controlled using a fixed-cone valve gate, which is also known as Howell-Bunger valve (see Figure 1.3). The fixed-cone valve gates have movable gates in a shape of a cone where the water flow is controlled by the opening of these gates.

Broken Weir is located approximately 26km downstream from Lake Nillahcootie. At Broken Weir, the hydraulic structure used to regulate the flow is an undershot gate. An example of the undershot gate is shown in Figure 1.4. The flow can be controlled through the lifting of the gates.

Further downstream from Broken Weir (after passing through Lake Benalla), we have

[1]Obtained by approximating the rivers by straight lines between the hydraulic structures (HS) on the map

Figure 1.2: Picture of a pump used to draw water from the river.

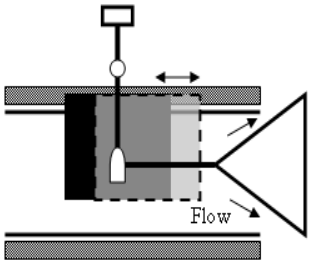

Figure 1.3: Top: Picture of a fixed-cone valve. Bottom: Picture of water release from Lake Nillahcootie.

two more hydraulic structures, i.e. at Casey's Weir and Gowangardie Weir. Both these weirs resemble a sharp-crested weir. An example of the sharp-crested weir is shown in Figure 1.5. These weirs have fix weir height that is not adjustable and hence no control of water release is possible.

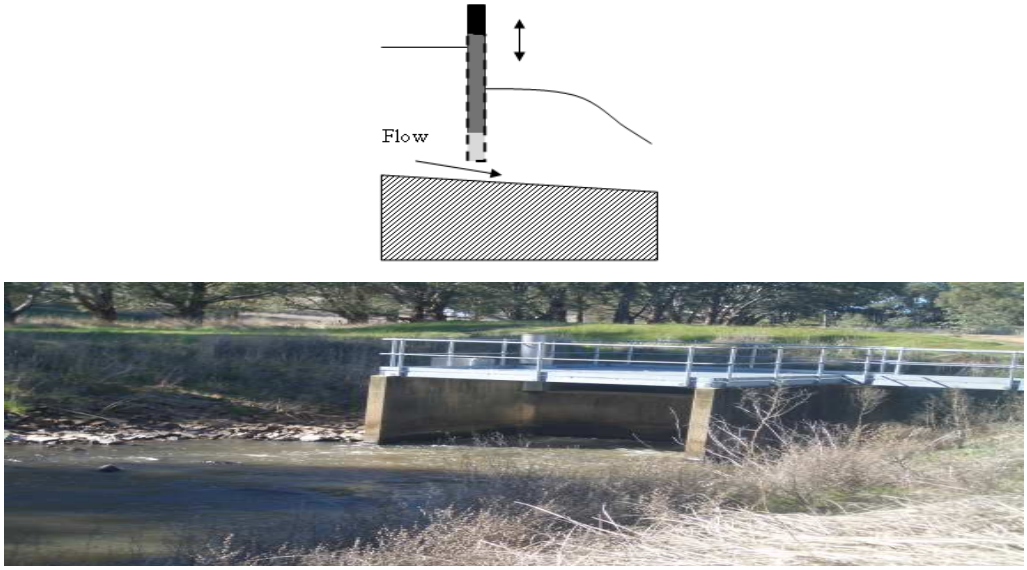

Figure 1.4: Top: Picture of an submerged undershot gate. Bottom: Picture of the submerged undershot gate at Broken Weir.

1.2.1 Measurements of the Broken River

Referring to Figure 1.1, there are several locations (shown by the black dot), where the water levels are measured. If the water levels are measured at the hydraulic structure, (e.g. Broken Weir, Casey's Weir and Gowangardie Weir) the associated flows are computed based on the types of hydraulic structure used. Various examples of flow computation across different types of hydraulic structures can be found in (Bos, 1978) and (Booij, 2002).

In the event, where the measured water levels are not collected at the hydraulic structures (e.g. Moorngag, Lima Creek, Poison Creek, Hollands Creek and Lake Benalla), then the associated flows are computed using a rating curve. Most of the water levels are measured every 15 minutes and the unit is meter Australian Height Datum (mAHD), which is referenced to sea level.

1.3 The need for models

The primary aim of the modelling work carried out in this thesis is for control design. We need a model that captures the relevant dynamics of the system such that a good

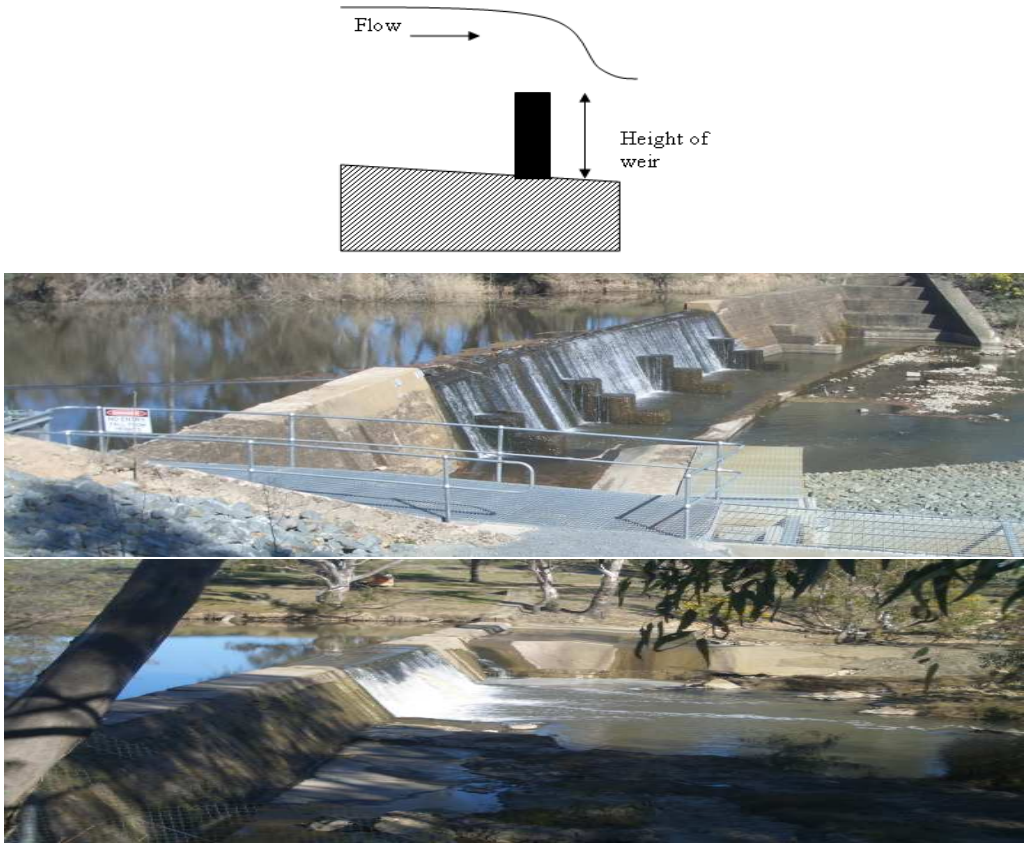

Figure 1.5: Top: Picture of a sharp crested weir. Middle: Picture of a sharp crested weir at Casey's Weir. Bottom: Picture of a sharp crested weir at Gowangardie Weir.

controller design can be achieved. If possible, linear models are preferred since the theory of linear controller design is well understood.

The secondary aim of the modelling work is for simulations. There are several reasons why we need model for simulations. Firstly, is the issue of limited access to perform experiments, which necessitate the use of a simulation model. Secondly, we may want to investigate what will happen if we put in new infrastructures such as regulation gates. This can be done using simulation models without actually putting the infrastructures in place. Thirdly, a simulation model can be used to generate useful data for system identification. In the case where good data are unavailable, we may use data generated from the simulation models to build and validate our model. And lastly, simulation models are used for scenarios simulation for decision support systems. The simulation models built

must satisfy both accuracy and computational requirements.

There are two approaches to modelling; physical modelling and empirical modelling. In physical modelling, the model is derived from the laws of physics. For river systems, the Saint Venant equations, which are derived from mass and momentum balance, are widely used. In general, the derivation of a physical model is usually time consuming but the model provides physical insight about the system. This approach needs the value of physical quantities of the system. Quite often these quantities are unknown, and they must be estimated from data.

On the other hand, empirical modelling does not require any physical quantities of the system. Empirical modelling builds model from operational data using system identification techniques. Hence, good operational data are required. It is usually simpler and easier to build models from data but the models do not provide physical insight about the system. Such models are known as black box models. When the model structure is chosen based on some prior knowledge about the physical system, the models are known as grey box model.

As mentioned above, good operational data are required for empirical modelling. Unfortunately, it is often absent in most river systems. Even if the data from rivers are available, they are often subjected to issues of varying sampling interval and infrequent data collection. The issue of varying sampling interval can be rectified by interpolation techniques. In the case of infrequent data, there is nothing much that can be done about it. In such cases, where good operational data are not available, we may use the Saint Venant equations to simulate fictitious "operational" data and then, use this data to build a river model using system identification techniques (see e.g. (Ooi and Weyer, 2008)). However, this approach is only valid if the accuracy of the Saint Venant equations for the river can be determined.

Although the accuracy of the Saint Venant equations has been demonstrated in lab scale experiments (Brutsaert, 1971) and for irrigation channels ((Ooi, 2003) and (Ooi *et al.*, 2005)), to author's knowledge well documented studies on the accuracy of the Saint Venant equations against real operational data from a river is very limited. Moreover, with the geometry of the river varies considerably, then there is also the question on how to represent river in the Saint Venant equations. Thus, part of the research aims at finding ways to represent the river using the Saint Venant equations in a simpler yet accurate manner and compare the Saint Venant equations against real data from the Broken River

to analyse its accuracy.

These analyses are important because without knowing the accuracy of the Saint Venant equations for the river systems, the simulated "fictitious" operational data is not valid, hence making the approach of building system identification models using data obtained from the simulation of the Saint Venant equations questionable.

1.4 The need for control

The Broken River serves as main water supply to the irrigators along the river and most of the irrigation areas are between Casey's Weir and Gowangardie Weir. Under current practice, the irrigators place water order four days in advance. Once the water order is approved, the water authority would release the water and the irrigators would draw water from the river using pump. Thus, it is important that the water would reach the irrigators on time and at the same time the water level in the river needs to be high enough such that the pump can be operated.

Water can only be supplied from Lake Nillahcootie, thus there is a long delay from the points of supply to the points of demand. In view of this, under current operation it is necessary for water authority to release water from the upstream end before it is required. Because there is uncertainty in the time delay, the water needs to be released a bit early in order to make sure that it reaches the location where the demand is on time. In order to compensate for losses on the way and inaccurate measurements of the flows, more water than necessary is released, which leads to water wastage. Furthermore, as higher priorities have been given to the environment, there is now a minimum and maximum flow requirement as well as the average daily flow variation has to be within a certain limit for the benefit of habitat preservation of aquatic creatures need to be considered in the Broken River.

Thus, the aim of the control system is to achieve a timely delivery of water to the irrigators, at the same time aim at reducing the total amount of water released from Lake Nillahcootie. The control system should also aims at improving water delivery services to the irrigators, by reducing the advance order time for the irrigators. The control system would also need to take into account the minimum and maximum allowable flows and permitted daily flow variations in Broken River.

To achieve those aims with a control system, then, there is a question on what type of controller should be considered. The choice of the controller needs to take into account issues such as ease of implementation, robust to uncertainties and ability to handle constraints well. From the description of the control problems mentioned above, the problem can be viewed as the flows and water levels in the Broken River are subjected to various constraints. Thus, the use of Model Predictive Control (MPC) is deemed a suitable control strategy due its ability to handle constraints well. However, finding the appropriate weights matrices in MPC cost function is not easy. The method of "reverse engineering" provides systematic way of obtaining these weight matrices and it will be explored. To measure how the designed controller would perform, the controller will be assessed through simulations. It is expected that with control in place, we would achieve timely delivery of water to satisfy the water demands from both the irrigators and the environment, minimise water wastage, improve water delivery services to the irrigators and satisfy all constraints.

1.5 Thesis Overview

This thesis is organised as follows.

Chapter 2 presents a literature review on modelling of open channel systems for the purpose of control design and simulation. A literature review on the control of open channel systems focused on river systems is also included in this chapter. Works on control of irrigation channels are briefly mentioned.

Chapter 3 focuses on physical modelling of river system. The model obtained is for the purpose of simulation. Here, the Saint Venant equations are introduced and derived. The numerical method for solving the Saint Venant equations is presented. The issue of how to segment a river is presented. Two simple segmentation strategies for a river are proposed and tested against real data from the Broken River and the Murray River. The treatment of a meandering river is addressed next by comparing the use of one-dimensional and two-dimensional flow models. The chapter concludes with nonlinearity tests of the Saint Venant equations, where we investigate how nonlinear the Saint Venant equations are by using several commonly used nonlinearity tests suggested in the literatures.

Chapter 4 focuses on empirical modelling of river systems with the purpose of obtaining models to be used for control design. The system identification procedures and the nonparametric and parametric methods for system identification are introduced. The use

of the two identification methods to obtain the river model is presented and it is shown that river reaches can be modelled using time delay models and integrator delay models. The quality of the parameters estimates in the models is investigated using the covariance matrix. The effect of varying flow conditions is investigated. A comparison between the physical and empirical modelling approaches is also presented.

Chapter 5 focuses on Model Predictive Control (MPC) design via reverse engineering. An introduction to MPC is first given, before presenting the details of reverse engineering. The design of MPC via reverse engineering is considered since it is difficult and time consuming to find the weight matrices in the MPC cost function from scratch. Thus, systematic methods of obtaining these weight matrices such that the MPC reproduces an existing controller are presented and illustrated with some examples.

Chapter 6 presents the control design for the Broken River. A detailed control problems, challenges and objectives for the Broken River is given. MPC is used to control the Broken River where two MPC designs are considered, i.e. MPC designed via reverse engineering and MPC designed from scratch. The performance of MPC are evaluated in terms of water savings, timely water delivery, improved water delivery services to the irrigators and improved environmental benefits compared to current manual operation and decentralised control.

Chapter 7 presents the conclusions and future works.

1.6 Thesis Contributions

The main contributions of this thesis are summarised as below.

- Investigations into how the Saint Venant equations should be segmented for simulations using the Preissmann scheme and how sensitive the simulation results are with respect to various parameters (Chapters 3.1 to 3.3).
- Comparison of the accuracy of one-dimensional and two-dimensional flow models (Chapter 3.3.2).
- Investigation of the nonlinearity in the Saint Venant equations using commonly used nonlinearity tests (Chapter 3.4).

- Using system identification procedures to obtain river models for the purpose of control design. The identified models are the time delay and the integrator delay models. These identified models are similar to the findings from literatures. The accuracy of these river models is compared against operational data as well as the Saint Venant equations (Chapters 4.3 to 4.5).

- Building on the works by (Maciejowski, 2007) and (Hartley and Maciejowski, 2009), two systematic methods of obtaining appropriate weights in the cost function of Model Predictive Control are developed (Chapter 5).

- Design of Model Predictive Control via reverse engineering and from scratch. These controllers are assessed on the Broken River through simulations (Chapter 6).

Chapter 2

Literature Review

In this chapter, a literature review on modelling and control of open channel systems[1] is given. The works on modelling and control of open channel systems are numerous (see (Malaterre and Baume, 1998) and (Zhuan *et al.*, 2009) and the references therein). As it is almost impossible to include all the works in this overview, only works that are directly relevant to the objective of this thesis as stated in Sections 1.3 and 1.4 will be presented.

2.1 Review on modelling of open channel system

Open channel systems are system where the flow of water is having a free surface. Example of open channel systems are rivers and irrigation channels, where water is delivered from a source (e.g. dam, lake, reservoir, etc) to a sink (e.g. consumers, sea, ocean, etc). To model an open channel system, the relation between the source (e.g. flow) and the sink (e.g. flow or water level) needs to be established. As mentioned in Section 1.3, this thesis explores modelling for control and modelling for simulation. The scope of the literature review on modelling will be focused on those two aspects. The review will not cover (details on) rainfall-runoff modelling, modelling of catchments, modelling for flood routing, etc.

The models of open channel systems used for control design can be obtained via two approaches, i.e. the physical approach and the empirical approach. We shall first present the literature reviews of models obtained via the physical approach, followed by models

[1]The term open channel systems is used here to include irrigation channels, river systems and other open channel systems.

obtained via the empirical approach.

2.1.1 Models for control

Physical models for control

To author's knowledge, the earlier works (see (Malaterre and Baume, 1998) and the references therein) on modelling of open channel system for control design have been based on the physical approach. The main governing equations are the Saint Venant equations derived in 1871 by Saint Venant (see e.g. (Cunge *et al.*, 1980), (Chaudhry, 1993) or (Akan, 2006)) based on the conservation of mass and momentum. The resultant model is a pair of nonlinear hyperbolic Partial Differential Equations (PDE) and these equations are not easy to use for control design. Nonetheless, the first attempt to design control using the full nonlinear Saint Venant equations was investigated in (Coron *et al.*, 1999). Coron et al. assumed the effect of viscous friction to be negligible and no lateral flow was considered, which simplified the momentum equation of the Saint Venant equations greatly, which was then used to design controller via a Lyapunov method. Subsequently, Bastin et al., extended the work by designing controller that handle open channel system with a steeper bottom slope (Bastin *et al.*, 2009*a*).

To use the Saint Venant equations directly for control design involve complex mathematical tools. Hence, these nonlinear equations are usually linearised. In (Papageorgiou and Messmer, 1985), assuming uniform flow, Papageorgiou and Messmer built a model by integrating three components; the reservoir, the regulator gate and the sewer (conveyance) that were normally encountered in open channel system. Linearising the Saint Venant equations around a steady flow, together with the gate equations and taking the Laplace transform, two transfer functions that relates the gate position with the flow and water level respectively were established. In the case of flow control, the resulting model was an integrator with delay, while in the case of water level control, the resulting model was a double integrator with delay. The model was not validated against any measured data.

The assumption of uniform flow that was considered in (Papageorgiou and Messmer, 1985) was not entirely valid as flow in open channel systems was seldom uniform. The nonuniform flow is the result of the effect of backwater which was not considered in (Papageorgiou and Messmer, 1985). The backwater effect arises when the flow of water is

obstructed (normally by a hydraulic structure) and leads to the rise of water level upstream of the obstructing structure. This effect was investigated in (Schuurmans *et al.*, 1995) and it was found that the dynamics of a reach consist of two parts, i.e. the part where the flow is uniform and the part where the flow is affected by the backwater effect. The part of the reach with uniform flow can be modelled by a pure time delay and the part affected by the backwater can be modelled by a pure integrator. Combining these two models led to the well known Integrator Delay Model (IDM), which is widely used as the model for control design in open channel system (see e.g (Silvis *et al.*, 1998), (van Overloop *et al.*, 2005)). The accuracy of the model was validated in (Schuurmans *et al.*, 1999*b*) where Schuurmans et al. compared the frequency response of IDM with the finite difference based model which was obtained from the linearised Saint Venant equations as well as the measured data from the WM Canal, Arizona, USA.

Litrico et al. have contributed vastly in obtaining models for control design either through simplification or from linearisation of the Saint Venant equations. Interested readers are referred to (Litrico and Fromion, 2009) for more details. In (Litrico and Georges, 1997) and (Litrico and Georges, 1999), under the assumption of zero lateral flow and negligible inertia term in the Saint Venant equations, the Saint Venant equations were simplified to a diffusive wave equations. Linearising this diffusive wave equations around a steady flow led to a linear Hayami model[2]. The Laplace Transform of the linear Hayami model was irrational and using the moment matching method, Litrico and Georges approximated the linear Hayami model with a second order system with time delay that relates the upstream flow to the downstream flow. The accuracy of the model was validated against measured data from the Baïse River, France. As a side note, there are works where the Hayami model is used directly for control design (see e.g. (Chentouf *et al.*, 2001)).

The Integrator Delay Zero (IDZ) model developed in (Litrico and Fromion, 2004*a*), (Litrico and Fromion, 2004*b*)) attempts to address several issues raised by Litrico and Fromion about how the IDM model in (Schuurmans *et al.*, 1995) was obtained. Litrico and Fromion pointed out that the integrator is always present in the linearised Saint Venant equations, and that the use of a pure time delay for the uniform flow part of the reach and the use of an integrator without delay in the modelling of the backwater effect part of the reach were not clearly justifiable. Litrico and Fromion derived the complete

[2]The model was named after Shoitiro Hayami (Hayami, 1951) for obtaining a linear model for flood waves propagation.

relation between the upstream and downstream flow and the upstream and downstream water level via the Saint Venant transfer matrices. The idea of obtaining the complete relation between the upstream and downstream flows and water levels is not new. This was first considered in (Baume *et al.*, 1998) with the assumption of uniform flow in the reach. Litrico and Fromion extended those ideas to the case of nonuniform flow. Through the transfer matrix of the Saint Venant equations, Litrico and Fromion found that the IDZ model is valid over a large frequency range. At the low frequency, where the integrator and time delay is dominant, the behaviour of the reach is the IDM model structure. At high frequency, the celerity[3] term and the time delay becomes dominant, hence they approximated the celerity (for simplicity) by a constant gain with the assumption that this constant gain represents the static behaviour of the oscillation. The IDZ model was validated against measured data from the experimental facilities of Hydraulics and Canal Control Center (HCCC), University of Évora, Portugal. In the author's opinion, since the model is going to be used for control design, where the low frequency behaviour is of more interest, the necessity of extend the modelling to the high frequency behaviour is questionable.

In addition, Litrico et al. also considered the use of simplified nonlinear Saint Venant equations for control design (Litrico and Pomet, 2003). Using moment matching method, the linear Hayami model in (Litrico and Georges, 1999) can be approximated by a class of linear Ordinary Differential Equations (ODE). Then, Litrico et al. obtained a single nonlinear ODE from the class of these linear ODEs and used the nonlinear ODE for control design. The work was extended in (Litrico *et al.*, 2010) to take into consideration of varying time delay due to variation in flow. In both those cases, Litrico et al. considered the case where the cross section of the canal was rectangular, where the analytical derivation was simpler. While this consideration is fairly valid for the case of irrigation canals[4], it may not be valid for the case of a river. Moreover, as pointed by Litrico et al. themselves, the analytical derivation becomes more involved and complicated (see (Litrico, 2001) and (Litrico and Pomet, 2003)). This model was validated against measured data from the Jacui River, France.

[3] In hydraulics, celerity is the speed of propagation of any disturbance introduced to the still body of water given by $c = \sqrt{gD}$, where g is the gravity constant and D is the water depth (Akan, 2006)

[4] Most of the time, the cross section of the irrigation channel is assumed to be trapezoidal.

Empirical models for control

All the modelling works mentioned above are based on the physical modelling approach. Models of open channel systems for control design can also be obtained based on the empirical modelling approach. This modelling approach is used in this thesis to obtain the model of the Broken River for control design. The choice of the model structure in empirical modelling is a choice between black box models and grey box models (Ljung and Glad, 1994). The black box models do not provide physical insight about the system and are used to only describe the relationship between the input and output. On the other hand, the grey box models use some prior knowledge about the physical system when selecting the appropriate model structure.

To the author's knowledge, the use of the system identification procedure to obtain model of open channel systems for control design is fairly recent (see the references in (Zhuan *et al.*, 2009)). This approach gained its popularity after Weyer in (Weyer, 2001) obtained a simple model of irrigation channel useful for control design using the system identification procedures. Using a simplified mass balance equation and gate equations, Weyer obtained a grey box model that relates the upstream head over the gate to the downstream water level for irrigation channel and it turned out that this model was a parameterised IDM, which is in agreement with the findings by (Schuurmans *et al.*, 1995) and (Litrico and Fromion, 2004*b*). The unknown parameters in the model were estimated from data. The model was validated against measured data from Haughton Main Channel (HMC), Australia and was shown to be accurate in capturing the relevant dynamics of the irrigation channels. In (Eurén and Weyer, 2007), the work was extended to consider different gate structures used in the irrigation channels. Again, the model was validated against measured data from Coleambally Main Channel (CMC), Australia and it was shown to be accurate to capture the relevant dynamics in the irrigation channel. The controller designed based on this model had been successfully implemented in irrigation channels in Australia (see e.g. (Weyer, 2008) and (Cantoni *et al.*, 2007)), where the efficiency of the water delivery system had improved significantly (Mareels *et al.*, 2005).

The identification in (Weyer, 2001) was carried out in open loop. Open loop experiments conducted on site normally cause substantial deviations from normal operating conditions. In view of that, closed loop identification of irrigation channels was considered in (Ooi and Weyer, 2001). The model obtained via closed loop identification had the same model structure as the one obtained via open loop identification.

A grey box model was also used in the work Sohlberg and Sernfält in (Sohlberg and Sernfält, 2002) to model the Dalälven River in Sweden. The obtained model was also the parameterised IDM, that relates the upstream flow over the turbine to the downstream water level. On the other hand, the work of Maxwell and Warnick in (Maxwell and Warnick, 2006) used a time delay model that relates the upstream flow to the downstream flow to model the Sevier River in USA. Both the models mentioned above had been validated against measured data. In addition, these two findings are useful to this thesis as they provide a good intuition for the initial choice of model structure as part of the system identification procedures.

The use of black box models was considered in (Rivas-Pérez *et al.*, 2007) and (Rivas-Pérez *et al.*, 2008) to model irrigation channels. Rivas-Perez et al. pointed out that the channel characteristic were time varying parameters due to the change of flow and this would affect the robust specification of the controller. They considered a robust identification using recursive least square to address this issue. They considered four types of model structures and concluded that the Auto Regressive Moving Average with Exogenous Input (ARMAX) model that relates the upstream gate position to the downstream water level best describe the dynamics of the irrigation canal with validation against measured data from Guira de Melena Irrigation Main Canal (GMIMC), Cuba. The varying parameters mentioned by Rivas-Perez et al., did not include the time delay. It is the variation of time delay due to varying flow conditions that is of more concern in the robust specification of the controller as this limits the closed loop bandwidth of the controller (Litrico and Fromion, 2004*a*). In the author's opinion, it is the inappropriate choice of the input signal in the model that led to the variability in the system dynamics. Instead of choosing the upstream head over the gate as input signal like in the case of (Weyer, 2001) or flow over the turbine in the case of (Sohlberg and Sernfält, 2002), they chose upstream gate position instead.

In a similar work, Sepúlveda and Rodellar concluded that the Auto Regressive with Exogenous Input (ARX) model that relates the upstream flow to the downstream water level best describe the dynamic of the irrigation channels (Sepúlveda and Rodellar, 2005). The author wishes to express some doubt regarding the validity of the choice of the model they used. The reason is due to the data, which they used for identification were generated from the Saint Venant equations, in which the accuracy of the Saint Venant equations for the channel they were investigating was not validated. While it is common to use the simulated data from the Saint Venant equations to do system identification, without

the Saint Venant equations been validated against measured data, the accuracy of the identified model could be questionable.

A nonlinear version of an ARX model that relates upstream flow to downstream flow was considered in (Elfawal-Mansour *et al.*, 2000). The motivation to use NARX model as mentioned by Elfawal-Mansour et al. was that the dynamics of the river system is nonlinear and no further detail justifications were given. Furthermore, they did not validate the model against any measured data, but proceed straight away to illustrate the performance of the designed controller.

Another different approach of empirical modelling was considered in (Bolea *et al.*, 2009). Bolea et al., considered Linear Parameter Varying (LPV) model for irrigation channels. The motivation behind was to use this model to design a fractional controller which was shown to give satisfactory performance for irrigation channels (see (Feliu-Batlle *et al.*, 2007)). From the series of step responses conducted by Bolea et al., they arrived at a second order system with time delay that relates pump input voltage to downstream water level. The model was validated against measured data from the test canal in the Automatic Control Department, Polytechnic University of Catalunya (UPC), Spain. To design a fractional controller, the second order model was then approximated by an equivalent fractional model. As a side note, using similar approach, Bolea et al. also approximated a fractional model from Hayami model (Bolea *et al.*, 2010).

A summary of the different models used for control are given in Table 2.1.

Other models

There are works that model open channel systems for other purposes than control. Those models are aimed at describing the relation between precipitations[5] or unmeasured flow and the main flow of the open channel systems. From this thesis point of view, these models can be useful in estimating the precipitation or the unmeasured flow, which can be used in "feedforward" control of the river systems. As mentioned earlier, these works will not be discussed in detail but a short summary is given below.

[5]In meteorology, one of the definition of precipitation is the interaction between water, atmosphere and ground surface (Sumner, 1988). Thus precipitation includes rainfall and snow.

Table 2.1: Summary of models used for control.

Reference	**Approach**	**Model**	**Input**	**Output**	**Model Validated**
Coron et al. (1999)	Physical	Full Saint Venant	Gate position	Water level	No
Papageorgiou & Messmer (1985)	Physical	Linearised Uniform Flow Saint Venant	(i) Flow (ii) Flow	(i) Flow (ii) Water level	No
Schuurman et al. (1995, 1999b)	Physical	IDM	Flow over gates	Water level	Yes WM Canal, USA
Litrico & Georges (1997, 1999)	Physical	Approx. Linear Hayami 2nd order with delay	Flow	Flow	Yes Baïse River, France
Litrico & Fromion (2004a, 2004b)	Physical	IDZ	Flow	Water level	Yes HCCC, Portugal
Litrico & Pomet (2003, 2010)	Physical	Simplified Nonlinear Saint Venant	Flow	Water level	Yes Jacui River, France
Weyer et al. (2001, 2007)	Empirical	Parameterised IDM	Head over gates	Water level	Yes HMC, CMC, Australia
) Solhberg & Sernfält (2002)	Empirical	Parameterised IDM	Flow over turbines	Water level	Yes Dalälven River, Sweden
Maxwell & Warnick (2006)	Empirical	Time Delay Model	Flow	Flow	Yes Sevier River, USA
Rivas-Perez et al. (2007, 2008)	Empirical	ARMAX	Gate position	Water level	Yes GMIMC, Cuba
Sepúlveda & Rodellar (2005)	Empirical	ARX	Flow	Water level	No
Elfawal-Mansour et al. (2000)	Empirical	NARX	Flow	Flow	No
Bolea et al. (2009, 2010)	Empirical	Fractional LPV 2nd order with delay	Pump input voltage	Water level	Yes UPC, Spain

Young and co-workers have done a lot of works on rainfall-runoff modelling (see e.g. (Young and Chotai, 2001), (Young, 2003), (Young *et al.*, 2009) and reference therein). They used a Data Based Mechanistic (DBM) modelling approach in their attempt to model the rainfall-runoff. The backbone of DBM was a black box model but with the attempt to give a physical interpretation of the model through the observations of the measured data. DBM was also used to model the effect of snowmelt on river flow (Castelletti *et al.*, 2009). In (Bastin *et al.*, 2009*b*), Bastin et al., combined the use of grex box and black box modes to model a reservoir subject to precipitation and the surface runoff.

For the modelling of open channel systems with unmeasured flow (e.g., unmeasured creeks, unmeasured offtake to irrigations), Jacobsen et al. used a three-reservoir model to describe the dynamics of the open channel systems (Jacobsen *et al.*, 1997) subject to the contribution of unmeasured sewer systems during rain. The work was extended to consider the unmeasured flow from creeks (Jónsdóttir *et al.*, 2001). Jónsdóttir et al. concluded that a two-reservoir model best describe the system. The use of several reservoirs models in series is not new. In fact, this model was first proposed by Nash et al. (see (Nash, 1957) and (Nash, 1959)), and the comparison against measured data revealed that this simple model describes the dynamics of open channel systems relatively well (see the three-part paper (Nash and Sutcliffe, 1970), (O'Connell *et al.*, 1970) and (Mandeville *et al.*, 1970)).

2.1.2 Models for simulation

Simulation models for open channel system are important for two reasons. Firstly, due to that access to carry out experiments on the real open channel systems is normally restricted, the simulation model thus acts as a substitute for experimentation. The simulation model can also be used for generating useful data for system identification in the absence of quality measured data. Secondly, it is used for quick simulation for scenarios assessment. In this section, a literature review on models for simulation centered around these two reasons will be given. However, the focus is on the use of these models from a control point of view, i.e. to assess the performance of the controller. The controller is normally designed using simple model as discussed in Section 2.1.1. To assess the performance of the controller, the full Saint Venant equations are normally used as a simulation model as they depict the "real" open channel systems, which induces model mismatch and varying time delay due to varying flow conditions. The review will cover very briefly on some aspects on the accuracy of the Saint Venant equations. It will however, not

cover the nuts and bolts of the methodologies used as it is a vast field of research on its own. Interested readers can consult texts on open channel (e.g. (Cunge *et al.*, 1980) or (Akan, 2006)) for more details.

Simulation models for experimentation

The full Saint Venant equations are used extensively in the simulation of open channel systems. This is evident from the development of various commercial softwares (e.g. InfoSys-CS, HEC-RAS, CONCEPT, SIC, MIKE11), which are based on the discretisation of the Saint Venant equations. The reason for the discretisation is that the full Saint Venant equations have no analytic solution available and they have to be solved numerically. Generally, the Preissmann scheme, which is an implicit finite difference method, is used to discretise the Saint Venant equations. A comprehensive list of commercial hydrological softwares and other schemes used can be found in (Singh and Yadava, 2003).

In principal, the Saint Venant equations are valid for an arbitrary geometry. For open channel systems, where the geometry does not vary much, for e.g. in irrigation channels, solving the discretised Saint Venant equations numerically is relatively easy. However, things get more involved and complicated in treating open channel systems with varying geometry for e.g. in rivers. The general practice used in those commercial softwares mentioned earlier is to do segmentation. Segmentation is where the river is approximated with several segments of straight stretches, where the river geometry is constant. In each of the segment, the river geometries are then assigned (see e.g. (Langendoen, 2000), (Baume *et al.*, 2005), (Brunner, 2008)).

In regards to the treatment of rivers that meander, the friction coefficient plays a crucial role as it affects the flow resistance (Fread, 1991). Hence, by adjusting the friction coefficient, one can represent the meandering river pretty well. This was investigated in (Bleninger *et al.*, 2006). Bleninger et al. compared the simulation results from CasCade[6] with a simple discretised Saint Venant equations they developed. In CasCade, the friction coefficients were adjusted to treat the meandering river. In their findings, they concluded that the accuracy of their simplified Saint Venant equations was relatively good compared to CasCade in representing meandering river by adjusting the friction coefficient.

[6]The CasCade software is an in house software developed by the German Federal Waterways Engineering and Research Institute that model the Rhine River. The CasCade software have the details of the river geometry of the river.

Nonetheless, there was no comparison made against real data. An alternative is to use a two-dimensional flow model to treat river meandering. This, however increases computational complexity. Nonetheless, the literatures on two-dimensional flow will not be discussed here as it is not the main scope of this thesis.

The Saint Venant equations are also normally used as the simulation models to generate data for system identification. To use the Saint Venant equations to generate these fictitious data for system identification, the accuracy of the Saint Venant equations themselves have to be ascertained first. Although the accuracy of the Saint Venant equations have been verified in lab scale experiments (Brutsaert, 1971), the accuracy of the Saint Venant equations in large scale system remains an open question. To author's knowledge, other than the work by Brutsaert, there are only three works that validate the accuracy of the Saint Venant equations for open channel systems. This section will cover those three works that have compared the accuracy of the Saint Venant equations against measured data.

In (Ooi *et al.*, 2005), Ooi et al. compared the Saint Venant equations with the measured data from Haughton Main Channel (HMC), Australia. In their findings, they showed that the Saint Venant equations were accurate in capturing the relevant dynamics of the irrigation channels. Subsequently, in (Ooi and Weyer, 2008), controllers were designed from the model identified using the data generated from the Saint Venant equations.

The simplified nonlinear Saint Venant equations developed by Litrico et al. in (Litrico *et al.*, 2010) can be used to generate data for system identification. In fact that was one of the three main purposes of developing this model as mentioned by Litrico et al. This simplified Saint Venant equations had been validated against measured data from Jacui River, France (see Table 2.1).

Shrestha and Nestmann made the comparison of the Saint Venant equations with measured data from Rhine River, Germany (Shrestha and Nestmann, 2005). They went a step further by comparing the Muskingum-Cunge[7] model against the measured data as well. They concluded that the accuracy of both the Saint Venant equations and the Muskingum-Cunge models are similar.

[7]The Muskingum-Cunge model (Cunge, 1969) is a simplified Saint Venant equations in the momentum equation, which is widely used by the hydrologic community for channel routing.

Simulation models for scenarios assessment

To author's knowledge, almost all the literatures on control of open channel systems use the full Saint Venant equations as the simulation model (unless they have access to do experiment on site). However, there are some exceptions and they are highlighted here. The use of the full Saint Venant equations tends to be computational heavy and this is not preferred if we want to perform a quick simulations. In (Litrico *et al.*, 2010), Litrico et al. proposed a simplified Saint Venant equations where the simulation was computationally less demanding. The idea was to reduce the Saint Venant equations to a simple nonlinear Delay Differential Equations (DDE), by linearising around a steady flow. The varying time delay due to varying flow condition was accounted for by deriving the nonlinear DDE that coincides with the linear DDE for every flow. The derivation, however considered only rectangular cross section for simplicity. For other cross sections, the derivations were more complicated. Thus, this simulation model would be more appropriate for open channel systems with minor variations in geometry.

In (Sohlberg and Sernfält, 2002), a parameterised IDM model was used for simulation but with an addition of white noise. Although adding white noise to the model to simulate the "real" world is not uncommon, in author's opinion, for river systems, this practice is not appropriate as the dynamics of river systems are greatly affected by the time delay. The Dalälven River that they considered had huge flow variations (up to $100\text{m}^3/\text{s}$) and naïvely just adding white noise and not considering the variation of time delay could lead to robustness issues for the designed controller, when implemented.

2.2 Review on control of open channel system

To properly classify the different control methodologies for open channel systems is a very difficult task. Nonetheless, in this thesis, the author will focus on presenting works on control methodologies for river systems, whereas the control methodologies for other open channel systems in particular irrigation channels will be briefly highlighted. A comprehensive list of references on control methodologies for irrigation channels can be found in (Malaterre, 1995), (Malaterre *et al.*, 1998) and (Zhuan *et al.*, 2009). The author will categorise the review into control of single reach river and multi-reach river.

2.2.1 Control of single reach river

One of the earlier works on control of river systems is (Papageorgiou and Messmer, 1989). The control objectives considered in that paper were to ensure that the downstream flow was maintained at two different setpoints over two different seasons. During the dry season, the flow in the river need to be maintained at a minimum flow Q_{min} set by the water authority. While, during the raining season, the flow in the river need to reach the new setpoint $Q_{high} > Q_{min}$ as fast as possible. In other words, they wanted a fast setpoint tracking when there was positive flow setpoint change (from Q_{min} to Q_{high}) and no undershoot during negative flow setpoint change (from Q_{high} to Q_{min}). The control variable was the upstream flow and the controlled variable was the downstream flow. Three controllers were considered and designed using the model obtained in (Papageorgiou and Messmer, 1985). The first one was a PI-controller. The second one was a switching controller between feedforward and feedback controller, where during the positive flow setpoint change, the feedforward would be used while during the negative flow setpoint change, the PI-controller would be used. Conditions to ensure bumpless switch between the two controllers were considered. In view of the large time delay in the river system, a Smith Predictor was considered and tuned through several experimentations until a satisfactory performance was achieved. The comparison between the three controllers was made. All three controllers produced no undershoot during negative flow setpoint change. For the positive flow setpoint change, the Smith Predictor performed the best in terms of a small rise time and less overshoot. However, Papageorgiou and Messmer preferred implementing the switching controller instead as the tuning of the Smith Predictor would be difficult in the real implementation.

Litrico and Georges considered the LQG controller to control a dam-river system (Litrico and Georges, 2001). Their control objectives were to ensure delivery of water to farmers and to maintain the downstream flow at setpoint defined by environmental and ecological needs. The control and controlled variables were the upstream flow and downstream flow respectively. The controller was designed using the linearised Hayami model obtained in (Litrico and Georges, 1999). To ensure zero steady state error, the integral state was augmented to the model. The flow setpoint errors, the control actions and the integral states were included in the criterion to be minimised. The criterion weighting matrices Q and R were tuned using the "de Larminat method" where a tuning parameter N_c and N_o were multiplied to the controllability and observability gramian of the system respectively. The tuning of N_c and N_o were carried out through trial-and-error. As not all

states were measured, an observer was designed. The controller showed good performance in the simulation but it was not tested on the real river system.

An H-infinity controller was considered in (Litrico and Fromion, 2002) to control a two-dam river system. The controller was also designed using the linearised Hayami model. In the considered river system, there were two dams of different volume with the dam nearer to the irrigation area had smaller volume capacity compared to the dam located at the most upstream. Litrico and Fromion looked at how to determine appropriate releases from the dams so that the smaller dam would not be emptied due to water withdrawal by the farmers. The simulation results showed that the H-infinity controller was able to release appropriately the water from both the dams without emptying the smaller dam in the presence of offtakes to irrigation.

The use of Model Predictive Controller (MPC) has increased in popularity due to its constraints handling capability. MPC was considered in (Sohlberg and Sernfält, 2002) to control the Dalälven River. The flow in the Dalälven River was determined by the amount of energy generated by the hydropower station according to demand, which led to large variation of water levels along the river. The control objectives were to ensure the variation of water levels at the three specific locations were within a tolerable range, to achieve high efficiency of power generation from the hydropower station and to minimise the rate of change of flow over the hydropower station. The water level setpoint errors and the control actions were included in the criterion to be minimised subject to the mentioned constraints. The performance of the MPC was compared with current control configurations via simulation where MPC not only was able to keep water levels within the specified range, but the water level variations were smaller compared to the current control configuration. From a power generation point of view, this smaller variation was preferred as that led to a high power generation efficiency.

2.2.2 Control of multi-reach river

In control of multi-reach river, broadly speaking, there are two main control configurations, i.e. the centralised and the decentralised. For other variants of configurations, readers are referred to (Malaterre, 1995) for more details. In the centralised configuration, all the control actions in the river reach are governed by a central controller. In the decentralised configuration, each reach is controlled by a local controller. The drawback of a centralised controller is that the design phase can be time consuming due to the many required trials

with the high computational demanding centralised controller. In the implementation, the performance is susceptible to data communication failure. For the decentralised configuration, the drawback lies in the disturbance amplification or error propagation (see e.g. (Schuurmans *et al.*, 1999*a*), (Li *et al.*, 2005) or (Cantoni *et al.*, 2007)). Most works used MPC to control multi-reach river system. The choice of using MPC in river control is not surprising considering its good constraints handling ability, which most river systems are subjected to. In view of this, one can notice almost all of the works given below uses MPC.

In (Glanzmann *et al.*, 2005), a centralised MPC was designed using the linearised Saint Venant equations to control a four-reach river in Aare River, Switzerland. The flow discharge through the turbine at the most upstream end of the river was used to generate power. The effect of this flow discharge led to large water level variations along the river, which was not desirable due to environmental considerations. Thus, their control objectives were to ensure the deviation of water levels from setpoints were within a tolerable range and to reduce the damping effect of the flow discharge variation. The criterion to be minimised included water level setpoint errors and the control actions. The weight matrices Q and R were tuned through trial-and-error and the Kalman filter was used for states estimation. Glanzmann et al. compared the performance of MPC against the PI-controller with feedforward through simulation. As expected, due to the constraints handling capability in MPC, the performance of MPC was better compared to the PI-controllers as the effect of damping was reduced and the variations in the water levels were kept small.

An extension of the work by Glanzmann et al. was carried out in (Setz *et al.*, 2008), where an additional control problem of making the river navigable was considered. When the Aare River was used for navigation, locks were used for the vessels to by-pass the hydropower station. The use of locks not only greatly affected the flow discharge through the turbine, which may lead to turbine wear, it also introduced large water level variations in the river. Thus, on top of the control objectives mentioned in (Glanzmann *et al.*, 2005), effort to reduce the mechanical wear of the turbine was also considered. Instead of designing the centralised MPC using the linearised Saint Venant equations, they designed the controller using IDM. Setz et al. further divided the tolerable range of water levels to two zones i.e. the "preferred zone" and the "emergency zone". With this, the control effort will be on damping the flow discharge variation, when the water levels were in the preferred zone and to get out of the emergency zone (as soon as possible) when the water

levels enters the emergency zone. Since these constraints on water levels were considered as soft constraints, slack variables were included in the criterion. To limit the number of movements of the actuator to reduce mechanical wear, a dead band was considered in the optimisation problem. However, no specific details on how the weights they used in the criterion function were given. The controllers in (Setz *et al.*, 2008) were compared via simulation with the PI-controller with feedforward and their findings shows that the centralised MPC controller outperformed the PI-controller with feedforward in terms of keeping the deviation of water levels within the tolerable operating range. None of the MPC controllers used in (Glanzmann *et al.*, 2005) and (Setz *et al.*, 2008) were tested on the real river.

Due to the large computational effort in using centralised MPC, Şahin and Morari considered a decentralised MPC to control a 35-reach river (Sahin and Morari, 2010) with the same control objectives as in (Setz *et al.*, 2008). The controller was also designed using IDM and augmented with integrating disturbance states to ensure zero steady state error. The unmeasured states were estimated using the Kalman filter. Şahin and Morari introduced a third operating zones, i.e. "forbidden zone" which resulted in an additional slack variable introduced in the criterion. Large weight were given to the slack variable of the forbidden zone to ensure water levels will avoid this zone if possible at the same time ensuring feasibility in the optimisation problem. In view of the disturbance amplification or error propagation of using the decentralised configuration, they included a feedforward of information between adjacent local MPC controllers. The information between the local controllers was one way from upstream to the downstream local controllers. The performance between the two setups (with and without feedfoward) of decentralised MPC was compared via simulation and as expected the decentralised MPC with feedforward performs better than the one without using the feedforward. In addition, the computation time between the centralised and the decentralised control were compared, and showed a smaller computation time when using the decentralised control. No test was carried out on the real river.

The centralised MPC was used in (van Overloop *et al.*, 2010) to control the North Sea and the Amsterdam-Rhine Canals in the The Netherlands. For a navigable river, pumps were used to minimise the variations of water level. Thus, the control objectives considered were minimal energy consumption through the use of flow pump and to ensure a navigable river. The IDM model was used to design the MPC. Through on-site experimentation, van Overloop et al. showed that with MPC, significant energy savings were achieved

(with a more efficient pumping operation) compared to the current operation while at the same time ensuring a navigable river. van Overloop et al. planned to extend the implementation of MPC to the whole Dutch water system. Due to the size of the system, the use of centralised MPC would incur a large computational burden. They proposed a distributed MPC configuration based on the work of (Negenborn *et al.*, 2009*b*) but the implementation of the controller had not been carried out yet.

In (Evans *et al.*, 2011), the centralised MPC and LQ controller were considered to control a network of reaches in the Murray River, Australia. The intention of the paper is not meant for comparison of performance between the two controllers but rather to explore the use of optimal control theory to control a river. The operations in the Murray River are divided into three modes, i.e. supplying mode, storing mode and spilling model where it is possible that different reaches in the river are operating in different mode. In the supplying mode, the river is used to supply water according to demand in particular during irrigation season. In the storing mode, the excess flow of the water not used to satisfy the demands are stored within the river and in the spilling mode, the flow in the river exceeds the capacity due to the effect of rain. Putting all these modes together, their control objectives were to meet the water demands from respective users, maintain the storage levels at setpoints and maintain water levels at the designated location of interest at setpoints. In addition, the secondary control objectives considered were to reduce the effort of the gates movement and keep the rise and fall rate of the flow within a reasonable limit to reduce the activity of river bank slumping. For the LQ controller, the criterion to be minimised included the water level setpoint errors, control actions and gate movements, while for the MPC controller, the criterion to be minimised included the water level setpoint errors and the rate of change of the control actions were included instead. The weights in the criterion function were tuned through trial-and-error. Simulation results showed both controllers performed well.

In (Puig *et al.*, 2009), a centralised MPC was considered to control a three-reach Arrêt-Darré/Arros system, which is a dam river system in France. Their control objectives were to maintain the flow at the downstream end of the river at setpoint while ensuring the flow at the intermediate points in the river stayed above the defined minimum ecological flow. The criterion to be minimised included the flow setpoint errors and the rate of change of the control actions. The weights in the criterion function were tuned through trial-and-error. The MPC was designed using the ARX model, which they had identified for each of the reaches, using the measured data from the river. Three simulation scenarios were

considered; downstream flow setpoint tracking, disturbance rejection subject to rainfall and disturbance rejection subject to offtakes to farms. In all cases, the MPC was able to maintain the downstream flow at setpoint and ensured the flow at the intermediate points in the river did not breach the defined minimum ecological flow. In addition, the MPC was compared with the decentralised PID-controller. As expected, while the PID-controller was able to maintain the downstream flow at setpoint, the PID-controller could not maintain the flow at the intermediate point of the river to stay above the defined minimum ecological flow.

Centralised MPC was considered in (Wagenpfeil *et al.*, 2010) to control a four-reach Elbe River, Germany. The Elbe River serves as the transport route for the shipping industry. Under normal operation, the water level in the river was often low, which was unsafe for shipping navigation, thus necessitated the use of pumps to channel the water into the river. The use of pump led to high electrical power consumption. The control objectives were to maintain water at levels deemed safe for navigation and to minimise the pumping cost. Hence, the electrical energy tariffs were included in the criterion to be minimised. The MPC was designed using the linearised Saint Venant equations and the Kalman filter was used for state estimation. Simulation results showed that water level variations were kept minimal taking into account the pump cost in the criterion.

A similar work was considered in (Linke, 2010) to control a three-reach Moselle River, Germany. Along the Moselle River, instead of locks (used in Aare River), barrages were used for shipping navigation. The opening and closing of the barrages create variation in water levels and the coordination between different barrages are vital so that these water level variations do not pose danger to the river navigation. The river also have hydropower stations for power generation. Therefore, the control objectives were to achieve a navigable river and to maximise hydropower output. Linke proposed a two-layer control configuration. In the lower layer control, the decentralised PI-controller was used to maintain the water level in each reach at setpoint. These setpoints were determined by the MPC, which was the higher layer control. Like (Wagenpfeil *et al.*, 2010), the controllers were designed using linearised Saint Venant equations. The criterion to be minimised included water level setpoint errors and control actions with more effort to attaining good flow discharge such that maximum power generation was achieved. Simulation results showed that as more effort was given in attaining good flow discharge for maximum power generation, simulation results also showed an increase of hydropower output compared to the current existing controller configuration.

A centralised MPC was used in flood regulation in (Barjas Blanco *et al.*, 2008) and (Barjas Blanco *et al.*, 2010). The Demer River in Belgium is flood prone and the current controller configuration, although it helped in reducing the risk of flood, it failed to avoid the big flood in 1998 due to a large amount of rainfall. In the MPC problem formulation, Barjas Blanco et al. constrained the water level to avoid river bank spilling and incorporated the rainfall measurements into the prediction horizon. The MPC was designed using a simplified reservoir model (see (Nash, 1957) or (Jacobsen *et al.*, 1997)). Simulations using the data from the 1998 flood showed that MPC was able to avoid river bank spilling, which suggests that the flood risk could potentially have been reduced with the use of MPC.

Similar works on flood mitigation using MPC was investigated in (Kearney *et al.*, 2011*b*) with the Wivenhoe Dam along the Brisbane River, Australia used as a case study. The Wivenhoe Dam, which was built to safeguard the city from flood was not able to prevent the 2011 huge flood event. Two MPC strategies were considered with the difference between the two was that one of the MPC utilised the measured flow in the prediction model over the horizon, while the other MPC utilised the predicted flow in the prediction model over the horizon. These MPCs were designed using the combination of a time delay and a reservoir model. Simulation results using the data from the 2011 flood event showed that with MPC, the huge flow released by the dam that led to the flood was reduced significantly. This suggests that the potential damage incurred by the flood could have been reduced with the use of MPC.

MPC was also considered in (Romera *et al.*, 2011) for flood mitigation in the Ebro River, Spain. There were several "flooding areas" along the river where in the event of high flow in the river, gates could be regulated to route the high flow to these flooding areas. Thus, the control objective considered were flow routing in the event when the flow in the river goes above a defined maximum safety value. The MPC was designed using the IDZ model proposed in (Litrico and Fromion, 2004*a*). Simulation results showed that MPC was able to regulate the gate to route the flow to the flooding areas when the flow in the river went above a defined maximum safety value.

A hybrid MPC was considered in (van Ekeren *et al.*, 2011), where the MPC was used to control the opening of different barriers, which were used to protect the area against flood. The term hybrid was used due to the opening and closing of these barriers were designed to operate in discrete manner while the water levels and flows are operating in continuous manner. The Rhine-Meuse Delta in the Netherlands was considered as their case study

and van Ekeren et al., proposed the so-called time-instant optimisation (TIO) MPC to reduce the computational load, which were often incurred when solving MPC optimisation that involve a mixture of continuous and discrete dynamics. The idea behind TIO MPC was to optimise the time instants of when the control action should take place. The control objectives considered were to achieve a good performance trade-off between minimising the cost of using these barriers and keeping the water levels within a safety level. The cost of using the barrier and the amount of water levels exceeding the defined safety reference level were included in the criterion. However, no details were given on how the weights used in the criterion were selected. The MPC was designed using the IDM. The performance of MPC was compared with the current control systems via simulation and the results showed that with MPC, significant reduction in the cost of using the barriers was achieved while maintaining the water levels within the defined safety level.

2.2.3 Control of irrigation channels

In this section, a brief review on control of irrigation channels are given. The PI-controller, which was first properly implemented in (Schuurmans, 1997) is now commonly used and was considered in many works (see e.g. (Baume *et al.*, 1999), (Chentouf *et al.*, 2001), (Litrico *et al.*, 2003) and (Aguilar *et al.*, 2009)). While those works focused on control of single irrigation channel, the decentralised PI-controller of multiple irrigation channels was considered in (Schuurmans *et al.*, 1999*a*), (van Overloop *et al.*, 2005), (Weyer, 2002) and (Ooi and Weyer, 2008). The PI-controller is normally used with the combination of low pass filter and feedforward of current measurements for wave attenuation and improved performance respectively. However, in scenarios where farmers may cancel or withdraw the water earlier or later than the scheduled time, no significant improvement is observed when the feedforward of scheduled offtakes is used (Weyer, 2002).

In (Malaterre, 1998), the LQ controller with feedforward was designed using the linearised Saint Venant equations to control two different eight-pool irrigation channels. To achieve zero steady state error, an integral state was included in the state space model. The water level setpoint errors, the control actions and the integral states were included in the criterion to be minimised. The weighting matrices Q and R were tuned through trial-and-error. In addition, due to unknown disturbance and as not all the states were measured, the Kalman filter was used for states estimation. The controller showed good performance in simulations but was not tested in real operation irrigation channels.

The LQ controller was also considered in (Weyer, 2003) to control a three-pool irrigation channels in HMC, Australia. Instead of using the linearised Saint Venant equations or Hayami equation, the controller was designed using the parameterised IDM obtained in (Weyer, 2001). The state space model was augmented with integral states and high pass filter states to ensure zero steady state error and avoiding excitation of wave frequencies respectively. The criterion to be minimised included water level and head over gate setpoint errors, the control actions, the integral states and the high pass filter states. As all the states were measured, no observer was designed. As a note, the criterion involved a cross term matrix due to one of the control objectives was to ensure minimal gate movement. The tuning matrices Q, R and N were tuned through trial-and-error. The controller was tested on HMC (Weyer, 2008) and compared with the decentralised PI-controller with feedforward designed in (Weyer, 2002). Although the performance of LQ controller was better compared to the decentralised PI-controller with feedforward, Weyer pointed that more design effort was needed for the centralised LQ controller and whether the better performance justified the design effort was case dependent.

The centralised H-infinity loop shaping controller was considered in (Li *et al.*, 2004) to control a three-pool irrigation channels in HMC, Australia. The were two steps to the design procedure using H-infinity loop shaping. The first step was to shape the loop gain of the plant to the desired loop gain shape. Then, the controller was synthesized to achieve the desired performance by minimising the H-infinity norm of the shaped loop gain. Li et al. compared the performance of the centralised H-infinity loop shaping controller with the decentralised PI-controller with feedforward designed in (Weyer, 2002) and the centralised LQ controller designed in (Weyer, 2003) via simulation and found that the H-infinity loop shaping controller had the best performance in terms of setpoints tracking and disturbances rejection. The advantage of H-infinity loop shaping controller lied in the ease of tuning compared to the LQ controller. The distributed controller configuration was later considered in (Li and Cantoni, 2008). The main difference between this configuration and the centralised configuration in (Li *et al.*, 2004) was that the loop shaping weights and the structure of the controller imposed ensures information was exchanged unidirectional between local adjacent controllers from downstream to upstream. The performance of the centralised and distributed H-infinity loop shaping controller was compared with the decentralised PI-controller with feedforward. The error propagation was lesser when the H-infinity loop shaping controller was used compared to the decentralised PI-controller with feedforward. Secondly, a properly fine tuned distributed H-infinity loop shaping

controller performed as well as the centralised H-infinity loop shaping controller.

The use of MPC controller in the control of irrigation channels can be found in many works (see e.g. (Ruiz and Ramirez, 1998), (Begovich *et al.*, 2007), (Wahlin, 2007), (van Overloop, 2006)). Most of those works mentioned considered centralised MPC configuration with the control objective of maintaining water level at setpoints. The criterion to be minimised include water level setpoint errors and rate of change of the control actions and most of the weights in the criterion function were tuned through trial-and-error. A decentralised version were considered in (Sawadogo *et al.*, 1998) and (Gómez *et al.*, 2002). A distributed version of MPC was considered in the following two papers (Negenborn *et al.*, 2009*b*) and (Negenborn *et al.*, 2009*a*) to control a seven-pool irrigation channels. The main difference between the two works, lied in the way the information was exchanged between the local MPC controllers. In the former work, information exchange between the adjacent local MPC was bidirectional where each local controller would strive to achieve the best performance. Negenborn et al. termed this as iterative schemes. The drawback of this scheme was heavy computation time and the optimal solution may not be computed fast enough (within a control cycle). A non-iterative scheme was proposed in the later work, where a hierarchy was given to the local MPC controller where the controller in the higher hierarchy could enforce the decision it made on the local MPC of lower hierarchy. In other words, the information exchange became unidirectional from the higher hierarchy controller to the lower one. Although this scheme was faster, the drawback of this scheme was that the higher hierarchy controller will not know what was going on with the lower hierarchy controller. The performance of the two schemes was compared and Negenborn et al. concluded that the use of which schemes was case dependant. A similar variant of non-iterative distributed MPC was considered in (Kearney *et al.*, 2011*a*).

There are also work that designed open loop controller via model inversion (Liu *et al.*, 1994), open loop controller designed using differential flatness (Rabbani *et al.*, 2010) and nonlinear controller designed using Lyapunov method (Coron *et al.*, 1999) and (Bastin *et al.*, 2009*b*) to control irrigation channels.

Chapter 3

Physical modelling

In this chapter, the physical modelling approach for river systems is presented. The dynamics of one-dimensional flow of the river systems are modelled by a set of nonlinear partial differential equations, which are also known as the Saint Venant equations derived by Adhémar Jean Claude Barré de Saint-Venant in 1871. Despite the wide usage in the field of hydrology, there are very few well documented studies on the accuracy of the Saint Venant equations validated against measured data (see e.g. (Brutsaert, 1971), (Ooi *et al.*, 2005) for some works in this direction). In this chapter, the main aim is to determine the accuracy of the Saint Venant equations for the river systems. This problem is investigated by comparing the Saint Venant equations against measured data from a river. In addition, we further investigate how to represent a river using the Saint Venant equations given that the geometries of the river can vary considerably and river meanders. Through simulation studies, we found that a simple representation of the river can be achieved with good accuracy. The findings are validated using operational data from two rivers in Australia. Moreover, our studies also reveal that simple adjustment of the friction coefficient suffices in treatment of meandering river without the need to use a two-dimensional flow model. Lastly, we investigate through several nonlinearity detection tests on how nonlinear the Saint Venant equations are.

In Section 3.1, we will derive the Saint Venant equations from the conservation of mass and momentum. Then, the Preissmann scheme, which is the most common numerical method for solving the Saint Venant equations is presented. Section 3.2 addresses the issue of segmentation where we look at how the river should be represented in the Saint

Venant equations in order to obtain an accurate representation of the dynamics of the river system. The segmentation approaches are compared against real data from the Broken and Murray Rivers. The discussion of meandering river and whether a two-dimensional flow model is required to treat a meandering river is presented in Section 3.3. The penultimate section investigates the nonlinearities in the Saint Venant equations and a summary is given in Section 3.5.

3.1 Derivation of the Saint Venant equations

The Saint Venant equations (assuming no lateral flow contribution) are given by

$$\frac{\partial Q}{\partial x} + \frac{\partial A}{\partial t} = 0$$

$$\frac{\partial Q}{\partial t} + \frac{\partial}{\partial x}\left(\frac{Q^2}{A}\right) + gA\frac{\partial y}{\partial x} + gA(S_f - S_0) = 0$$

where $Q = VA$ is the flow, V is the velocity, A is the wetted cross sectional area of the channel, y is the water depth, g is the gravity constant, S_0 is the bottom slope and S_f is the friction slope. These equations are derived from the conservation of mass and momentum under the following assumptions.

(i) The flow is one-dimensional.

(ii) The distribution of pressure is hydrostatic.

(iii) The velocity is uniform over a channel section.

(iv) The average channel bed slope is small. This implies that the angle (θ in Figure 3.2) formed between the channel bed and reference datum is very small. This means the measured flow depth in vertical direction is considered equal to the measured flow depth perpendicular to the channel bottom.

(v) The flow is incompressible.

A simplified derivation of the Saint Venant equations will be presented here. More detailed derivations can be found in standard open channel textbook (e.g. (Akan, 2006), (Chaudhry, 1993) or (Cunge *et al.*, 1980)). We begin by considering the conservation of mass.

3.1.1 Mass equation

Consider a volume element as shown in Figure 3.1 (Akan, 2006), where ρ is the density of the fluid (water), A is the wetted cross sectional area of the channel, Q is the flow, the subscript U and D denote the upstream and downstream end respectively, Δx is the distance between the upstream and downstream end and the flow direction is along the x-axis.

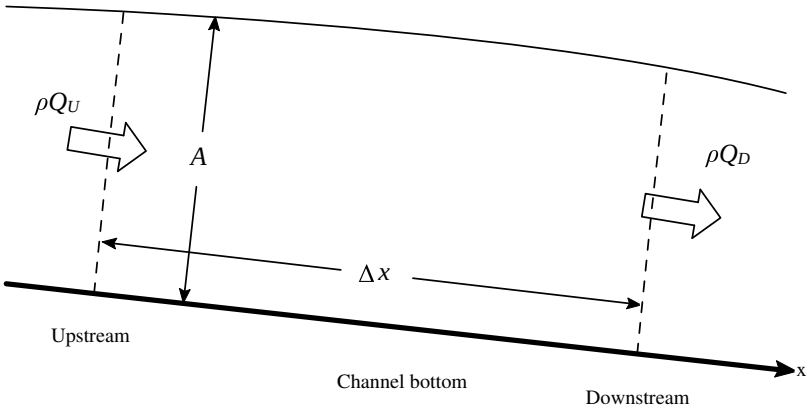

Figure 3.1: Sketch for the derivation of the conservation of mass equation. (Akan, 2006)

The conservation of mass states that

$$\begin{aligned} &\text{Net rate of mass entering/leaving the volume element} \\ &= \\ &\text{Rate of change of mass in the volume element} \end{aligned} \tag{3.1}$$

From Figure 3.1, the mass of the water is given by $\rho A \Delta x$. The water enters the volume element at the rate of ρQ_U and leaves the volume element at the rate of ρQ_D over a finite time, Δt. Equating both sides of the conservation of mass yields,

$$\rho Q_U - \rho Q_D = \frac{\Delta(\rho A \Delta x)}{\Delta t} \tag{3.2}$$

Generally, water is considered an incompressible fluid. This implies that the density, ρ is

constant. Then, Equation (3.2) is rewritten as

$$\begin{aligned} Q_U - Q_D &= \frac{\Delta(A\Delta x)}{\Delta t} \\ \frac{Q_U - Q_D}{\Delta x} &= \frac{\Delta A}{\Delta t} \\ \frac{Q_D - Q_U}{\Delta x} + \frac{\Delta A}{\Delta t} &= 0 \\ \frac{\Delta Q}{\Delta x} + \frac{\Delta A}{\Delta t} &= 0 \end{aligned} \tag{3.3}$$

where $\Delta Q = Q_D - Q_U$. As Δx and Δt approach zero, Equation (3.3) becomes

$$\frac{\partial Q}{\partial x} + \frac{\partial A}{\partial t} = 0 \tag{3.4}$$

where t and x are the time and displacement in the main flow direction (i.e. x-direction in our case). Equation (3.4) is known as the *continuity equation*.

3.1.2 Momentum equation

Here, the second Saint Venant equations is derived from the conservation of momentum. Consider the volume element as shown in Figure 3.2. where ρ, Q, A, Δx and subscript U and D have the same meaning as before (Figure 3.1). $\bar{y}$ is water depth of the centroid[1] (see Figure 3.2), V is the velocity, F_p is the pressure force, F_f is the friction force and W is the force due to the weight of the water. According to the conservation of momentum,

Rate of change of momentum within the volume element
=
Net rate of momentum transfer into the volume element (3.5)
+
Sum of all forces that acts on the volume element

The left hand side of the conservation of momentum is given by

$$\frac{\Delta(\rho\Delta x A V)}{\Delta t} \tag{3.6}$$

[1]The center of the trapezoidal wetted cross sectional area.

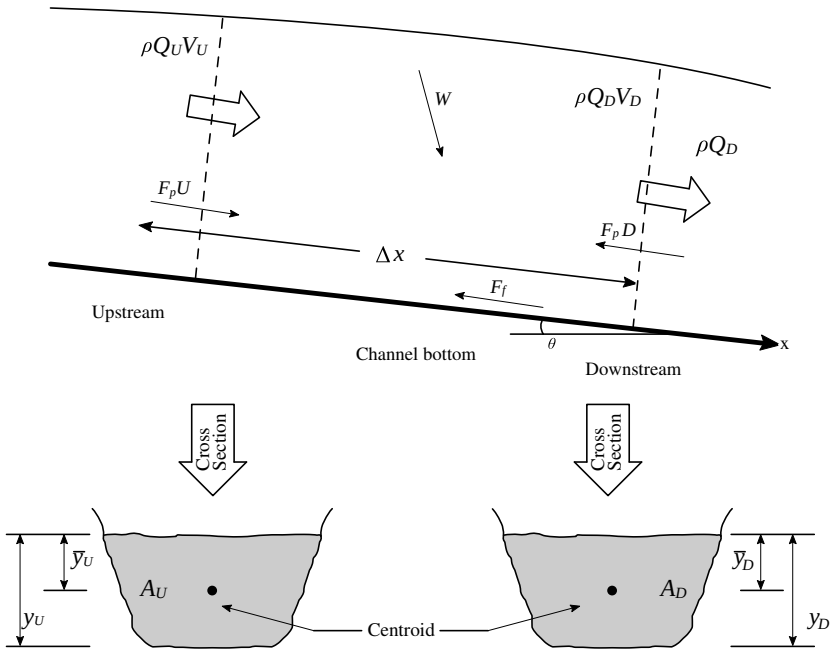

Figure 3.2: Sketch of the derivation of the conservation of momentum equation. (Akan, 2006)

The first term on the right hand side is given by

$$\rho Q_U V_U - \rho Q_D V_D \tag{3.7}$$

The second term on the right hand side comprises of the pressure force, the friction force and the force due to the weight of the water along the direction of the flow i.e. along the x-direction. The pressure force is denoted by

$$F_{p,U} - F_{p,D} = \rho g A_U \bar{y}_U - \rho g A_D \bar{y}_D \tag{3.8}$$

The friction force F_f is given by

$$F_f = -\rho g A \Delta x S_f \tag{3.9}$$

where S_f is the friction slope and the negative sign is due to the force acting in the opposite direction of the flow (see Figure 3.2). Using the Manning's friction coefficient, S_f can be

expressed as $\frac{n^2Q^2}{A^2R^{4/3}}$, where n is the Manning friction coefficient and $R = A/P$, P is the wetted perimeter[2]. The force due to the weight of the water is given by

$$W = \rho g A \Delta x S_0 \tag{3.10}$$

where $S_0 = \sin(\theta)$. Putting all these terms together yield

$$\frac{\Delta(\rho \Delta x A V)}{\Delta t} = (\rho Q_U V_U - \rho Q_D V_D) + (\rho g A_U \bar{y}_U - \rho g A_D \bar{y}_D) + \rho g A \Delta x S_0 - \rho g A \Delta x S_f \tag{3.11}$$

Again, ρ is constant as the water is assumed incompressible. Dividing Equation (3.11) by Δx leads to

$$\frac{\Delta(AV)}{\Delta t} + \frac{\Delta(QV)}{\Delta x} + g\frac{\Delta(A\bar{y})}{\Delta x} + gAS_f - gAS_0 = 0 \tag{3.12}$$

where $\Delta QV = Q_D V_D - Q_U V_U$ and $\Delta(A\bar{y}) = A_D \bar{y}_D - A_U \bar{y}_U$. As Δx and Δt approach zero, then, Equation (3.12) becomes

$$\frac{\partial Q}{\partial t} + \frac{\partial}{\partial x}\left(\frac{Q^2}{A}\right) + gA\frac{\partial y}{\partial x} + gAS_f - gAS_0 = 0 \tag{3.13}$$

In arriving with Equation (3.13), we used the following approximation $\frac{\Delta(A\bar{y})}{\Delta x} \approx A\frac{\partial y}{\partial x}$ (see (Akan, 2006) and (Chow *et al.*, 1988) for the derivation). Equation (3.13) is also known as the *dynamic equation*. Equations (3.4) and (3.13) form the Saint Venant equations.

3.1.3 Finite difference method

When solving a nonlinear PDE such as the Saint Venant equations, we normally have to resort to numerical methods due to the absence of a closed form solution. Finite Difference Methods (FDM) are usually used to discretise the PDE. The FDMs discretise the PDE in space and in time, where the partial derivatives are approximated using Taylor series expansion. The discretised equations are then solved on a computational grid (see Figure 3.3).

From Figure 3.3, the horizontal grid lines represent the discrete time k, while the vertical grid lines represent the discrete space i. The time and spatial increments are denoted by Δt and Δx respectively. In the case of the Saint Venant equations, each vertical grid line represents a spatial point of a river reach with the left most vertical

[2]The perimeter of the assumed cross sectional area minus the surface.

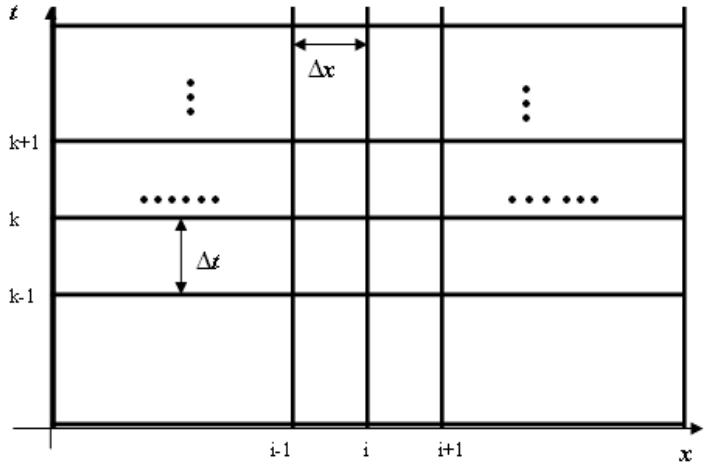

Figure 3.3: Computation grid.

grid line represents the upstream end and the right most vertical grid line represents the downstream end. We use a superscript to denote time while a subscript is used to denote space. For example, by Q_i^k, we are referring to the flow Q at spatial grid point i and time grid point k.

The FDM scheme can either be explicit or implicit. In an explicit scheme, the approximations based on the Taylor series expansions are expressed in variables at the current time, while in the implicit scheme, the approximation based on the Taylor series expansions is expressed in variables at future times.

3.1.4 Courant-Frederichs-Lewy (CFL) condition

When using Taylor series approximation for approximating the PDE, only a few terms of the series are retained. This leads to truncation errors. The truncation errors need to be treated with care as the accumulation of the truncation errors can lead to numerical instability. Courant, Frederichs and Lewy investigated the numerical instability in relation to the truncation error for PDEs in 1928 (Courant *et al.*, 1967)[3].

For the Saint Venant equations, which are hyperbolic PDEs, in order to avoid numerical instability, the following condition, called the CFL condition has to be satisfied (Cunge *et*

[3]This article was originally published in German in 1928. The English version was from 1967.

al., 1980).

$$\left| c_0 \frac{\Delta t}{\Delta x} \right| \leq 1 \tag{3.14}$$

where $c_0 = \sqrt{gy}$, g and y are the gravitational constant and the water depth respectively. In the explicit schemes, when solving the Saint Venant equations, the CFL condition may not be satisfied. To illustrate the CFL condition, we use an example given in (Cunge *et al.*, 1980).

In the example, the Saint Venant equations are solved for a river with water depth $y = 3$ m using a spatial increment of $\Delta x = 1000$ m. Equation (3.14) gives

$$\Delta t < \frac{1000}{(9.81 \times 3)^{1/2}} \simeq 180s$$

This means, that to ensure numerical stability using an explicit finite difference method, we can only solve the Saint Venant equations for a computational time step of at most 3 minutes. We can increase Δx to obtain a larger computational time step, but increasing Δx reduces the spatial resolution, which may result in poor accuracy of the obtained solution.

On the other hand, in the implicit finite difference schemes there are no problems with the CFL condition. This can be shown through a stability analysis procedure called the *von Neumann* analysis procedure (see (Lyn and Goodwin, 1987) and (Julien, 2002)). For this reason, implicit schemes are widely used when solving PDEs like the Saint Venant equations.

3.1.5 Preissmann scheme

As explained in the previous section, explicit schemes are not preferred as they may suffer from numerical instability (see e.g. (Vreugdenhil, 1994), (Beam and Warming, 1976), (Lyn and Goodwin, 1987) or (Julien, 2002)). The implicit schemes, on the other hand, do not suffer from numerical instability, and are hence preferred. There are several implicit schemes that can be used (see e.g. (Chaudhry, 1993) and the reference therein) when discretising the Saint Venant equations. The most widely used scheme is the Preissmann scheme[4] (see e.g. (Cunge *et al.*, 1980), (Chaudhry, 1993) or (Akan, 2006)), and it will also be used in this thesis. We will briefly explain the scheme here.

[4]The Preissmann scheme is also known as the 4-point implicit scheme

To recapitulate, the Saint Venant equations are given by,

$$\frac{\partial A}{\partial t} + \frac{\partial Q}{\partial x} = 0$$

$$\frac{\partial Q}{\partial t} + \frac{\partial}{\partial x}\left(\frac{Q^2}{A}\right) + gA\frac{\partial y}{\partial x} + gA(S_f - S_0) = 0$$

which can be rewritten in conservational matrix form,

$$\frac{\partial \mathbf{U}}{\partial t} + \frac{\partial \mathbf{F}}{\partial x} + \mathbf{S} = 0 \tag{3.15}$$

where

$$\mathbf{U} = \begin{bmatrix} A \\ Q \end{bmatrix} \quad \mathbf{F} = \begin{bmatrix} Q \\ \frac{Q^2}{A} + gAy \end{bmatrix} \quad \mathbf{S} = \begin{bmatrix} 0 \\ gA(S_f - S_0) \end{bmatrix} \tag{3.16}$$

By approximating the variables (Q and A) and their partial derivatives by

$$\begin{aligned} \frac{\partial f}{\partial t} &= \frac{(f_i^{k+1} + f_{i+1}^{k+1}) - (f_i^k + f_{i+1}^k)}{2\Delta t} \\ \frac{\partial f}{\partial x} &= \frac{\alpha(f_{i+1}^{k+1} - f_i^{k+1}) + (1-\alpha)(f_{i+1}^k - f_i^k)}{\Delta x} \\ f &= \frac{1}{2}\alpha(f_{i+1}^{k+1} + f_i^{k+1}) + \frac{1}{2}(1-\alpha)(f_{i+1}^k + f_i^k) \end{aligned}$$

where $f = A$ or Q. α is a weighting coefficient, Equation (3.15) can be rewritten as

$$\begin{aligned} (\mathbf{U}_i^{k+1} + \mathbf{U}_{i+1}^{k+1}) - (\mathbf{U}_i^k + \mathbf{U}_{i+1}^k) + \frac{2\Delta t}{\Delta x}\left[\alpha(\mathbf{F}_{i+1}^{k+1} - \mathbf{F}_i^{k+1}) + (1-\alpha)(\mathbf{F}_{i+1}^k - \mathbf{F}_i^k)\right] \\ + \Delta t\left[\alpha(\mathbf{S}_{i+1}^{k+1} + \mathbf{S}_i^{k+1}) + (1-\alpha)(\mathbf{S}_{i+1}^k + \mathbf{S}_i^k)\right] = 0 \end{aligned} \tag{3.17}$$

For $0.5 \leq \alpha \leq 1.0$, the Preissmann scheme is unconditionally stable (see e.g. (Chaudhry, 1993) or (Akan, 2006)). The Preissmann scheme is an implicit scheme since the approximation for the partial derivatives involved the future time point $k+1$. Equation (3.17) is a set of nonlinear algebraic equations that must be solved simultaneously.

Trapezoidal approximation

Here we approximate the wetted cross sectional area with a trapezoid (see Figure 3.4). Expressing A in terms of y (i.e. $A = (b+sy)y$, where b is the bottom width and s is the side slope), Equation (3.17) consists of two nonlinear algebraic equations with four unknowns (i.e. y_i^{k+1}, Q_i^{k+1}, y_{i+1}^{k+1} and Q_{i+1}^{k+1}), and $i = 1, \ldots, N$ where N is the number of spatial grid lines. In this case, Equation (3.17) yields $2(N-1)$ equations and $2N$ unknowns. Thus, we need boundary conditions at the upstream and the downstream end to uniquely determine all the unknowns.

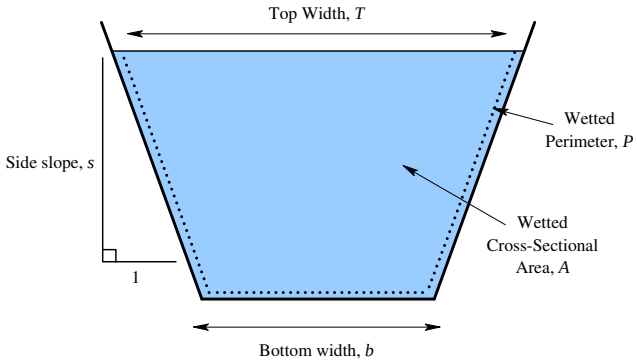

Figure 3.4: Trapezoidal approximation of the wetted cross section of a river reach.

Boundary conditions

The boundary conditions can be obtained as follow. At the upstream end, the boundary condition is given by

$$Q_{i=1}^{k+1} = Q_{up}^{k+1} \tag{3.18}$$

where Q_{up}^{k+1} is a given in-flow. At the downstream end, we will assume there is a weir. Using the flow over weir relationship (i.e. $Q(t) = ch^{3/2}(t)$ (Bos, 1978)), where c is the weir constant and h is the height of the water above the weir), the boundary condition can be expressed as

$$\begin{aligned} Q_{i=N}^{k+1} &= 0 && \text{if } h_N^{k+1} < 0 \\ Q_{i=N}^{k+1} &= c_{weir}(h_N^{k+1})^{3/2} && \text{otherwise} \end{aligned} \tag{3.19}$$

where $Q_{i=N}^{k+1}$ is the flow at the last spatial grid line and h_{down}^{k+1} is the downstream head over weir given by $y_N^{k+1} - p_{weir}$, where y_N and p_{weir} are the downstream water depth and height of the weir respectively. If a rating curve is used, then the downstream boundary conditions can be expressed as $Q_{i=N}^{k+1} = f(y_{i=N}^{k+1})$. If there is an undershot gate at the downstream end, the boundary condition can be expressed as $Q_{i=N}^{k+1} = c_{us} p_{us} \sqrt{y_{1,i=N}^{k+1} - y_{2,i=N}^{k+1}}$, where p_{us} is the gate opening, y_1 and y_2 are the water depth upstream and downstream of the undershot gate respectively.

Initial conditions

To start the numerical solution, we need the initial conditions, which are the initial flow and water depth at time point $k = 1$. The initial values can be obtained by solving the Saint Venant equations in steady state with the last spatial grid line being a given downstream water depth. Under steady state condition, all the time derivatives are set to zero. Equation (3.4) becomes

$$\frac{\partial Q}{\partial x} = 0 \tag{3.20}$$

Equation (3.20) implies that the flow is constant at each spatial increment Δx. Thus, the initial flow for all Δx is the constant upstream flow at time point $k = 1$. As the wetted cross sectional area is assumed trapezoidal, we have that $A = (b + sy)y$. Since the bottom width and side slope are varying with x, we have

$$\frac{\partial A}{\partial x} = (b + 2sy)\frac{\partial y}{\partial x} + y\frac{\partial b}{\partial x} + y^2\frac{\partial s}{\partial x}$$

Let $T = b + 2sy$. Using Equation (3.20), Equation (3.13) becomes

$$\begin{aligned}
gA(S_0 - S_f) &= \frac{\partial}{\partial x}\left(\frac{Q^2}{A}\right) + gA\frac{\partial y}{\partial x} \\
gA(S_0 - S_f) &= \left(\frac{1}{A}\frac{\partial Q^2}{\partial x}\right) - \left(\frac{Q^2}{A^2}\frac{\partial A}{\partial x}\right) + gA\frac{\partial y}{\partial x} \\
gA(S_0 - S_f) &= \left(-\frac{Q^2}{A^2}\right)\frac{\partial A}{\partial x} + gA\frac{\partial y}{\partial x} \\
gA(S_0 - S_f) &= \left(-\frac{Q^2}{A^2}\right)\left(T\frac{\partial y}{\partial x} + y\frac{\partial b}{\partial x} + y^2\frac{\partial s}{\partial x}\right) + gA\frac{\partial y}{\partial x}
\end{aligned} \tag{3.21}$$

Rearranging Equation (3.21) into differential form we get

$$\frac{dy}{dx} = \frac{gA(S_0 - S_f)}{\left(gA - \frac{Q^2T}{A^2}\right)} + \frac{\left(\frac{Q^2y}{A^2}\frac{\partial b}{\partial x}\right)}{\left(gA - \frac{Q^2T}{A^2}\right)} + \frac{\left(\frac{Q^2y^2}{A^2}\frac{\partial s}{\partial x}\right)}{\left(gA - \frac{Q^2T}{A^2}\right)} \tag{3.22}$$

Equation (3.22) is an Ordinary Differential Equation (ODE) and the solution of this ODE is a continuous function of water depths in x and it is used as the initial condition for the numerical solution of the Preissmann scheme.

Solution procedure

Equations (3.17), (3.18) and (3.19) constitute a set of $2N$ nonlinear algebraic equations with $2N$ unknowns, which can be solved using iterative technique. The most commonly used technique is the Newton-Raphson method (see e.g. (Kreyzig, 1988) or (Akan, 2006)) and it is also used in this thesis.

The solution procedure presented here follows (Akan, 2006) closely. The unknown quantities in Equation (3.17) are the Q_i^{k+1} and y_i^{k+1} for all spatial grid lines. The wetted cross-sectional area A and the friction slope S_f can be expressed in terms of those unknown quantities as well. Using the initial condition or the solution from the previous time step, we can obtain the solution for the next time step. Writing the continuity, dynamic, and boundary equations for all spatial grid lines, yield

$$\begin{aligned}
B_{up}(Q_1^{k+1}, y_1^{k+1}) &= 0 \\
C_1(Q_1^{k+1}, y_i^{k+1}, Q_2^{k+1}, y_2^{k+1}) &= 0 \\
D_1(Q_1^{k+1}, y_1^{k+1}, Q_2^{k+1}, y_2^{k+1}) &= 0 \\
C_2(Q_2^{k+1}, y_2^{k+1}, Q_3^{k+1}, y_3^{k+1}) &= 0 \\
D_2(Q_2^{k+1}, y_2^{k+1}, Q_3^{k+1}, y_3^{k+1}) &= 0 \\
&\vdots \\
C_{N-1}(Q_{N-1}^{k+1}, y_i^{k+1}, Q_N^{k+1}, y_N^{k+1}) &= 0 \\
D_{N-1}(Q_{N-1}^{k+1}, y_{N-1}^{k+1}, Q_N^{k+1}, y_N^{k+1}) &= 0 \\
B_{down}(Q_N^{k+1}, y_N^{k+1}) &= 0
\end{aligned} \tag{3.23}$$

In order to use Netwon-Raphson iteration method, we need to compute the partial derivatives of Equations (3.17), (3.18) and (3.19) with respect to Q_i^{k+1}, y_i^{k+1}, Q_{i+1}^{k+1} and y_{i+1}^{k+1}. The iteration method commences by assigning the initial condition to Q_i^{k+1} and y_i^{k+1} for all spatial grid lines to the left hand side of Equation (3.23).

There could be residuals in Equation (3.23). Thus, the new values of Q_i^{k+1} and y_i^{k+1} for all spatial grid lines for the next iteration are estimated such that these residuals approach to zero. To do so, we need to calculate the correction factor ΔQ_i and Δy_i to Q_i^{k+1} and y_i^{k+1} for all spatial grid lines such that partial derivatives of Equations (3.17), (3.18) and (3.19) with respect to Q_i^{k+1}, y_i^{k+1}, Q_{i+1}^{k+1} and y_{i+1}^{k+1} are equal to the negative of the residuals.

Mathematically,

$$
\begin{aligned}
\frac{\partial B_{up}}{\partial Q_1^{k+1}}\Delta Q_1 + \frac{\partial B_{up}}{\partial y_1^{k+1}}\Delta y_1 &= -\text{residual from } B_{up} \\
\frac{\partial C_1}{\partial Q_1^{k+1}}\Delta Q_1 + \frac{\partial C_1}{\partial y_1^{k+1}}\Delta y_1 + \frac{\partial C_1}{\partial Q_2^{k+1}}\Delta Q_2 + \frac{\partial C_1}{\partial y_2^{k+1}}\Delta y_2 &= -\text{residual from } C_1 \\
\frac{\partial D_1}{\partial Q_1^{k+1}}\Delta Q_1 + \frac{\partial D_1}{\partial y_1^{k+1}}\Delta y_1 + \frac{\partial D_1}{\partial Q_2^{k+1}}\Delta Q_2 + \frac{\partial D_1}{\partial y_2^{k+1}}\Delta y_2 &= -\text{residual from } D_1 \\
\frac{\partial C_2}{\partial Q_2^{k+1}}\Delta Q_2 + \frac{\partial C_2}{\partial y_2^{k+1}}\Delta y_2 + \frac{\partial C_2}{\partial Q_3^{k+1}}\Delta Q_3 + \frac{\partial C_2}{\partial y_3^{k+1}}\Delta y_3 &= -\text{residual from } C_2 \\
\frac{\partial D_2}{\partial Q_2^{k+1}}\Delta Q_2 + \frac{\partial D_2}{\partial y_2^{k+1}}\Delta y_2 + \frac{\partial D_2}{\partial Q_3^{k+1}}\Delta Q_3 + \frac{\partial D_2}{\partial y_3^{k+1}}\Delta y_3 &= -\text{residual from } D_2 \\
&\vdots \\
\frac{\partial C_{N-1}}{\partial Q_{N-1}^{k+1}}\Delta Q_{N-1} + \frac{\partial C_{N-1}}{\partial y_{N-1}^{k+1}}\Delta y_{N-1} + \frac{\partial C_{N-1}}{\partial Q_N^{k+1}}\Delta Q_N + \frac{\partial C_{N-1}}{\partial y_N^{k+1}}\Delta y_N &= -\text{residual from } C_{N-1} \\
\frac{\partial D_{N-1}}{\partial Q_{N-1}^{k+1}}\Delta Q_{N-1} + \frac{\partial D_{N-1}}{\partial y_{N-1}^{k+1}}\Delta y_{N-1} + \frac{\partial D_{N-1}}{\partial Q_N^{k+1}}\Delta Q_N + \frac{\partial D_{N-1}}{\partial y_N^{k+1}}\Delta y_N &= -\text{residual from } D_{N-1} \\
\frac{\partial B_{down}}{\partial Q_N^{k+1}}\Delta Q_N + \frac{\partial B_{down}}{\partial y_N^{k+1}}\Delta y_N &= -\text{residual from } B_{down}
\end{aligned}
\tag{3.24}
$$

Equation (3.24) can be written in the matrix form of

$$\mathbf{Ax} = \mathbf{b}$$

where $\mathbf{A}$, $\mathbf{x}$ and $\mathbf{b}$ are the big matrices consisting of all the partial derivatives, the correction factors and the residuals respectively. Here, any matrix inversion method (such as Gaussian elimination, LU Decomposition, etc) can be used to obtain the correction factor ΔQ_i and Δy_i for all spatial grid lines. Then, we substitute these correction factors into

$$\begin{aligned}(Q_i^{k+1})_{l+1} &= (Q_i^{k+1})_l + (\Delta Q_i)_l \\ (y_i^{k+1})_{l+1} &= (y_i^{k+1})_l + (\Delta y_i)_l\end{aligned} \tag{3.25}$$

where l and $l+1$ denote the iteration steps. This procedure is repeated until the difference between the left hand side and the first term on the right hand side is reduced below a tolerance value ϵ.

3.2 Segmentation analysis of river systems

The Saint Venant equations are widely used for modelling of river systems for scenario simulations, flow prediction, control design, etc. In order to represent a river using the Saint Venant equations, the river is usually divided into segments which are stretches where the river geometry and the friction are assumed constant. This lead to the question of how a river should be segmented, considering that the geometries of a river can vary considerably along a reach. In this section, we investigate the segmentation of rivers using the Saint Venant equations.

3.2.1 Geometrical segmentation

For our analysis, we focus on the reach from Casey's Weir to Gowangardie Weir in the Broken River (see Figure 1.1). For simplicity, we call this reach, Reach CG. Based on the on-site survey carried out by the Goulburn-Broken Catchment Management Authority (GBCMA) (GBCMA, 2009) and the Hydrologic Engineering Center - River Analysis System (HEC-RAS) model obtained from (Cottingham *et al.*, 2001), the approximate river parameters for Reach CG are summarised in Table 3.1. Both Casey's and Gowangardie Weirs are sharp crested weirs where the flow can be approximated by (Bos, 1978)

$$Q(t) \approx c_{weir} h(t)^{3/2} = c_{weir}[y(t) - p]^{3/2} \tag{3.26}$$

p is the height of the weir. $c_{weir} \approx 0.6\sqrt{g}b_{weir}$ (Boiten, 2002) is the weir constant where g is the gravity constant and b_{weir} is the width of the weir. The width of the weir at Casey's and Gowangardie Weirs are approximately 30m and 6m respectively.

Table 3.1: Summary of river parameters for Reach CG.

Parameters	**Reach CG**
Reach length, L_{CG}	26.7km
Bottom width, b_{CG}	9.0-12.0m
Side slope, s_{CG}	2.0-3.0
Bottom slope, $S_{0,CG}$	0.0008-0.0020
Manning friction coefficient, n_{CG}	0.060-0.085

In an attempt to get a close approximations of the river geometry for Reach CG, it is divided into segments, which are stretches where the river geometries are assumed constant. Thus, Reach CG was segmented using 20 segments as shown in Figure 3.5, with parameter values[5] given in Table 3.2.

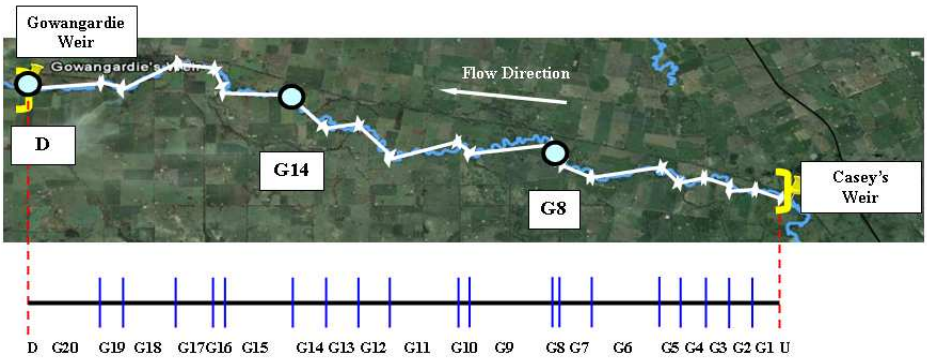

Figure 3.5: Geometrical segmentation of Reach CG. Source: Google Earth.

We called this way of segmentation, Geometrical segmentation. The setup time (i.e. the time it takes to find all parameters and implement the simulation model) for a Geometrical segmentation is large and the more a river meanders, the more segments are required for an accurate geometrical approximations. Sometimes we might only be inter-

[5]Values shown in Table 3.2 are obtained from GBCMA and the HEC-RAS model used in (Cottingham *et al.*, 2001). As there are no detailed surveyed data available for the whole of Reach CG, some of those values are just best guesses based on the observation using Google Earth.

ested in the flows or water levels at certain locations, e.g. the locations G8, G14 and D indicated by the circles in Figure 3.5. The question then arises; if we are only interested in the accuracy of the simulated flows and water levels at a few locations can we use a simplified description of the river with fewer segments? Next, two segmentation methods with less segments are suggested.

3.2.2 Single segmentation

We start with the simplest choice, i.e. we treat the whole river reach as one segment. We call this "Single segmentation". In Single segmentation, we treat the whole river reach as one segment with constant geometry such that the length is 26.7km, (i.e. the length of the reach) and b, s, S_0 and n are the average values from Table 3.1. S_0 is computed as $(161.04 - 137.04)/26700 \approx 9.00 \times 10^{-4}$, where 161.04mAHD and 137.04mAHD are the elevations at Casey's and Gowangardie Weirs measured in meter Australian Height Datum (mAHD), which is relative to sea level. Figure 3.6 and Table 3.2 summarise the Single segmentation for Reach CG.

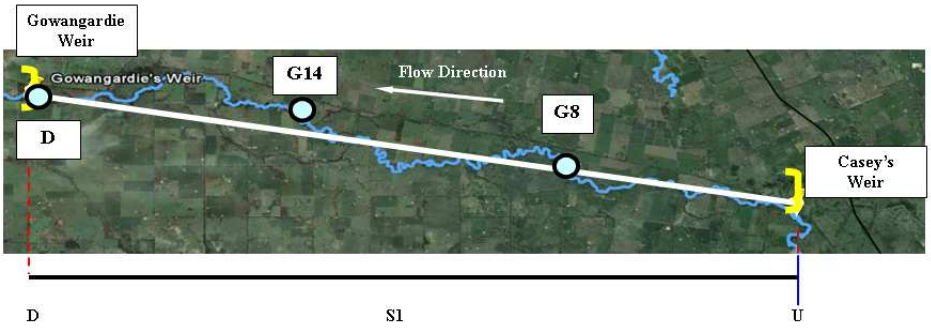

Figure 3.6: Single segmentation of Reach CG. Source: Google Earth.

Table 3.2: Summary of segmentation methods. The letter 'G', 'S' & 'M' denote Geometrical, Single and M-segment segmentation respectively.

Segment	**Geometry**	**Segment**	**Geometry**
G1	$b = 10.50$m, $s = 2.00$ $S_0 = 8.00 \times 10^{-4}$, $n = 0.070$	G11	$b = 12.00$m, $s = 2.85$ $S_0 = 9.00 \times 10^{-4}$, $n = 0.080$
G2	$b = 10.38$m, $s = 2.05$ $S_0 = 9.00 \times 10^{-4}$, $n = 0.075$	G12	$b = 11.49$m, $s = 3.00$ $S_0 = 11.00 \times 10^{-4}$, $n = 0.085$
G3	$b = 10.65$m, $s = 2.25$ $S_0 = 7.25 \times 10^{-4}$, $n = 0.060$	G13	$b = 12.00$m, $s = 2.85$ $S_0 = 9.00 \times 10^{-4}$, $n = 0.080$
G4	$b = 10.46$m, $s = 2.00$ $S_0 = 8.00 \times 10^{-4}$, $n = 0.072$	G14	$b = 10.97$m, $s = 2.00$ $S_0 = 18.00 \times 10^{-4}$, $n = 0.070$
G5	$b = 9.97$m, $s = 2.05$ $S_0 = 10.00 \times 10^{-4}$, $n = 0.077$	G15	$b = 11.26$m, $s = 2.45$ $S_0 = 15.00 \times 10^{-4}$, $n = 0.073$
G6	$b = 10.47$m, $s = 2.50$ $S_0 = 8.15 \times 10^{-4}$, $n = 0.068$	G16	$b = 9.68$m, $s = 2.08$ $S_0 = 10.00 \times 10^{-4}$, $n = 0.080$
G7	$b = 10.27$m, $s = 2.35$ $S_0 = 8.75 \times 10^{-4}$, $n = 0.070$	G17	$b = 10.80$m, $s = 2.35$ $S_0 = 10.65 \times 10^{-4}$, $n = 0.079$
G8	$b = 9.50$m, $s = 2.00$ $S_0 = 20.00 \times 10^{-4}$, $n = 0.078$	G18	$b = 11.00$m, $s = 2.50$ $S_0 = 9.00 \times 10^{-4}$, $n = 0.073$
G9	$b = 11.50$m, $s = 3.00$ $S_0 = 10.00 \times 10^{-4}$, $n = 0.085$	G19	$b = 10.50$m, $s = 2.60$ $S_0 = 12.55 \times 10^{-4}$, $n = 0.069$
G10	$b = 10.00$m, $s = 2.15$ $S_0 = 9.44 \times 10^{-4}$, $n = 0.071$	G20	$b = 11.96$m, $s = 2.65$ $S_0 = 10.00 \times 10^{-4}$, $n = 0.060$
S1	$b = 10.50$m, $s = 2.50$ $S_0 = 9.00 \times 10^{-4}$, $n = 0.073$		
M1	$b = 10.39$m, $s = 2.23$ $S_0 = 8.41 \times 10^{-4}$, $n = 0.070$	M3	$b = 11.10$m, $s = 2.47$ $S_0 = 11.20 \times 10^{-4}$, $n = 0.071$
M2	$b = 11.32$m, $s = 2.69$ $S_0 = 11.87 \times 10^{-4}$, $n = 0.080$		

3.2.3 M-segment segmentation

For M-segment segmentation, we segment the reach according to the locations of interest. M is the number of locations of interest along the river reach. In this example, we have M = 3 segments and the average value of the river parameters are used for the segments 'U-G8', 'G8-G14' and 'G14-D' (see Figure 3.7 and Table 3.2). As a note, instead of using average values based on surveys for the river parameters, they can also be estimated from

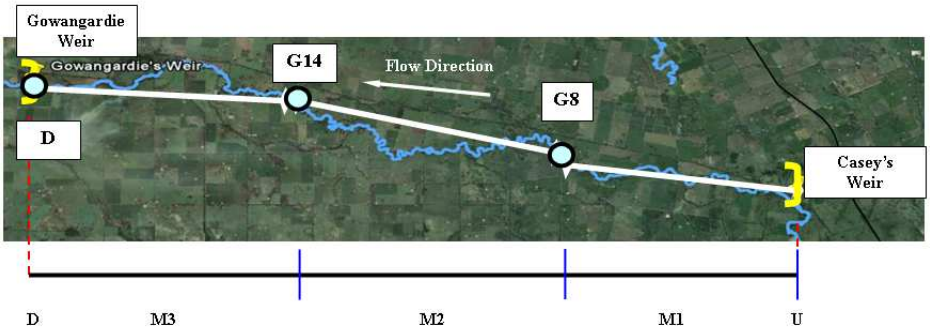

Figure 3.7: M-segment segmentation of Reach CG. Source: Google Earth.

measured data (see e.g. (Wu *et al.*, 2007)).

3.2.4 Illustrative examples

In this simulation, $\Delta t = 1$ minute and $n_{sec} = 100$, $\Delta x = L/n_{sec} = 26700/100 = 267$m are used. For the boundary flow condition at the upstream end we use a pseudorandom binary signal[6] with period 250 minutes and levels of 1.25m^3/s and 2.75m^3/s as shown in Figure 3.8. The downstream boundary condition is the flow given by Equation (3.26) using the simulated water level and $p_G = 137.33$mAHD. For the width of the weir, $b_{weir,G} = 6$m. The water levels at the three locations of interest are compared. For the three different segmentation methods, the simulated water levels are shown in Figure 3.9. The simulations ran from $t = 0$ minutes to $t = 6000$ minutes but for a clearer presentation, we only show the results from time 3000 to 5000 minutes. As a quantitative measure, the Mean Square Difference (MSD) is calculated i.e.,

$$\text{MSD} = \frac{1}{N}\sum_{t=1}^{N}[y_{geo}(t) - y_q(t)]^2 \tag{3.27}$$

where $N = 6000$ is the number of data points and y_{geo} and y_q are the simulated water level obtained using Geometrical segmentation and $q =$ Single or $q =$ M-segment respectively.

Remarks: The accuracy of the river parameters shown in Table 3.2 is not important as the comparison are made between simulated data. However, the accuracy of the river

[6] A pseudorandom binary signal is a two-level periodic and deterministic signal, which has the properties similar to a white noise. This allow excitation of multi harmonics in a single measurement.

parameters become more important when comparison are made against measured data. We address this in more detail in Sections 3.2.6.

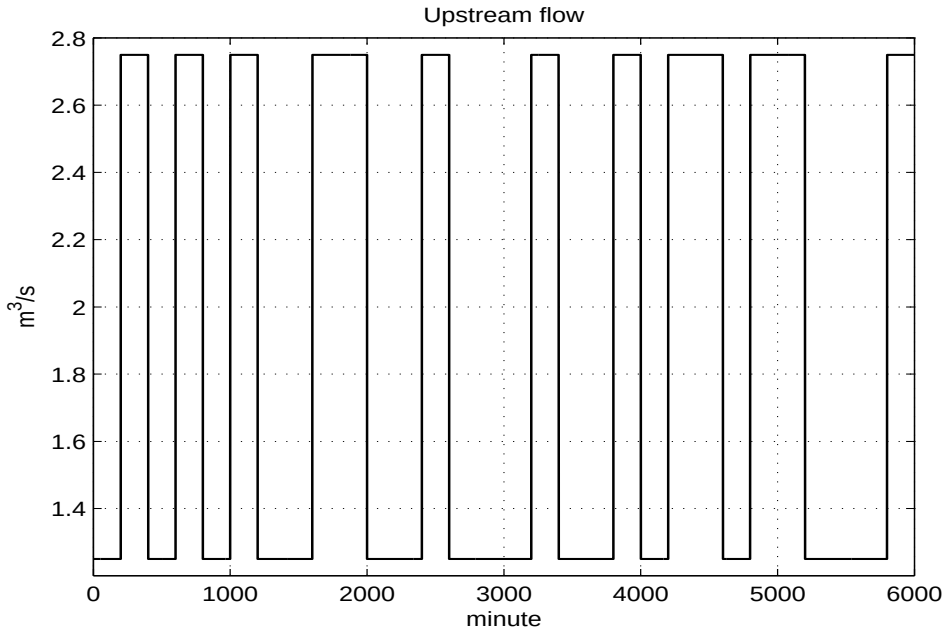

Figure 3.8: Input flow.

The values of the MSD are shown in Table 3.3.

Table 3.3: Values of MSD.

Location	**MSD** (10^{-4}m^2) (Geo. vs. Single)	**MSD** (10^{-4}m^2) (Geo. vs. M-segment)
G8	28.868	10.196
G14	118.391	30.694
D	0.604	0.112

From Figure 3.9 it is clear that all segmentations produce qualitatively similar simulated water levels with an offset between them. The difference in water level between different segmentations is small at the downstream end. If the water level at the downstream is all we are interested in, the results indicate that the Single segmentation is sufficient. At the other locations, M-segment segmentation is closer to the Geometrical

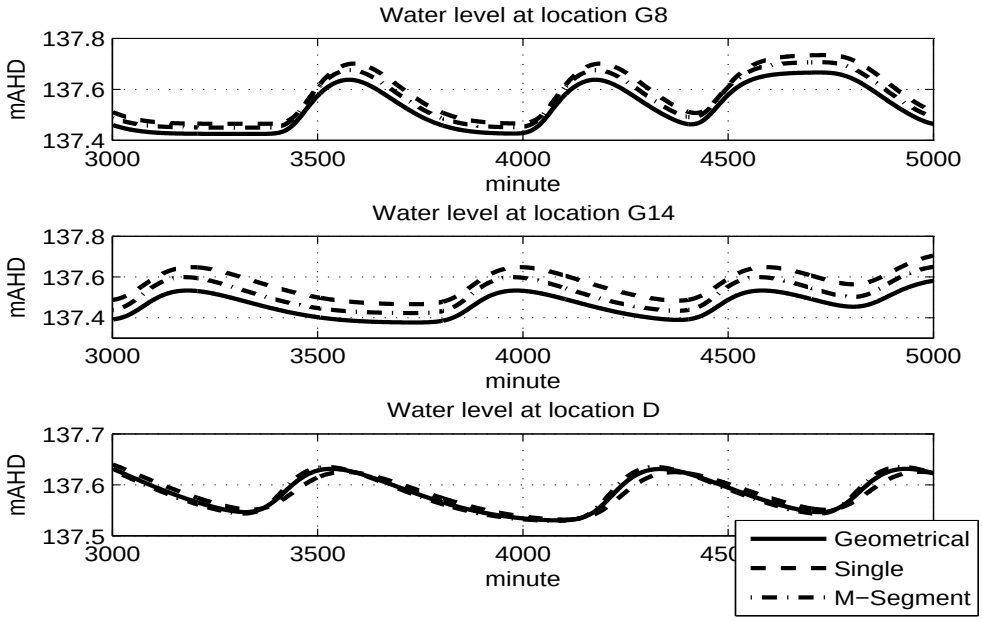

Figure 3.9: Water levels at the three locations.

segmentation than the Single segmentation. These findings are encouraging as it suggests that we do not loose much in accuracy by using fewer segments, particularly if we are only interested in the water level at the downstream end.

3.2.5 Validation against operational data

Single segmentation

Figure 3.10 shows the measurements of the flows and water levels at Casey's and Gowangardie Weir. The flows at Casey's Weir are not physically measured but computed from the water levels based on a water level-to-flow conversion table used by the water authority. Since the comparison of measurements can be made only at the downstream end and based on the results in Section 3.2.4, we use a Single segmentation to represent Reach CG. The upstream boundary condition is given by the measured flows at Casey's Weir, and the downstream boundary condition is obtained using Equation (3.26) with the simulated water level and $p_G = 137.33$mAHD, where the subscript 'G' denotes Gowangardie Weir. $c_{weir,G}$ and n_{CG} are calibrated from data using data from April to June 2001 (Figure 3.10)

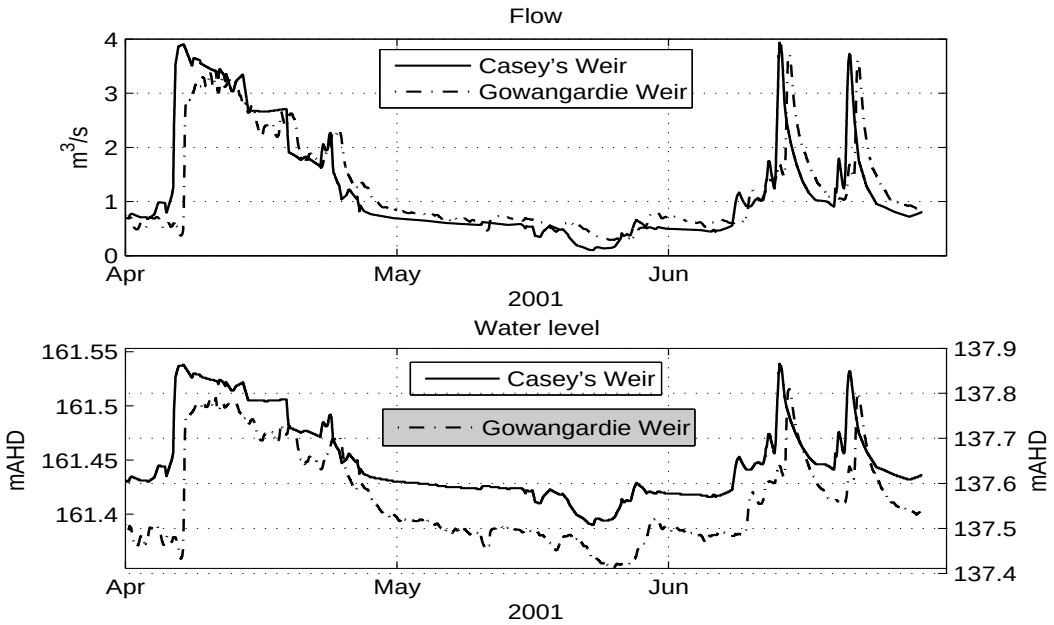

Figure 3.10: Top: Measured flows for Reach CG. Bottom: Measured water levels for Reach CG.

and the criterion

$$\hat{\theta}_{p,CG} = \underset{\theta_{p,CG}}{\operatorname{argmin}} \frac{1}{N} \sum_{t=1}^{N} [y_{mea,G}(t) - \hat{y}_{sim,G}(t, \theta_{p,CG})]^2 \tag{3.28}$$

where $N = 8640$ is the number of data points (the sampling period is 15 minutes), $\theta_{p,CG} = [c_{weir,G}, n_{CG}]^T$, $y_{mea,G}$ is the measured water level and $\hat{y}_{sim}$ is the simulated water level using the Saint Venant equations. The estimation procedure is a nonlinear least square problem and the Levenberg-Marquardt method is used to solve the problem iteratively, using the MATLAB® routine *lsqnonlin*.

The calibrated values are $c_{weir,G} = 10.10\text{m}^{3/2}/\text{s}$ and $n_{CG} = 0.1459$. The calibrated $c_{weir,G}$ indicates that the width of the weir $b_{weir,G} = 5.4\text{m}$, which is close to the actual width of the weir. The calibrated n is higher than the values given in Table 3.1. Those values correspond to a particular section of the river reach and do not include the effect of meandering. The meandering leads to a larger estimated value of n_{CG} (see e.g. (Arcement and Schneider, 1989)). Using the calibrated values, we validate our simulations on data sets not used for calibration. The data sets are from October to December 2001 and April

to June 2002 (see Figure 3.11) which roughly correspond to the Australian spring and autumn respectively. In the simulation, we used $n_{sec} = 100$ and $\Delta t = 15$ minutes. As a quantitative measure, the Mean Square Error (MSE) is calculated as

$$\text{MSE} = \frac{1}{N}\sum_{t=1}^{N}[y_{mea,G}(t) - \hat{y}_{sim}(t, \theta_{p,CG})]^2 \tag{3.29}$$

The MSE values are shown in Table 3.4.

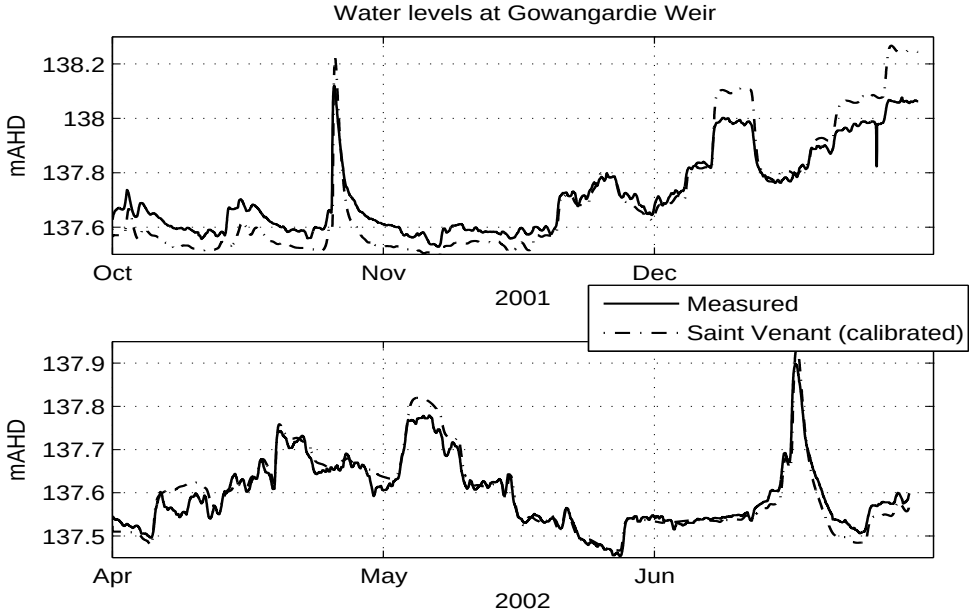

Figure 3.11: Top: Spring period (Start of irrigation season). Bottom: Autumn period (End of irrigation season).

Table 3.4: The MSE values (10^{-3}m^2).

Data Period	**MSE** (Single)	**MSE** (M-segment)	**MSE** (Geometrical)
Spring 2001	5.38	5.03	5.41
Autumn 2002	0.52	0.52	0.57

In addition, we calculated the MSE for the same data using M-segment and Geometrical segmentation. For M-segment and Geometrical segmentation, we calibrated $c_{weir,G}$ and n_{CG} for each segment. We can see from the values of the MSE that the Single segmentation is as accurate as the other segmentation methods.

Figure 3.11 shows that the Saint Venant equations after calibration using Single segmentation are accurate when compared to measured data. It picks up the trends in the water levels very well. Irrigation off-takes, rainfall and in-flows from creeks are not modelled, and further improved accuracy could possibly be achieved by taking those effects into consideration. Nonetheless, the results obtained are encouraging as they show that Single segmentation represents real river data well.

M-segment segmentation

In the Broken River, there is no available measurements where the method M-segment segmentation can be validated against data. In view of this, we validated this method against measurements from the Murray River in Australia.

For the Murray River, we study the reach between Doctor's Point and Yarrawonga Weir, and we call this reach, Reach DY. This reach is about 115km long and has a width between 40 and 60m making it larger than the Broken River. There are also two unmodelled creeks flowing into this reach. Along this reach, there is a measuring station at Corowa, which is located 63.1km downstream of Doctor's Point. There is no hydraulic structure at Corowa. Yarrawonga Weir is a sharp crested weir where the flow and water level relationship can be described using

$$Q(t) \approx ch(t)^{3/2} = c[y(t) - p]^{3/2} \tag{3.30}$$

where p is the height of the weir. $c \approx 0.6\sqrt{g}b_w$ (Boiten, 2002) where g is the gravity constant and b_w is the width of the weir. From a hydrological survey carried out by Victorian Water Resources (Victorian Water Resources, 2009) and Department of Primary Industries (Department of Primary Industries, 2009), Victoria, Australia, the (range of the) river parameters for Reach Doctor-Yarrawonga are summarised in Table 3.5.

For this reach, we are mainly interested in the flows and water depths at two locations, Yarrawonga Weir and Corowa. We only have measurements of flows and water levels at Doctor's Point and Corowa. In view of the absence of measurements at Yarrawonga Weir,

Table 3.5: Summary of river parameters.

Parameters	**Reach Doctor-Yarrawonga**
Reach length, L	115.0km
Bottom width, b	40.0-60.0m
Side slope, s	3.0-5.0
Bottom slope, S_0	0.002-0.003
Manning friction coefficient, n	0.07-0.09

comparisons can only be made at Corowa. As boundary conditions can only be obtained at Yarrawonga Weir, the reach is segmented using M = 2 segments as shown in Figure 3.13 with parameter values given in Table 3.6. The upstream boundary condition is the flow at

Table 3.6: Summary of M-segment segmentation.

Segment	**Geometry**
DY1	$b = 50.0$m, $s = 4.0$ $S_0 = 0.00244$, $n = 0.1176$
MU2	$b = 55.0$m, $s = 5.0$ $S_0 = 0.00233$, $n = 0.0684$

Doctor's Point, and the downstream boundary condition is given by Equation (3.30) using the simulated water level. For Yarrawonga Weir, the height of the weir p_Y and the weir coefficient c_Y are unknown and they are estimated together with the friction coefficients on each segment, which we denote by $n_{DY,1}$ and $n_{DY,2}$ respectively. The criterion used is

$$\hat{\theta}_{p,DY} = \underset{\theta}{\operatorname{argmin}} \frac{1}{N} \sum_{t=1}^{N} [y_{mea,Cr}(t) - y_{sim,Cr}(t, \theta_{p,DY})]^2 \tag{3.31}$$

where $N = 365$, $\theta_{p,DY} = [c_Y, p_Y, n_{DY,1}, n_{DY,2}]^T$, $y_{mea,Cr}$ and $y_{sim,Cr}$ are the measured and simulated water levels at Corowa. As for the remaining river parameters (i.e. b, s and S_0), the average values from Doctor's Point to Corowa and from Corowa to Yarrawonga Weir are used. The measurements for the year 2000 shown in Figure 3.12 are used for calibration.

The sampling interval is 1 day. The calibrated values are $c_Y = 77.76\text{m}^{3/2}/\text{s}$, $p_Y =$

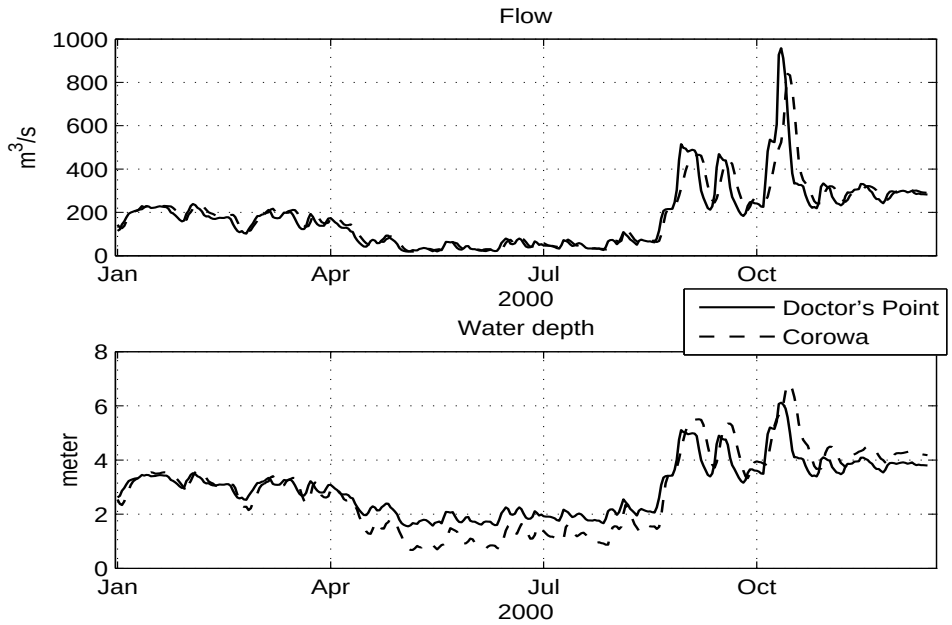

Figure 3.12: Measured flows and water levels at Corowa for year 2000. Top: Flow. Bottom: Water level.

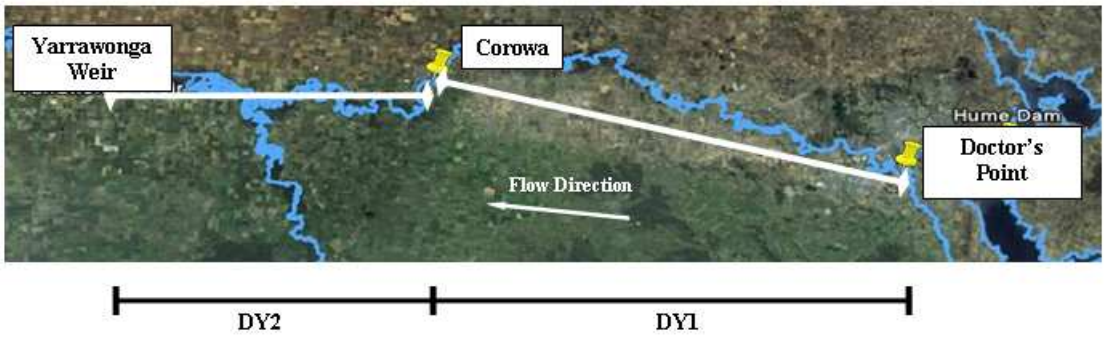

Figure 3.13: M-segment segmentation of Reach DY. Source: Google Earth.

2.41m, $n_{DY,1} = 0.1176$ and $n_{MU2} = 0.0684$. Using these calibrated parameters, we validate our models on data from 2001 (see Figure 3.14) which are not used for calibration. In the simulations, $n_{sec} = 100$ and $\Delta t = 1$ day. We also use Single and Geometrical Segmentation to represent the reach and calculated the MSEs. They are given in Table 3.7. From Figure 3.14, we see that the simulated water level picks up the trends in the measured water level very well. As expected, from the MSE in Table 3.7, we see that the accuracy of using Single

Table 3.7: The MSE values for Reach DY.

Data Period	**MSE** (Single) m^2	**MSE** (M-segment) m^2	**MSE** (Geometrical) m^2
2001	0.080	0.038	0.032

segmentation is not as good as the Geometrical segmentation, while the accuracy of the M-segment segmentation is as good compared to the Geometrical segmentation. As before, in- and outflows from the creeks, rainfall, etc are not taken into account. These results are again encouraging as they illustrate that the M-segment segmentation represents real river data well.

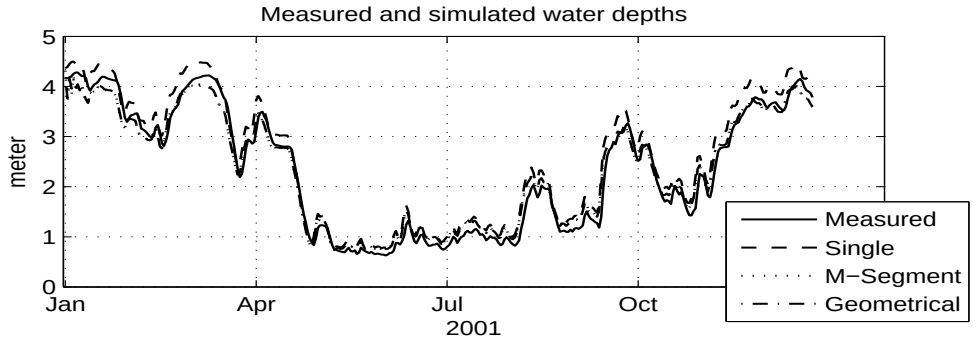

Figure 3.14: Measured and simulated water depths at Corowa using different segmentations.

3.2.6 Sensitivity analysis

Variations in river parameters

In Section 3.2.5, we used Single segmentation to represent Reach CG where the average values of each of the river parameters are used. As these values are only approximate, we study the effect of uncertainty in the parameters in this section.

We use the measured data from April to June 2002 for Reach Casey-Gowangardie. The MSE found in Section 3.2.5 is used as the nominal MSE and it is denoted by MSE_0. We vary each of the four river parameters (i.e. bottom width, side slope, bottom slope and Manning friction coefficient), one at a time from $\pm 5\%$ to $\pm 40\%$ and calculate the

respective MSE. For comparison, the relative MSE is calculated as

$$\text{Relative MSE} = \frac{\text{MSE}_j - \text{MSE}_0}{\text{MSE}_0} \tag{3.32}$$

where MSE_j represents the MSE obtained for each of the varied parameters, $j = b_{CG}, s_{CG}, S_{0,CG}, n_{CG}$. From Figure 3.15 (top), we observe that the variation in b_{CG} and s_{CG} do not affect the

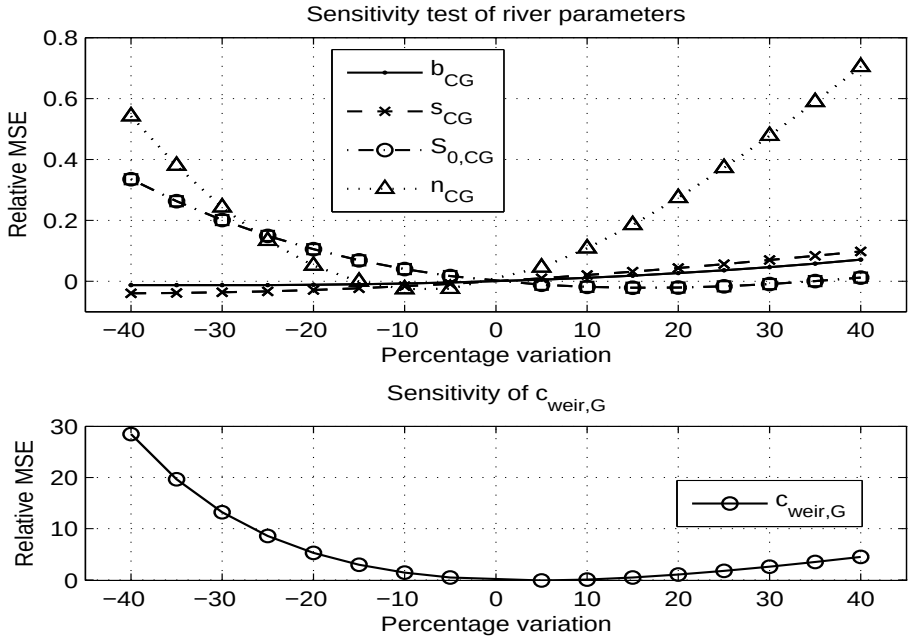

Figure 3.15: Top: Relative MSE versus percentage variation of the river parameters. Bottom: Relative MSE versus percentage variation in $c_{weir,G}$.

accuracy much. For $S_{0,CG}$, the accuracy decreases with 10% when the variation is more than -20%, and n affects the accuracy greatly. However, $S_{0,CG}$ which is the average bottom slope, can be relatively accurate measured and will not change much due to human or natural activities. Thus, realistically the simulations will only be sensitive to the variations in n_{CG}. This finding is in agreement with the common practice of calibrating n_{CG} against data (see e.g. (Lebosse, 1989)). In addition, we also investigate the sensitivity of $c_{weir,G}$. From Figure 3.15 (bottom), we notice that variation of $c_{weir,G}$ also affects the accuracy significantly with very large relative MSE. Thus, it is of importance to calibrate $c_{weir,G}$ as well.

Changing Δx and Δt

In Section 3.2.5, $\Delta t = 15$ minutes and $\Delta x = 267$m, corresponding to $n_{sec} = 100$ are used and yield a simulation time of 205 seconds. In this section, we analyse how much the time and spatial resolution can be allowed to increase before the accuracy drops significantly. Δt and Δx are varied each at a time, while fixing the river parameters to those used in

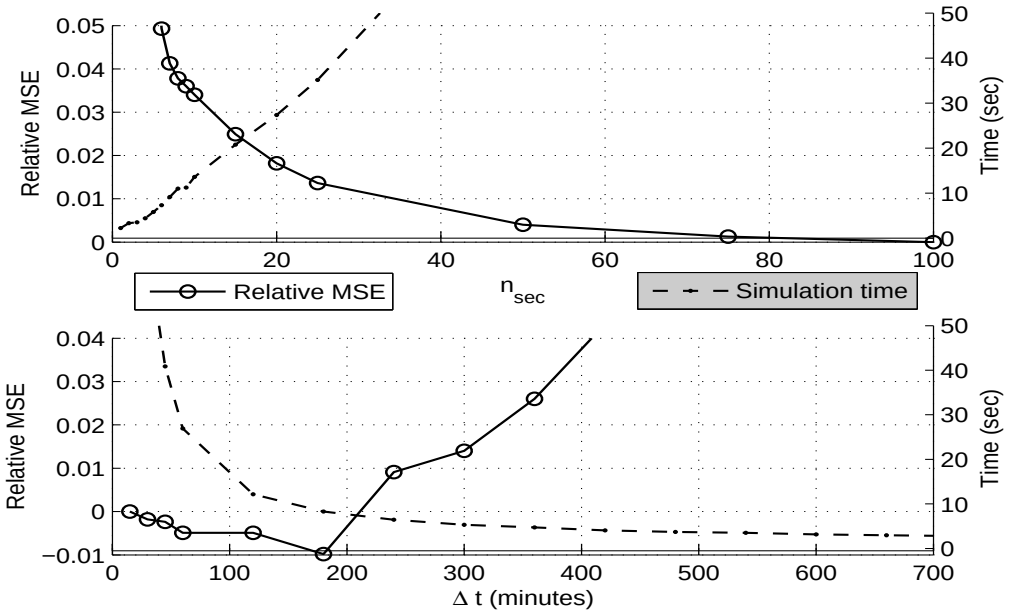

Figure 3.16: Relative MSE and simulation time as a function of n_{sec} (top) and Δt (bottom).

Section 3.2.5. Δx is varied by varying n_{sec} such that Δx is given by $\Delta x = L/n_{sec}$. We then compute the relative MSE and the simulation time. All the simulations are carried out in MATLAB® on the same computer[7]. The simulation time is calculated using the *tic* and *toc* functions in MATLAB®. The results are shown in Figure 3.16.

From Figure 3.16, we observe the following. As expected, the accuracy of the simulation improves as n_{sec} increases but at the expense of longer simulation time. On the other hand, as Δt increases, we get similar accuracy but it gets worse when Δt is greater than 200 minutes but we get a shorter simulation time. $\Delta t = 240$ minutes (i.e. data sampled every 4 hours) and $\Delta x = 1068$m (i.e. $n_{sec} = 25$) both give an increase of 0.01 in relative MSE. We therefore expect a relative increase of about 0.02 if we use $\Delta t = 240$ minutes

[7]Intel Core 2 CPU 1.73GHz processor with 2GB RAM

and $\Delta x = 1068$m. Next we used these values and compared with the measured data and the results from Section 3.2.5 with $\Delta x = 267$m and $\Delta t = 15$ minutes. The results

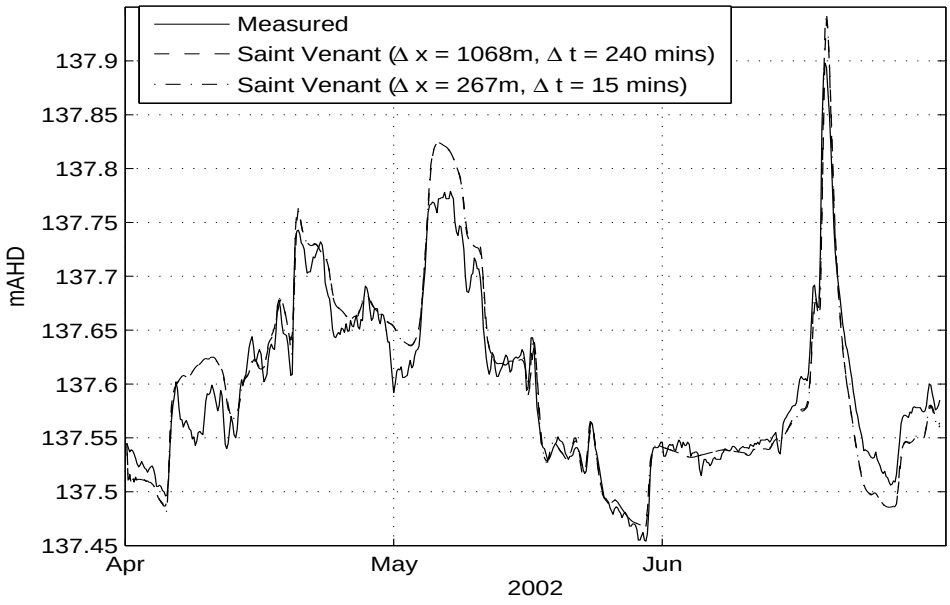

Figure 3.17: Measured and simulated water level using $\Delta t = 240$ minutes and $\Delta x = 1068$m.

are shown in Figure 3.17. Note that the two simulated water levels are nearly identical and therefore difficult to distinguish. The simulation time is 1.35 seconds, which is a substantial reduction compared to 205 seconds for $\Delta t = 15$ minutes and $n_{sec} = 100$, while the calculated MSE increased from 0.52 (10^{-3}m^2) to 0.53 (10^{-3}m^2), which is in agreement with our expectations. These findings show that we do not loose much accuracy by using a lower spatial and time resolutions, at the same time reduces the simulation time.

3.3 Treatment of meandering river

In our analyses thus far, we have accounted the effect of meandering river by adjusting the friction coefficient. This way of treating a meandering river is not uncommon (see e.g. (Fread, 1991) or (Langendoen, 2000)). Here, we present the illustration used in (Langendoen, 2000) on how the hydraulic software, CONCEPT handles a meandering river (see Figure 3.18).

Meandering regions e.g. between number 6-7 or 9-10 in Figure 3.18 will be assigned a larger friction coefficient, i.e. a larger Manning's friction coefficient n. This is because a meandering region create resistance to the flow of the water. This method is sensible and commonly employed in practice.

Another alternative for treating a meandering river is to use a two-dimensional flow model. This lead us to the question of how accurate is a one-dimensional flow model with an adjusted friction coefficient compared to a two-dimensional flow model? This question is discussed in the next section.

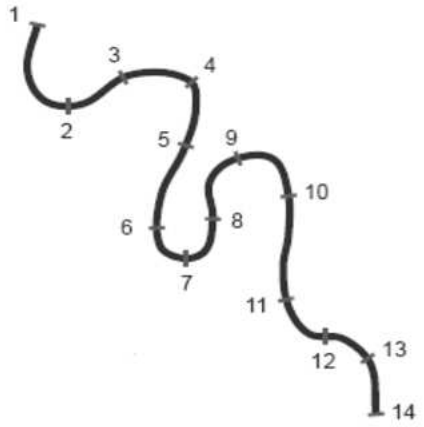

Figure 3.18: A meandering river. Source: (Langendoen, 2000)

3.3.1 The Navier Stoke equations

The Saint Venant equations which are derived in Section 3.1 are a special case of the Navier-Stoke equations for one-dimensional flow. Here, we will just present the Navier-Stoke equations. For a detailed derivation of the Navier-Stoke equations, see Appendix A.

The Navier-Stokes equations are given by,

$$\frac{\partial u}{\partial x} + \frac{\partial v}{\partial y} + \frac{\partial w}{\partial z} = 0 \tag{3.33}$$

$$\rho \left[\frac{\partial(u)}{\partial t} + u\frac{\partial(u)}{\partial x} + v\frac{\partial(u)}{\partial y} + w\frac{\partial(u)}{\partial z} \right] - g_x\rho + \frac{\partial p}{\partial x} - \mu\nabla^2 u = 0 \tag{3.34}$$

$$\rho\left[\frac{\partial(v)}{\partial t}+u\frac{\partial(v)}{\partial x}+v\frac{\partial(u)}{\partial y}+w\frac{\partial(v)}{\partial z}\right]-g_y\rho+\frac{\partial p}{\partial y}-\mu\nabla^2 v=0 \tag{3.35}$$

$$\rho\left[\frac{\partial(w)}{\partial t}+u\frac{\partial(w)}{\partial x}+v\frac{\partial(w)}{\partial y}+w\frac{\partial(w)}{\partial z}\right]-g_z\rho+\frac{\partial p}{\partial z}-\mu\nabla^2 w=0 \tag{3.36}$$

where u, v, w are the velocity in the x, y, z direction respectively, ρ is the density of the water, g is the gravitational constant, p is pressure, ∇^2 is the Laplacian operator given by $\frac{\partial^2}{\partial x^2}+\frac{\partial^2}{\partial y^2}+\frac{\partial^2}{\partial z^2}$ and μ is a constant related to the stress in the fluid. Equation (3.33) is the *continuity equation*, while Equations (3.34), (3.35) and (3.36) are the *dynamic equations*.

The Navier-Stokes equations describe three-dimensional flow. To describe a two-dimensional flow, we need to integrate the continuity and the dynamic equations over water depth. After some algebraic manipulation (see Appendix A), the continuity and dynamic equations for a two-dimensional flow are given by,

$$\frac{\partial h}{\partial t}+\frac{\partial(uh)}{\partial x}+\frac{\partial(vh)}{\partial y}=0 \tag{3.37}$$

$$\frac{\partial uh}{\partial t}+\frac{\partial}{\partial x}\left(u^2h+\frac{1}{2}gh^2\right)+\frac{\partial(uvh)}{\partial y}=gh(S_{0x}-S_{fx}) \tag{3.38}$$

$$\frac{\partial vh}{\partial t}+\frac{\partial(uvh)}{\partial x}+\frac{\partial}{\partial y}\left(v^2h+\frac{1}{2}gh^2\right)=gh(S_{0y}-S_{fy}) \tag{3.39}$$

where h is the water depth, S_0 is the channel bottom slope, S_f is the friction slope and subscripts x and y indicate the direction of the slope. Using Manning's friction coefficient, S_{fx} and S_{fy} are given by $un^2\sqrt{u^2+v^2}/h^{4/3}$ and $vn^2\sqrt{u^2+v^2}/h^{4/3}$ respectively.

The continuity and dynamic equations can be expressed in conservation form i.e.

$$\frac{\partial \mathbf{U}}{\partial t}+\frac{\partial \mathbf{E}}{\partial x}+\frac{\partial \mathbf{F}}{\partial y}+\mathbf{S}+\mathbf{T}=0 \tag{3.40}$$

where

$$\mathbf{U}=\begin{bmatrix}h\\uh\\vh\end{bmatrix}\quad \mathbf{E}=\begin{bmatrix}uh\\u^2h+\frac{1}{2}gh^2\\uvh\end{bmatrix}\quad \mathbf{F}=\begin{bmatrix}vh\\uvh\\v^2h+\frac{1}{2}gh^2\end{bmatrix} \tag{3.41}$$

$$\mathbf{S}=\begin{bmatrix}0\\-gA(S_{0x}-S_{fx})\\0\end{bmatrix}\quad \mathbf{T}=\begin{bmatrix}0\\0\\-gA(S_{0y}-S_{fy})\end{bmatrix} \tag{3.42}$$

Note here that the terms uh and vh have the SI unit of m^2/s, which is the flow per unit distance.

Numerical method for two-dimensional flow

Like the one-dimensional model, implicit finite difference schemes are more attractive since the explicit schemes suffers from issue with numerical instability. There are several types of implicit schemes that can be used for solving the two-dimensional PDE. These schemes include the Preismann scheme for two-dimensional flow (Holly and Preismann, 1977) as well as Beam and Warming schemes (Beam and Warming, 1976). The Preismann scheme for two-dimensional flow has shown to be stable in (Venutelli, 2002) and (Venutelli, 2007). For that reason, the Preismann scheme is also used here.

When using implicit schemes for solving two-dimensional unsteady flow, one has to deal with a large system of nonlinear algebraic equations at each time step. To reduce the computational burden while maintaining the advantages of the implicit schemes, Alternate Direction Implicit (ADI) method is utilised (Vreugdenhil, 1994). ADI was first introduced by Holland for solving Maxwell's equations (Holland, 1984). The ADI method is particularly useful for solving multi-dimensional problem as one solve the system in one particular dimension followed by the next dimension until the problem is solved in all dimensions. Each solution in a particular dimension will be used as the initial solution for the next dimension. Venutelli in (Venutelli, 2007) illustrated how the ADI is used with Preissmann scheme for solving the two-dimensional flow equations. In view of the high computational cost in solving the full Preissmann scheme, the scheme used in (Venutelli, 2007) will be used here with the difference that the solution of the nonlinear algebraic equations is solved using Newton-Raphson method instead of the double sweep method, used in (Venutelli, 2007).

3.3.2 Illustrative examples

Here, we will consider (i) a single bend and (ii) multiple bends, as illustrated in Figure 3.19. The solid arrow represents the direction of the flow per unit distance along the x-axis while the dashed arrow represents the direction of the flow per unit distance along y-axis. The higher (lighter color) area represents the permanent structure (e.g. river side bank), and the lower (darker color) area represents the wetted area. To account for these

permanent structures, we set the velocity at these permanent structures to zero, since there is no flow per unit distance at these structures (Venutelli, 2007).

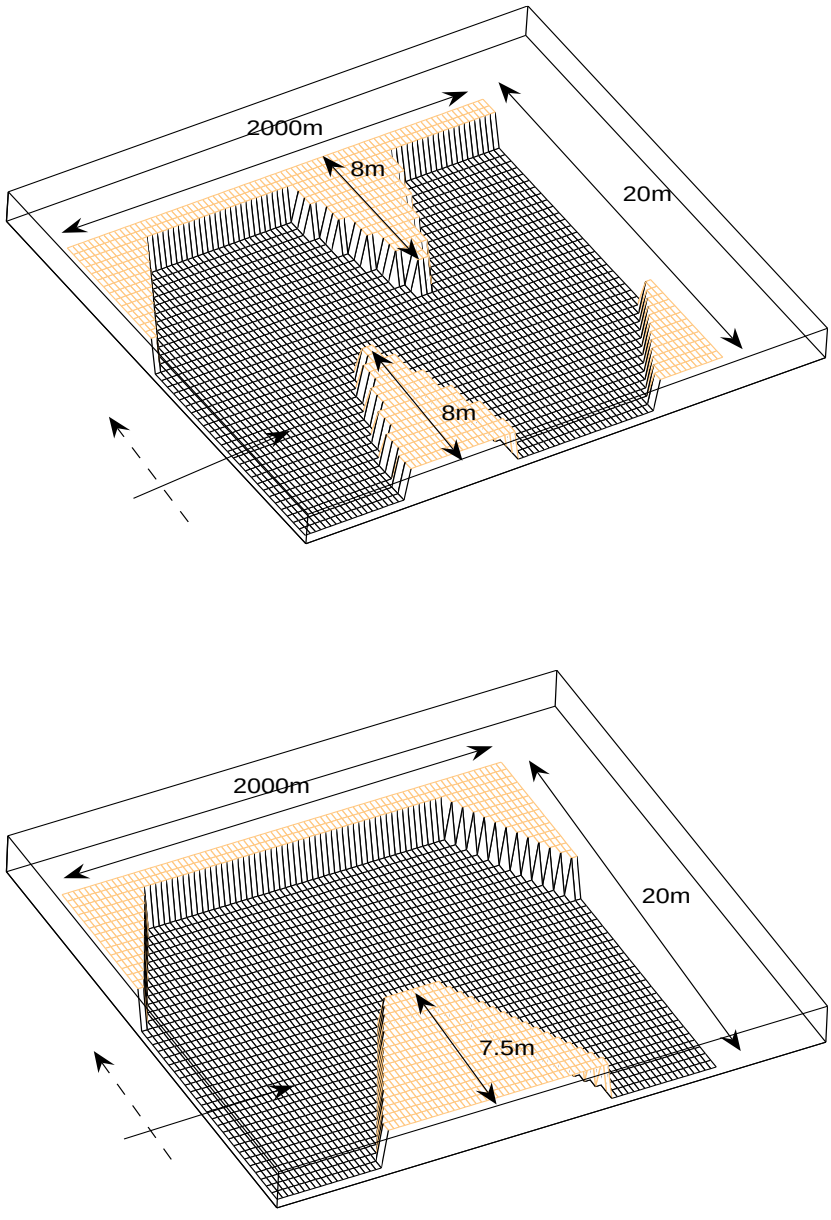

Figure 3.19: Illustration of multiple bends (top) and single bend (bottom).

Despite Figure 3.19 showing only a portion of the meandering river, intuitively the results should hold when considering the whole river reach as most of the meandering in river can be represented by Figure 3.19. Before proceeding, the simulation setup is first explained.

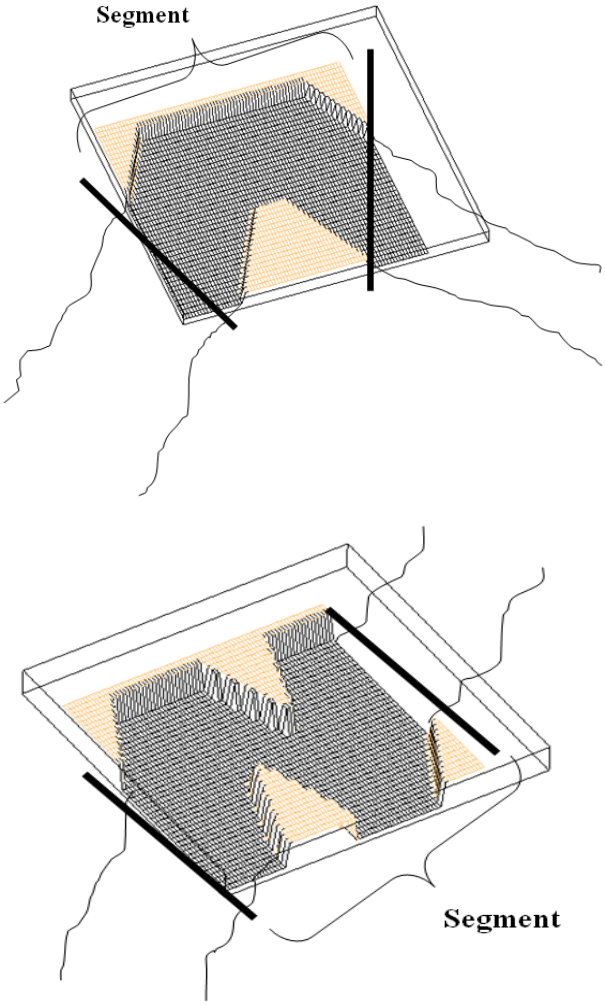

Figure 3.20: Top: Treating single bend as a segment. Bottom: Treating multiple bends as a segment. Flow direction is from left to right.

We consider the bend(s) as a segment (see Figure 3.20). The length of the segment with bend(s) is 2 km with $\Delta x = 50$m. The bottom width is $b = 20$m with $\Delta y = 0.5$m. Thus, we have the both $n_{sec,x} = n_{sec,y} = 40$. The bottom slope in the x-direction, $S_{0x} = 0.001$,

bottom slope in y-direction, $S_{0y} = 0$ and Manning's friction coefficient is $n = 0.04$. The characteristic of the bend(s) are shown in Figure 3.19.

The same input at the upstream end will be applied to both the one- and two-dimensional flow models. The flow per unit distance at these bend(s) for the one- and two-dimensional flow models will be compared in terms of Mean Square Error (MSE) given by

$$\text{MSE} = \frac{1}{N}\sum_{t=1}^{N}[q_{1d}(t) - q_{2d}(t)]^2 \tag{3.43}$$

where $N = 160$, q_{1d}[8] and q_{2d} are the flow per unit distance for one- and two-dimensional flow models respectively. For the two-dimensional flow, as we have several flows per unit distance across the y-direction, we use the average flow per unit distance computed along the y-axis.

We shall then estimate the friction coefficient for the one-dimensional flow model from the two-dimensional flow model. The friction coefficient, $\theta_{2d} = n$ is estimated using the quadratic criterion, i.e.

$$\hat{\theta}_{2d} = \underset{\theta_{2d}}{\text{argmin}}\, \frac{1}{N}\sum_{t=1}^{N}[q_{2d}(t) - \hat{q}_{1d}(t, \theta_{2d})]^2 \tag{3.44}$$

where N is the number of data points, $\hat{q}_{1d}$, q_{2d} are the output flows per unit distance with estimated friction coefficient using the one-dimensional flow model and the output flow per unit distance using the two-dimensional flow model respectively. The plots of the input and the output flow per unit distance are shown in Figure 3.21.

The estimated friction coefficient and the values of the MSE are shown in Table 3.8. From the plots, we can see that output flow per unit distance of the one-dimensional flow model with the estimated friction coefficient is as accurate as the two-dimensional flow model. This is reflected in the values of MSE. The values of the estimated friction coefficient are larger than 0.04, which makes sense considering that the meandering region creates larger flow resistance, hence larger friction coefficient.

The results presented here show that by tweaking the friction coefficient of the one-dimensional flow model, we can get a fairly accurate representation of a meandering river as compared to using a two-dimensional flow model. This suggests that there is no need

[8]For the one-dimensional case, the unit for input and the output flows are in m^3/s. To get the unit of flow per unit distance, m^2/s, we divided them by Δx.

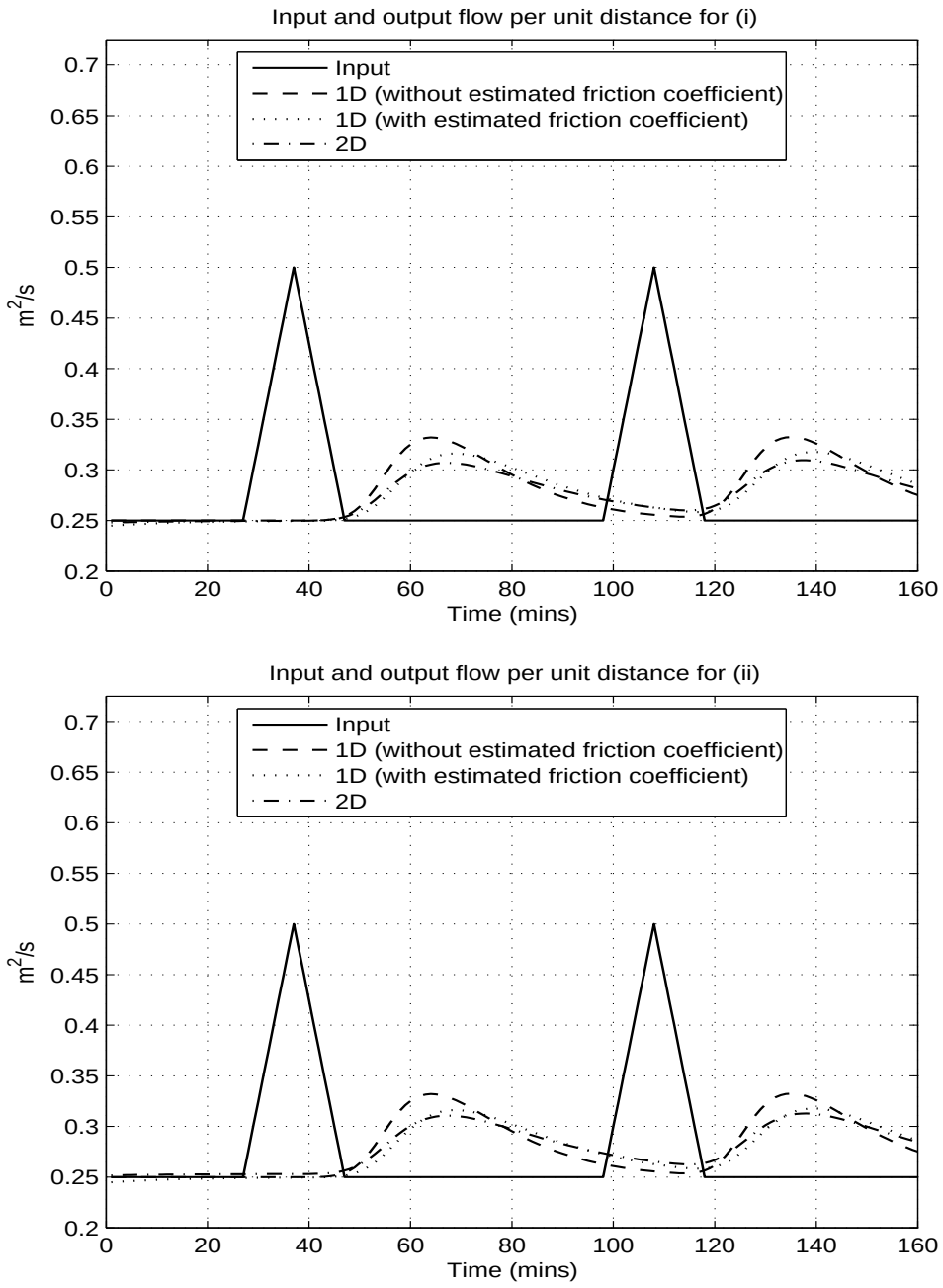

Figure 3.21: Flow per unit distance. Top: Single bend, Bottom: Multiple bends.

to use a two-dimensional flow model for a meandering river. Note however that, in more complex situations such as simulations of dam-break waves, coastal flows, tsunamis, etc,

Table 3.8: Estimated friction coefficients and the values of MSE.

Structure	Estimated Friction Coefficient $\hat{n}$	MSE (without estimated parameter) ($\times 10^{-5}$ $(\mathrm{m}^2/\mathrm{s})^2$)	MSE (with estimated parameter) ($\times 10^{-5}$ $(\mathrm{m}^2/\mathrm{s})^2$)
(i)	$\hat{n} = 0.0541$	12.330	2.564
(ii)	$\hat{n} = 0.0526$	10.984	2.069

the two-dimensional model becomes important.

3.4 Nonlinearities in the Saint Venant equations

The Saint Venant equations, are two nonlinear PDEs. Thus, there is an interest to determine "how nonlinear" the Saint Venant equations are and we investigate this question in this section. In Section 3.4.1, a brief literature review of the existing techniques on nonlinearity detection for arbitrary systems is presented. The application of these techniques to river systems and the obtained result are discussed in Section 3.4.2.

3.4.1 Review on nonlinearity detection

An extensive list of works on nonlinearity detection can be found in (Natke *et al.*, 1988). The more prominent works are by Haber (Haber, 1985), (Haber and Keviczky, 1999), Billings (Billings and Voon, 1983) and more recently Pintelon and Schoukens (Pintelon and Schoukens, 2001).

There are several nonlinearity tests. They include time domain tests, coherence tests, nonlinear cross-correlation tests, higher order autocorrelation tests, etc. An extensive list can be found in (Haber and Keviczky, 1999). We will discuss some of the more commonly used tests and highlight some of the advantages and disadvantages of these tests.

The simplest and the most popular test is the time domain test (Pintelon and Schoukens, 2001). In this test, the input signal $u_1(t)$ is scaled by a factor α_1 (i.e. $u_1(t)$ is replaced by $\alpha_1 u_1(t) = u_2(t)$). If the system is linear, the output will be scaled by the same factor, i.e. $y_2(t)/y_1(t) = \alpha_2(t) = \alpha_1$. Although this test is simple, it is not widely used in practice as at least two experiments must be carried out. The choice of α_1 may be limited by

process constraints. If a small value of α_1 is applied, the effect of noise is more significant, jeopardising the overall test.

Coherence test or the linear spectral density test (Haber, 1985) is another test used in nonlinear detection. The idea was originally developed by Sir Francis Galton and further developed by Karl Pearson (Rodgers and Nicewander, 1988). The coherence between two signals, $x(t)$ and $y(t)$ is given by

$$\gamma_{xy}^2(e^{j\omega}) = \frac{|S_{xy}(e^{j\omega})|^2}{S_{xx}(e^{j\omega})S_{yy}(e^{j\omega})} \tag{3.45}$$

where $S_{xy}(e^{j\omega}) = X(e^{j\omega})Y^*(e^{j\omega})$. $X(e^{j\omega})$ and $Y(e^{j\omega})$ are the Discrete Time Fourier Transform (DTFT) of $x(t)$ and $y(t)$ respectively. The notation * denotes the complex conjugate. For linear system, the values of $\gamma_{xy}^2(e^{j\omega})$ is close to unity. A drawback with this method is that the separation between noise and a nonlinearity cannot be made ((Haber, 1985), (McCormack *et al.*, 1994) and (Pintelon and Schoukens, 2001)).

A test called nonlinear cross-correlation test was introduced in (Haber, 1979). In this test, the input signal is a nonzero mean white Gaussian noise or a pseudorandom signal. This signal is symmetrically distributed around the mean and have zero odd order moment and nonzero even order moment (Haber and Keviczky, 1999). Introducing the term called multiplier, i.e.,

$$x(t) = \frac{\bar{u}^2(t) - \mathbb{E}\{\bar{u}^2(t)\}}{\sigma(\bar{u}^2(t))} \tag{3.46}$$

where $\sigma(.)$ denotes the standard deviation and $\bar{u}^2(t) = [u^2(t) - \mathbb{E}\{u^2(t)\}]/\sigma(u^2(t))$. The cross-correlation,

$$R_{x\bar{y}}(\tau) = \mathbb{E}\{x(t-\tau)\bar{y}(t)\} \tag{3.47}$$

is computed, where

$$\bar{y}(t) = \frac{y(t) - \mathbb{E}\{y(t)\}}{\sigma(y(t))} \tag{3.48}$$

If the system is linear, the cross-correlation, $R_{x\bar{y}}(\tau) = 0$ for all τ. If the system is nonlinear, then $R_{x\bar{y}}(\tau) \neq 0$. In (Haber and Keviczky, 1999), it was claimed that this method is robust against noise.

The higher order autocorrelation test in (Billings and Voon, 1983) is another nonlinearity test. Using a similar input signal as the nonlinear cross-correlation test but this

time with zero mean, the autocorrelation given by,

$$R_{\bar{y}^2\bar{y}}(\tau) = \mathbb{E}\{\bar{y}^2(t-\tau)\bar{y}(t)\} \tag{3.49}$$

is computed, where $\bar{y}^2(t) = [y^2(t) - \mathbb{E}\{y^2(t)\}]/\sigma(y^2(t))$ and $\bar{y}(t) = [y(t) - \mathbb{E}\{y(t)\}]/\sigma(y(t))$. $R_{\bar{y}^2\bar{y}}(\tau)$ is zero for all τ for linear system. This test method becomes very popular as it is simple and easy to apply (Várlaki *et al.*, 1985). Despite its popularity, this test method do raise some questions (Korenberg and Hunter, 1990) since while the zero value for the autocorrelation $R_{y^2y}(\tau)$ for all τ is necessary, it is not sufficient, and the test method fails for a simple cubic relationship (i.e. $y(t) = x^3(t)$).

A more recent nonlinearity test suggested in (Pintelon and Schoukens, 2001) is based on using a broadband periodic excitation input signal. The idea originated from (Evans *et al.*, 1994). The method involves choosing a signal that only contain certain harmonic. One example of such signal is the odd-odd multisines signal. The frequencies that are excited by the odd-odd multisines signal are $(4k+1)f_0$, $k = 0, 1, \ldots, F$, where F is the number of frequencies and f_0 is the fundamental frequency. If the system is linear, only the frequencies at $(4k+1)f_0$ will appear in the output. If the system is nonlinear, the nonlinearity plus noise would excite the non-excited harmonics i.e. at frequencies, $(4k+2)f_0$, $(4k+3)f_0$ and $(4k+4)f_0$. This technique can serve as an qualitative indication of a nonlinearity but not a quantitative measure (Pintelon and Schoukens, 2001).

3.4.2 Nonlinearity tests for river systems

In this section, all the nonlinearity tests mentioned in Section 3.4.1 will be utilised to determine "how nonlinear" the Saint Venant equations are. We applied the tests to the calibrated Saint Venant equations for Reach CG using Single segmentation (see Section 3.2.5).

Time domain test

The input signal $u_1(t)$ is applied to the system and the corresponding output $y_1(t)$ is obtained. The experiment is then repeated with the input scaled with a constant term, i.e. $u_2(t) = \alpha_1 u_1(t)$ and the output $y_2(t)$ is obtained. The ratio of $y_1(t)$ and $y_2(t)$ is then computed, i.e. $\frac{y_2(t)}{y_1(t)} = \alpha_2(t)$. If the system is linear, $\alpha_2(t) = \alpha_1$. The time domain test is the simplest test for nonlinearity. This method do however, possesses some drawbacks as highlighted in (Pintelon and Schoukens, 2001). These drawbacks mainly deal with practicality issues when applying this method to the real systems. Since we are not applying this method to a real river, these issues do not arise here.

Sinusoids with different offsets and amplitudes are used as input signals. They are given by $u_{LF}(t) = 0.1\sin(\omega t) + 0.35$ m^3/s, $u_{MF}(t) = 0.75\sin(\omega t) + 3.00$ m^3/s and $u_{HF}(t) = 0.5\sin(\omega t) + 7.50$ m^3/s, where the subscript "LF", "MF" and "HF" denotes Low Flow, Medium Flow and High Flow respectively. The frequencies ω used are 0.001, 0.002, 0.004, 0.008, 0.01, 0.02, 0.04 and 0.08 rad/min. These frequencies are in the frequency range that we are interested in for control. We use $\alpha_1 = 0.25$, 0.75, 1.25, 1.75, 2.25 and 3.00. For illustration, only the results for $\omega = 0.004$ rad/min are presented. Similar results are observed for the other frequencies. In addition, a $\pm 5\%$ tolerance bound is included. Figure 3.22 shows the plot of $\alpha_2(t) = y_2(t)/y_1(t)$ for different values of α_1. From Figure 3.22, we observe that $\alpha_2(t)$ almost always stay within the $\pm 5\%$ tolerance bound except for the case when $\alpha_1 = 0.25$ under LF condition. For this case, $\alpha_2(t)$ exceeds the bound at time 500 minutes and quite often stay close to the bound.

To ensure more frequencies are excited, we can use a broadband excitation signal. The choice of broadband excitation signal is advocated in (Pintelon and Schoukens, 2001) as this input signal can excite a broad range of the spectrum enabling collection of all the required information from a single measurement (Pintelon and Schoukens, 2001). Pseudo-random binary signal (PRBS) is an example of a broadband excitation signal. Figure 3.23 shows the PRBS signal applied to the Saint Venant equations. The period of the signal is 300 minutes. We repeat the time domain test with the PRBS using the same α_1 values. The value of $\alpha_2(t) = y_2(t)/y_1(t)$ is plotted and shown in Figure 3.24.

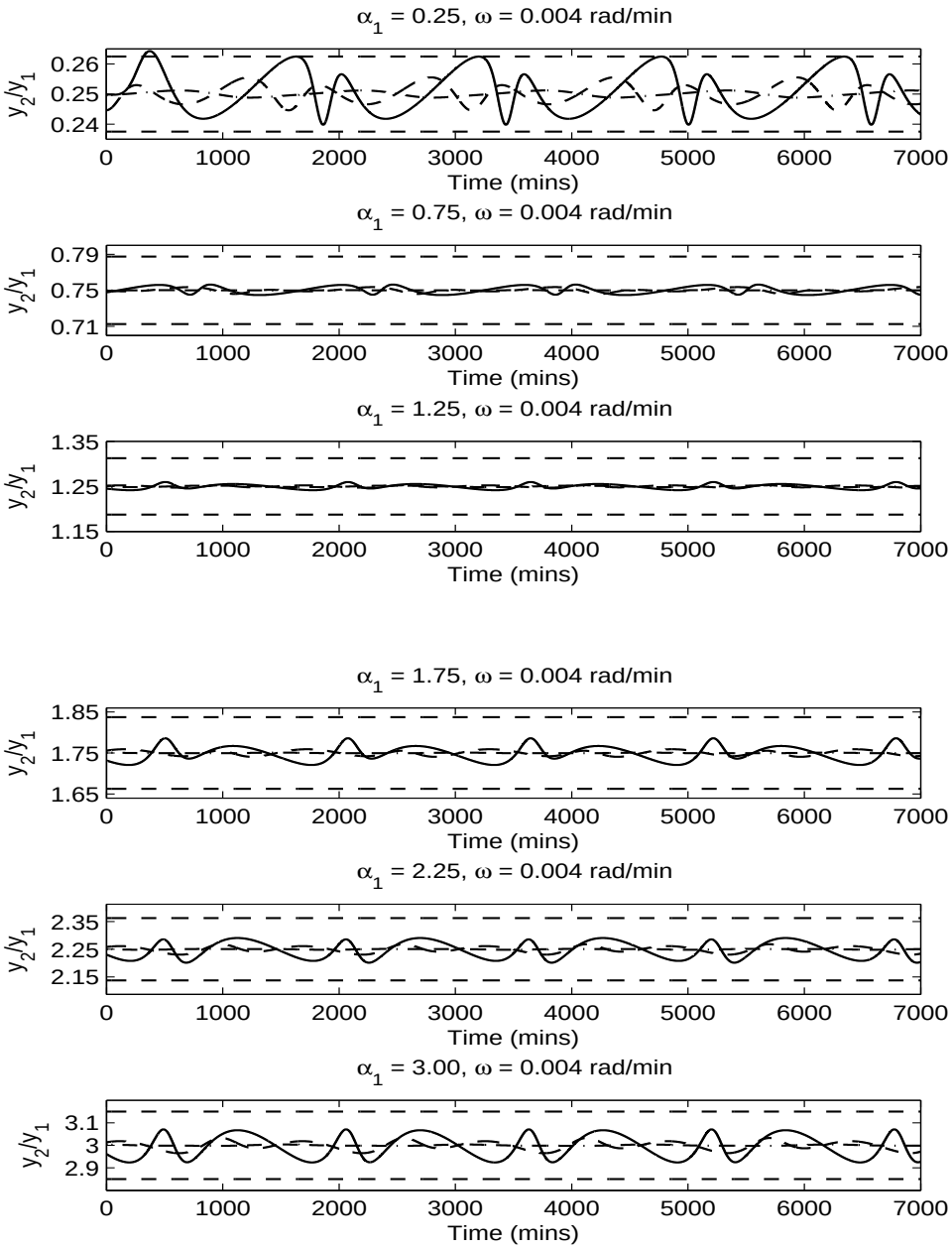

Figure 3.22: Plots of $y_2(t)/y_1(t) = \alpha_2(t)$ for different flow conditions. Input frequency: ω = 0.004 rad/min. Bold dashed line: $\pm 5\%$ tolerance bound. Dotted line: α_1. Solid line: LF. Dashed line: MF. Dash dotted line: HF.

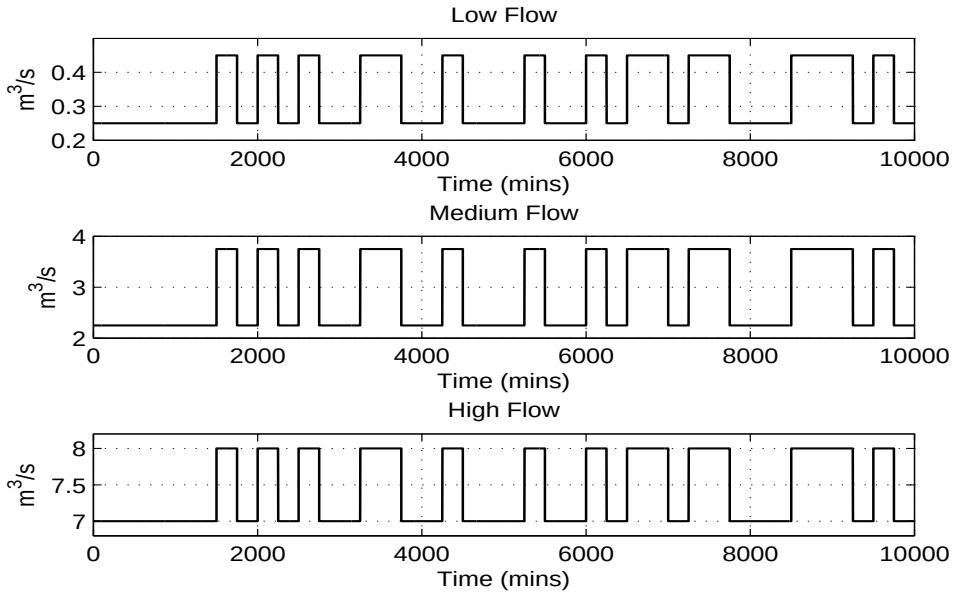

Figure 3.23: Pseudorandom binary signal (PRBS). Signal period = 300 minutes.

Again, we can see that under LF condition with $\alpha_1 = 0.25$, $\alpha_2(t)$ are not within the $\pm 5\%$ tolerance bound. For the rest of the plots, $\alpha_2(t)$ stays within the tolerance bound. In addition, the results are consistent with the results using a sinusoidal input flow. Other than for LF condition, $\alpha_2(t)$ stay within the $\pm 5\%$ tolerance bound. The reason that the LF condition show larger deviations is that the resonances tends to occur more clearly at low flow. Based on the results from time domain test, we can say that the Saint Venant equations are approximately linear within an operating region.

Coherence test

The coherence test is not a suitable nonlinearity test in our case as we are simulating the Saint Venant equations in a "noise-free" environment. McCormack et al. pointed that for a noise free input and output signal, the coherence will always be unity regardless of whether the output y is obtained through a linear or a nonlinear function. Moreover, if only input u is noise free, the coherence can be computed without the effect from input signal, which suggests the poor ability of coherence function to detect nonlinearity given the input and output relationship, thus it not a good test for nonlinearity detection in our

case.

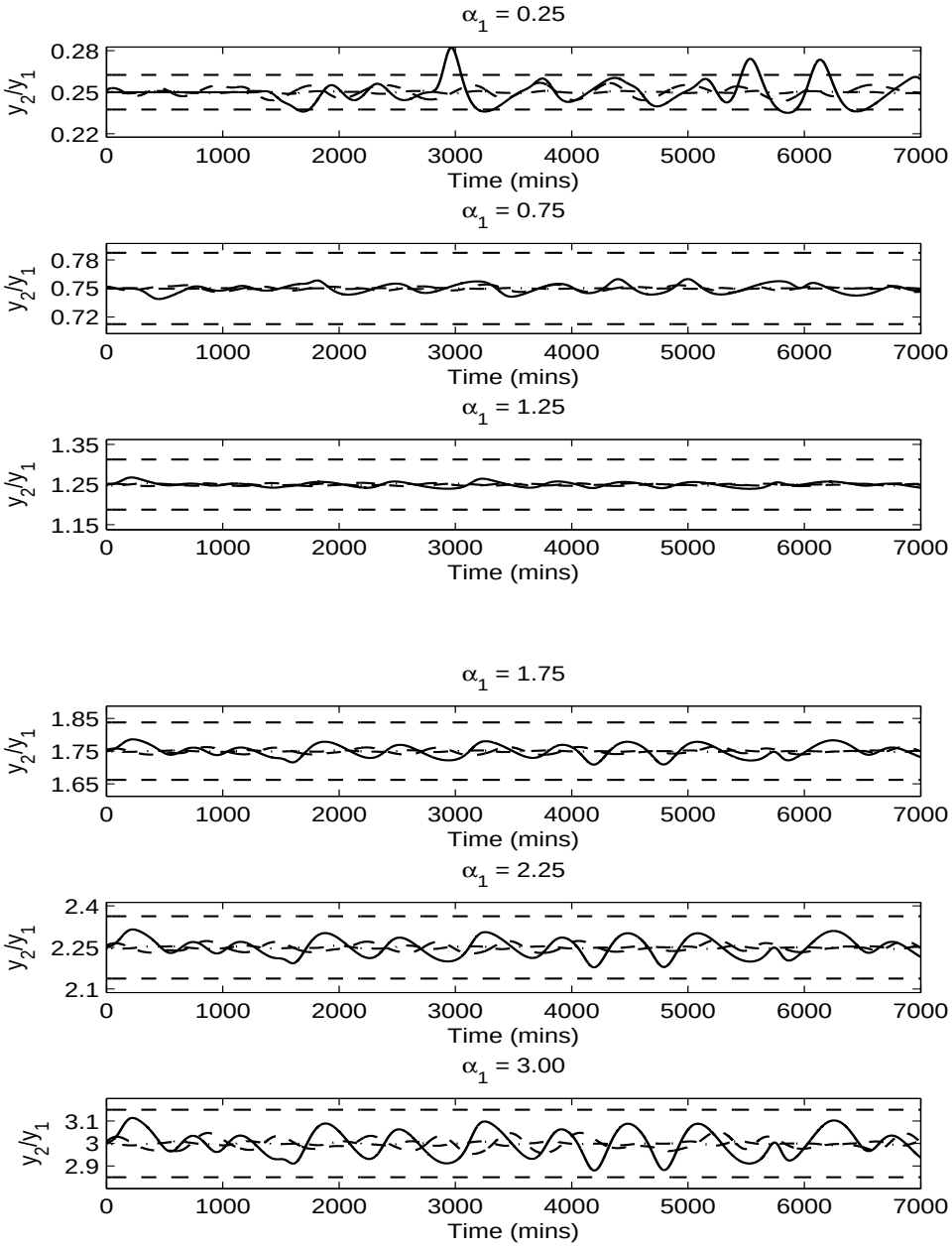

Figure 3.24: Plots of $y_2(t)/y_1(t) = \alpha_2(t)$ for different flow conditions. Input signal: PRBS with period = 300 minutes. Bold dashed line: $\pm 5\%$ tolerance bound. Dotted line: α_1. Solid line: LF. Dashed line: MF. Dash dotted line: HF.

Nonlinear cross-correlation test

In this test, the input signal is Gaussian or PRBS with nonzero mean. We use the PRBS for the three different flow conditons, LF, MF and HF as input signal and compute the cross-correlation in Equation (3.47). The cross-correlation plot is shown in Figure 3.25.

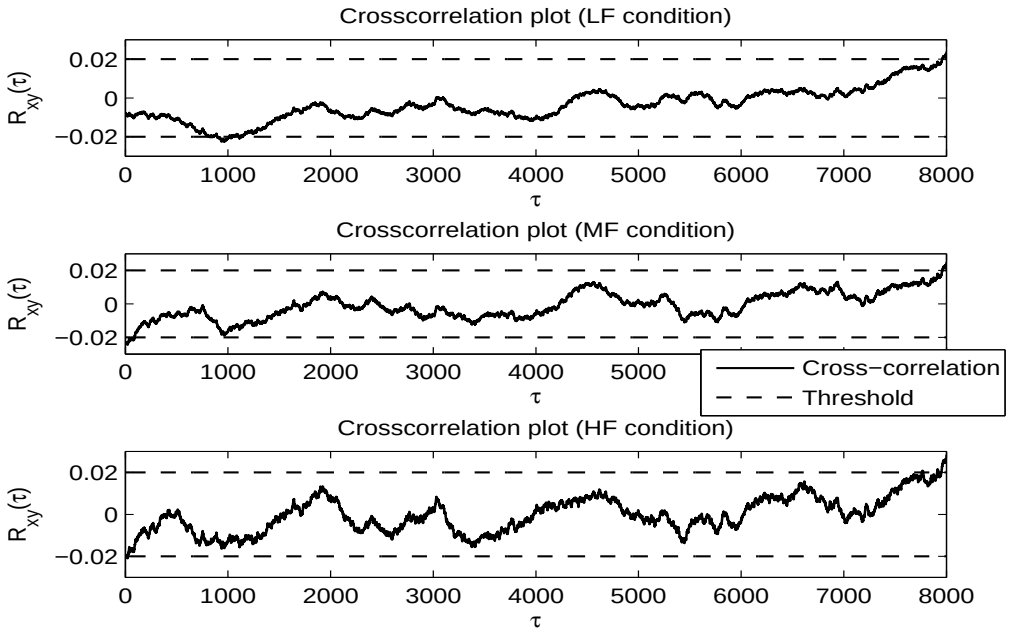

Figure 3.25: Nonlinear cross-correlation test plot. Top: LF condition, Middle: MF condition, Bottom: HF condition.

From the plot, we see that $R_{x\bar{y}}(\tau)$ is small for all values of τ. Using the threshold value $2/\sqrt{N}$ given in (Haber, 1985)[9] we see that, the cross-correlation stays within the threshold for almost all τ. There are some instances where the cross-correlation just exceeds the threshold (e.g. around $\tau = 1000$ for LF condition). Based on the results from this test, we can conclude that the Saint Venant equations are approximately linear within an operating region.

[9]For large N, the standard deviation of the correlation estimate is $1/\sqrt{N}$. The 95% confidence limit is approximately $2/\sqrt{N}$ (Billings and Voon, 1983).

Higher order autocorrelation test

This test is similar to the nonlinear cross-correlation test. The differences are the input signal is zero mean and we compute the autocorrelation using Equation (3.49). If the system is linear the autocorrelation is zero for all τ.

Note that a zero mean input signal means that, we are dealing with negative flows, which is not physically feasible. Thus, we apply an input signal to the Saint Venant equations and remove the mean at the output of the Saint Venant equations. In our simulation, only the MF condition is considered. The reason we only consider one flow condition is that due to the removal of the mean from the output, we observe that the computed autocorrelation plot are very similar for all other flow conditions. The plot is shown in Figure 3.26. From the plot, we see that $R_{\bar{y}^2\bar{y}}(\tau)$ is small for all values of τ.

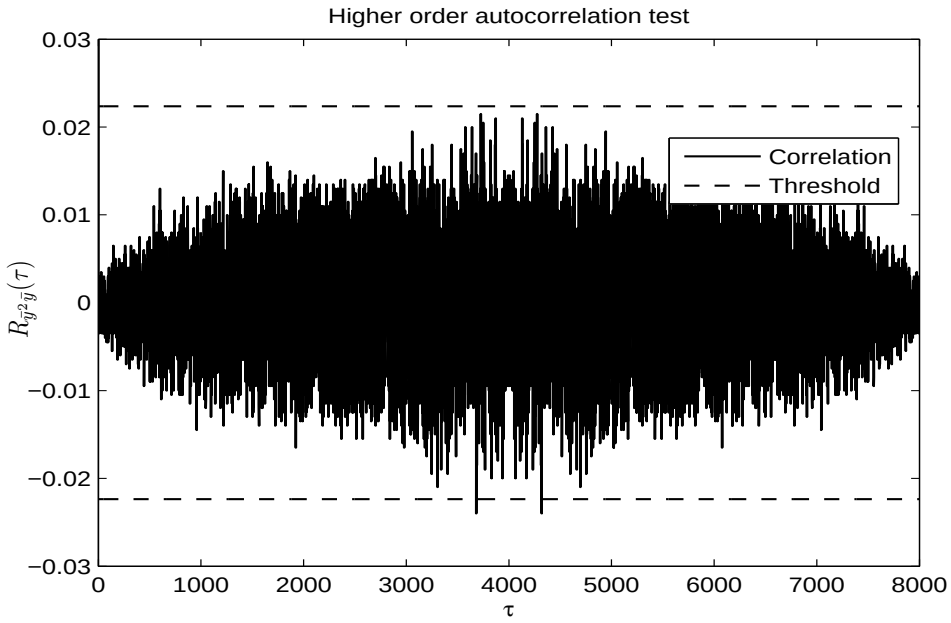

Figure 3.26: Higher order autocorrelation test plot.

Using the threshold value, $2/\sqrt{N}$ given in (Haber, 1985), we see that, the autocorrelation just stays within the threshold for almost all τ. There are some instances where the autocorrelation just exceeds the threshold (e.g. around $\tau = 4000$). Based on the results from this test, we can again conclude that the Saint Venant equations are approximately linear within an operating region.

Broadband periodic excitation

The odd-odd multisines signal is given by

$$u(t) = \sum_{t=1}^{F} [A \sin(\omega_0 i(k)t + \phi_k)] + B \tag{3.50}$$

where A is the amplitude, B is a constant offset to ensure positive flow, F is the number of frequencies, $i(k) = 4k+1$, with $i = 0, 1, ...$ and $\phi_k = -k(k-1)\pi/F$. ϕ_k is called Schroeder

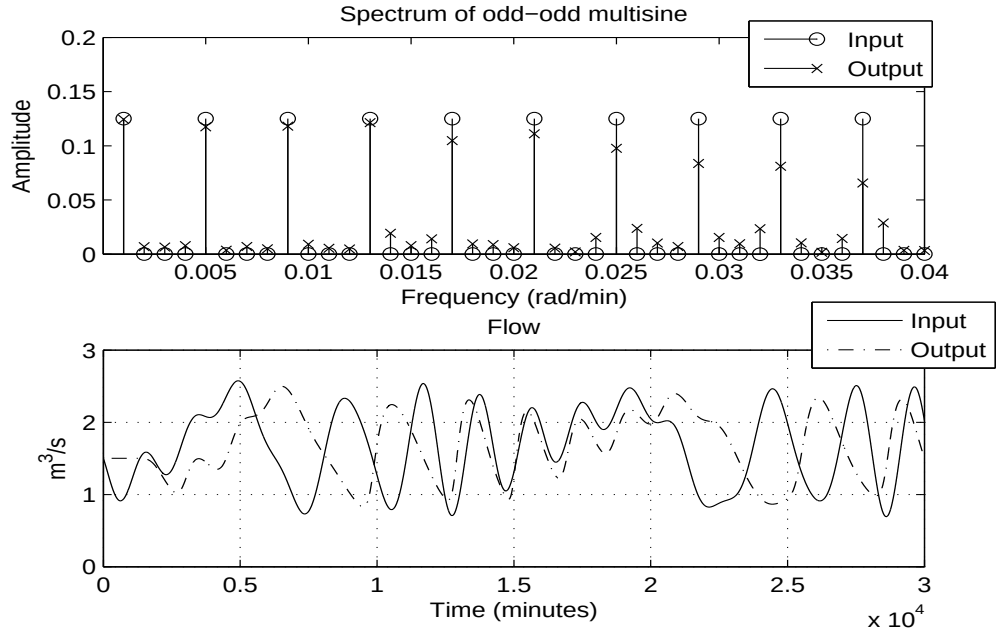

Figure 3.27: Top: Spectrum of odd-odd multisines signal. Bottom: Time domain plot of odd-odd multisines signal.

phase (Schroeder, 1970) and they are constructed such that the peak to peak amplitude of the sum of the sinusoid signals is minimised. The odd-odd multisines is applied as the input to the Saint Venant equations, with $F = 10$, $A = 0.75$ and $B = 1.75$. As we are interested in the low frequency region, we chose $\omega_0 = 0.001$ rad/min. The simulation result is shown in Figure 3.27.

In the frequency region of $\omega = 0.001$ to 0.02 rad/min, we observe that the spectrum of the output signal is similar to the spectrum of the input signal. The amplitude at the excited frequencies for the output signal is similar to the amplitude of the input signal

at the excited frequencies. Although the other harmonics are also excited for the output signal, the amplitude is small compared to the amplitude of the excited frequencies. In the high frequency region, e.g. $\omega > 0.02$ rad/min, we see that the amplitude at the non excited frequencies is larger compared to the low frequency region. This test indicates that the Saint Venant equations are linear within the low frequency region.

3.5 Summary

In this chapter, we have investigated the segmentation of a river using the Saint Venant equations. From the segmentation analysis, it has been shown that a few segments are often sufficient for obtaining an accurate representation of a river. The findings are validated using real data from two rivers in Australia, the reach between Casey's Weir and Gowangardie Weir in the Broken River, and the reach between Doctor's Point and Yarrawonga Weir in the Murray River. Through the analysis, we also validate the accuracy of the Saint Venant equations against real data. From the sensitivity analysis with respect to the river parameters, we find that the variations in the Manning friction coefficient and the weir constant have the biggest influence on the simulation results. Hence, they should be calibrated against data. Moreover, it has been shown that the simulation time can be reduced significantly by using lower spatial and time resolutions. In regards to the treatment of a meandering river, our findings suggest that by adjusting the friction coefficient of the one-dimensional flow model, one can get a fairly accurate representation of a meandering river as compared to the use of a two-dimensional model. In the analysis of nonlinearity detection of the Saint Venant equations, based on the results of several nonlinearity tests, we can say that the Saint Venant equations are close to being linear within an operating region.

Chapter 4

Empirical modelling

In Chapter 3, we have introduced the Saint Venant equations, and being partial differential equations, they are not easy to use for control design. Thus, we seek a simpler alternative model. In this chapter, the main aim is to build a model of a river for control design using the system identification procedures and to determine the accuracy of the model. The accuracy of the system identification models is investigated by comparing the model against the measured data from a river. In addition, we want to determine the accuracy of the system identification models against the Saint Venant equations. This is investigated by comparing the two models against each other. Through experimentation validation, the system identification model are found to capture the important dynamics of the river useful for control design and are found to be of a similar accuracy as the Saint Venant equations. The effect of different flow conditions that lead to varying time delays is investigated as this factor affects robustness specifications for the controller, given that the system identification models are going to be used for control design. The accuracy of the estimate of the parameters in the system identification models are then analysed using the theory of asymptotic distribution of parameter estimates.

The outlines of Chapter 4 is as follow. In Section 4.1, we present an overview of the system identification procedures. Then, we derive model using nonparametric and parametric identification methods in Sections 4.2 and 4.3 respectively. The effect of varying flow conditions are analysed in Section 4.4. Section 4.5 looks at further modelling of river reaches when the downstream flow can be regulated and when there is a storage in the river. The accuracy of the estimated parameters for the empirical models is analysed using

the covariance matrix of the estimate and this is discussed in Section 4.6. A summary is presented at the end of the chapter.

4.1 System identification procedures

The general procedures for system identification are shown in Figure 4.1 ((Ljung, 1999) and (Söderström and Stoica, 1988)). There are four main steps; experiment design, model structure selection, parameter estimation and model validation.

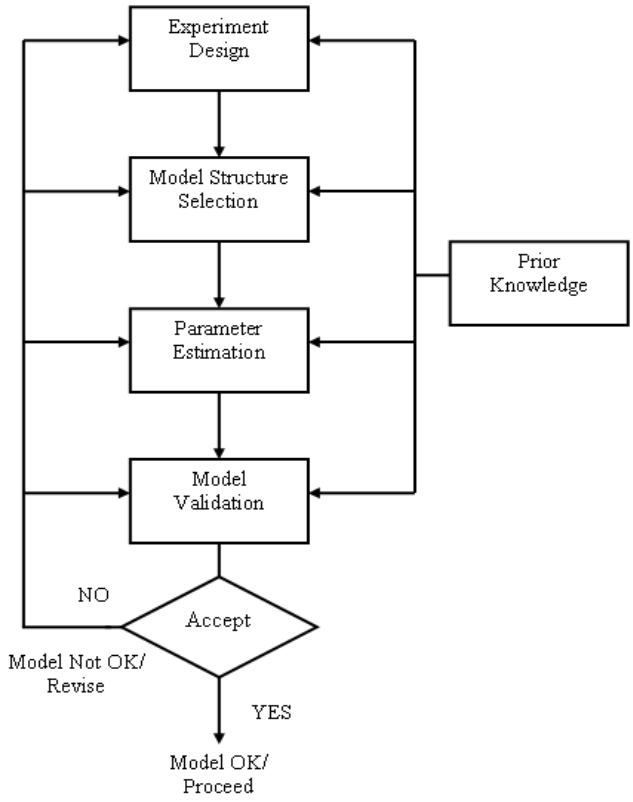

Figure 4.1: General system identification procedures.

Experiment design: The operational data should be as informative as possible. The best way is to conduct a dedicated experiment to collect data. In performing the experiment, we need to ensure that the data we collect are of good quality and capture information about the relevant dynamics. The quality of the data depends on several factors

such as sampling interval, signal-to-noise ratio, input signal shape, etc. Post treatment of data such as pre-filtering, checking for drift, outlier, etc is also done in this stage. In cases where experiments cannot be conducted, we just have to use whatever operational data that is available.

Model structure selection: In this stage, the selection of the model structure is to be made. A model structure is a class of models in which we are looking for a good one to describe the system. There is a choice between parametric or nonparametric model structures. Parametric models are models of the system that are described by a finite dimensional parameters vector. Nonparametric models have the feature that the models are curves or functions. There is also a choice between the "ready-made models" and the "tailor-made model" (Ljung and Glad, 1994). The ready-made models are a set of model with general applicability while the tailor-made models are constructed from basic physical principles. In addition, for the ready-made models, this stage also involve choice of model order, linear or nonlinear model, etc.

Parameter estimation: The selected model structure has parameters, which need to be estimated from the operational data. There are several methods available to estimate these parameters. These methods include prediction error method, maximum likelihood method, instrumental variable method, etc.

Model validation: A good model is a model which is useful for its purpose. The model needs to be able to reproduce the system behaviour given a new set of data. If the model fails the validation stage, the modeller needs to make modifications by repeating parts of the system identification procedure until an acceptable model is obtained. Model validation tools include crossvalidation (i.e. simulating the model on a data set not used for estimation), residual analysis, checking the value of the cost function, etc (Pintelon and Schoukens, 2001).

4.1.1 Identification methods

System identification methods can be classified as nonparametric or parametric. Nonparametric identification methods often have the feature that the resulting model are curves or functions (Söderström and Stoica, 1988). They are not described by a finite dimensional parameter vector (Ljung, 1999). Often we use nonparametric identification when we are interested in conducting a simple experiment to gain insight in how the variables influence

one another.

In parametric identification, the model of the system is described by a finite dimensional parameter vector. Generally, θ is used to denote this parameter vector. The main focus is to determine the value of θ such that the "best" model in the model structures is found (Ljung, 1999).

We shall apply both these identification methods to the Broken River. We first present nonparametric identification method followed by the parametric identification method.

4.2 Nonparametric identification

Initially, the modeller may have little knowledge about the important dynamics of a system. To gain insight into the behaviour of the system, a simple experiment can be conducted. This simple experiment (e.g. step test or frequency analysis) is not aimed at collecting quality operational data for parameter estimation, but rather to give the modeller some knowledge about the system dynamics (e.g. how the variables affect each other, the important time constant, etc). Two commonly used nonparametric identification methods are step response analysis and frequency analysis[1].

Since performing experiments such as step tests and sine sweeping tests on a river is in most cases not practical due to economical, environmental and operational reasons, we will simulate the step test and the sine sweeping test using the calibrated Saint Venant equations instead. The step test can give us information regarding the time constant and the time delay of the system. The frequency analysis can provide us with information regarding the order of the system and also the suitable frequency range for control design. We focus on the reach from Casey's Weir to Gowangardie Weir. As in Chapter 3, we call this reach, Reach CG. The calibrated Saint Venant equations using the Single segmentation as in Section 3.2.5 will be used for simulations.

[1]This is also known as sine sweeping test (Pintelon and Schoukens, 2001).

4.2.1 Step response analysis

In step response analysis, the input is a step. A step response is a good way to obtain a rough model (Söderström and Stoica, 1988). A step function is defined by

$$u(t) = \begin{cases} A + A_0 & t \geq 0 \\ A_0 & t < 0 \end{cases} \tag{4.1}$$

A_0 is the nominal amplitude and A is the size of the step.

From a visual inspection of the measured flow in Reach CG (see Figure 3.10), the flow ranges from about 0.7m^3/s ($\approx$ 61ML/day) to 3.0m^3/s ($\approx$ 260ML/day). Thus, a step input flow from 0.8 m^3/s ($\approx$ 70ML/day) to 2.5 m^3/s ($\approx$ 216 ML/day) is given to the Saint Venant equations to obtain the step response. Moreover, this flow are also the expected flow in the Broken River during the irrigation season with the control system is operating. Figure 4.2 shows the step response of Reach CG. At the downstream end, we converted the water level to flow using the flow over weir relationship so that a comparison between in-flow and out-flow can be made, i.e. $Q_G(t) = c_{weir,G}[y_G(t) - p_G]^{3/2}$ where Q is the flow and y is the water level where the subscript "G" denotes Gowangardie Weir. The weir constant $c_{weir,G} = 10.10$ m$^{3/2}$/s which has been calibrated against measured data (see Section 3.2.5) and $p_G = 137.33$ mAHD is the height of the weir.

From the step response in Figure 4.2, we see that the time delay is large compared to the time constant of the system. The time constant T_c is the time for the output response to reach 63% of the final value. The time constant $T_{c,CG} \approx 300$ minutes. As a remark, if the time constant is estimated based on the output response reaches steady state after 5 time constants, a smaller time constants of approximately 200 minutes is obtained. In this thesis, the definition of the time constant based on output response reaching 63% of the final value will be used. The time delay is found to be $\tau_{CG} \approx 1600$ minutes. The gain of the system $K_{CG} = 1$ as the steady state value for both input and output the system is the same. As the delay of the system is much larger than the time constant, it indicates that the system can be modelled as a pure time delay system, i.e.

$$\frac{Q_G(s)}{Q_C(s)} = \exp(-s\tau_{CG}) \tag{4.2}$$

or in time domain representation,

$$Q_G(t) = Q_C(t - \tau_{CG}) \tag{4.3}$$

where Q is the flow, τ_{CG}, is the time delay, subscript "C" and "G" denote the Casey's Weir and Gowangardie Weir respectively. Moreover, the measured data (see Figures 3.10 or 4.6) also indicated that the system can be modelled as a time delay system.

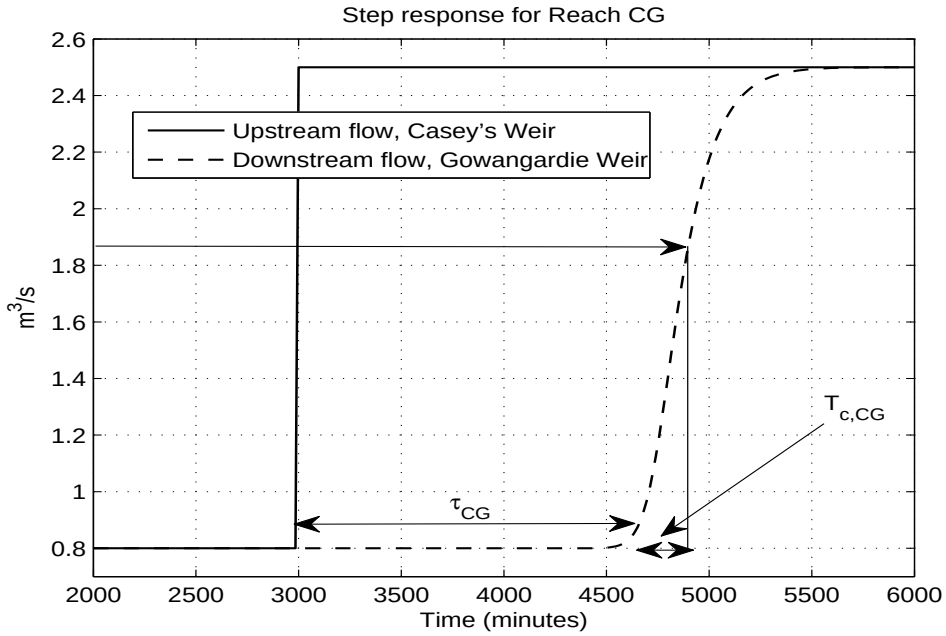

Figure 4.2: Step response.

4.2.2 Frequency response analysis

Frequency analysis is the analysis of the system in steady state when the system is subjected to a sinusoidal input signal. By varying the frequency of the input signal over a range of frequencies, the obtained output response can be analysed. The advantage of frequency response analysis is that the Bode plot of the system can be easily obtained. The disadvantage of this method is that in practice, many processes do not allow the sinusoidal input during normal operation. Moreover, the experiment time is also long as the experiment need to be repeated over the different frequencies of interest.

In our case, it is not sensible to conduct field experiments using sinusoidal signals as input to the river to obtain the Bode plot. However, given that we have calibrated the Saint Venant equations for Reach CG, we can carry out the frequency response analysis by performing sine sweeping experiment throughs simulation. We emphasize that the purpose of frequency response analysis is to gain some rough idea about what the Bode plot of the river system looks like, it is not meant as a practical method, which can be applied in practice.

Consider a sinusoidal input,

$$u(t) = A\sin(\omega_0 t) \tag{4.4}$$

where A is the amplitude and ω_0 is the frequency.

If the system is linear and time invariant, the output would be a sinusoidal signal with the same frequency, a scaled amplitude, and a phase shift. In a real system, the output $y(t)$ to the sinusoidal input also comprises of transient effects, effect of nonlinearities and disturbances (e.g., noise).

$$y(t) = B\sin(\omega_0 t + \phi) + D(t) + \text{transient} + \text{nonlinearities} \tag{4.5}$$

where $B = A|G(j\omega_0)|$, $\phi = \angle G(j\omega_0) = \tan^{-1}\frac{\text{Im}[G(j\omega_0)]}{\text{Re}[G(j\omega_0)]}$, $D(t)$ is the disturbance and $G(j\omega)$ is the transfer function relating the input and the output.

Here, we assume that the linear contribution dominates the nonlinearities (see Chapter 3.4). The effect of $D(t)$ can be reduced by using a correlation method (Ljung, 1999)[2]. The transient effect can be reduced by not considering the initial parts of the data. The idea behind the correlation method is to correlate the output signal $y(t)$ with a sine and cosine of the same frequency ω_0 as the input signal, and then average over the length of the data, N (Ljung, 1999) (see Figure 4.3).

From Figure 4.3, the following equation can be obtained.

$$M_c(N) = \frac{1}{N}\sum_{t=1}^{N} y(t)\cos(\omega_0 t) \tag{4.6}$$

and

$$M_s(N) = \frac{1}{N}\sum_{t=1}^{N} y(t)\sin(\omega_0 t) \tag{4.7}$$

[2]This is also known as improved frequency method (Söderström and Stoica, 1988)

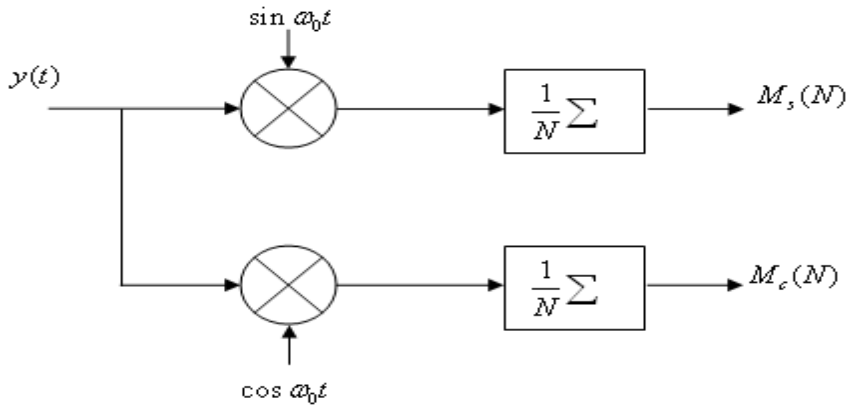

Figure 4.3: Improved frequency method.
(Söderström and Stoica, 1988)

Substituting Equation (4.5) into both Equations (4.6) and (4.7) and assuming that the effect of the transient is negligible, yields the following expression,

$$\begin{aligned}
M_c(N) &= \frac{1}{N}\sum_{t=1}^{N} y(t)\cos(\omega_0 t) \\
&= \frac{1}{N}\sum_{t=1}^{N}(B\sin(\omega_0 t+\phi)+D(t))\cos(\omega_0 t) \\
&= \frac{1}{N}\sum_{t=1}^{N}(A|G(j\omega_0)|\sin(\omega_0 t+\phi)\cos(\omega_0 t)+D(t)\cos(\omega_0 t)) \\
&= \frac{1}{N}\sum_{t=1}^{N} A|G(j\omega_0)|\frac{\sin(2\omega_0 t+\phi)+\sin(\phi)}{2}+\frac{1}{N}\sum_{t=1}^{N} D(t)\cos(\omega_0 t) \\
&= \frac{A}{2}|G(j\omega_0)|\sin(\phi)+\frac{A}{2}|G(j\omega_0)|\frac{1}{N}\sum_{t=1}^{N}\sin(2\omega_0 t+\phi) \\
&\quad +\frac{1}{N}\sum_{t=1}^{N} D(t)\cos(\omega_0 t) \qquad (4.8)
\end{aligned}$$

For large N, the average of the sinusoidal signal tends to zero and hence, the second term will go to zero when $N \to \infty$. Assuming that $D(t)$ is a stationary stochastic process

with covariance function $R_D(\ell)$ such that

$$\sum_{\ell=0}^{\infty} \ell |R_D(\ell)| < \infty$$

then, the decay rate of the variance of the third term will be $\frac{1}{N}$. Thus, as $N \to \infty$, the third term will go to zero as well. For a detailed proof, see (Ljung, 1999).

Doing the similar calculations for $M_s(N)$ we get,

$$M_s(N) = \frac{A}{2}|G(j\omega_0)|\cos(\phi) - \frac{A}{2}|G(j\omega_0 t)|\frac{1}{N}\sum_{t=1}^{N}\cos(2\omega_0 t + \phi) + \frac{1}{N}\sum_{t=1}^{N} D(t)\sin(\omega_0 t) \tag{4.9}$$

From Equations (4.8) and (4.9), $|G(j\omega_0)|$ and $\phi = \angle G(j\omega_0)$ can be estimated as

$$|\hat{G}(j\omega_0)| = \frac{2\sqrt{M_c^2(N) + M_s^2(N)}}{A} \tag{4.10}$$

and

$$\hat{\phi} = \tan^{-1}\frac{M_c(N)}{M_s(N)} \tag{4.11}$$

Having derived the expression for the magnitude and the phase of the transfer function, we shall now apply frequency response analysis to Reach CG. The sinusoidal input flow $u(t) = 0.75\sin(\omega_0 t) + 3.0$ m^3/s is applied to the Saint Venant equations for Reach CG, and the experiment is repeated for several frequencies ω_0 in the frequency range of interest. The input and output flow (i.e. the flow over Casey's Weir and Gowangardie Weir respectively) are shown in Figure 4.4.

By visual inspection of Figure 4.4, the output looks like a sinusoid with the same frequency, and no harmonic or subharmonic is observed in the output. This suggests that the Saint Venant equations are almost linear in a small operating region, and the nonlinearity tests we carried out in Section 3.4, do reveal that the Saint Venant equations are close to linear in an operating region. By repeating the sine sweeping test over different frequencies and obtaining the magnitude and phase at each frequency, a Bode plot can be

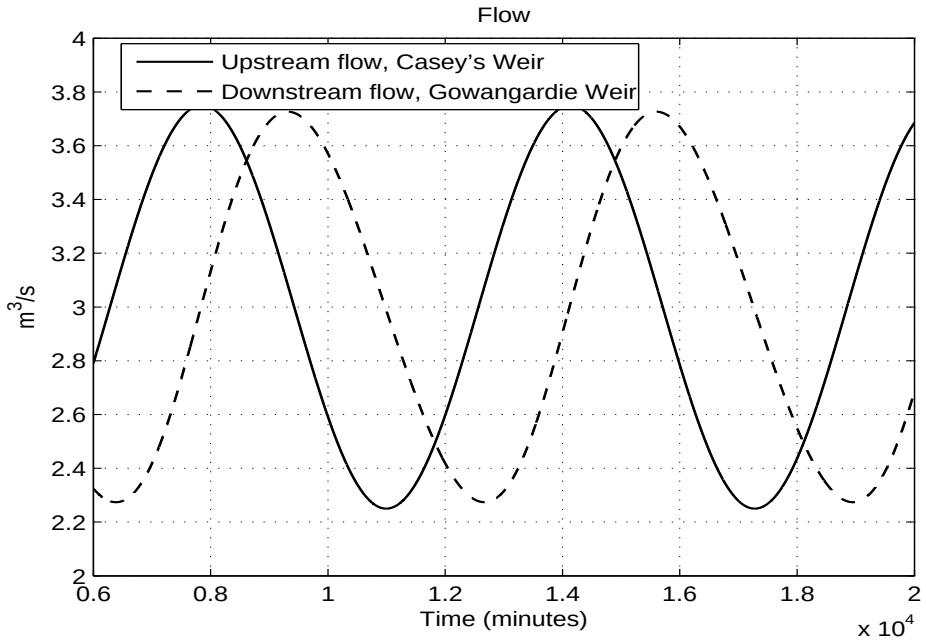

Figure 4.4: Input and output flow given sinusoidal input at frequency $\omega_0 = 0.001$ rad/min.

constructed.

The Bode plot for Reach CG obtained from the sine sweeping test is plotted in Figure 4.5. From the step response, the time delay is approximately 1600 minutes and the time constant is approximately 300 minutes. The inverse of the time constant corresponds to the corner frequency, i.e. $\omega_{corner} = 1/T_{c,CG} = 1/300 = 0.0033$ rad/min. The corner frequency is where the "bend" occurs in the magnitude plot. From the theory of linear time invariant system in the frequency domain, for a first order system without time delay, the magnitude and the phase at the corner frequency are -3dB and -45° respectively, and the roll-off is -20dB/dec.

From the zoomed in Bode plot, i.e. Figure 4.5 (bottom), we can see that in the frequency range relevant for control the frequency response is similar to the frequency response of a pure time delay system. The 3dB bandwidth of the system is approximately 0.0032 rad/min, but we note that the phase shift is already more than $-180°$ at 0.0023 rad/min indicating a dominant time delay. In regards to the roll-off of the magnitude plot, the roll-off is -20dB/dec at ω_{corner} but it becomes approximately -60dB/dec at the frequency of 0.02 rad/min (see Figure 4.5 (top)), due to the unmodelled dynamics and

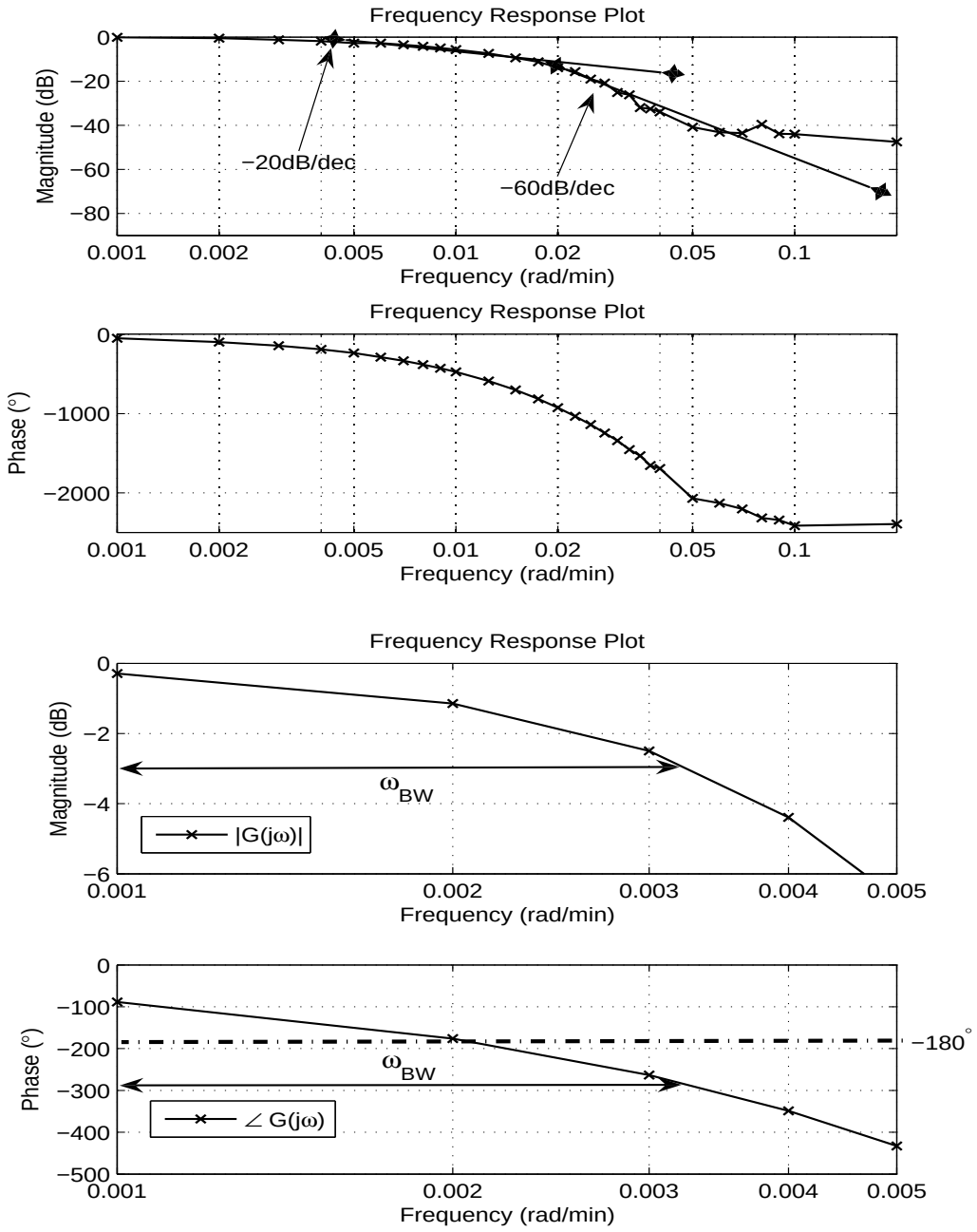

Figure 4.5: Top: Bode plot for Reach CG. Bottom: Zoomed in Bode plot for the frequency range 0.001 to 0.005 rad/min.

nonlinearities not captured by a first order model.

4.2.3 Summary of nonparametric identification method

The step response analysis gives us information about the time constant and time delay of the river reach. From the step response, we observe that the response can be approximated by a pure time delay model. The results from the frequency response analysis concur with the findings of the step response in the low frequency range. We shall use this information to determine the appropriate model structure for the parametric identification method.

4.3 Parametric identification

Parametric models can be classified into the "ready-made models" and the "tailor-made models" (Ljung and Glad, 1994). These models are also commonly known as black box models and grey box models respectively. In the ready-made models (black box), a model structure, which in general provides no physical interpretation of the system is used. Its function is mainly to describe the input-output relationships of the system. These models are useful if the physical laws governing the system are poorly known. On the other hand, a tailor-made model (grey box) is built with some insights of the physical system and the parameter θ represents the unknown values of the system parameters. θ would in this case have some physical interpretation. For river system, the "tailor-made" models are used as initial model selection considering that we know from physics that for incompressible flow, the sum of all in-flows and out-flows is equal to zero and the volumes and flows of water obey mass and momentum balance equation.

Remarks on notation: In the system identification literature, the variable θ is used to represent the unknown parameters. In order not to create a confusion, we use different subscripts, i.e. $\theta_{x,y,z}$ to distinguish between different θs associated with different models used in this thesis. The first subscript $x = p, e$ where "p" stands for physical approach to modelling while "e" stands for the empirical approach to modelling. The second subscript $y = CG, LBC$, etc is used to represent the associated river reach, while the third subscript $z = 1, 2, \ldots$ is used for numbering the unknown parameters. For example, $\theta_{e,CG,1}$ means this θ represents the first unknown parameter in a model of Reach CG obtained using empirical modelling.

4.3.1 Model structure selection

The same measurements of flows and water levels at Casey's and Gowangardie Weir as used in Section 3.2.5 are shown again in Figure 4.6. From Figure 4.6, we observe that the

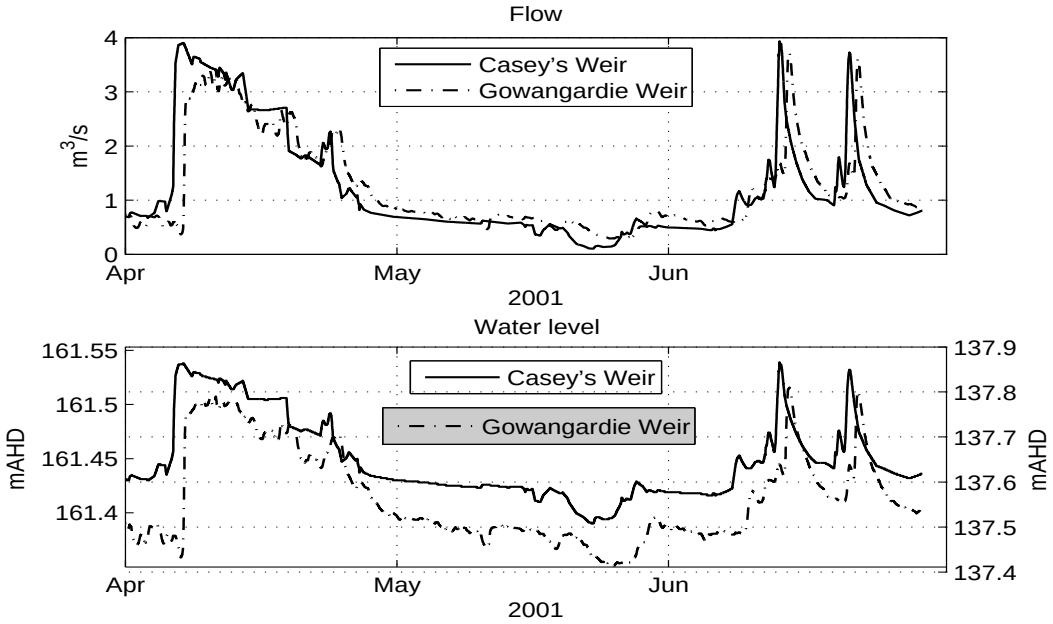

Figure 4.6: Top: Measured flows for Reach CG. Bottom: Measured water levels for Reach Casey-Gowangardie.

flow measurements show a lag between Casey's and Gowangardie Weirs and this indicates that the system can be modelled as a time delay system. The simulations of the step response and frequency response in Section 4.2 are in agreement with this finding as well. By modelling this reach as a time delay system we get,

$$Q_G(t) = Q_C(t - \tau_{CG}) \tag{4.12}$$

where τ_{CG} is the time delay and the subscripts 'C' and 'G' denotes the Casey's and Gowangardie weirs respectively.

Both Casey's and Gowangardie Weirs resemble a sharp crested weir (see Figure 4.7). There is a well established relationship between water levels and flows for sharp crested weirs, which can be found in most open channel text book, (see e.g. (Chaudhry, 1993),

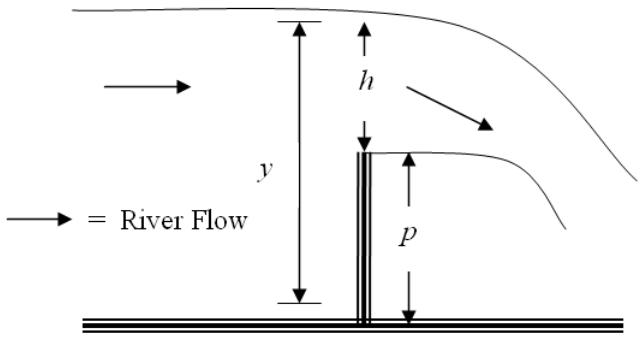

Figure 4.7: Sharp-crested weir structure.

(Cunge *et al.*, 1980), (Bos, 1978)). The flow over a sharp crested weir can be approximated by (Bos, 1978)

$$Q(t) = c_{weir} h^{3/2}(t) = c_{weir}[y(t) - p]^{3/2} \tag{4.13}$$

where c_{weir} is the weir constant, $h = y(t) - p$ is the head over weir and p is the height of the weir. The weir constant is (Boiten, 2002)

$$c_{weir} \approx 0.6\sqrt{g} b_{weir} \tag{4.14}$$

where g is the gravitational constant and b_{weir} is the width of the weir. Substituting Equation (4.13) into Equation (4.12), we get

$$\begin{aligned} c_{weir,G} h_G^{3/2}(t) &= c_{weir,C} h_C^{3/2}(t - \tau_{CG}) \\ &\Downarrow \\ c_{weir,G}[y_G(t) - p_G]^{3/2} &= c_{weir,C}[y_C(t - \tau_{CG}) - p_C]^{3/2} \qquad (4.15) \\ &\Downarrow \\ y_G(t) &= \theta_{e,CG,1} y_C(t - \tau_{CG}) + \theta_{e,CG,2} \qquad (4.16) \end{aligned}$$

where $\theta_{e,CG,1} = (c_{weir,C}/c_{weir,G})^{2/3}$ and $\theta_{e,CG,2} = p_G - (c_{weir,C}/c_{weir,G})^{2/3} p_C$ are unknown constants, which are estimated from the observed data together with the time delay. The associated predictor for (4.16) is given by

$$\hat{y}_G(t, \theta_{e,CG}, \tau_{CG}) = \theta_{e,CG,1} y_C(t - \tau_{CG}) + \theta_{e,CG,2} \tag{4.17}$$

where $\hat{y}$ is the predicted water level. Note that, the use of a time delay model to model a river is in agreement with the findings by (Maxwell and Warnick, 2006). Maxwell and Warnick consider the parameterised time delay model $Q_G(t) = \alpha Q_C(t-\tau)$. Nonetheless, this leads to the same predictor, Equation (4.17) but with different expressions for $\theta_{e,CG,1}$ and $\theta_{e,CG,2}$. However, this is of no importance as $\theta_{e,CG,1}$ and $\theta_{e,CG,2}$ are estimated from data, and hence Equation (4.16) is the same as the parameterised time delay model from (Maxwell and Warnick, 2006).

Remarks: Although Equation (4.12) contains no parameter apart from τ_{CG}, the flow is rarely measured, but obtained from rating curves or based on Equations (4.13) to (4.14). There are often large uncertainties in these rating curves and hence the necessity of estimating the parameters in the model given by Equation (4.17).

4.3.2 Parameter estimation

The time delay model has three unknown parameters $\theta_{e,CG,1}$, $\theta_{e,CG,2}$ and τ_{CG}. As in (Maxwell and Warnick, 2006), the time delay τ_{CG} is obtained from the cross-correlation between the measurements at the upstream and the downstream ends. The cross-correlation function is given by

$$R_{Q'_G Q'_C}(\tau) = \frac{1}{N}\sum_{n=1}^{N} Q'_G(n) Q'_C(n-\tau) \qquad \tau = 0, \pm 1, \ldots \tag{4.18}$$

where $N = 8640$ (the sampling interval is 15 minutes), $Q'(n) = \frac{1}{\sigma(Q(n))}\left[Q(n) - \frac{1}{N}\sum_{j=1}^{N} Q(j)\right]$ and σ is standard deviation. $R_{Q'_G Q'_C}$ is shown in Figure 4.8. The estimate of τ_{CG} is given

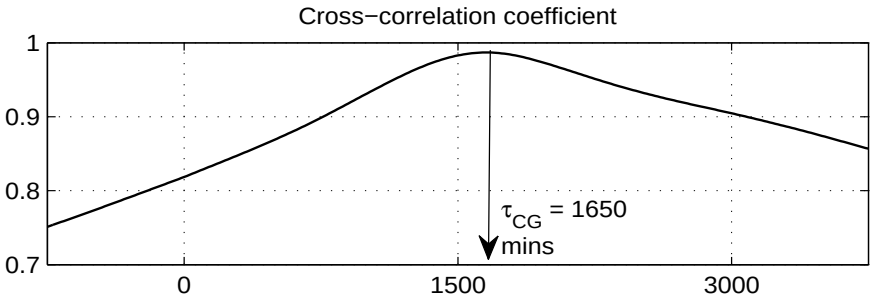

Figure 4.8: Cross-correlation coefficient.

by $\hat{\tau} = \text{argmax}_\tau R_{Q'_G Q'_C}(\tau)$.

The parameter $\theta_{e,CG} = [\theta_{e,CG,1}, \theta_{e,CG,2}]^T$ is estimated using least squares, i.e.

$$\hat{\theta}_{e,CG} = \left[\sum_{t=1}^{N} \varphi(t)\varphi^T(t)\right]^{-1} \left[\sum_{t=1}^{N} \varphi(t) y_G(t)\right] \tag{4.19}$$

where $\varphi(t) = [y_C(t - \hat{\tau}_{CG}), 1]^T$ and y_G is the measured water level. The data set shown in Figure 4.6 is used for estimation and the estimated values are $\hat{\theta}_{e,CG,1} = 2.711$, $\hat{\theta}_{e,CG,2} = -300.05$mAHD and $\hat{\tau}_{CG} = 1650$ minutes.

4.3.3 Accuracy of the model

Having selected the model structure and estimated the parameters, following the system identification procedures, the model needs to be validated. In this section, we include the results from Section 3.2.5 such that the time delay model and the Saint Venant equations can be evaluated together and compared.

Time domain analysis

The accuracy of the Saint Venant equations for Reach CG using Single segmentation and the time delay model are compared on data sets not used for estimation. These data sets are from summer 2001 and winter 2002. Figure 4.9 shows the measured water levels, predicted water levels using the time delay model and the simulated water levels from the calibrated Saint Venant equations.

Table 4.1: Values of MSE.

Data Period	**Time Delay Model** (10^{-3}m^2)	**Saint Venant equations** (10^{-3}m^2)
Summer 2001	2.25	5.38
Winter 2002	0.72	0.52

For quantitative comparison, the mean square errors, (MSE) between the predicted and simulated water levels and the measured water levels are calculated. The MSE is

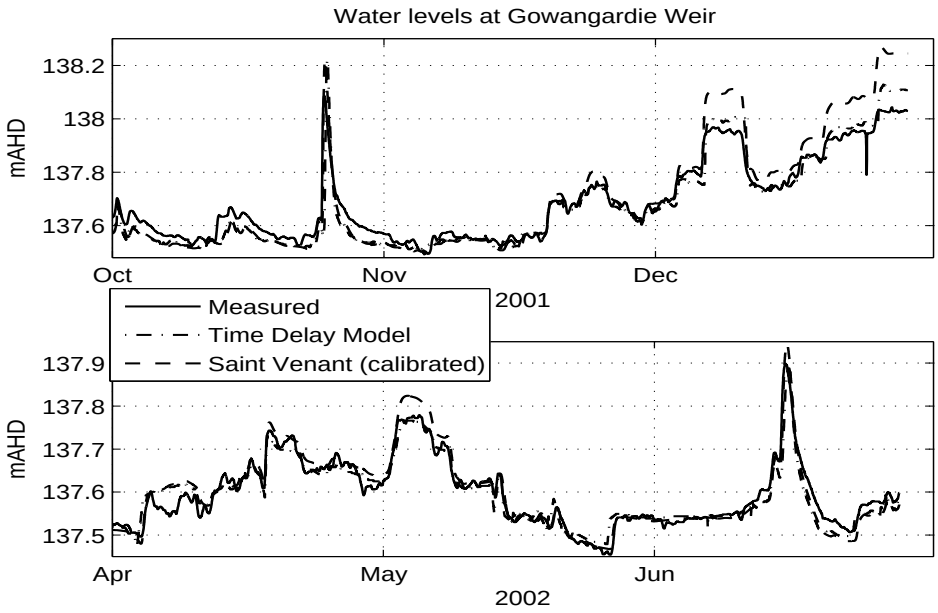

Figure 4.9: Top: Summer period 2001 (start of irrigation season). Bottom: Winter period 2002 (end of irrigation season).

given by

$$\text{MSE} = \frac{1}{N}\sum_{t=1}^{N}[y_G(t) - \hat{y}_G(t, \theta_{e,CG}, \tau_{CG})]^2 \tag{4.20}$$

and given in Table 4.1. From Figure 4.9 (bottom), it can be seen that the Saint Venant equations after calibration are accurate when compared to data during the winter period. It picks up the trends in the measured water levels very well. We also included the result from the summer period (see Figure 4.9 (top)) when larger water volumes are taken from the river for irrigation. We can see that the water levels simulated using the calibrated Saint Venant equations are higher than the measured water levels. This is expected as the irrigation off-takes are not taken into account in the simulation model. The results show that the calibrated Saint Venant equations are accurate in describing the relevant dynamics of the river systems.

There is also good agreement between the time delay model and the measured data. The time delay model has a similar accuracy in terms of the MSE as the Saint Venant equations. In general, the MSE values are small and the time delay model follows the main trends in the water level very well. Compared to the Saint Venant equations, the time

delay model is much simpler, and it is preferred for control design. Both the Saint Venant equations and the time delay model could be further improved by taking the effects of irrigation off-takes, rainfall, etc into consideration.

Frequency domain analysis

The Saint Venant equations and the time delay model show similar behaviour when compared against time domain data. As mentioned before, as many control design methods

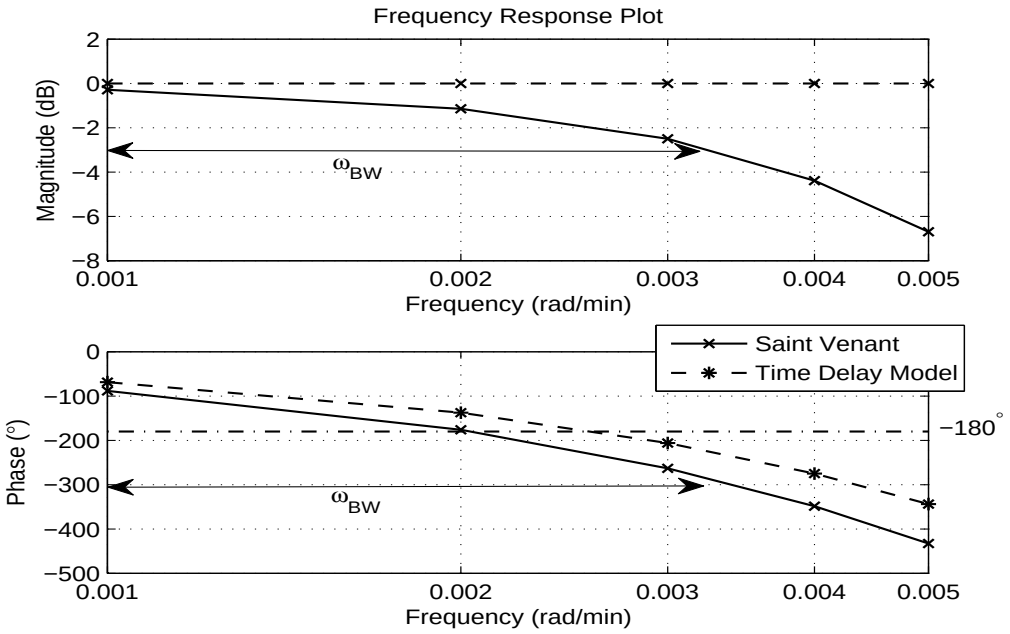

Figure 4.10: Bode plot for the reach between Casey's Weir and Gowangardie Weir.

are based on frequency domain considerations, and it is therefore of interest to compare the frequency domain properties of the two models. The Bode plot of the Saint Venant equations and the time delay model are shown in Figure 4.10. In the frequency range relevant for control the frequency response of the Saint Venant equations is similar to the frequency response of the time delay model. The 3dB bandwidth of the Saint Venant equations model is approximately 0.0032rad/min, but we notice that the phase shift is already more than -180° at 0.0023rad/min, indicating a dominant time delay.

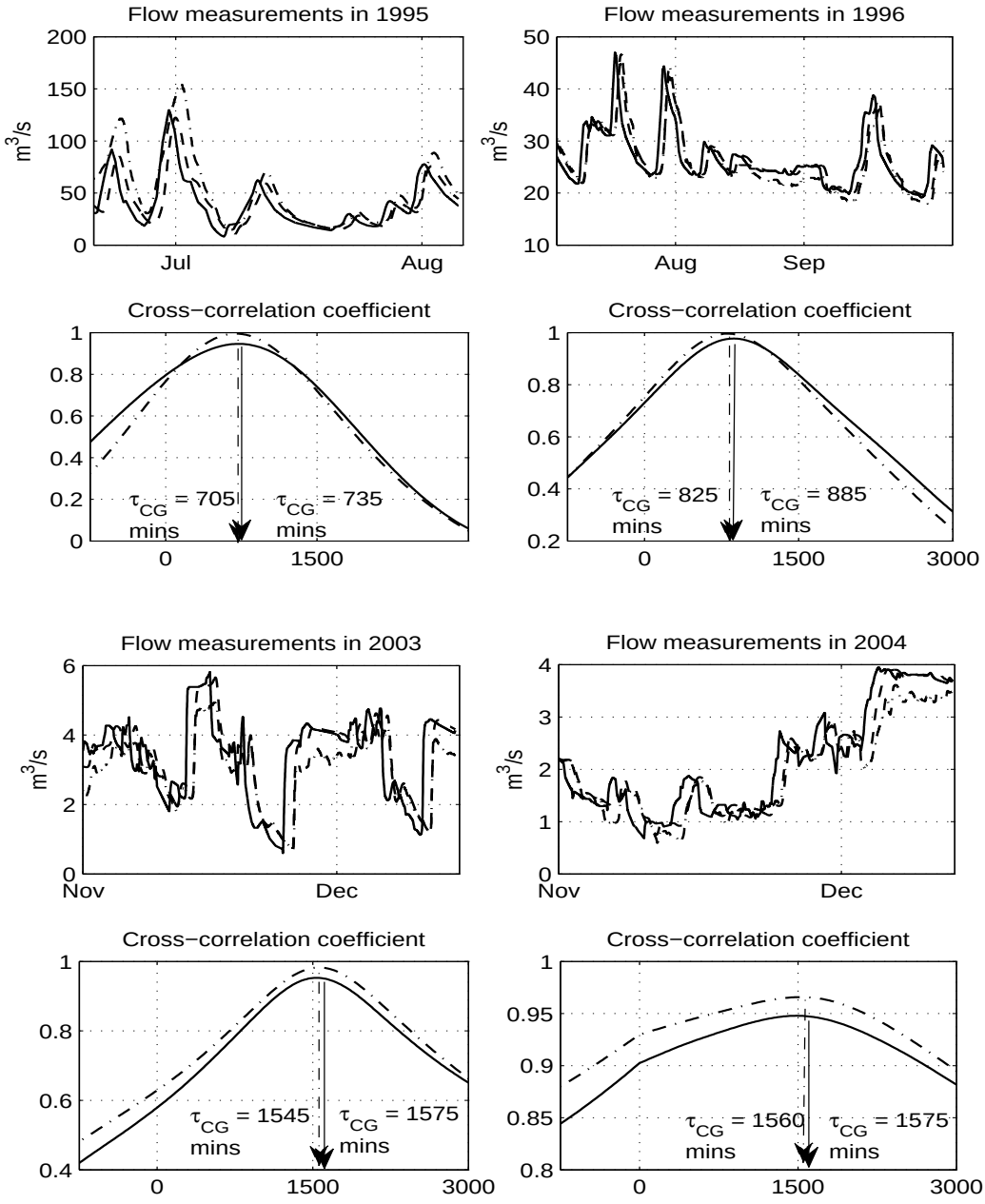

Figure 4.11: Cross-correlation coefficients and estimated time delays. Flow measurements. Solid line: Casey's Weir, Dash-dotted: Gowangardie Weir. Cross-correlation coefficient. Solid line: Measured data. Dash-dotted line: Simulated data.

4.4 Effect of varying flow condition

It is known (see e.g. (Litrico and Pomet, 2003), (Thomassin *et al.*, 2009)) that the flow conditions affect the time delay in a river, which will affect the robustness margins of a control system. In view of that, further investigations on the effect of varying flow condition are carried out.

From the available data, sets with different flows are found. The time delays for those data sets are estimated using cross-correlation analysis as in Section 4.3.2. In addition, we also include the cross-correlation between the upstream flow measurements at Casey's Weir and the simulated downstream flow at Gowangardie Weir obtained from the Saint Venant equations. The estimated time delays are shown in Figure 4.11, and as expected the estimated time delay decreases with higher flows. In addition, there is good agreement between the cross-correlations obtained using the measured data and those obtained using the Saint Venant equations, reconfirming the accuracy of the Saint Venant equations. The varying time delay must be taken into account in the robustness specification of the controllers.

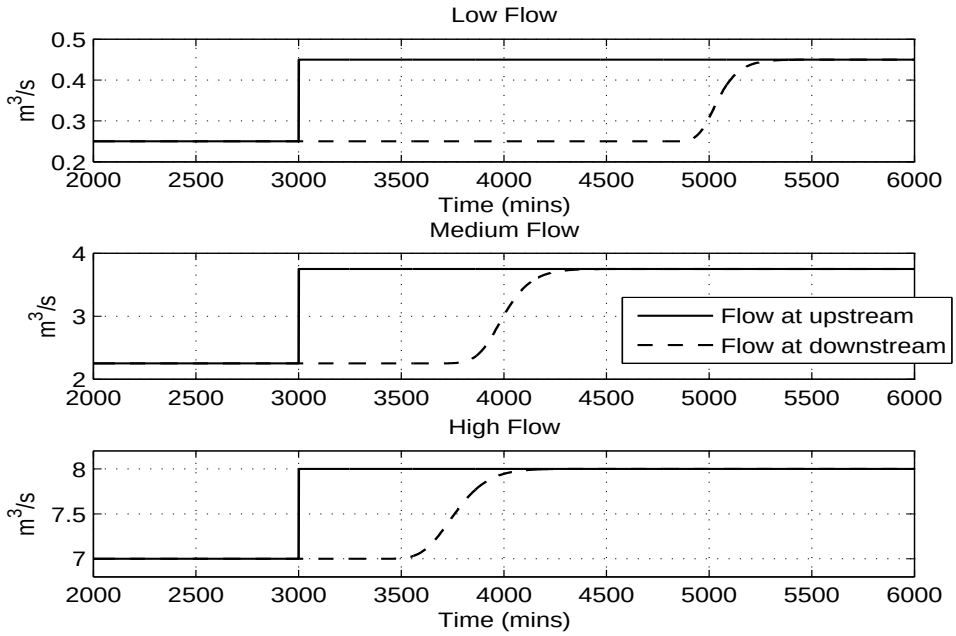

Figure 4.12: Step responses for LF, MF and HF condition.

In addition, we repeat both the step response and frequency response analysis. We simulated three different flow conditions, 0.25-0.45 m^3/s ($\approx$ 22-39 ML/Day), 2.25-3.75 m^3/s ($\approx$ 195-324 ML/Day) and 7.00-8.00 m^3/s (605-692 ML/Day). We call these three flow conditions, Low Flow (LF), Medium Flow (MF) and High Flow (HF) condition respectively. We performed three new step tests where the flow is stepped from 0.25 m^3/s to 0.45 m^3/s for LF condition, from 2.25 m^3/s to 3.75 m^3/s for MF condition and from 7.00 m^3/s to 8.00 m^3/s for HF condition. These step responses are shown in Figure 4.12.

From Figure 4.12, we see that the time delay changes substantially with the flow conditions. A larger time delay is obtained for lower flow condition and a smaller time delay is obtained for the higher flow condition. The time delay for LF, MF and HF conditions are $\tau_{LF} \approx 1800$ minutes, $\tau_{MF} \approx 800$ minutes and $\tau_{HF} \approx 500$ minutes respectively. This trend is in agreement with the findings from the cross-correlation analysis. The time constant, on the other hand, does not change much for the three flow conditions, i.e. between $200 - 300$ minutes. Again, we note that if the definition of time constant where the output response reaches its steady state value in 5 time constants is used, the time constants seems to be larger as flow condition increases. Nonetheless, as the time delay is larger than the time constant, a time delay model is still the suitable model structure, thus the effect of the time constant can be neglected.

We repeat the sine sweeping test using these three flow conditions. The Bode plots are plotted in Figure 4.13. The respective corner frequencies for all the three flow conditions (marked by the intersection with the -3dB line) indicate that the time constant for all three flow conditions are within 200-300 minutes, which is in agreement with the step response obtained above. As for the phase plot, a large time delay for LF conditions contributes to the phase dropping below -180° much sooner as compared to the MF and HF conditions. As for the MF and HF conditions, the frequencies where the phase drops below -180° is quite close. As a note, resonance peaks are observed at high frequencies but as control design is the main interest, the behaviour at lower frequencies are more of interest.

The Bode plots suggest that the low flow condition is the most challenging due to the drop in phase. Note that the gains in Figure 4.13 are never more than -3dB apart so a modest gain margin will be sufficient. So essentially any robust controller designed for low flow condition should work for medium and high flow conditions.

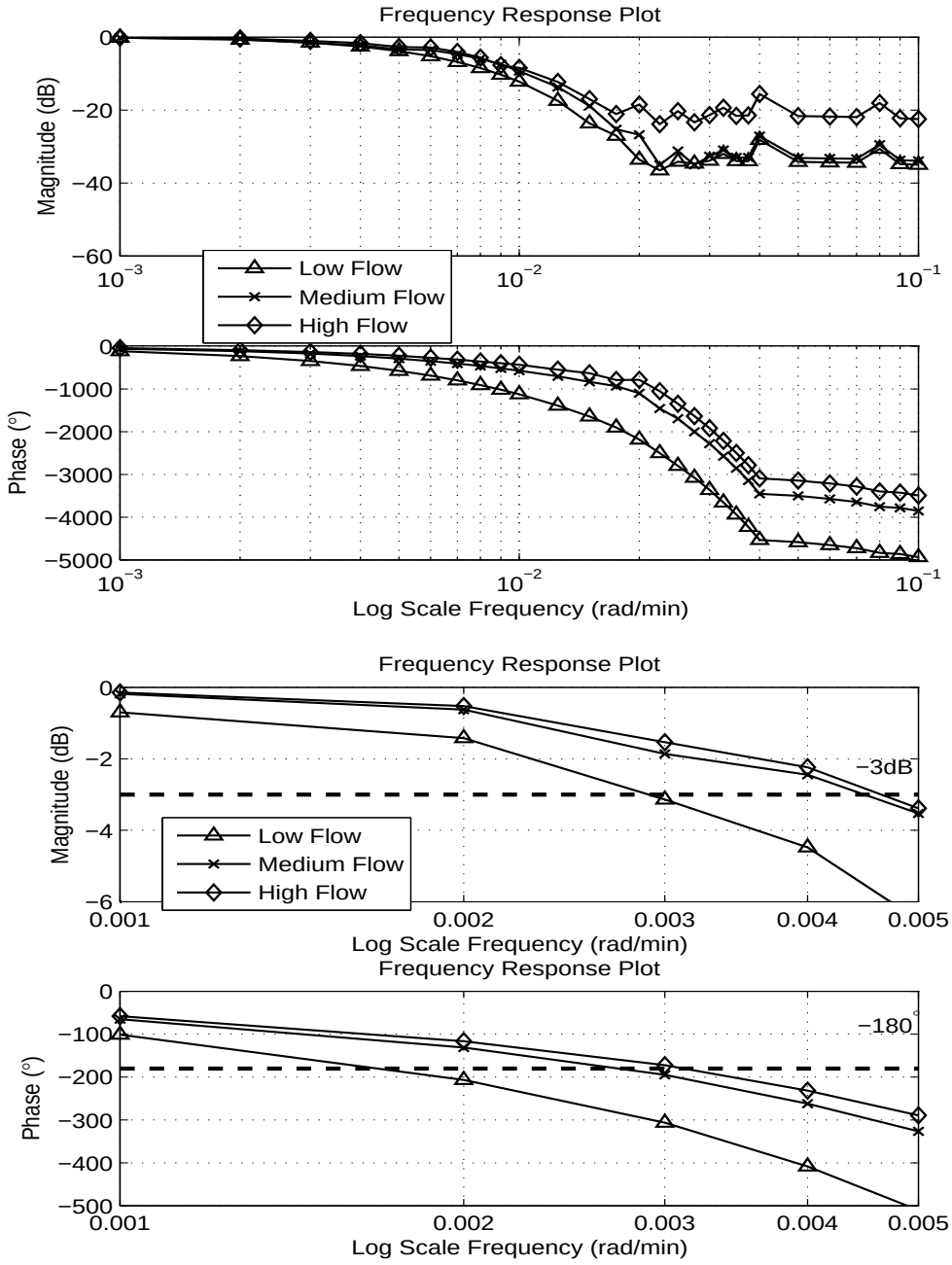

Figure 4.13: Top: Bode plot for LF, MF and HF condition. Bottom: Zoomed in version.

4.4.1 Discussion of the models

Undermodelling

A number of factors such as in-flows and out-flows from creeks, rainfall, water withdrawals for irrigation, evaporation and surface-water/ground-water interactions have been ignored in the models. Here, we briefly discuss the influence of these factors taking into account that the models are going to be used for control design.

Surface-water/ground-water interactions: Some stretches of the Broken River are gaining water from the ground water, while others are loosing. The reach between Casey's Weir and Gowangardie Weir is a loosing reach (Adams and Western, 2010). However, the surface-water/ground-water dynamics is slow, and it is not considered important for control. Moreover, if the surface-water/ground-water interaction is modelled as a constant in- or out-flow $Q_{SW/GW}$, then Equation (4.12) becomes $Q_G(t) = Q_C(t - \tau_{CG}) - Q_{SW/GW}$, and we will still end up with the model structure, Equation (4.16), but with a different expression for $\theta_{e,CG,2}$. This is however of no importance as $\theta_{e,CG,2}$ is estimated from data. Furthermore a controller with integral action will reject constant unmodelled in- or out-flows.

Evaporation: The rate of evaporation is dependent on temperature, solar radiation, wind speed, atmospheric pressure, area of water surface, etc (Deodhar, 2009). In (Young, 1998), temperature is included as an input variable in a rainfall-flow model, and the flow shows a long term dependence on temperature which could account for the effect of evaporation. As with the surface-water/ground-water interactions, the loss due to evaporation from the river is a disturbance and its effect on the levels and flows is of lesser importance for control. Evaporation from storages may be significant (Craig *et al.*, 2007), and this may influence how the storages are operated and hence also the control objectives. In such case, it would be of interest to obtain models that relates the surface area of the storage and the evaporation and use this model to as part of feedforward control for the in- and out-flow of the storage.

Water withdrawal from the river for irrigation: The withdrawals can be large and they can have a big impact on the predictive accuracy of the models. From a control point of view the withdrawals are load disturbances which should be rejected. The irrigators order their water some days in advance, and better control can be achieved by releasing water early using feedforward action to match the amount of ordered water.

However, as water withdrawals act as disturbances the transfer function from the in-flow (that we can manipulate) to the water level or flow (that we want to control) remains the same. That is, the transfer function on which a feedback control design is based remains the same, although the estimate of it may become more uncertain if there are large water withdrawals which have not been taken into account.

In- and out-flows from creeks and rainfall: If measured, the in- and out-flows from creeks can easily be included in the models (see Section 4.5), and they can also be accounted for in the controller by e.g. regarding them as part of the flow to be released by the controller. When the flows in the creeks are not measured, rainfall-runoff models (see e.g. (Bastin *et al.*, 2009*b*), (Young, 1998), (Young and Chotai, 2001), (Young, 2002), (Young, 2003) and the references therein) are useful for estimating the additional contributions from creeks and rain. Even when the flows and water levels in creeks are measured, it may be of interest to predict flows into the future if the time delays associated with the flows in the creeks are much smaller than the time delays of the flows commanded by the control system. The information about the predicted flows can then be used as part of feedforward control.

Use of the time delay model for control

Although the time delay model gives a good representation of a river reach in the time and frequency domain as illustrated in the previous sections, some care needs to be exercised when using it for control design. One key aspect in the previous sections is that the downstream flow could not be manipulated, and the downstream flow is simply modelled as the delayed upstream flow, i.e. $Q_D(t) = Q_U(t-\tau)$. However, if the downstream flow Q_D can be set independently of the upstream flow Q_U (e.g. by regulation gates or valves), the time delay model is obviously not going to be a good model. This point must be kept in mind if hydraulic structures are changed, e.g. if fixed weirs are replaced by regulation gates.

The time delay model also assumes that there is little storage capabilities in the river reach in the sense that the volume of water in the reach is nearly constant. This may not be a valid assumption, particularly if the river flows through a lake as the Broken River does at Lake Benalla. In both the above cases, an integrator delay model of the type

$$\dot{V}(t) = Q_U(t-\tau) - Q_D(t)$$

seems more appropriate where V is the volume of water in (a part of) the reach. This model structure will be discussed in the next section.

4.5 Further modelling

As mentioned in the previous section, the time delay model is only valid when the flow at the downstream end cannot be regulated or when there is little storage capabilities in the river reach. Here, we explore different model structures for cases where the time delay model may no longer be appropriate. To be consistent with the presentation of the results in Section 4.3.3, we include the results using the Saint Venant equations as well. Only the results from the time domain analysis are presented.

4.5.1 Modelling of river reach with regulation of downstream flow

Reach Lake Nillahcootie to Broken Weir

Physical modelling:

We consider the reach from Lake Nillahcootie to Broken Weir. For simplicity, we call this reach, Reach LNB. For this reach, there is in-flow from a creek called Lima Creek. Based on the on-site survey carried out by Goulburn-Broken Catchment Management Authority (GBCMA) (GBCMA, 2009), the approximate river parameters for this reach are summarised in Table 4.2. The measured flows and water levels for Lake Nillahcootie

Table 4.2: Summary of river parameters for Reach LNB.

Parameters	**Values**
Reach Length, L_{LNB}	25.9km
Bottom width, b_{LNB}	10-12m
Side slope, s_{LNB}	2.5-3
Bottom slope, $S_{0,LNB}$	0.002-0.003
Manning friction coefficient, n_{LNB}	0.07-0.10

and Broken Weir are shown in Figure 4.14. As there is no information about the elevation

at Lima Creek, the water depths[3] are shown instead. The data is sampled every 3 hours (180 minutes). The elevations at Lake Nillahcootie and Broken Weir are 249.26mAHD and 173.00mAHD respectively. In view of the poor quality of the data (there is missing data), only the data from the period from April to July for both 2007 and 2008 are considered (see Figure 4.14).

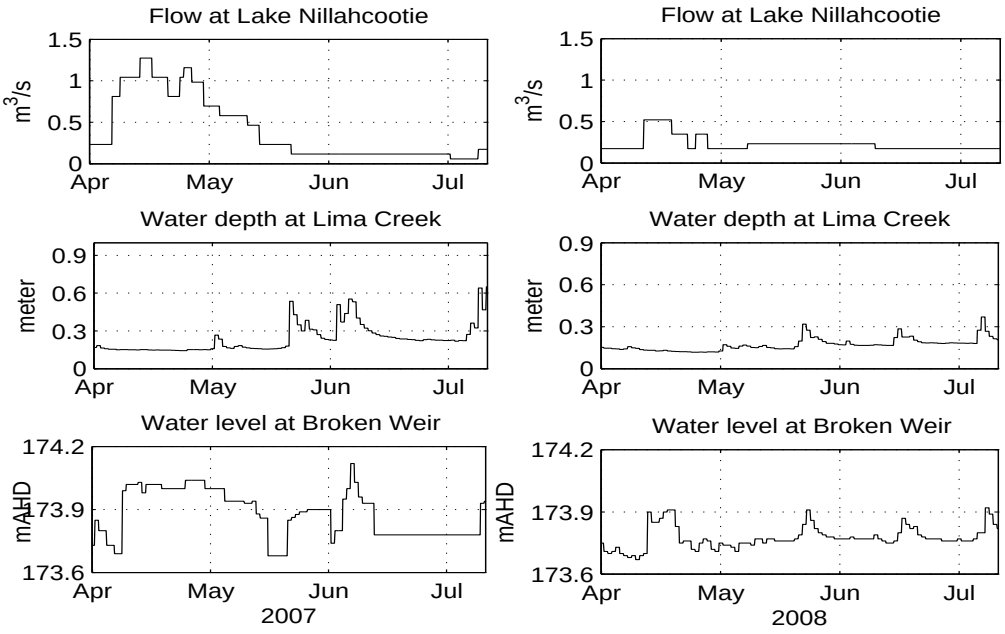

Figure 4.14: Flows, water depths and water levels measurements for Reach LNB.

We aim to validate the Saint Venant equations for Reach LNB against measured data. As the values in Table 4.2 are only approximate, the Saint Venant equations are calibrated against the measured data. The input to the Saint Venant equations is the flow at Lake Nillahcootie. As for the flow at Lima Creek, as we do not have any information regarding the flow, we make the assumption that the flow at Lima Creek can be modelled using a local linear relationship $Q_{LC} \approx a_{LC} y_{LC} + \Delta_{LC}$. a_{LC} is chosen based on visual inspection of the data on how the dynamics of Lima Creek would affect the water level at Broken Weir and we choose $a_{LC} = 4$ and $\Delta_{LC} = 0$. This flow is treated as a lateral in-flow to the Saint Venant equations.

[3]Water depth is measured from the surface of the river to the bottom of the river. It is not reference to datum, i.e. the sea level.

For the Broken Weir, we want to point out that Broken Weir is actually a submerged undershot gate (see Section 1.2) and to model the flow over an undershot gate, two measurements of water level are required, i.e. the water levels upstream and downstream of the gate. Given that we only have measurements of water level upstream of the gate at Broken Weir, obviously the model of the submerged undershot gate cannot be used and we need to seek an alternative model. With the manual regulation gate at Broken Weir is in the process of being replaced by an overshot gate, thus we assume that the flow over Broken Weir can be modelled by a sharp crested weir[4] and the flow over Broken Weir is approximated using

$$Q_{BW}(t) \approx c_{weir,BW} h_{BW}^{3/2}(t) = c_{weir,BW}[y_{BW}(t) - p_{BW}]^{3/2} \tag{4.21}$$

where $p_{BW} = 173.1$mAHD is the height of the weir, $c_{weir,BW} \approx 0.6\sqrt{g} b_{weir,BW}$ is the weir constant, with g is the gravity constant and $b_{weir,BW}$ is the width of the weir.

From the segmentation and sensitivity analysis carried out in Section 3.2, we use Single segmentation to represent this reach. The value of $b_{LNB} = 9.5$m and $s_{LNB} = 2.5$, which are the average values of the bottom width and the side slope respectively are used. Using the elevations, the average bottom slope $S_{0,LNB}$ is given by (249.26-173.00)mAHD/25900 ≈ 0.003. The weir constant $c_{weir,BW}$ and the Manning friction coefficient n_{LNB} will be estimated from the data.

Table 4.3: Estimated parameters for Reach LNB.

Estimation Set	$\hat{c}_{BW}$	$\hat{n}_{LNB}$
Apr-Jul 2007	$3.76\text{m}^{3/2}/\text{s}$	0.1489
Apr-Jul 2008	$4.13\text{m}^{3/2}/\text{s}$	0.1501

The data set on the left of Figure 4.14 (April to July 2007) is used for estimation and validation will be made on the data set on the right of Figure 4.14. In addition, we also use the data set on the right of Figure 4.14 (April to July 2008) for estimation and validate it on the data set on the left of Figure 4.14. These parameters are estimated using prediction

[4] An overshot gate behaves approximately like a sharp crested weir (Bos, 1978)

error method with quadratic criterion, i.e.

$$\hat{\theta}_{p,LNB} = \underset{\theta_{p,LNB}}{\operatorname{argmin}} \frac{1}{N} \sum_{t=1}^{N} [y_{mea,BW}(t) - \hat{y}_{sim,BW}(t, \theta_{p,LNB})]^2 \tag{4.22}$$

where $N = 800$ is the length of the data used for estimation, $\theta_{p,LNB} = [c_{weir,BW}, n_{LNB}]^T$. $y_{mea,BW}$ and $\hat{y}_{sim,C}$ are the measured and simulated water level using the Saint Venant equations at Broken Weir respectively. The estimated parameters are shown in Table 4.3 and the estimated parameters between the two data sets are quite similar. The results are discussed on page 113 together with the results from empirical modelling.

Empirical modelling:

As mentioned, the manual regulation gate at Broken Weir is in the process of being replaced by a fully automated regulation gate. With this infrastructure upgrade, the flow at Broken Weir can be regulated independently of the upstream flow. Thus, the time delay model is no longer suitable and we consider the integrator delay model to model this reach. Using the mass balance equations, we have

$$\dot{V}_{BW}(t) = Q_{LN}(t - \tau_{LN}) + Q_{LC}(t - \tau_{LC}) - Q_{BW}(t) \tag{4.23}$$

where V is the volume, Q_i with $i =$ LN (Lake Nillahcootie), LC (Lima Creek) and BW (Broken Weir) are the flows and τ_{LN} and τ_{LC} are the time delays. Normally, a rating curve would be used to relate the water depth to flow. In the absence of a reliable rating curve at Lima Creek, we use a local linear relationship, which is given by

$$Q_{LC} \approx a_{LC} \breve{y}_{LC} + \Delta_{LC} \tag{4.24}$$

where a_{LC} and Δ_{LC} are constants. We use the notation $\breve{y}$ to denote water depth to avoid any confusion.

Substituting Equations (4.21) and (4.24) into (4.23), assuming that the water level is proportional to the volume and using an Euler approximation for the derivative, we arrive

at

$$y_{BW}(k+1) = y_{BW}(k) + \left(\frac{T_s}{A}\right) Q_{LN}(k-\tau_{LB}) + \left(\frac{T_s}{A}\right) a_{LC}\breve{y}_{LC}(k-\tau_{LC}) - \left(\frac{T_s}{A}\right) c_{BW}[y_{BW}(k)-p_{BW}]^{3/2} + \left(\frac{T_s}{A}\right)\Delta_{LC} \tag{4.25}$$

where k denotes the discrete time. T_s is the sampling interval, A is the surface area and $p_{BW} = 173.10$ mAHD.

The associated "Output Error" (OE) predictor for Equation (4.25) is

$$\hat{y}_{BW}(k+1,\theta_{e,LNB},\tau_{LN}) = \hat{y}_{BW}(k,\theta_{e,LNB},\tau_{LB}) + \theta_{e,LNB,1}Q_{LB}(k-\tau_{LB}) + \theta_{e,LNB,2}\breve{y}_{LC}(k-\tau_{LC}) + \theta_{e,LNB,3}[\hat{y}_{BW}(k,\theta_{e,LNB},\tau_{LN}) - p_{BW}]^{3/2} + \theta_{e,LNB,4} \tag{4.26}$$

$\theta_{e,LNB} = [\theta_{e,LNB,1},\theta_{e,LNB,2},\theta_{e,LNB,3},\theta_{e,LNB,4}]^T = [\left(\frac{T_s}{A}\right), \left(\frac{T_s a_{LC}}{A}\right), \left(\frac{T_s c_{BW}}{A}\right), \left(\frac{T_s \Delta_{LC}}{A}\right)]^T$. An OE model is used here as it usually gives a good description of a system in the low frequency range (see e.g. (Ljung, 1999)), which is of most interest for control design. Notice that this predictor makes use of only the initial values of the water level and makes prediction using the previously predicted water levels.

As in Section 4.3.2, the time delays τ_{LN} and τ_{LC} are estimated from the cross-correlation between the measurements at Lake Nillahcootie and Broken Weir and Lima Creek and Broken Weir. The cross-correlation coefficient plots are shown in Figure 4.15 and the estimated time delays are $\tau_{LN} = 3060$ minutes and $\tau_{LC} = 1620$ minutes. We note that there is a lot uncertainty in the cross-correlation coefficient plot as shown by the almost flat curve near the maximum value of the plot.

The parameter $\theta_{e,LNB}$ is estimated using a prediction error method with quadratic criterion, i.e.,

$$\hat{\theta}_{e,LNB,\tau_{LN}} = \underset{\theta_{e,LNB,\tau_{LN}}}{\operatorname{argmin}} \frac{1}{N}\sum_{k=1}^{N}[y_{BW}(k) - \hat{y}_{BW}(k,\theta_{e,LNB},\tau_{LN})]^2 \tag{4.27}$$

where $N = 800$, y_{BW} is the measured water level and $\hat{y}_{BW}$ is the predicted water level using Equation (4.26). As in the physical modelling approach, the data set on the left of

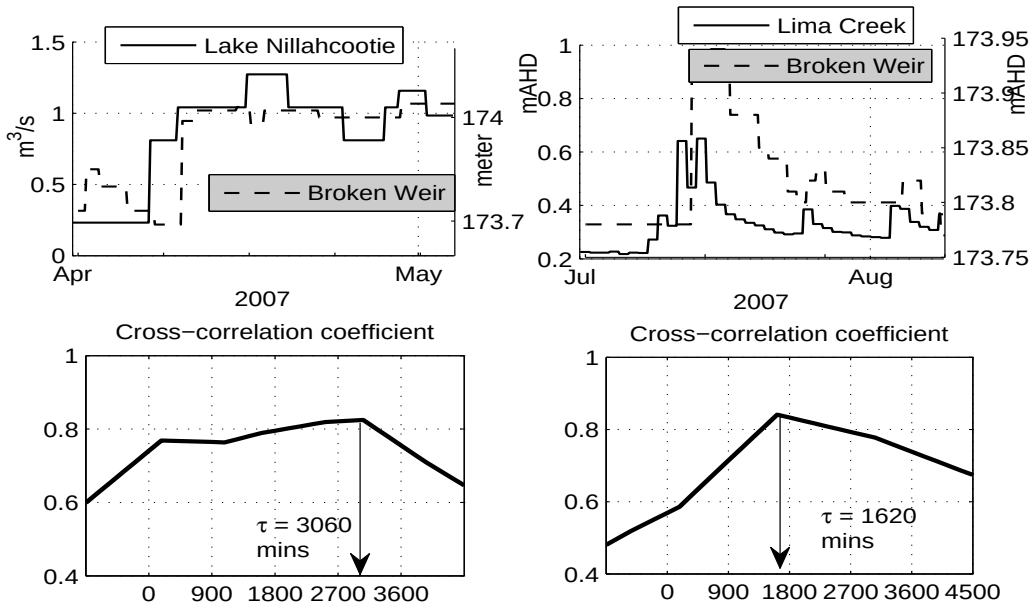

Figure 4.15: Cross-correlation coefficients and estimated time delays for Reach LNB.

Figure 4.14 are used for estimation and validated on the data set on the right of Figure 4.14. We also use the data set on the right of Figure 4.14 for estimation and validate on the data set on the left of Figure 4.14. The estimated parameters are given in Table 4.4. From Table 4.4, we can see that the values of $\hat{\theta}_{e,LNB,1}$ and $\hat{\theta}_{e,LNB,2}$ are positive,

Table 4.4: Parameter estimates for Reach LNB.

Estimation Set	$\hat{\theta}_{e,LNB,1}$	$\hat{\theta}_{e,LNB,2}$	$\hat{\theta}_{e,LNB,3}$	$\hat{\theta}_{e,LNB,4}$
Apr-Jul 2007	0.048	0.117	-0.108	0.028
Apr-Jul 2008	0.335	0.754	-0.691	0.180

which is in agreement with the interpretation of in-flow and the negative value of $\hat{\theta}_{e,LNB,3}$ is in agreement with the interpretation of out-flow. We also notice that these estimated parameters are very different between the two years with larger values observed for the data from April to July 2008. The difference of the estimated parameter between the two data set is approximately with a factor of 7. An inspection on the data (Figure 4.14), we noticed that the flows at Lake Nillahcootie and the water depths at Lima Creek in

2008 data set are smaller than the flows and water depths in 2007 data despite having the almost similar water levels at Broken Weir. This difference of flow conditions may have led to the large difference in the estimated parameters between the two years. The decommissioning of Lake Mokoan in middle of 2008 ((Mokoan Wetlands, 2006)) is another source of uncertainty. Another possible reason is the local linear assumption for Lima Creek, which may not be a suitable to model the flow and water depth relationship. The assumption where Broken Weir can be modelled as a sharp crested weir also add to the uncertainty. The asymptotic covariance of the parameter estimates is further investigated in Section 4.6.

Discussion:

One thing we want to highlight is that the estimated parameters in the Saint Venant equations are similar between the two data sets but large variations is observed for the integrator delay model between the two data sets. As there is a lot of assumption made and uncertainties present, we do not want to make any further conclusion but merely point out this matter.

Using the values of the estimated parameter in Tables 4.2 and 4.4, we simulate the water level using the Saint Venant equations and Equation (4.26) on the data set not used for estimation to validate our model. Figure 4.16 shows the measured water levels, the predicted water levels using the integrator delay model and the simulated water levels using the Saint Venant equations.

Table 4.5: Values of MSE.

Validation Set	Predictor (4.26) MSE	Saint Venant MSE
Apr-Jul 2007	3.71 (10^{-3}m^2)	5.81 (10^{-3}m^2)
Apr-Jul 2008	1.36 (10^{-3}m^2)	1.30 (10^{-3}m^2)

For quantitative comparison, the MSEs are calculated using Equation (4.28) and they are given in Table 4.5.

$$\text{MSE} = \frac{1}{N}\sum_{k=1}^{N}[y_{mea,BW}(k) - \hat{y}_{BW}(k, \theta_{x,LNB}, \tau_{LNB})]^2 \tag{4.28}$$

where the subscript $x = p, e$, $y_{mea,BW}$ is the measured water levels and $\hat{y}_{BW}$ is either the simulated water levels from Saint Venant equations or the predicted water levels using Equation (4.26) at Broken Weir.

From Figure 4.16, it is observed that in general, both the integrator delay model and the Saint Venant equations pick up the general trend of the water level well. Although the simulated water levels do not pick up some of the peaks and dips well, the difference is small, i.e. within ±5cm. In view of the effect of rainfall and offtakes to irrigation are not considered in the model, the assumption of a local linear relationship at Lima Creek and the assumption of the flow at Broken Weir can be modelled using a sharp crested weir, we do not want to draw any strong conclusion. However, what is encouraging is that the integrator delay model picks up the general trends well and it is as accurate as the Saint Venant equations.

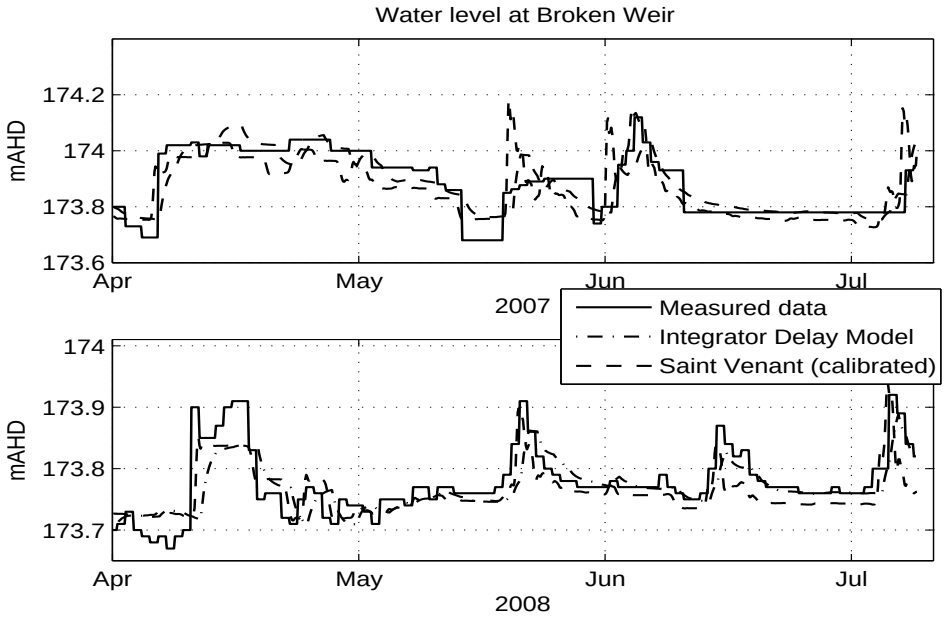

Figure 4.16: Measured and simulated water levels. Top: April to July 2007. Bottom: April to July 2008.

4.5.2 Modelling of river reach with storage capabilities

Reach Lake Benalla to Casey's Weir

Physical modelling:

We consider the reach from Lake Benalla to Casey's Weir. For simplicity, we call this reach, Reach LBC. For this reach, there is a weir pool at Casey's Weir. There is also an out-flow to Broken Creek just upstream of Casey's Weir. Based on the on-site survey carried out by GBCMA (GBCMA, 2009), the approximate river parameters for this reach are summarised in Table 4.6. Notice that the range of values shown in Table 4.6 are rather big as it

Table 4.6: Summary of river parameters for Reach LBC.

Parameters	**Values**
Reach Length, L_{LBC}	12260m
Bottom width, b_{LBC}	15-150m
Side slope, s_{LBC}	2.5-10
Bottom slope, $S_{0,LBC}$	0.0003-0.0010
Manning friction coefficient, n_{LBC}	0.08-0.20

includes Lake Benalla. The measurements at Lake Benalla, are obtained approximately 400m upstream of the weir at Lake Benalla. The measured data are shown in Figure 4.17, which are taken from October 2010 to April 2011. The sampling interval is 3 hours (180 minutes). There is no measurement of flow available at Lake Benalla. In addition, the flows at Casey's Weir and Broken Creek shown in Figure 4.17 are not physically measured but computed from the water level based on a water level-to-flow conversion table used by the water authority. The elevation at Lake Benalla is 167.62mAHD while for Casey's Weir and Broken Creek, the elevation is 161.07mAHD.

Like before, we aim to validate the Saint Venant equations for Reach LBC by calibrating it against the measured data. The input to the Saint Venant equations is the flow out of Lake Benalla. The hydraulic structure at Lake Benalla can be approximated by a sharp crested weir using

$$Q_{LB}(t) \approx \bar{c}_{weir,LB} h_{LB}^{3/2}(t) = \bar{c}_{LB}[y_{LB}(t) - p_{LB}]^{3/2} \tag{4.29}$$

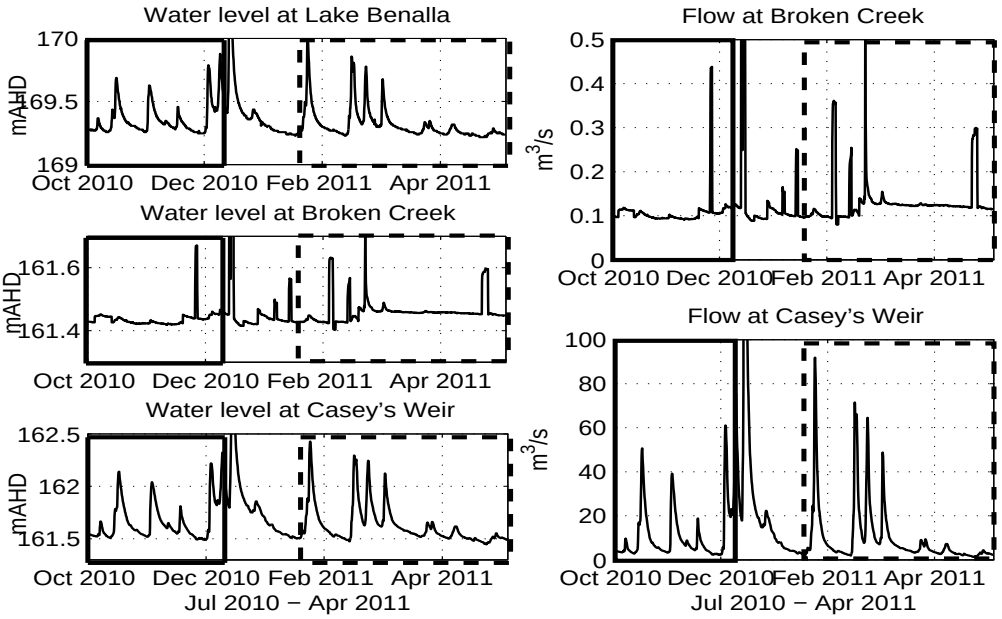

Figure 4.17: Flow and Water level for Reach LBC. Right: Water level. Left: Flow. NOTE: There is no flow measurement available at Lake Benalla.

where $p_{LB} = 169.12$mAHD is the height of the weir and $\bar{c}_{weir,LB}$ is the "modified" weir constant. We use the term "modified" weir constant here, as we make the assumption that the water levels are almost constant from the location where the measurements are obtained (i.e. the middle of the lake) to the weir at Lake Benalla. Thus, we use $\bar{c}_{weir,LB}$ to denote the "modified" weir constant to avoid any confusion with the interpretation of weir constant used throughout the thesis. The use of Equation (4.29) to relate the flow and water level at Lake Benalla may not be a suitable choice, and ideally a rating curve should be used. However, in the absence of a rating curve, we have used Equation (4.29).

At the downstream, Casey's Weir resembles a sharp crested weir where the flow can be approximated by

$$Q_C(t) \approx c_{weir,C} h_C^{3/2}(t) = c_{weir,C}[y_C(t) - p_C]^{3/2} \tag{4.30}$$

where $p_C = 161.37$mAHD is the height of the weir. $c_{weir,C} \approx 0.6\sqrt{g} b_{weir,C}$ is the weir constant for Casey's Weir.

Again, we use Single segmentation for this reach, where the average bottom width

$b_{LBC} = 20.9$m and side slope $s_{LBC} = 3.5$ after the lake is used. Using the elevations, the average bottom slope is (167.62-161.07)mAHD/9260 ≈ 0.0007. The weir constant $c_{weir,C}$ and the Manning friction coefficient n_{LBC} will be estimated from the data. In addition, considering that the measurements are not obtained near the weir $\bar{c}_{weir,LB}$ will also be estimated from data. We use the data set in the solid rectangular box (October to December 2010) for estimation and validate the model on the data set in the dotted rectangular box (January to April 2011). We also use the data set in the dotted rectangular box for estimation and validate the model on the data set in the solid rectangular box. The data set outside both the rectangular boxes (i.e. late December 2010 to early January 2011) are not used due to the abnormal high flows. These parameters are estimated using prediction error method with quadratic criterion, i.e.

$$\hat{\theta}_{p,LBC} = \underset{\theta_{p,LBC}}{\operatorname{argmin}} \frac{1}{N} \sum_{t=1}^{N} [y_{mea,C}(t) - \hat{y}_{sim,C}(t, \theta_{p,LBC})]^2 \tag{4.31}$$

where N is the length of data used for estimation (i.e. $N = 530$ (October to December 2010) and $N = 795$ (January to April 2011)), $\theta_{p,LBC} = [\bar{c}_{weir,LB}, c_{weir,C}, n_{LBC}]^T$. $y_{mea,C}$ and $\hat{y}_{sim,C}$ are the measured and simulated water level using the Saint Venant equations at Casey's Weir respectively. The estimated parameters are shown in Table 4.7. We simulate the Saint Venant equations using the estimated parameters on the data set not used for estimation and the results are shown in Figure 4.19, where we observe that the estimated parameters between the two data sets are similar. The results are discussed in page 120 together with the result using empirical modelling.

Table 4.7: Estimated parameters for Reach LBC.

Estimation Set	$\hat{\bar{c}}_{weir,LB}$	$\hat{c}_{weir,C}$	$\hat{n}_{LBC}$
Oct-Dec 2010	131.55m$^{3/2}$/s	84.49m$^{3/2}$/s	0.1372
Jan-Apr 2011	133.42m$^{3/2}$/s	83.04m$^{3/2}$/s	0.1503

Empirical modelling:

In view of the weir pool at Casey's Weir, which acts as a storage, we consider the integrator delay model to model this reach. Using the mass balance equations, we have

$$\dot{V}_C(t) = Q_{LB}(t - \tau_{LB}) - Q_C(t) - Q_{BC}(t) \tag{4.32}$$

where V is the volume, Q_i with $i =$ LB (Lake Benalla), C (Casey's Weir) and BC (Broken Creek) are flows and τ_{LB} is the time delay.

Substituting Equations (4.29) and (4.30) into (4.32), assuming that the water level is proportional to the volume and using an Euler approximation for the derivative, we arrive at

$$\begin{aligned} y_C(k+1) = y_C(k) &+ \left(\frac{T_s}{A}\right) \bar{c}_{weir,LB}[y_{LB}(k - \tau_{LB}) - p_{LB}]^{3/2} \\ &- \left(\frac{T_s}{A}\right) c_{weir,C}[y_C(k) - p_C]^{3/2} - \left(\frac{T_s}{A}\right) Q_{BC}(k) \end{aligned} \tag{4.33}$$

where k is the discrete time index. T_s is the sampling interval, A is the surface area. The associated OE predictor for Equation (6.9) is

$$\begin{aligned} \hat{y}_C(k+1, \theta_{e,LBC}, \tau_{LB}) = \hat{y}_C(k, \theta_{e,LBC}, \tau_{LB}) &+ \theta_{e,LBC,1}[y_{LB}(k - \tau_{LB}) - p_{LB}]^{3/2} \\ &+ \theta_{e,LBC,2}[\hat{y}_C(k, \theta_{e,LBC}, \tau_{LB}) - p_C]^{3/2} + \theta_{e,LBC,3} Q_{BC}(k) \end{aligned} \tag{4.34}$$

where $\theta_{e,LBC} = [\theta_{e,LBC,1}, \theta_{e,LBC,2}, \theta_{e,LBC,3}]^T = [\left(\frac{T_s}{A}\right) \bar{c}_{weir,LB}, \left(\frac{T_s}{A}\right) c_{weir,C}, \left(\frac{T_s}{A}\right)]^T$.

The time delay $\tau_{LB} = 540$ minutes is estimated from the cross-correlation between the measurements at Lake Benalla and Casey's Weir as shown in Figure 4.18. The parameter $\theta_{e,LBC}$ is estimated using prediction error method with a quadratic criterion, i.e.

$$\hat{\theta}_{e,LBC,\tau_{LB}} = \underset{\theta_{e,LBC,\tau_{LB}}}{\operatorname{argmin}} \frac{1}{N} \sum_{k=1}^{N} [y_C(k) - \hat{y}_C(k, \theta_{e,LBC}, \tau_{LB})]^2 \tag{4.35}$$

where N is the length of the data set used for estimation (i.e. $N = 530$ (October to December 2010) and $N = 795$ (January to April 2011)), y_C is the measured water levels and $\hat{y}_C$ is the predicted water levels using Equation (4.34). The data set in the solid rectangular box (October to December 2010) shown in Figure 4.17 is used for estimation and validated against the data set in the dotted rectangular box (January to April 2011).

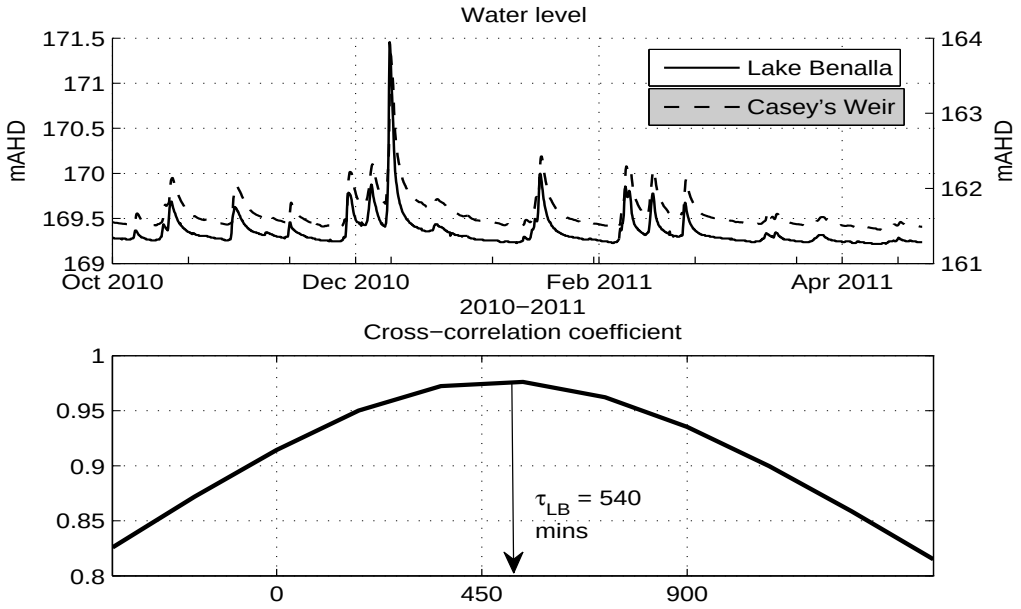

Figure 4.18: Cross-correlations and estimated time delays for Reach LBC. Right-axis: Casey's Weir, Left-axis: Lake Benalla

We also use the data set in the dotted rectangular box (January to April 2011) for estimation and validate the model against the data set in the solid rectangular box (October to December 2010). The data set outside the rectangular boxes are not used due to the abnormal high flows. Furthermore, these abnormal flow is beyond the operating range of the controller. The estimated parameters are given in Table 4.8. From Table 4.8, we can

Table 4.8: Parameter estimates for Reach LBC.

Estimation Set	$\hat{\theta}_{e,LBC,1}$	$\hat{\theta}_{e,LBC,2}$	$\hat{\theta}_{e,LBC,3}$
Oct-Dec 2010	2.200	-1.394	-0.226
Jan-Apr 2011	2.069	-1.316	-0.098

see that the values of $\hat{\theta}_{e,LBC,1}$ are positive which is in agreement with an in-flow and the values of $\hat{\theta}_{e,LBC,2}$ and $\hat{\theta}_{e,LBC,3}$ are negative which is in agreement with an out-flow. The estimated parameters are very similar between the two data sets with the exception of $\hat{\theta}_{e,LBC,3}$. The asymptotic covariance matrices are computed in Section 4.6.

Discussion:

Using the values of the estimated parameter in Tables 4.6 and 4.8, we simulate the water level using the Saint Venant equations and Equation (4.34) on the validation data set in order to validate our model. For quantitative comparison, the MSE is calculated using Equation (4.36) and the values are given in Table 4.9.

$$\text{MSE} = \frac{1}{N}\sum_{k=1}^{N}[y_{mea,C}(k) - \hat{y}_C(k, \theta_{x,LBC}, \tau_{LB})]^2 \tag{4.36}$$

Here, the subscript $x = p, e$, $y_{mea,C}$ is the measured water levels at Casey's Weir and $\hat{y}_C$ is either the simulated water level using the Saint Venant equations or the predicted water levels using Equation (4.34).

Figure 4.19 shows the measured water levels, and predicted water levels using the integrator delay model and simulated water levels the Saint Venant equations. The values of MSE are shown in Table 4.9 From Figure 4.19, it is observed both the integrator delay

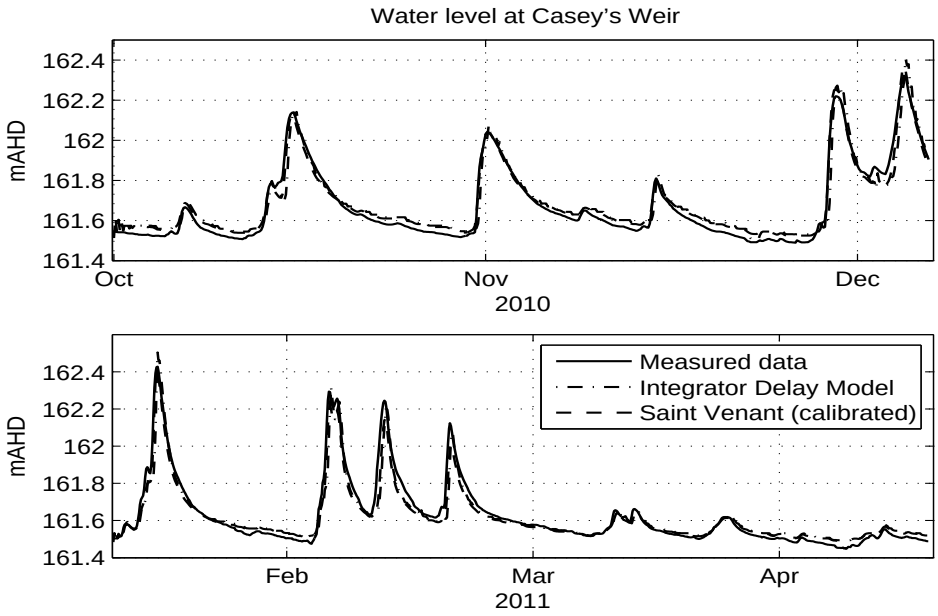

Figure 4.19: Measured and simulated water levels. Top: October to December 2010. Bottom: January to April 2011.

model and the Saint Venant equations are able to pick up the general trend of the water

Table 4.9: Values of MSE.

Validation Set	Predictor (4.34) MSE	Saint Venant MSE
Oct-Dec 2010	2.65 (10^{-3}m^2)	0.96 (10^{-3}m^2)
Jan-Apr 2011	2.82 (10^{-3}m^2)	0.83 (10^{-3}m^2)

level very well. The predictive capabilities of the integrator delay model is very good, bearing in mind that the predictor only make use of the initial value of the water level to make predictions. In terms of MSE, the integrator delay model has a slightly larger MSE compared to the Saint Venant equations but in general the MSE is small. Since the aim is to obtain a model to be used for control design, the integrator delay model is preferred as it is simpler compared to the Saint Venant equations.

Reach Poison Creek to Lake Benalla

Physical modelling:

We consider the reach from Poison Creek to Lake Benalla and we call this reach, Reach PLB. Ideally, we would like to build the river model from Broken Weir[5] to Lake Benalla. However, due to the absence of data at Broken Weir, the data from Poison Creek are used instead. Despite the name, the data is not collected at Poison Creek but in the Broken River itself. Poison Creek is located approximately 2km upstream of Broken Weir. This reach includes Lake Benalla, which acts as a storage. There is in-flow from a creek called Hollands Creek. Based on the on-site survey carried out by GBCMA (GBCMA, 2009), the approximate river parameters for this reach are summarised in Table 4.10. The large range of values for the bottom width and the side slope is due to Lake Benalla. The measurements at Lake Benalla are obtained approximately 400m upstream of the weir at Lake Benalla. The measured water levels are shown in Figure 4.20. These measurements are from October to November 2010 and are taken every 3 hours (180 minutes). The elevation at Poison Creek, Hollands Creek and Lake Benalla are 177.81mAHD, 181.63mAHD and 167.62mAHD respectively. The elevation at the in-let of Lake Benalla is 168.09mAHD.

[5]The data for Broken Weir is only available for the period from 2007-2008 and no data is available at Lake Benalla for the same time period.

Table 4.10: Summary of river parameters for Reach PLB.

Parameters	**Values**
Reach Length, L_{PLB}	13.4km
Bottom width, b_{PLB}	10-150m
Side slope, s_{PLB}	2.5-10
Bottom slope, $S_{0,PLB}$	0.00072-0.00075
Manning friction coefficient, n_{PLB}	0.07-0.10

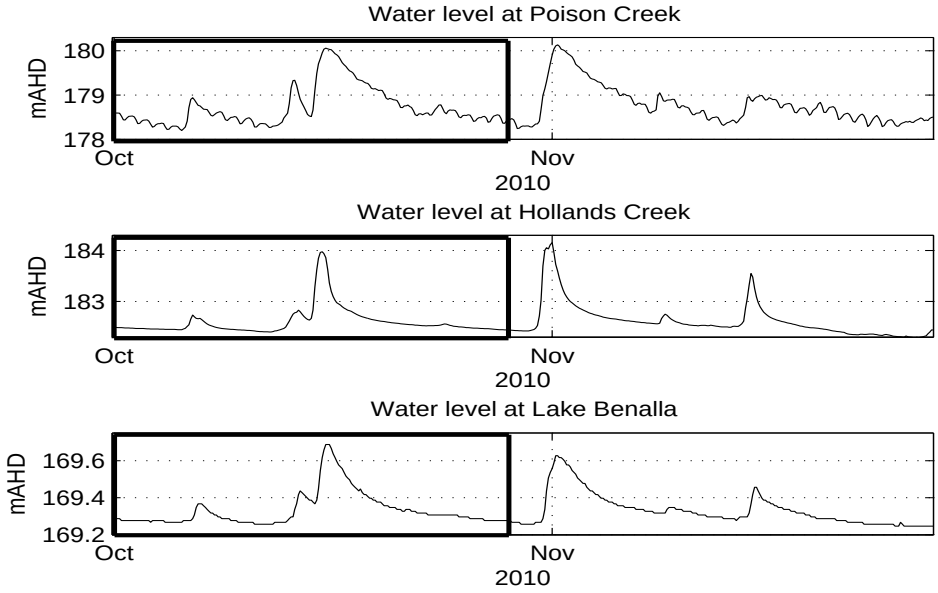

Figure 4.20: Water levels measurements for Reach PLB.

The input to the Saint Venant equations is the flow at Poison Creek. The in-flow from Hollands Creek is treated as a lateral flow to the Saint Venant equations. As there is no flow measurements available at these two locations, we use a rating curve. Note that, water depth is normally used instead of water level in rating curves. The water depth $\breve{y}$ is obtained from the water level y by subtracting the elevation, i.e. $y = \breve{y} + \text{elevation}$.

The flow for Poison Creek and Hollands Creek can be computed from the water depth using

$$Q_{PC} \approx m_{PC} \breve{y}_{PC}^{k_{PC}} \tag{4.37}$$

$$Q_{HC} \approx m_{HC} \breve{y}_{HC}^{k_{HC}} \tag{4.38}$$

where $m_{PC} = 1.8$, $m_{HC} = 2.4$, $k_{PC} = 1.2$ and $k_{HC} = 3.1$. The rating curve for Hollands Creek is obtained from Victorian Water Resources Data Warehouse (Victorian Water Resources, 2009) while the rating curve for Poison Creek is obtained from (Costelloe, 2010). The hydraulic structure at Lake Benalla resembles a sharp crested weir, where the flow can be approximated using

$$Q_{LB}(t) \approx c_{weir,LB} h_{LB}^{3/2}(t) = c_{weir,LB} [\breve{y}_{LB}(t) - p_{LB}]^{3/2} \tag{4.39}$$

where $p_{LB} = 1.5$m is the height of the weir, $c_{weir,LB} \approx 0.6\sqrt{g} b_{weir,LB}$. Note that $c_{weir,LB}$ is used here to denote the conventional weir as opposed to $\bar{c}_{weir,LB}$ used in Reach LBC.

For this reach, we use M-segment segmentation (see Section 3.2) with M = 2. One segment is from Poison Creek to the start of Lake Benalla and a separate segment for Lake Benalla. The average bottom widths $b_{PLB,1} = 13.2$m and $b_{PLB,2} = 112.0$m and the average side slopes $s_{PLB,1} = 2.9$ and $s_{PLB,2} = 7.8$ are used for the two segments. Using the given elevations, the average bottom slopes are given by (177.81-168.09)mAHD/12400 ≈ 0.0008 and (168.09-167.62)mAHD/1000 ≈ 0.0005. The Manning friction coefficients for the two segments, i.e. $n_{PLB,1}$ and $n_{PLB,2}$ will be estimated from the data together with the weir constant $c_{weir,LB}$.

The data set shown in the rectangular box is used for estimation while the data set outside the rectangular box is used for validation. We also use the data set outside the rectangular box for estimation and validate it on the data set in the rectangular box. The parameters are estimated using a prediction error method with quadratic criterion, i.e.

$$\hat{\theta}_{p,PLB} = \underset{\theta_{p,PLB}}{\operatorname{argmin}} \frac{1}{N} \sum_{t=1}^{N} [\breve{y}_{mea,LB}(t) - \hat{\breve{y}}_{sim,LB}(t, \theta_{p,PLB})]^2 \tag{4.40}$$

where N is the length of the data used for estimation (i.e. $N = 170$ (October 2010) and $N = 280$ (November 2010)), $\theta_{p,PLB} = [c_{LB}, n_{PLB,1}, n_{PLB,2}]^T$. $\breve{y}_{mea,PC}$ and $\hat{\breve{y}}_{sim,PC}$ are the measured and simulated water depths using the Saint Venant equations at Lake Benalla.

The estimated parameters are shown in Table 4.11.

From Table 4.11, one would notice that the estimated value for $\hat{c}_{weir,LB}$ is different compared to the value of $\hat{\bar{c}}_{weir,LB}$ obtained in Table 4.7. The reason for this is that the estimated value of $\hat{\bar{c}}_{weir,LB}$ in Reach LBC is inferring that the width of the weir is similar

Table 4.11: Estimated parameters for Reach PLB.

Estimation Set	$\hat{c}_{weir,LB}$	$\hat{n}_{PLB,1}$	$\hat{n}_{PLB,2}$
Oct 2010	$20.67\text{m}^{3/2}/\text{s}$	0.08	0.10
Nov 2010	$22.55\text{m}^{3/2}/\text{s}$	0.09	0.09

to the width of the lake, which make sense considering the width of the lake is much larger than the width of an actual weir. On the other hand, the estimated value of $\hat{c}_{weir,LB}$ in Reach PLB is referring to the actual weir itself, thus resulting in the difference between the two values.

Using the values of the estimated parameter, we simulate the Saint Venant equations and the results are shown in Figure 4.22. The estimated parameters between the two data sets again is similar. Again, the discussion of the results are given in page 126 together with the empirical modelling.

Empirical modelling:

As Lake Benalla acts as a storage, we again consider the integrator delay model to model this reach. Using the mass balance equations, we have

$$\dot{V}_{LB}(t) = Q_{PC}(t - \tau_{PC}) + Q_{HC}(t - \tau_{HC}) - Q_{LB}(t) \tag{4.41}$$

where V is the volume, Q_i and τ_i with $i =$ PC (Poison Creek) and HC (Hollands Creek) are the flows and time delays respectively. As we are using the rating curve to compute the flows at Poison Creek and Hollands Creek, we need to work with water depth instead of water level. Substituting Equations (4.37), (4.38) and (4.39) into (4.41), assuming that the water depth is proportional to the volume and using an Euler approximation for the derivative, we arrive at

$$\begin{aligned}\breve{y}_{LB}(k+1) = \breve{y}_{LB}(k) &+ \left(\frac{T_s}{A}\right) m_{PC} \breve{y}_{PC}^{k_{PC}}(k - \tau_{PC}) + \left(\frac{T_s}{A}\right) m_{HC} \breve{y}_{HC}^{k_{HC}}(k - \tau_{HC}) \\ &- \left(\frac{T_s}{A}\right) c_{LB}[\breve{y}_{LB}(k) - p_{LB}]^{3/2}\end{aligned} \tag{4.42}$$

where k is the discrete time. T_s is the sampling interval, A is the surface area.

The associated OE predictor for Equation (4.42) is

$$\hat{\breve{y}}_{LB}(k+1,\theta_{e,PLB},\tau_{PC}) = \hat{\breve{y}}_{LB}(k,\theta_{e,PLB},\tau_{PC}) + \theta_{e,PLB,1}\breve{y}^{1.2}_{PC}(k-\tau_{PC}) + \theta_{e,PLB,2}\breve{y}^{3.1}_{HC}(k-\tau_{HC}) + \theta_{e,PLB,3}[\hat{\breve{y}}_{LB}(k,\theta_{e,PLB},\tau_{PC}) - p_{LB}]^{3/2} \tag{4.43}$$

where $\theta_{e,PLB} = [\theta_{e,PLB,1}, \theta_{e,PLB,2}, \theta_{e,PLB,3}]^T = [(\frac{T_s}{A})\, m_{PC}, (\frac{T_s}{A})\, m_{HC}, (\frac{T_s}{A})\, c_{LB}]^T$ and $\tau = [\tau_{PC}, \tau_{HC}]$.

The time delays $\tau_{PC} = 540$ minutes and $\tau_{HC} = 540$ minutes are estimated from the cross-correlations between Poison Creek and Lake Benalla and Hollands Creek and Lake Benalla and they are shown in Figure 4.21. The estimated τ_{PC} and τ_{HC} are the same as the distance of the measuring station at Hollands Creek to the measuring station at Lake Benalla is similar to the distance from the measuring station at Poison Creek to the measuring station at Lake Benalla.

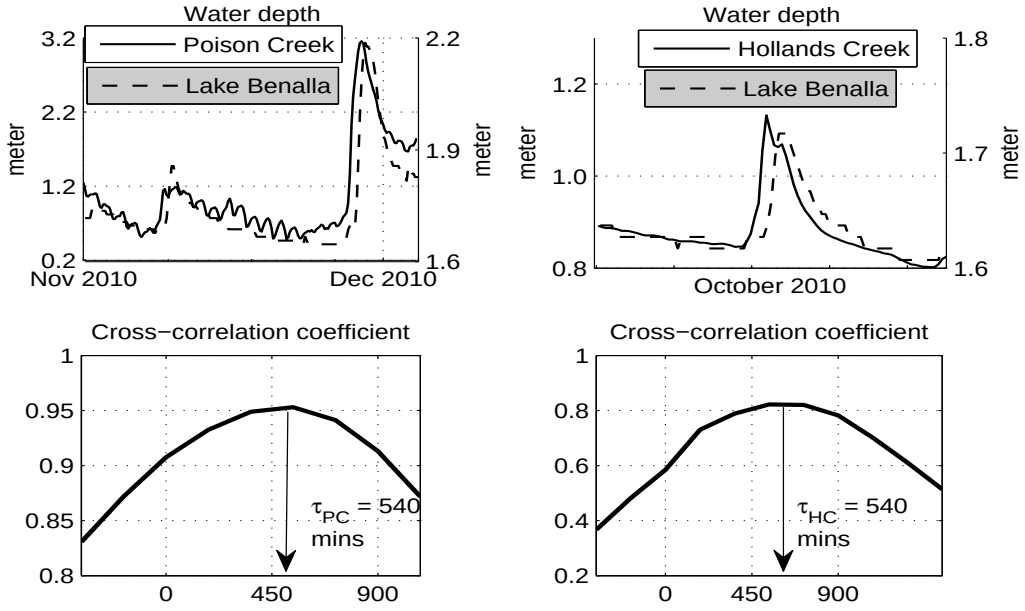

Figure 4.21: Cross-correlation coefficients and estimated time delays for Reach PLB. Water level plots: Right-axis: Lake Benalla, Left-axis: Poison Creek (top left) and Holland Creek (top right)

The parameter $\theta_{e,PLB}$ is estimated using a prediction error method with a quadratic

criterion, i.e.

$$\hat{\theta}_{e,PLB,\tau_{PC}} = \underset{\theta_{e,PLB,\tau_{PC}}}{\operatorname{argmin}} \frac{1}{N}\sum_{k=1}^{N}[\breve{y}_{LB}(k) - \hat{\breve{y}}_{LB}(k,\theta_{e,PLB},\tau_{PC})]^2 \tag{4.44}$$

where N is the length of the data set used for estimation (i.e. $N = 170$ (October 2010) and $N = 280$ (November 2010)), $\breve{y}_{LB}$ is the measured water depth and $\hat{\breve{y}}_{LB}$ is the predicted water depth using Equation (4.43). The estimated parameters are given in Table 4.12. From Table 4.12, we can see that the values of $\hat{\theta}_{e,PLB,1}$ and $\hat{\theta}_{e,PLB,2}$ are positive which is in

Estimation Set	$\hat{\theta}_{e,PLB,1}$	$\hat{\theta}_{e,PLB,2}$	$\hat{\theta}_{e,PLB,3}$
Oct 2010	0.173	0.022	-1.906
Nov 2010	0.163	0.021	-1.837

Table 4.12: Parameter estimates for Reach PLB.

agreement with an in-flow and the value of $\hat{\theta}_{e,PLB,3}$ is negative which is in agreement with an out-flow. The estimated parameters for the two data sets are similar. The asymptotic covariance are computed in Section 4.6.

Discussion:

Using the estimated parameters shown in Tables 4.10 and 4.12, we simulate the Saint Venant equations and Equation (4.43) using the data sets which are not used for estimation to validate our model. The MSE are calculated using

$$\text{MSE} = \frac{1}{N}\sum_{k=1}^{N}[\breve{y}_{mea,LB}(k) - \hat{\breve{y}}_{LB}(k,\theta_{x,PLB},\tau_{PC})]^2 \tag{4.45}$$

where the subscript $x = p, e$, $\breve{y}_{mea,LB}$ is the measured water levels at Lake Benalla and $\hat{\breve{y}}_{LB}$ is either the simulated water level using the Saint Venant equations or the predicted water level using Equation (4.43). When we plot the results, we add the elevation back to the water depth to obtain the water level. Figure 4.22 shows the measured and simulated water levels using Equation (4.43) and the Saint Venant equations, and the values of MSE are shown in Table 4.13.

From Figure 4.22, it is observed that in general both the models are able to pick up the general trend of the water level very well. The integrator delay model has good prediction

capability, bearing in mind again that it makes prediction using only the initial values of the water level. From the values of MSE, the integrator delay model is as accurate as the Saint Venant equations.

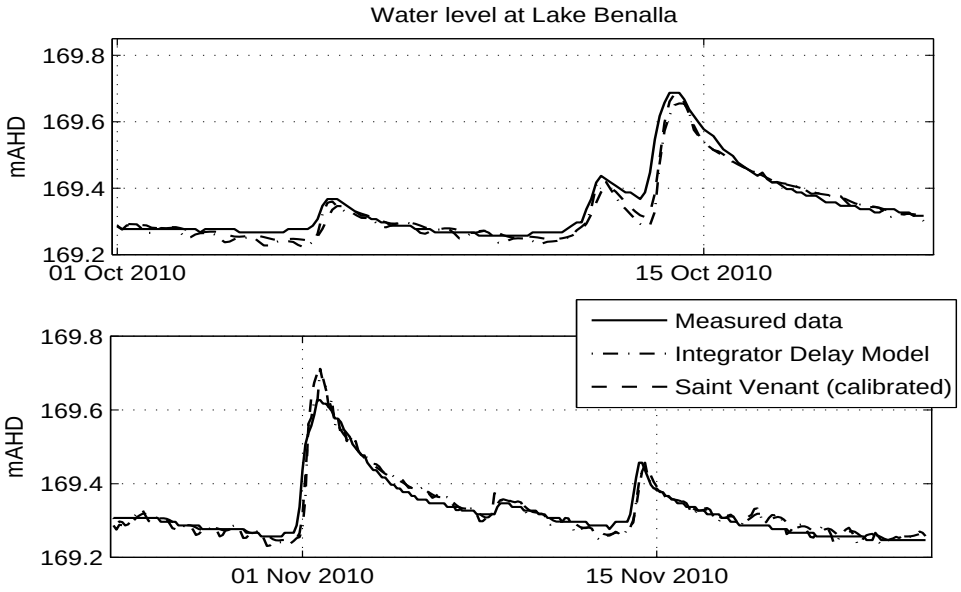

Figure 4.22: Measured and simulated water levels. Top: October 2010. Bottom: November 2010.

Validation Sets	Predictor (4.43) MSE	Saint Venant MSE
Oct 2010	1.21 (10^{-3}m^2)	0.80 (10^{-3}m^2)
Nov 2010	0.59 (10^{-3}m^2)	0.45 (10^{-3}m^2)

Table 4.13: Values of MSE.

4.6 Asymptotic distribution of parameter estimates

In the previous section, we have used the time delay and the integrator delay models to describe the dynamics of a river. The unknown parameters in those models are estimated using prediction error methods. An important question is how accurate is the estimate of

the parameters in the model. A measure of the quality of the estimate of the parameters in the model is given by the covariance matrix of the estimate.

4.6.1 Expression of the covariance matrix

We present a simplified version of the derivation of the expression for the covariance matrix. For more details see (Ljung, 1999) or (Söderström and Stoica, 1988). The unknown parameters are estimated using a prediction error method with quadratic criterion (e.g. Equation (4.27))

$$\begin{aligned}\hat{\theta}_N &= \underset{\theta}{\operatorname{argmin}}\, J_N(t,\theta) \\ &= \underset{\theta}{\operatorname{argmin}}\, \frac{1}{N}\sum_{t=1}^{N} e(t,\theta)^2 \end{aligned} \tag{4.46}$$

where $e(t,\theta) = y(t) - \hat{y}(t,\theta)$. The minimum can be found by differentiating $J_N(t,\theta)$ with respect to θ and set this to zero, i.e.

$$J'_N(t,\hat{\theta}_N) = 0 \tag{4.47}$$

where $'$ is used to represent the derivative. We will drop the variable t to avoid overloading of variables. Let θ^* be the true parameters (assuming they exists). Assume that $\hat{\theta}$ is located close to θ^* and that N is large enough. Expanding Equation (4.47) into a Taylor series around θ^* using the first two terms, we get

$$J'_N(\hat{\theta}_N) \approx J'_N(\theta^*) + J''_N(\theta^*)(\hat{\theta} - \theta^*) = 0 \tag{4.48}$$

Provided $J''_N(\theta^*)$ is invertible, we get

$$(\hat{\theta} - \theta^*) \approx -[J''_N(\theta^*)]^{-1} J'_N(\theta^*) \tag{4.49}$$

$J'_N(\theta^*)$ and $J''_N(\theta^*)$ are given by

$$J'_N(\theta^*) = \frac{2}{N}\sum_{t=1}^{N} -\frac{d}{d\theta^*}\hat{y}(t,\theta)\bigg|_{\theta=\theta^*} [y(t) - \hat{y}(t,\theta^*)] \tag{4.50}$$

$$J_N''(\theta^*) = \frac{2}{N}\sum_{t=1}^{N}\left(\frac{d}{d\theta^*}\hat{y}(t,\theta)\Big|_{\theta=\theta^*}\right)\left(\frac{d}{d\theta^*}\hat{y}(t,\theta)\Big|_{\theta=\theta^*}\right)^T + \frac{2}{N}\sum_{t=1}^{N}\left(\frac{d^2}{d\theta^{*2}}\hat{y}(t,\theta)\Big|_{\theta=\theta^*}\right)[y(t)-\hat{y}(t,\theta^*)] \tag{4.51}$$

The term $\frac{d^2}{d\theta^{*2}}\hat{y}(t,\theta^*)$ is small and thus can be neglected. Introducing $\psi(t,\theta) = \frac{d}{d\theta}\hat{y}(t,\theta)$, then Equations (4.50) and (4.51) becomes,

$$J_N'(\theta^*) = -\frac{2}{N}\sum_{t=1}^{N}\psi(t,\theta^*)e(t,\theta^*) \tag{4.52}$$

$$J_N''(\theta^*) = \frac{2}{N}\sum_{t=1}^{N}\psi(t,\theta^*)\psi(t,\theta^*)^T \tag{4.53}$$

For N large enough, Equation (4.53) is close to its expected value, i.e.

$$J_N''(\theta^*) \approx 2\mathbb{E}\psi(t,\theta^*)\psi(t,\theta^*)^T := 2R \tag{4.54}$$

Equation (4.52) is zero by definition (see Equation (4.47)) and if $\psi(t,\theta^*)$ is independent from $e(t,\theta^*)$, by central limit theorem $-\sqrt{N}J_N'(\theta^*)$ converges to a normal distribution with zero mean and variance given by

$$\mathbb{E}NJ_N'(\theta^*)J_N(\theta^*)^T = \frac{4}{N}\sum_{t=1}^{N}\sum_{s=1}^{N}\mathbb{E}\psi(t,\theta^*)\psi(s,\theta^*)\mathbb{E}e(s,\theta^*)E(t,\theta^*) = 4\lambda R \tag{4.55}$$

where we have assumed that $\mathbb{E}e(s,\theta^*)e(t,\theta^*) = \delta_{t-s}\lambda$. Putting together Equations (4.49), (4.54) and (4.55), we obtain

$$\sqrt{N}(\hat{\theta}_N - \theta^*) \to \mathcal{N}(0,P) \tag{4.56}$$

where $\mathcal{N}(0,P)$ denotes normal distribution with zero mean and covariance matrix P, which is given by

$$P = (2R)^{-1}[4\lambda R](2R)^{-1} = \lambda R^{-1} \tag{4.57}$$

In practice, P and λ can be approximated by using

$$\hat{P}_N = \hat{\lambda}_N \left[\frac{1}{N} \sum_{t=1}^{N} \psi(t, \hat{\theta}_N) \psi(t, \hat{\theta}_N)^T \right]^{-1} = \hat{\lambda}_N \hat{R}_N^{-1} \tag{4.58}$$

with

$$\hat{\lambda}_N = \frac{1}{N} \sum_{t=1}^{N} e(t, \hat{\theta}_N) = \frac{1}{N} \sum_{t=1}^{N} [(y(t) - \hat{y}(t, \hat{\theta}_N)]^2 \tag{4.59}$$

which is the MSE value. The value of $\hat{P}_N$, is an approximation of P, which is the covariance matrix of the asymptotic distribution. The covariance of $\hat{\theta}_N$ is given by

$$\text{Cov}\hat{\theta}_N \approx \frac{1}{N} \hat{P}_N \tag{4.60}$$

$\text{Cov}\hat{\theta}_N$ is proportional to $\hat{\lambda}_N$ and inversely proportional to the number of data point N, which make sense as the smaller the value of MSE and the more data point we have, the smaller the value of $\text{Cov}\hat{\theta}_N$. $\text{Cov}\hat{\theta}_N$ is also inversely proportional to $\psi(t, \hat{\theta}_N)$, which is the gradient of the prediction with respect to $\hat{\theta}_N$. Again this make sense, since the prediction error is most sensitive to changes in the direction of the gradient.

From the material presented above, to compute $\hat{P}_N$, we need to compute the gradient $\psi(t, \hat{\theta}_N)$. For the least square estimate, the gradient is the regressor $\varphi(t)$. For the nonlinear least square estimate, the gradient is normally computed in the minimisation algorithm. In MATLAB®, the gradient can be computed using the function *lsqnonlin* in the minimisation of the prediction error. The value of $\hat{P}_N$ also tells use how each of the elements of $\hat{\theta}_N$ are correlated. Thus, we can use this to compute the confidence intervals or ellipsoids to measure the quality of the estimates. As $\hat{\theta}_N - \theta^* \to \mathcal{N}(0, P_N)$, using the definition of χ^2-distribution, we have (Ljung, 1999)

$$(\hat{\theta}_N - \theta^*)^T P_N^{-1} (\hat{\theta}_N - \theta^*) \in \chi^2(d) \tag{4.61}$$

and the probability that

$$|\hat{\theta}_N - \theta^*|^2_{P_N^{-1}} = (\hat{\theta}_N - \theta^*)^T P_N^{-1} (\hat{\theta}_N - \theta^*) \geq \alpha \tag{4.62}$$

is given by $\chi^2(d)$-distribution, where d is the degree of freedom and α is the level of $\chi^2(d)$-distribution. Equation (4.62) is an ellipsoid. The direction of the ellipsoid is determined by the eigenvectors of P_N while the "size" of the principal axes of the ellipsoid is determined

by the eigenvalues of P_N.

4.6.2 Quality estimate of models

We compute the covariance matrices for the models of the reaches in Broken River. In addition, we construct the 95% confidence ellipsoid.

Notational remarks: In order to be consistent with the material presented in Section 4.57, the time index t is used to denote the discrete time index instead of k.

Reach Casey's Weir to Gowangardie Weir

The predictor for of the time delay model is given by

$$\hat{y}_G(t, \theta_{e,CG}, \tau_{CG}) = \theta_{e,CG,1} y_C(t - \tau_{CG}) + \theta_{e,CG,2} \tag{4.63}$$

with $\theta_{e,CG,1} = 2.711$ and $\theta_{e,CG,2} = -300.05$. The associated covariance matrix is given by

$$\hat{P}_{CG,N}(\hat{\theta}_{e,CG,N}) = \begin{bmatrix} 0.00005 & -0.00770 \\ -0.00770 & 1.24296 \end{bmatrix} \tag{4.64}$$

From Equation (4.64), the variances, given by the diagonal entries of Equation (4.64) for both $\theta_{e,CG,1}$ and $\theta_{e,CG,1}$ are small relative to the estimated parameters. The correlation between the two parameters are given by the off-diagonal entries of Equation (4.64). In constructing the confidence ellipsoid, we make use of Equations (4.61) and (4.62). As we have two parameters, χ^2-distribution with 2 degrees of freedom is the relevant distribution and the value of $\alpha = 5.99$ corresponds to a 95% confidence ellipsoid. The ellipsoid for the parameter estimates for Reach CG is shown in Figure 4.23.

The eigenvalues of $\hat{P}^{-1}_{CG,N}$ are given by $\lambda_{CG,1} = 0.805$ and $\lambda_{CG,2} = 4.349 \times 10^5$. The larger eigenvalue is the principal major axes of the ellipsoid while the smaller eigenvalue is the principal minor axes of the ellipsoid. The orientation of the ellipsoid is determined by the eigenvectors. The largest eigenvalue in the direction defined by its eigenvector represents the largest uncertainties of the parameter estimate.

The two parameters are negatively correlated. This means that if the uncertainty increases in the direction of $\theta_{e,CG,1}$ and the value of $\theta_{e,CG,2}$ decreases with it, the accuracy

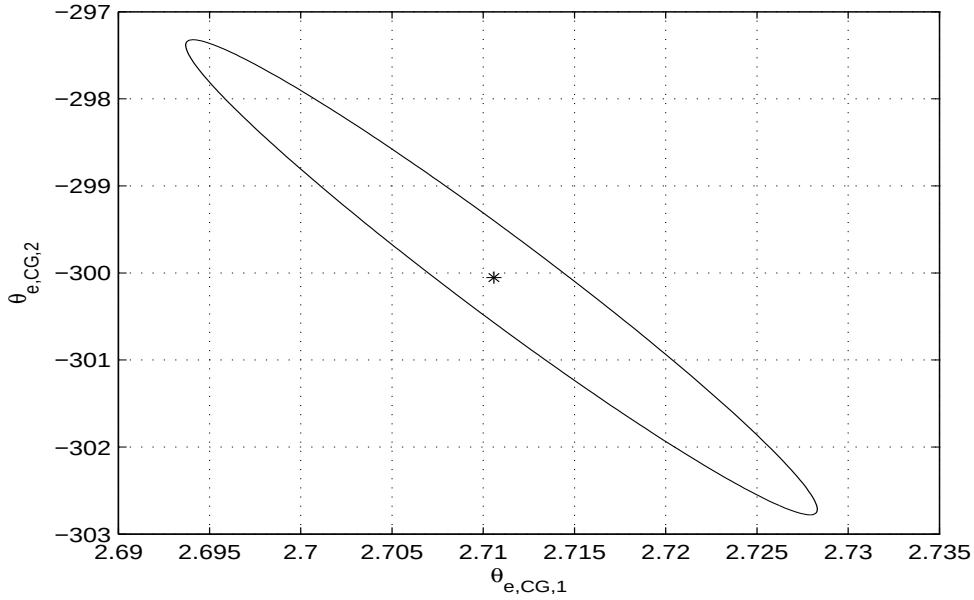

Figure 4.23: Ellipsoid for $\theta_{e,CG}$. '*' denotes the estimated values.

of the prediction made using Equation (4.63) is not affected much by the uncertainty. As an example, the water level at Casey's Weir y_C is always positive. Due to the uncertainty, we have an increase in $\theta_{e,CG,1}$ to $\theta_{e,CG,1,new} = 2.72$. The accuracy of the prediction model, i.e. Equation (4.63) will not be affected much if the offset value, $\theta_{e,CG,2}$ decreases to $\theta_{e,CG,2,new} = -301$, and still within the ellipsoid.

Reach Lake Nillahcootie to Broken Weir

The integrator delay model is used to model this reach. The associated predictor is given by

$$\begin{aligned}\hat{y}_{BW}(t+1, \theta_{e,LNB}, \tau_{LN}) = \hat{y}_{BW}(t, \theta_{e,LNB}, \tau_{LB}) + \theta_{e,LNB,1} Q_{LB}(t - \tau_{LB}) \\ + \theta_{e,LNB,2} \breve{y}_{LC}(t - \tau_{LC}) + \theta_{e,LNB,3} [\hat{y}_{BW}(t, \theta_{e,LNB}, \tau_{LN}) - p_{BW}]^{3/2} \\ + \theta_{e,LNB,4} \qquad (4.65)\end{aligned}$$

with $\theta_{e,LNB,1} = 0.048$, $\theta_{e,LNB,2} = 0.117$, $\theta_{e,LNB,3} = -0.108$ and $\theta_{e,LNB,4} = 0.028$ estimated from data set from April to July 2007 and $\theta_{e,LNB,1} = 0.335$, $\theta_{e,LNB,2} = 0.754$,

$\theta_{e,LNB,3} = -0.691$ and $\theta_{e,LNB,4} = 0.180$ estimated from data set from April to July 2008.

The associated covariance matrices for the two estimates are given by

$$\hat{P}_{LNB,N}(\hat{\theta}_{e,LNB,N})\Big|_{\text{Apr-Jul,2007}} = \begin{bmatrix} 0.1292 & 0.2858 & -0.2901 & 0.0820 \\ 0.2858 & 0.7250 & -0.6383 & 0.1577 \\ -0.2901 & -0.6383 & 0.6982 & -0.2167 \\ 0.0820 & 0.1577 & -0.2167 & 0.0804 \end{bmatrix} \times 10^{-4}$$

$$\hat{P}_{LNB,N}(\hat{\theta}_{e,LNB,N})\Big|_{\text{Apr-Jul,2008}} = \begin{bmatrix} 0.00120 & 0.00261 & -0.00243 & 0.00063 \\ 0.00261 & 0.00611 & -0.00531 & 0.00129 \\ -0.00243 & -0.00531 & 0.00510 & -0.00140 \\ 0.00063 & 0.00129 & -0.00140 & 0.00044 \end{bmatrix} \tag{4.66}$$

From Equation (4.66), we can see that the correlations between the parameters are large as some of the off-diagonal entries are larger than the diagonal entry. Looking at the diagonal entries, which are the variances of the parameters estimate, we observe that the variance for $\theta_{e,LNB,2}$ and $\theta_{e,LNB,3}$ is larger compared to the variance of $\theta_{e,LNB,1}$ and $\theta_{e,LNB,4}$. The large variance for $\theta_{e,LNB,2}$ could suggest that the local linear assumption for the rating curve at Lima Creek is not valid, while the large variance for $\theta_{e,LNB,3}$ could suggest that the assumption of the flow over Broken Weir can be modelled using a sharp crested weir is not a good approximation.

$\theta_{e,LNB,1}$ is positively correlated with $\theta_{e,LNB,2}$ and $\theta_{e,LNB,4}$. Likewise, $\theta_{e,LNB,2}$ is also positively correlated with $\theta_{e,LNB,4}$. On the other hand, $\theta_{e,LNB,3}$ is negatively correlated to $\theta_{e,LNB,1}$, $\theta_{e,LNB,2}$ and $\theta_{e,LNB,4}$. This means, if any uncertainty that lead to the increase of $\theta_{e,LNB,1}$, the values of $\theta_{e,LNB,2}$ and $\theta_{e,LNB,4}$ would also increase, while the value of $\theta_{e,LNB,3}$ would decrease and this would not affect the accuracy of the prediction made using Equation (4.65). In terms of physical interpretation, the accuracy of the predicted water level y_{BW} will not be affected much if there is the presence of uncertainties lead to an increase in the flow at Lake Benalla and Lima Creek, an increase in the offset value and a decrease in the flow at Broken Weir.

As we have 4 parameters, the degree of freedom for χ^2-distribution is 4 and for a 95% confidence ellipsoid, we need $\alpha = 9.49$. The eigenvalues of $\hat{P}^{-1}_{LNB,N}$ for both the data sets are shown in Table 4.14.

For both the data sets, we observe that the uncertainty is the largest in the direction of $\theta_{e,LNB,4}$.

Data set	$\lambda_{LNB,1}$	$\lambda_{LNB,2}$	$\lambda_{LNB,3}$	$\lambda_{LNB,4}$
April to July 2007	6.551×10^3	1.003×10^5	1.615×10^6	2.264×10^7
April to July 2008	80.404	2.691×10^3	3.057×10^4	4.285×10^5

Table 4.14: Eigenvalues of $\hat{P}^{-1}_{LNB,N}$.

Since it is difficult to visualise a 4-dimensional ellipsoid, we consider three parameters at a time and the ellipsoids for the two data sets are plotted in Figures 4.24 and 4.25. In both figures, we can see the largest uncertainties are in the direction of $\theta_{e,LNB,3}$ for the figures on the left and in the direction of $\theta_{e,LNB,4}$ for the figures on the right as indicated by the eigenvalues shown in Table 4.14. Nonetheless, any uncertainties in the parameters within the ellipsoid do not affect much the accuracy of the prediction made using Equation (4.65).

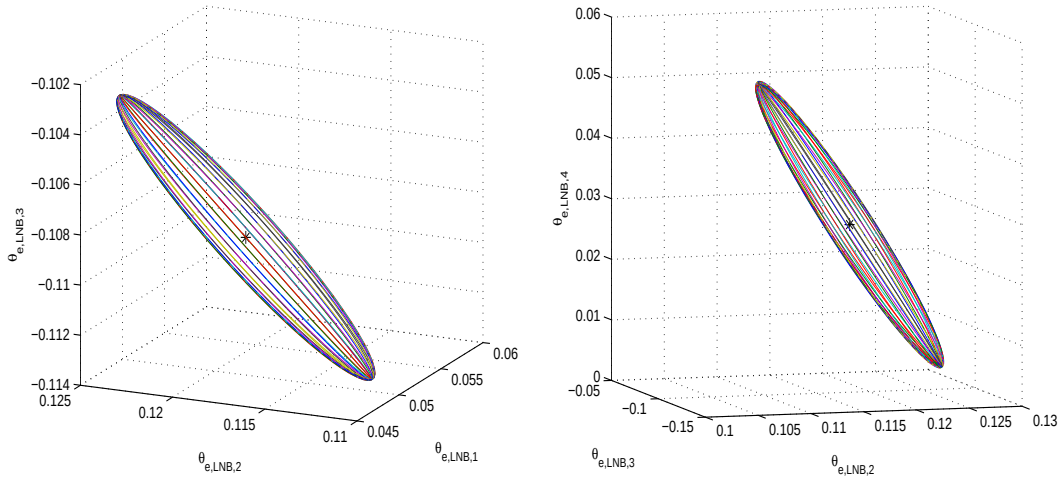

Figure 4.24: Ellipsoid for $\theta_{e,LNB}$ I. '*' denotes the estimated values using data set from April to July 2007. Left: Plots of $\theta_{e,LNB,1}$ to $\theta_{e,LNB,3}$. Right: Plots of $\theta_{e,LNB,2}$ to $\theta_{e,LNB,4}$.

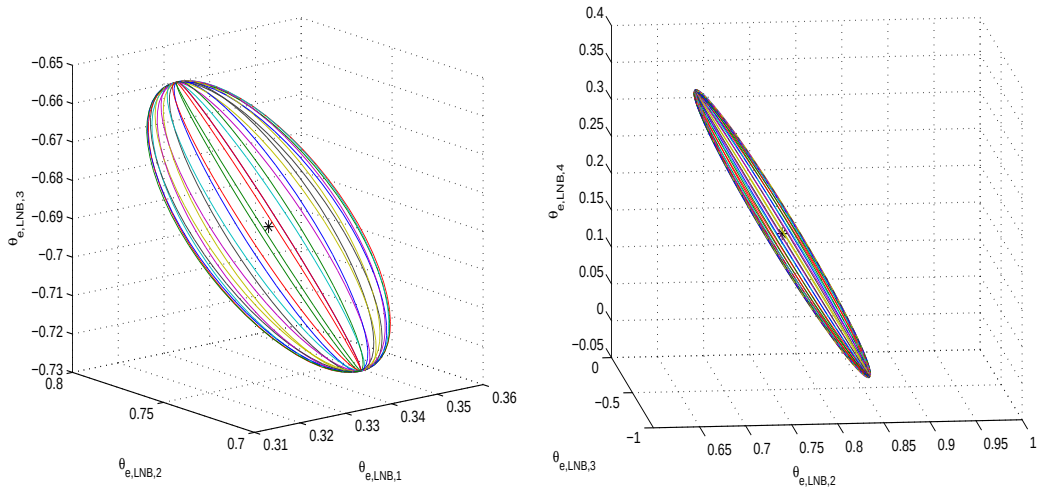

Figure 4.25: Ellipsoid for $\theta_{e,LNB}$ II. '*' denotes the estimated values using data set from April to July 2008. Left: Plots of $\theta_{e,LNB,1}$ to $\theta_{e,LNB,3}$. Right: Plots of $\theta_{e,LNB,2}$ to $\theta_{e,LNB,4}$.

Reach Poison Creek to Lake Benalla

The integrator delay model is used to model this reach and the associated predictor is given by

$$\begin{aligned}\hat{\breve{y}}_{LB}(t+1,\theta_{e,PLB},\tau_{PC}) = \hat{\breve{y}}_{LB}(t,\theta_{e,PLB},\tau_{PC}) + \theta_{e,PLB,1}\breve{y}^{1,2}_{PC}(t-\tau_{PC}) \\ + \theta_{e,PLB,2}\breve{y}^{3,1}_{HC}(t-\tau_{HC}) + \theta_{e,PLB,3}[\hat{\breve{y}}_{LB}(t,\theta_{e,PLB},\tau_{PC}) - p_{LB}]^{3/2}\end{aligned} \tag{4.67}$$

with $\theta_{e,PLB,1} = 0.173$, $\theta_{e,PLB,2} = 0.022$ and $\theta_{e,PLB,3} = -1.906$ when estimated using the data set from October 2010 and $\theta_{e,PLB,1} = 0.163$, $\theta_{e,PLB,2} = 0.021$ and $\theta_{e,PLB,3} = -1.837$ when estimated using the data set from November 2010.

The associated covariance matrices for the two data sets are given by

$$\hat{P}_{PLB,N}(\hat{\theta}_{e,PLB,N})\Big|_{\text{Oct,2010}} = \begin{bmatrix} 0.00037 & 0.00003 & -0.00367 \\ 0.00003 & 0.00001 & -0.00039 \\ -0.00367 & -0.00039 & 0.03958 \end{bmatrix}$$

$$\hat{P}_{PLB,N}(\hat{\theta}_{e,PLB,N})\Big|_{\text{Nov,2010}} = \begin{bmatrix} 0.00081 & 0.00008 & -0.00865 \\ 0.00008 & 0.00002 & -0.00093 \\ -0.00865 & -0.00093 & 0.09509 \end{bmatrix} \tag{4.68}$$

From the covariance matrices, we observe that there are some correlations between the parameters indicated by the large values in the off-diagonal entries in the covariance matrices. Looking at the variances of the estimated parameters, which are the diagonal entries of the covariance matrix, we observe that the largest variance is for $\theta_{e,PLB,3}$. As $\theta_{e,PLB,3}$ is related to the weir at Lake Benalla, the large variance suggests that with the measurement of Lake Benalla is obtained in the middle of the lake, modelling the flow out of Lake Benalla with a sharp crested weir equations, may not be a good approximation. $\theta_{e,PLB,1}$ and $\theta_{e,PLB,2}$ are positively correlated and both of them are negatively correlated with $\theta_{e,PLB,3}$. Thus, any uncertainty that lead to the increase in $\theta_{e,PLB,1}$ would increase the value of $\theta_{e,PLB,2}$ and decrease the value of $\theta_{e,PLB,3}$. Again, in terms of physical interpretation, the predicted water level at Lake Benalla y_{LB} would not be greatly affected by any uncertainties that lead to an increase in the flow at Poison Creek and Hollands Creek and the decrease in the flow at Lake Benalla.

As we have 3 parameters, the degree of freedom for χ^2-distribution is 3 and for a 95% confidence ellipsoid, $\alpha = 7.81$. The eigenvalues of $\hat{P}^{-1}_{PLB,N}$ for both the data sets are given in Table 4.15. From Table 4.15, the largest uncertainties is in the direction of $\theta_{e,PLB,3}$ for both the data sets. From Figure 4.26, the largest uncertainties are in the

Data set	$\lambda_{PLB,1}$	$\lambda_{PLB,2}$	$\lambda_{PLB,3}$
October 2010	25.045	3.427×10^4	3.819×10^5
November 2010	10.428	3.409×10^4	3.786×10^5

Table 4.15: Eigenvalues of $\hat{P}^{-1}_{PLB,N}$.

direction of $\theta_{e,PLB,3}$ for both the plots as indicated by the eigenvalues given in Table 4.15. Nonetheless, any uncertainties to the parameters that is within the ellipsoid do not affect much the accuracy of the prediction made using Equation (4.67).

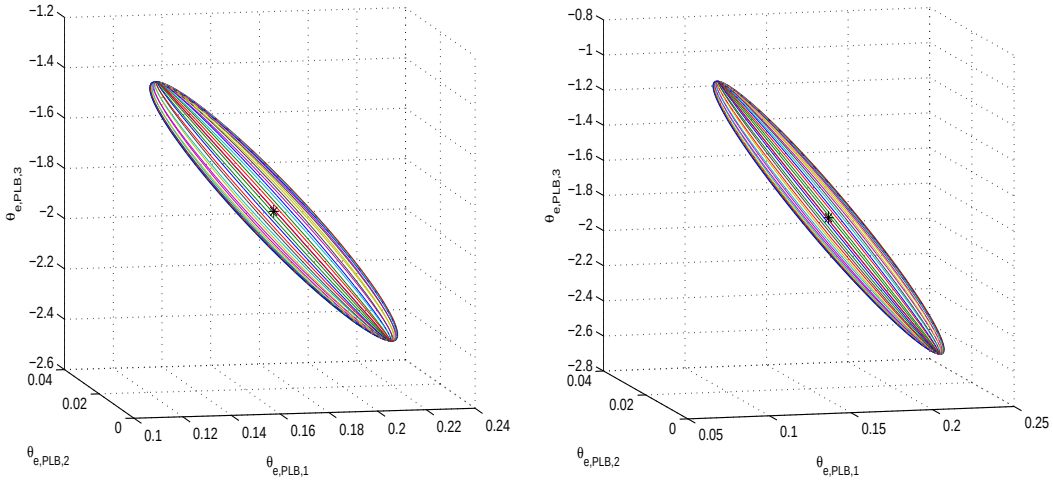

Figure 4.26: Ellipsoid for $\theta_{e,PLB}$. '*' denotes the estimated values. Left: Estimated using data set October 2010. Right: Estimated using data set November 2010.

Reach Lake Benalla to Casey's Weir

This reach is modelled using integrator delay model and the associated predictor is given by

$$\begin{aligned}\hat{y}_C(t+1,\theta_{e,LBC},\tau_{LB}) = \hat{y}_C(t,\theta_{e,LBC},\tau_{LB}) + \theta_{e,LBC,1}[y_{LB}(t-\tau_{LB}) - p_{LB}]^{3/2} \\ + \theta_{e,LBC,2}[\hat{y}_C(t,\theta_{e,LBC},\tau_{LB}) - p_C]^{3/2} + \theta_{e,LBC,3}Q_{BC}(t) \qquad (4.69)\end{aligned}$$

with $\theta_{e,LBC,1} = 2.200$, $\theta_{e,LBC,1} = -1.394$ and $\theta_{e,LBC,1} = -0.226$ estimated using data set from October to December 2010 and $\theta_{e,LBC,1} = 2.069$, $\theta_{e,LBC,1} = -1.316$ and $\theta_{e,LBC,1} = -0.098$ estimated using data set from January to April 2011.

The associated covariance matrices are given by

$$\begin{aligned}\hat{P}_{LBC,N}(\hat{\theta}_{e,LBC,N})\Big|_{\text{Oct-Dec,2010}} &= \begin{bmatrix} 0.00381 & -0.00217 & -0.00058 \\ -0.00217 & 0.00146 & 0.00017 \\ -0.00058 & 0.00017 & 0.00048 \end{bmatrix} \\ \hat{P}_{LBC,N}(\hat{\theta}_{e,LBC,N})\Big|_{\text{Jan-Apr,2011}} &= \begin{bmatrix} 0.01273 & -0.00784 & -0.00090 \\ -0.00784 & 0.00510 & 0.00027 \\ -0.00090 & 0.00027 & 0.00070 \end{bmatrix} \qquad (4.70)\end{aligned}$$

From the covariance matrices, we observe that correlation between the parameters is small suggesting there is little correlation between the parameters. Likewise, the variances of the estimated parameters are also small relative to the estimated parameters. $\theta_{e,LBC,2}$ and $\theta_{e,LBC,3}$ are positively correlated and both of these two parameters are negatively correlated with $\theta_{e,LBC,1}$. Any uncertainty that in lead to the increase of $\theta_{e,LBC,1}$ would decrease the value of $\theta_{e,LBC,2}$ and $\theta_{e,LBC,3}$ and this would not affect much the prediction made using Equation (4.69). Physically, this can be interpreted as the accuracy of the predicted water level at Casey's Weir would be affected much by the uncertainties that lead to an increase of flow at Lake Benalla and the decrease of flows at Broken Creek and Casey's Weir. The eigenvalues of $\hat{P}^{-1}_{LBC,N}$ for the two data sets are given in Table 4.16.

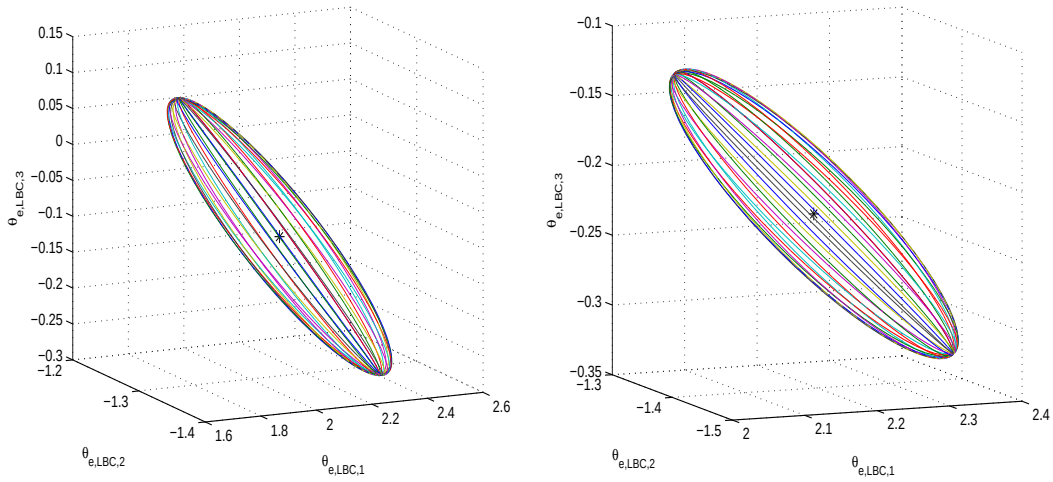

Figure 4.27: Ellipsoid for $\theta_{e,LBC}$. '*' denotes the estimated values. Left: Estimated using data set October to December 2010. Right: Estimated using data set January to April 2011.

From Table 4.16, we observe that the largest uncertainty is in the direction of $\theta_{e,LBC,3}$ for both the data sets. The ellipsoids shown in Figure 4.27 show that the uncertainties are

Data set	$\lambda_{LBC,1}$	$\lambda_{LBC,2}$	$\lambda_{LBC,3}$
October to December 2010	1.931×10^2	2.069×10^3	1.126×10^4
January to April 2011	56.55	1.321×10^3	1.141×10^4

Table 4.16: Eigenvalues of $\hat{P}^{-1}_{LBC,N}$.

largest in the direction of $\theta_{e,LBC,3}$ as indicated by the eigenvalues shown in Table 4.16.

Nonetheless, any uncertainties in the parameters within the ellipsoid do not affect much the accuracy of the prediction made using Equation (4.69).

4.7 Summary

In this chapter, we have used system identification procedures to obtain models for the reaches in the Broken River. Both nonparametric and parametric identification methods are explored. The step response and frequency response analysis for Reach CG reveals that the reach is a time delay dominant system. Based on this information and observation from data, we select the time delay model as our model structure in our parametric identification method. The validation of the time delay model shows that the model is accurate in capturing the relevant dynamics of the river and it is as accurate as the Saint Venant equations. From a control design point of view, the time delay model is preferred as it is simpler. The effect of varying time delay due to varying flow condition is investigated and this needs to be considered in the robustness specifications for the controller.

We further explore the use of the integrator delay model and the simulation results from Reach LBC and Reach PLB show that the integrator delay model is accurate in capturing the relevant dynamics of the reaches. For these two reaches, the integrator delay models are as accurate as the Saint Venant equations and they are preferred for control design. For Reach LNB, the integrator delay model seem to be a promising model candidate but in view of the poor quality of the data and the absence of a reliable rating curve, we do not want to draw any further conclusion. The analyses of the covariance matrix reveal that the parameter estimate for Reach CG and Reach LBC is good. For the other reaches, the absence of a good flow to water level relationship lead to the parameter estimates with a larger uncertainty.

Chapter 5

Model Predictive Control (MPC) design via reverse engineering

In Chapters 3 and 4 we have looked at modelling of river systems, where the purpose of the model is for control design. In the next two chapters, using the obtained models, we will look at the design of controllers, which will later be simulated on the Broken River. As the operation of the Broken River is subjected to various constraints, Model Predictive Control (MPC) is deemed the appropriate controller and will be explored in this thesis. In this chapter, we focus on the design of MPC via reverse engineering, i.e. we let MPC reproduces an existing controller. In the next chapter, we apply the reverse engineered MPC to control the Broken River.

The motivation behind the design of MPC via reverse engineering is as follow. The ability to take constraints explicitly into account in the formulation of the optimisation problem has made MPC a popular control strategy. However, finding the weights in the MPC optimisation criterion is often non-trivial and requires a fair bit of trial-and-error. Conventional controllers such as PI-controllers, on the other hand are relatively easy to tune and they often achieve satisfactory performance in the absence of constraints. In this chapter, we present three systematic methods of designing an MPC such that it reproduces the conventional controller when the constraints are not active. The first approach is from existing literature, where a full order observer is used for reverse engineering. The second and third approach proposed here use a reduced order observer and state augmentation respectively. The obtained controller can also serve as an initial MPC tuning weights,

which can be further fine tuned and constraints can later be added to evaluate any potential benefit of using MPC compared to the conventional controller.

This chapter is organised as follows. An introduction to MPC is first given in Section 5.1. This is followed by the motivation and a brief review of the concept of inverse optimal control, which is the main idea behind reverse engineering in Section 5.2 and 5.3 respectively. Methods for reverse engineering are discussed in Section 5.5. Illustrative examples are given in Section 5.6. Some remarks on reverse engineering are addressed in Section 5.7 and a summary is given in Section 5.8.

5.1 Introduction to MPC

Before going into a detail discussion of the methods of reverse engineering, a brief discussion on MPC is first given. For a more in depth discussion, see ((Maciejowski, 2002), (Rossiter, 2005), (Rawlings and Mayne, 2009) or (Wang, 2009)).

5.1.1 Basic idea

MPC is an online optimal controller, where the controller generates a sequence of control input based on the predicted behaviour of the plant, which is described by the plant model, over a finite prediction horizon[1] N_p, by solving an optimisation criterion[2], i.e.

$$\begin{aligned} u = & \underset{u(k),u(k+1),\ldots,u(k+N_p-1)}{\operatorname{argmin}} J(x,u,k,N_p) \\ \text{subject to: } & x(k+1) = Ax(k) + Bu(k) \\ & y(k) = Cx(k) \end{aligned} \tag{5.1}$$

where u is the control input, x is the state of the plant and y is the output of the plant. A, B and C are matrices that describe the dynamics of the plant. Here, we assume that we have measurements for all the states in steady states. The main attractive feature of MPC is its capability to handle constraints in the optimisation problem. Because of this feature, MPC has now becomes the standard choice of controller when dealing with

[1] Some works consider a control horizon N_u, which is different from the prediction horizon N_p and normally $N_u \leq N_p$. In this chapter, we consider only the case where $N_u = N_p$.

[2] This is also known as a cost function.

systems that are subjected to constraints.

Typically, the criterion $J(x, u, k, N_p)$ is a quadratic criterion and thus, the optimisation problem can be formulated as a quadratic programming[3] problem and the constraints are usually expressed in terms of linear equalities or linear inequalities.

Remarks: The plant model used in Equation (5.1) assumes that we have the full knowledge of the steady state values of the states $x(k)$ and the input $u(k)$, which are often not available in practical implementation. Thus, an alternate equivalent plant model that is often used in practical implementation of MPC takes the form of (Wang, 2009).

$$\begin{aligned}\begin{bmatrix}\Delta x(k+1)\\ y(k+1)\end{bmatrix} &= \begin{bmatrix}A & 0\\ CA & 1\end{bmatrix}\begin{bmatrix}\Delta x(k)\\ y(k)\end{bmatrix} + \begin{bmatrix}B\\ CB\end{bmatrix}\Delta u(k)\\ y(k) &= \begin{bmatrix}0 & 1\end{bmatrix}\begin{bmatrix}\Delta x(k)\\ y(k)\end{bmatrix}\end{aligned} \tag{5.2}$$

where $\Delta x(k) = x(k) - x(k-1)$ and $\Delta u(k) = u(k) - u(k-1)$. In this form, the model depends on the current and previous values of the states and the inputs. Moreover, $\Delta u(k)$, represents the change of the input, which physically, represents the rate of the opening of the valve, change of gate position, etc. Note that, Equation (5.2) also involves augmentation of the states to include an integrator, which is one the many ways of introducing an integrator[4] into the system (see (Maciejowski, 2002) and reference therein.). In this thesis, we will stick to the model used in Equation (5.1) as the materials related to the reverse engineering in the later section of this chapter use Equation (5.1).

5.1.2 Principle operation

The principle operation of MPC is illustrated as follows (see Figure 5.1). Suppose we want the output y to track a given setpoint. At time k, MPC obtains measurements (shown by the black dot) and updates the estimate of the states of the plant such that it reflects the current condition of the plant. Then, it generates a set of control input u, by optimising the predicted future behaviour of the plant over the prediction horizon N_p with respect to the input. Only the first control input is applied to the plant. At time $k+1$, the new measurements (shown by the grey dot), which reflects the effect of previous control are

[3] A quadratic programming solves the problem that is formulated in the form of $\min_x \frac{1}{2}x^TQx + p^Tx$ subject to $Ax \leq b$ (inequality constraint) and/or $Cx = d$ (equality constraint).

[4] In this thesis, the integrator is also introduced but in a slightly different manner, see Section 6.4.2.

obtained and the whole process is repeated until the output reaches the desired setpoint. The concept of prediction made over the finite horizon N_p is also known as "receding horizon" as the length of the prediction horizon remains the same as the initial time point shifts from time k (dotted black window) to $k+1$ (dotted grey window).

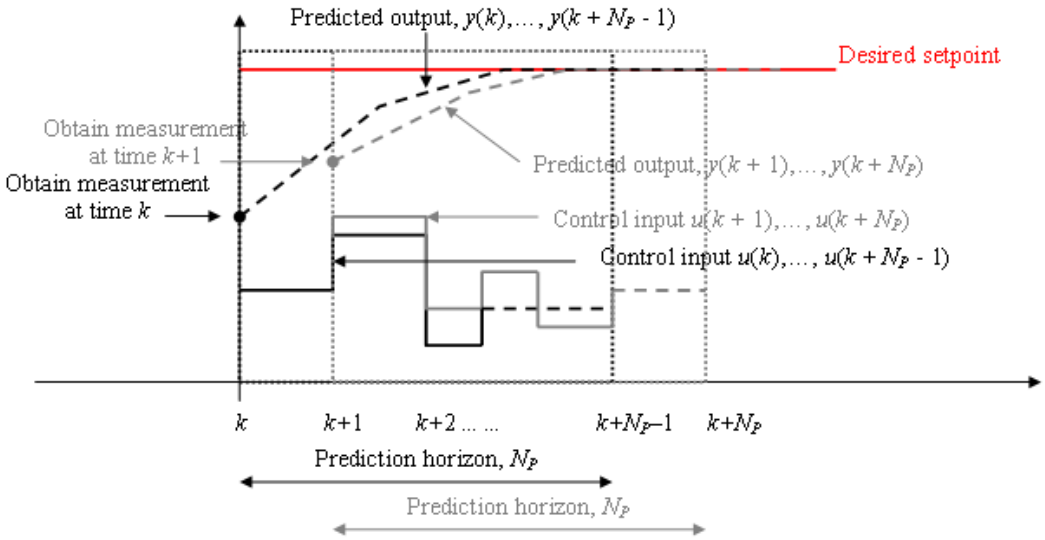

Figure 5.1: The basic working principle of MPC.

5.1.3 Constraints handling

As mentioned, the main attractive feature of MPC is its capability to handle constraints in the optimisation problem. Constraints can be included explicitly in the optimisation problem where Equation (5.1) becomes

$$\begin{aligned} u = & \underset{u(k),u(k+1),\ldots,u(k+N_p-1)}{\operatorname{argmin}} J(x,u,k,N_p) \\ \text{subject to: } & x(k+1) = Ax(k) + Bu(k) \\ & y(k) = Cx(k) \\ & x \in \mathcal{X},\ u \in \mathcal{U}\ ,\ y \in \mathcal{Y} \end{aligned} \tag{5.3}$$

where $\mathcal{X}$, $\mathcal{U}$ and $\mathcal{Y}$ are some defined constraints sets. A typical form of $J(x, u, k, N_p)$ is given by

$$J(x,u,k,N_p) = x^T(N_p)Px(N_p) + \sum_{k=1}^{N_p-1} x^T(k)Qx(k) + u^T(k)Ru(k) + s_L^T(k)Q_{s,L}s_L(k) + s_H(k)^TQ_{s,H}s_H(k) \tag{5.4}$$

where x and u are the state variables and the control input respectively. P, Q and R are weighting matrices where P and Q are positive definite matrices, while R is a positive semi definite weighting matrix. There are two types of constraints; the hard and the soft constraints. The hard constraints are constraints that cannot be violated at all. An example of a hard constraint is the opening of a gate to regulate flow that cannot go beyond its opening and closing limit. On the other hand, soft constraints are constraints that can be violated for a short period of time without causing any major consequences to the system.

The inclusion of the soft constraints is usually done to avoid the optimisation problem becoming infeasible. By infeasible, we mean that the optimiser is unable to find a solution that satisfies all the constraints simultaneously. One way to soften the constraints is to introduce the "slack variables" and include them in the criterion. These slack variables are defined in such a way that they will be non zero when constraint violation happens. Then, these variables are penalised with large weights in the criterion in order for the optimiser to maintain these slack variables at zero if possible. As an example, suppose the output $y(k)$ is constrained to be less than a value α and $y(k)$ is made a soft constraint with the slack variable $s_L(k)$. Rewriting in terms of linear inequalities, we have

$$y(k) + s_L(k) \leq \alpha \tag{5.5}$$

From Equation (5.5), we can see that $s_L(k) = 0$ when the constraints are inactive and $s_L(k) > 0$ when the constraints are active. With $s_L(k)$ penalised heavily in the criterion, Equation (5.4) will be very large if constraints violation occurs. Then, the optimiser will have the urge to keep $s_L(k)$ at zero if possible. In Equation (5.4), $s_L(k)$ and $s_H(k)$ are the slack variables that are associated with the minimum and the maximum values of the defined constraints. $Q_{s,L}$ and $Q_{s,H}$ are the weights matrices to penalise the slack variables $s_L(k)$ and $s_H(k)$ respectively.

5.1.4 Unmeasured states

So far, our discussions have assumed that we have measurements for all the states of the plant. In practice, quite often not all states are measured and in such scenario, an observer is required to estimate the states of the plant. MPC will then use this estimated states, which we denote as $\hat{x}$ in the place of the true states x for prediction of the future behaviour of the plant in order to determine the optimal sequence of the control inputs. That is the estimated states are used as the initial states to predict the future states within the controller.

5.1.5 Dealing with disturbances

Unmeasured or unknown disturbances

In practice, there are disturbances acting on the plant. Very often these disturbances are not measured or unknown and the controller needs to reject these disturbances such that a zero steady state error can be achieved. One standard way to deal with disturbance is to augment the plant with the model of the disturbance, use the observer to estimate this disturbance and use this estimated disturbance to cancel the effect of the actual disturbance (see e.g. (Franklin *et al.*, 1998) or (Rossiter, 2005)). If we assume the disturbance is constant, the disturbance model is given by

$$d_{UMD}(k+1) = d_{UMD}(k) \tag{5.6}$$

where the subscript "UMD" is used to denote the unmeasured disturbances. Depending on where the disturbances enter the plant (from the input or the output side), the state space model can be written as

$$\begin{aligned} x(k+1) &= Ax(k) + Bu(k) + B_{UMD}d_{UMD}(k) \\ y(k) &= Cx(k) \end{aligned} \tag{5.7}$$

if the disturbances enter from the input side, and

$$\begin{aligned} x(k+1) &= Ax(k) + Bu(k) \\ y(k) &= Cx(k) + d_{UMD}(k) \end{aligned} \tag{5.8}$$

if the disturbances enter from the output side. In both cases, we can use the observer to estimate these disturbances, the observer is designed based on the augmented plant with the disturbance model, which yields the following plant matrices,

$$A_{din,aug} = \begin{bmatrix} A & B_{UMD} \\ 0 & I \end{bmatrix} \qquad B_{din,aug} = \begin{bmatrix} B \\ 0 \end{bmatrix} \qquad C_{din,aug} = \begin{bmatrix} C & 0 \end{bmatrix} \tag{5.9}$$

if the disturbances enter from the input side, or

$$A_{dout,aug} = \begin{bmatrix} A & 0 \\ 0 & I \end{bmatrix} \qquad B_{dout,aug} = \begin{bmatrix} B \\ 0 \end{bmatrix} \qquad C_{dout,aug} = \begin{bmatrix} C & I \end{bmatrix} \tag{5.10}$$

if the disturbances enter from the output side with with $x_{d_{UMD},aug} = [x^T(k), d_{UMD}^T(k)]^T$

Measured or known disturbances

The measured or known disturbances can be either known at current time (e.g. the current measured value) or the known at future time (e.g. advanced order from the irrigators). In both cases, these disturbances can be used as "feedforward control" in MPC. The feedforward can be easily incorporated into MPC by including the disturbances directly into the prediction model over the prediction horizon (Maciejowski, 2002). When solving the optimisation problem, the control input signal is computed with the measured disturbances taken into account. To include the measured disturbances in our prediction model, Equation (5.3) is rewritten as

$$\begin{aligned} u = & \underset{u(k),u(k+1),\ldots,u(k+N_p-1)}{\operatorname{argmin}} J(x,u,k,N_p) \\ \text{subject to: } & x(k+1) = Ax(k) + Bu(k) + B_{MD}d_{MD}(k) \\ & y(k) = Cx(k) \\ & x \in \mathcal{X},\ u \in \mathcal{U}\ ,\ y \in \mathcal{Y} \end{aligned} \tag{5.11}$$

where d_{MD} is the measured disturbance.

5.2 Motivation behind reverse engineering

Having briefly introduced the idea of MPC, we now present the motivation behind MPC design via reverse engineering. Conventional controllers such as the PI-controllers are widely used because they are easy to tune, and they often achieve satisfactory performance in the absence of constraints. However, when constraints are active, these controllers often have to be de-tuned to avoid violating the constraints or be augmented with constraints handling mechanisms (e.g. anti windup), which in both cases may result in a reduced performance (Goodwin *et al.*, 2001).

MPC on the other hand, is known for its constraints handling capability since the constraints are directly included in the problem formulation. MPC uses the model of the plant to predict the behaviour of the plant over a finite prediction horizon and determine the best possible control action to be taken at each time step by solving an optimisation problem. Despite this attractive feature, finding good weights in the optimisation criterion for MPC is often non-trivial. As a rule of thumb, Bryson's Rule is often used for selecting the initial weights (Franklin *et al.*, 2006). Bryson's Rule requires knowledge of the largest possible value of the state of the plant and the control action.

Suppose the MPC criterion is given by

$$J(u, x, k, N_p) = \sum_{k=1}^{N_p} x(k)^T Q x(k) + u^T(k) R u(k) \tag{5.12}$$

Based on Bryson's Rule, the initial weight matrices of Q and R in Equation (5.12) can be chosen to be a diagonal matrices with the following values

$$\begin{aligned} Q_{ii} &= 1/\text{maximum acceptable values of } x_i^2 \\ R_{jj} &= 1/\text{maximum acceptable values of } u_i^2 \end{aligned} \tag{5.13}$$

where $i = 1, \ldots, n$ with n is the number of states and $j = 1, \ldots, p$ with p is the number of input. Then, these weight matrices are modified accordingly until an acceptable performance is obtained.

In this chapter, we present methods for finding the weights in an MPC criterion such that the obtained MPC controller reproduces an existing conventional controller when there are no constraints (see Figure 5.2). In other words, we reverse engineer these existing

conventional controller, for MPC. The benefit of doing this is that we ensure that the performance of the existing controller (which can be very good) is maintained, and we may potentially obtain the constraints handling capability of MPC as an added feature to the existing control configuration. This benefit may lead to a much wider acceptance of using MPC over different range of applications by the industry.

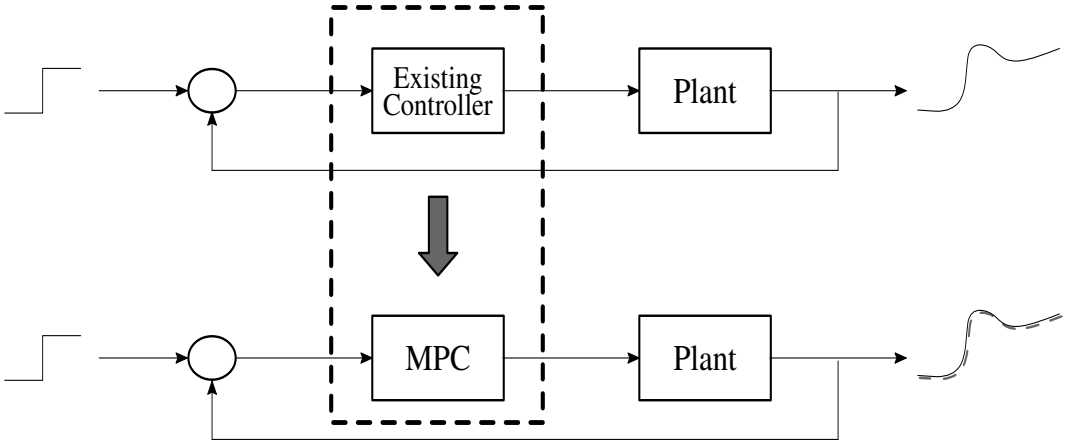

Figure 5.2: Block diagram for reverse engineering.

5.3 Brief review on reverse engineering

The idea of "reverse engineering" was first addressed in (Kalman, 1964), when Kalman addressed the question, "When is a linear control system optimal?" In other words, Kalman was interested in finding the performance indices such that the given control law is optimal. This led to a great interest in the inverse regulator problem (see e.g. (Kreindler and Jameson, 1972), (Molinari, 1973) and (Fujii, 1987)).

One approach to reverse engineering is to use an observer-based compensator. This was considered in (Bender and Fowell, 1985) and it is the key idea used throughout this chapter. Bender and Fowler utilised a state feedback/observer controller to reproduce the existing controller and they considered the case where the order of the plant is equal to the order of the controller. In (Alazard and Apkarian, 1999) and (Delmond *et al.*, 2006), the authors generalised the work of (Bender and Fowell, 1985) by considering different types of controllers and the order of the controller and the plant do not have to be equal.

The work in (Maciejowski, 2007) and subsequently, (Hartley and Maciejowski, 2009)

extended the idea of reverse engineering using the observer-based compensator to MPC. There are alternative methods for reverse engineering for MPC, which do not make use of an observer and they can be found in (Di Cairano and Bemporad, 2010). However, the methods in (Di Cairano and Bemporad, 2010) had some drawbacks such as large computational time and no guarantee of feasibility.

In this chapter, we build on the work in (Hartley and Maciejowski, 2009), and consider two additional reverse engineering procedures using a reduced order observer and state augmentation. The emphasis is on reproducing controllers with integral action (e.g. PI or I-controller), motivated by the widespread use of such controllers.

5.4 MPC implementation for reverse engineering

Given a state feedback controller, $u(k) = -Kx(k)$, a zero value infinite horizon cost function with this controller as its minimiser is given by (Kreindler and Jameson, 1972)

$$J = \sum_{k=0}^{\infty} [u(k) + Kx(k)]^T [u(k) + Kx(k)] = \sum_{k=0}^{\infty} \begin{bmatrix} x(k) \\ u(k) \end{bmatrix}^T \begin{bmatrix} K^T K & K^T \\ K & I \end{bmatrix} \begin{bmatrix} x(k) \\ u(k) \end{bmatrix} \tag{5.14}$$

Equation (5.14) is an LQR cost function with cross terms. In MPC, the optimisation is carried out over a finite horizon N_p. An equivalent MPC formulation is given by

$$\begin{aligned} J_{MPC} = & \sum_{k=0}^{N_p-1} \begin{bmatrix} x(k) \\ u(k) \end{bmatrix}^T \begin{bmatrix} K^T K & K^T \\ K & I \end{bmatrix} \begin{bmatrix} x(k) \\ u(k) \end{bmatrix} \\ & + x^T(N_p) P x(N_p) \end{aligned} \tag{5.15}$$

where P is a solution to a Discrete Algebraic Riccati Equation, (DARE). Since Equation (5.14) has a zero value cost for $u(k) = -Kx(k)$, the terminal weight P is zero (Hartley and Maciejowski, 2009). This reduces Equation (5.15) to

$$J_{MPC} = \sum_{k=0}^{N_p-1} \begin{bmatrix} x(k) \\ u(k) \end{bmatrix}^T \begin{bmatrix} K^T K & K^T \\ K & I \end{bmatrix} \begin{bmatrix} x(k) \\ u(k) \end{bmatrix} \tag{5.16}$$

Rewriting Equation (5.16) in standard form

$$J_{MPC} = \sum_{k=0}^{N_p-1} x(k)^T Q x(k) + u(k)^T R u(k) + x(k)^T S u(k) + u^T(k) S^T x(k) \tag{5.17}$$

we observe that $Q = K^T K$, $R = I$ and $S = K^T$, where I denotes identity matrix. These weights are dependent on K. In the event, where not all states are measured, the control law is then given by $u = -K\hat{x}$, where $\hat{x}$ is the output of an observer. The goal here, which will be further illustrated in the subsequent sections is to find a feedback gain K and an observer gain such that the controller $u = -K\hat{x}$ reproduces the existing controller when there are no constraints.

5.5 Methods for reverse engineering

We now present three methods for designing MPC such that it reproduces the conventional controller when there are no constraints. The first method where a full order observer is used in the reverse engineering is from the work of (Maciejowski, 2007) and (Hartley and Maciejowski, 2009). We build on those works and proposed two more reverse engineering methods, which use a reduced order observer and state augmentation.

5.5.1 Using full order observer

In this section, the method of reverse engineering, which uses a full order observer is presented. We use the notation K_{fav} to denote the existing "favourite" controller that the MPC should reproduce.

Consider the plant and the favourite controller,
Plant

$$\begin{aligned} x(k+1) &= Ax(k) + Bu(k) \\ y(k) &= Cx(k) \end{aligned} \tag{5.18}$$

Controller

$$x_K(k+1) = A_K x_K(k) + B_K y(k)$$
$$u(k) = C_K x_K(k) + D_K y(k) \tag{5.19}$$

where $A \in \mathbb{R}^{n\times n}$, $B \in \mathbb{R}^{n\times p}$, $C \in \mathbb{R}^{m\times n}$, $A_K \in \mathbb{R}^{n_K\times n_K}$, $B_K \in \mathbb{R}^{n_K\times m}$, $C_K \in \mathbb{R}^{p\times n_K}$ and $D_K \in \mathbb{R}^{p\times m}$. n, p, m and n_K are the order of the plant, input of the plant, output of the plant and the controller respectively and $n_K \leq n$. Next, we represent K_{fav} as a state feedback controller. This is achieved by using an observer where the controller states are mapped to the observer states (see Figure 5.3). For simplicity of analysis, we have made

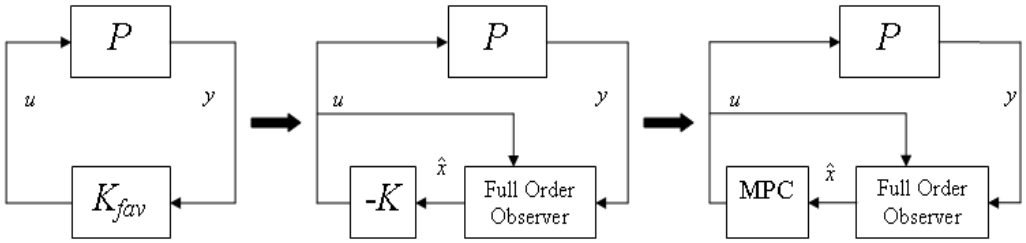

Figure 5.3: Reverse engineering using full order observer.

the assumption that there are no feed-through terms in the plant and the controller (i.e. $D = 0$ and $D_K = 0$). In the case where $D_K \neq 0$ (e.g. PI-controller), some extra steps (either by introducing a unit delay or by loop shifting) can be taken to obtain a problem formulation where the controller is strictly proper (see (Hartley and Maciejowski, 2009)).

For the method of adding a unit delay, some care has to be taken prior reverse engineering. A unit delay introduces additional phase shift, which would change the phase margin of the loop transfer function. Thus, the controller that we want to reproduce has to be robust against such a scenario.

As for the method of loop shifting, following the procedure in (Zhou *et al.*, 1996) the D_K term is moved to the plant (see Figure 5.4). The loop shifting results in the modified plant having the following new A matrix, which we denote $\bar{A} = (A + BD_KC)$, while the B and C matrices remain the same. This method preserves the original closed loop transfer function. In this chapter, whenever we are dealing with $D_K \neq 0$, loop shifting is used instead of adding a unit delay (see Section 5.6).

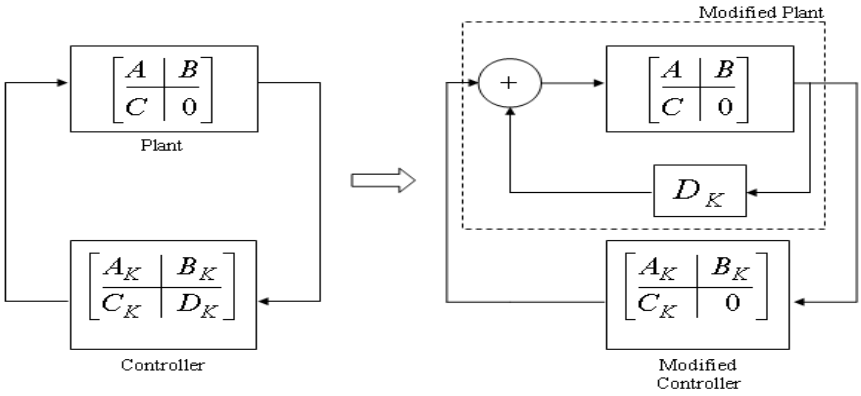

Figure 5.4: Loop shifting.

We proceed with showing the simplified derivation on how the full order observer is used for reverse engineering. We follow the derivation from (Bender and Fowell, 1985) and (Hartley and Maciejowski, 2009) closely. The A matrix of the closed loop system of Equation (5.18) and (5.19) is given by

$$A_{CL} = \begin{bmatrix} A & BC_K \\ B_K C & A_K \end{bmatrix} \tag{5.20}$$

The idea is to map the states of K_{fav} to the full order observer such that the dynamics of the closed loop system of the plant and the full order observer is similar to A_{CL}.

A full order observer is given by

$$\hat{x}(k+1) = A\hat{x}(k) + Bu(k) + L(y(k) - C\hat{x}(k)) \tag{5.21}$$

and the control input is expressed as

$$u(k) = -K\hat{x}(k) \tag{5.22}$$

where $\hat{x}$ denotes the estimate of the state of the plant. K and L are the state feedback gain and the observer gain respectively. Substituting Equation (5.22) into Equation (5.21), we

get

$$\begin{aligned} \hat{x}(k+1) &= (A - LC - BK)\hat{x}(k) + Ly(k) \\ u(k) &= -K\hat{x}(k) \end{aligned} \tag{5.23}$$

The closed loop system given by Equations (5.18) and (5.23) is

$$\begin{bmatrix} x(k+1) \\ \hat{x}(k+1) \end{bmatrix} = \begin{bmatrix} A & -BK \\ LC & A - LC - BK \end{bmatrix} \begin{bmatrix} x(k) \\ \hat{x}(k) \end{bmatrix} =: \breve{A} \begin{bmatrix} x(k) \\ \hat{x}(k) \end{bmatrix} \tag{5.24}$$

We need to find K and L such that the closed loop dynamics between the plant and the full order observer contains the closed loop dynamics of the plant and K_{fav}.

In order to map the states of the controller to the states of the observer, the relationship

$$x_K(k) = T\hat{x}(k) \tag{5.25}$$

is imposed where T is a full row rank matrix. This idea was used in (Bender and Fowell, 1985), where they considered the case where $n_K = n$. With $n_K = n$, T is a square matrix and nonsingular (as T is a full row rank matrix). Thus, substituting Equation (5.25) into Equation (5.19) with $D_K = 0$, we have

$$\begin{aligned} T\hat{x}(k+1) &= A_K T\hat{x}(k) + B_K y(k) \\ u(k) &= C_K T\hat{x}(k) \end{aligned} \tag{5.26}$$

Pre-multiply by T^{-1} on both sides for the first equation, we get

$$\begin{aligned} \hat{x}(k+1) &= T^{-1}A_K T\hat{x}(k) + T^{-1}B_K y(k) \\ u(k) &= C_K T\hat{x}(k) \end{aligned} \tag{5.27}$$

Comparing Equations (5.23) and (5.26) term by term, we get

$$\begin{aligned} T^{-1}A_K T &= A - LC - BK \\ T^{-1}B_K &= L \\ C_K T &= -K \end{aligned} \tag{5.28}$$

Substituting Equation (5.28) into Equation (5.24), pre-multiply and post-multiply $\breve{A}$ with $\begin{bmatrix} I & 0 \\ 0 & T \end{bmatrix}$ and $\begin{bmatrix} I & 0 \\ 0 & T^{-1} \end{bmatrix}$ respectively, we get

$$\begin{aligned} \begin{bmatrix} x(k+1) \\ \hat{x}(k+1) \end{bmatrix} &= \begin{bmatrix} I & 0 \\ 0 & T \end{bmatrix} \begin{bmatrix} A & -BK \\ LC & A - LC - BK \end{bmatrix} \begin{bmatrix} I & 0 \\ 0 & T^{-1} \end{bmatrix} \begin{bmatrix} x(k) \\ \hat{x}(k) \end{bmatrix} \\ &= \begin{bmatrix} A & BC_K \\ B_K C & A_K \end{bmatrix} \begin{bmatrix} x(k) \\ \hat{x}(k) \end{bmatrix} \end{aligned} \tag{5.29}$$

It is clear from Equation (5.29) that the closed loop dynamics of the plant and the full order observer is the same as the closed loop dynamics of the plant and K_{fav}. T is a solution to the non-symmetric algebraic Riccati equation,

$$\begin{aligned} \begin{bmatrix} -T & I \end{bmatrix} A_{CL} \begin{bmatrix} I \\ T \end{bmatrix} &= 0 \\ \begin{bmatrix} -T & I \end{bmatrix} \begin{bmatrix} A & BC_K \\ B_K C & A_K \end{bmatrix} \begin{bmatrix} I \\ T \end{bmatrix} &= 0 \\ -TA - TBC_K T + B_K C + A_K T &= 0 \end{aligned} \tag{5.30}$$

We will discuss the method to find T later in this section.

For the case when $n_K \leq n$, $T \in \mathbb{R}^{n_K \times n}$ is now a wide rectangular matrix. Hence, the left inverse of T does not necessarily exists and the steps in Equations (5.26) and (5.27) cannot be used to obtain K and L. We need an alternate derivation. It turns out that the state feedback gain K and the observer gains L are given by

$$K = -C_K T \tag{5.31}$$

and

$$L = T^{\#} B_K \tag{5.32}$$

where T^{-1} is replaced by $T^{\#}$, a right inverse of T, i.e. $TT^{\#} = I$. In the following, we show that with Equations (5.31) and (5.32), we can get the closed loop dynamics between the plant and the full order observer to be similar with the closed loop dynamics between the plant and K_{fav}.

Before that, some notations associated with T are first introduced. As stated before,

$T^{\#}$ is the right inverse of T. Let $T^{\perp}$ be a matrix whose column form an orthonormal basis for the nullspace of T (i.e. $TT^{\perp} = 0$) and let T^{+} be the Moore-Penrose pseudoinverse[5] of T.

Substituting Equations (5.31) and (5.32) into Equation (5.24), we get

$$\begin{bmatrix} x(k+1) \\ \hat{x}(k+1) \end{bmatrix} = \begin{bmatrix} A & BC_K T \\ T^{\#}B_K C & A + BC_K T - T^{\#}B_K C \end{bmatrix} \begin{bmatrix} x(k) \\ \hat{x}(k) \end{bmatrix} \tag{5.33}$$

Using a similarity transformation to decompose $\hat{x}$ into components belonging to the rowspace and null space of T, we get $\hat{x} = x_{RS} + x_{NS}$ where $x_{RS} \in \text{Row}(T)$ and $x_{NS} \in \text{Null}(T)$. Equation (5.33) becomes

$$\begin{bmatrix} x(k+1) \\ x_{RS}(k+1) \\ x_{NS}(k+1) \end{bmatrix} = \begin{bmatrix} I & 0 \\ 0 & T \\ 0 & T^{\perp T} \end{bmatrix} \begin{bmatrix} A & BC_K T \\ T^{\#}B_K C & A + BC_K T - T^{\#}B_K C \end{bmatrix} \begin{bmatrix} I & 0 & 0 \\ 0 & T^{+} & T^{\perp} \end{bmatrix} \begin{bmatrix} x(k) \\ x_{RS}(k) \\ x_{NS}(k) \end{bmatrix} \tag{5.34}$$

Expanding $\breve{A} = \begin{bmatrix} I & 0 \\ 0 & T \\ 0 & T^{\perp T} \end{bmatrix} \begin{bmatrix} A & BC_K T \\ T^{\#}B_K C & A + BC_K T - T^{\#}B_K C \end{bmatrix} \begin{bmatrix} I & 0 & 0 \\ 0 & T^{+} & T^{\perp} \end{bmatrix}$, we get

$$\begin{bmatrix} A & BC_K TT^{\#} & BC_K TT^{\perp} \\ TT^{\#}B_K C & (TA - B_K C + TBC_K T)T^{+} & (TA - B_K C + TBC_K T)T^{\perp} \\ T^{\perp T}T^{\#}B_K C & T^{\perp T}(A + BC_K T - T^{\#}B_K C)T^{+} & T^{\perp T}(A + BC_K T - T^{\#}B_K C)T^{\perp} \end{bmatrix} \tag{5.35}$$

To simplify Equation (5.35), from Equation (5.30) we have

$$TA - B_K C + TBC_K T = A_K T \tag{5.36}$$

Moreover $TT^{\#} = I$ and $TT^{\perp} = 0$, and substituting these equations into Equation (5.35), we then have Equation (5.34) becomes,

$$\begin{bmatrix} x(k+1) \\ x_{RS}(k+1) \\ x_{NS}(k+1) \end{bmatrix} = \begin{bmatrix} A & BC_K & 0 \\ B_K C & A_K & 0 \\ A_{NS1} & A_{NS2} & A_{NS3} \end{bmatrix} \begin{bmatrix} x(k) \\ x_{RS}(k) \\ x_{NS}(k) \end{bmatrix} \tag{5.37}$$

where $A_{NS1} = T^{\perp T}T^{\#}B_K C$, $A_{NS2} = T^{\perp T}(A + BC_K T - T^{\#}B_K C)T^{+}$ and $A_{NS3} =$

[5] A pseudoinverse is a generalised inverse for any matrix and the matrix need not be a square matrix.

$T^{\perp^T}(A + BC_KT - T^{\#}B_KC)T^{\perp}$. By identifying x_{RS} with x_K, it is clear that Equation (5.37) contains the dynamics of A_{CL}. The dynamics of x and x_{RS} are not affected by the dynamics of x_{NS} due to the zero appearing at the (1,3) and (2,3) element of the matrix in Equation (5.37).

With the expression for K and L found for the case of $n_K \leq n$, the problem now boils down to finding T. There are many solutions for T, which can be found using an invariant subspace method (Laub, 1979). One possibility is to use the eigenvalues[6] decomposition of A_{CL} such that

$$U^{-1}A_{CL}U = \Lambda \tag{5.38}$$

where $U \in \mathbb{R}^{(n_K+n)\times(n_K+n)}$, and its columns are the eigenvectors of A_{CL}. Λ is a diagonal matrix with the eigenvalues of A_{CL} on the diagonal. The matrix U can be partitioned as

$$U = \left[\begin{array}{c|c} U_{11} & U_{12} \\ U_{21} & U_{22} \end{array}\right] \tag{5.39}$$

where the partitioned left column of U consists of the first n eigenvectors of A_{CL}. T can be chosen as $T = U_{21}U_{11}^{-1}$. The choice of this column also determines the eigenvalues which will be assigned to the dynamics of the state feedback and which will be assigned to the observer with the constraints that a pair of complex conjugate eigenvalues cannot be split, the uncontrollable poles and the unobservable poles must be assigned to the state feedback controller and the full order observer dynamic respectively. The choice of the eigenvalue assignment does not affect the closed loop transfer function in the absence of constraints, but it affects the rate of convergence of the dynamics of the observer. Guidelines for choosing the appropriate eigenvalues are given in (Bender, 1985).

Because $n_K \leq n$, the system with the full order observer will be a non-minimal realisation of K_{fav}. The closed loop system of Equations (5.18) and (5.21) will have $n - n_K$ extra eigenvalues which are not present in A_{CL}. The designer can choose any of these extra eigenvalues through the choice of $T^{\#}$, which is used to compute the gain of the full order observer, i.e. $L = T^{\#}B_K$. To compute $T^{\#}$, the following method, which derivation is based entirely on (Delmond *et al.*, 2006) is used. Any right invertible matrix can be written in the following form (Brookes, 2005),

$$T^{\#} = T^{+} + T^{\perp}X \tag{5.40}$$

[6] Another possibility is to use Schur decomposition.

where $X \in \mathbb{R}^{(n-n_K)\times n_K}$ is an arbitrary matrix and it is through the matrix X, that the designer can select these extra $n - n_K$ eigenvalues.

Let $A_{ob} := A - LC = A - T^{\#}B_K C$. Note that, eig$(A_{ob})$ consist of the eigenvalues of the full order observer, which contains the eigenvalues of A_{CL} assigned to the full order observer by solving for T and the extra $n - n_K$ eigenvalues. Performing similarity transformation by pre-multiplying A_{ob} with $\begin{bmatrix} T & T^{\perp^T} \end{bmatrix}^T$ and post-multiplying A_{ob} with $\begin{bmatrix} T^+ & T^{\perp} \end{bmatrix}$ leads to

$$\begin{aligned}
&\begin{bmatrix} T \\ T^{\perp^T} \end{bmatrix} A_{ob} \begin{bmatrix} T^+ & T^{\perp} \end{bmatrix} \\
&= \begin{bmatrix} A_K - TBC_K & A_K TT^{\perp} - TBC_K TT^{\perp} \\ T^{\perp^T}(A - T^{\#}B_K C)T^+ & T^{\perp^T}(A - T^{\#}B_K C)T^{\perp} \end{bmatrix} \\
&= \begin{bmatrix} A_K - TB_K C & 0 \\ T^{\perp^T}(A - T^{\#}B_K C)T^+ & T^{\perp^T}(A - T^{\#}B_K C)T^{\perp} \end{bmatrix}
\end{aligned} \tag{5.41}$$

The eigenvalues of $A_K - TBC_K$ are the eigenvalues of A_{CL} which is assigned to the full order observer by solving for T. The extra $n - n_K$ eigenvalues are the eigenvalues of $T^{\perp^T}(A - T^{\#}B_K C)T^{\perp}$. Substituting Equation (5.40) to $T^{\perp^T}(A - T^{\#}B_K C)T^{\perp}$ and after some algebraic rearrangement, yields $T^{\perp^T}AT^{\perp} - XB_K CT^{\perp}$. X^T can be computed using standard pole placement techniques with its canonical matrix given by the pair of $((T^{\perp^T}AT^{\perp})^T, (B_K CT^{\perp})^T)$. Using the obtained value of X, $T^{\#}$ can then be computed using Equation (5.40).

With T found, the weights in the MPC cost function are

$$\begin{aligned}
Q &= K^T K = (-C_K T)^T(-C_K T) \\
R &= I \\
S &= K^T = (-C_K T)^T
\end{aligned} \tag{5.42}$$

For MPC to reproduce K_{fav}, the MPC implementation must be based on the feedback of the states estimated by the full order observer with the observer gain must be chosen as $L = T^{\#}B_K$ as illustrated in Figure 5.3.

5.5.2 Using reduced order observer

In this section, we explore the use of a reduced order observer for reverse engineering. We will first briefly introduce the reduced order observer before showing how it can be used for reverse engineering. The introductory material follows the derivation in (Vaccaro, 1995) closely.

As some of the states are measured, the states of the plant can be partitioned into measured and non-measured states (here we use the subscript "M" and "NM" to denote "measured" and "not measured" respectively), i.e.

$$x(k) = \begin{bmatrix} x_M(k) \\ \hline x_{NM}(k) \end{bmatrix} \begin{matrix} \}m \\ \}(n-m) \end{matrix} \tag{5.43}$$

The partition of $x(k)$ leads to the following partition of the plant matrices,

$$A = \begin{array}{c} \overset{m}{} \quad \overset{n-m}{} \\ \left[\begin{array}{c|c} A_{11} & A_{12} \\ \hline A_{21} & A_{22} \end{array}\right] \begin{matrix} \}m \\ \}n-m \end{matrix} \end{array} \quad B = \begin{bmatrix} B_1 \\ \hline B_2 \end{bmatrix} \begin{matrix} \}m \\ \}n-m \end{matrix}$$

$$C = \begin{array}{c} \overset{m}{} \quad \overset{n-m}{} \\ \left[\begin{array}{c|c} C_1 & 0 \end{array}\right] \end{array} \tag{5.44}$$

where m is the number of measured states and n is the order of the plant. It follows that,

$$\begin{aligned} x_M(k+1) &= A_{11}x_M(k) + A_{12}x_{NM}(k) + B_1u(k) \\ x_{NM}(k+1) &= A_{21}x_M(k) + A_{22}x_{NM}(k) + B_2u(k) \end{aligned} \tag{5.45}$$

The reduced order observer will estimate x_{NM} given by

$$\hat{x}_{NM}(k+1) = A_{22}\hat{x}_{NM}(k) + B_2u(k) + A_{21}C_1^{-1}y(k) \tag{5.46}$$

where we have used $x_M(k) = C_1^{-1}y(k)$. For simplicity, C_1 is assumed to be invertible. In general, the matrix C can be any rank m matrix (see (Vaccaro, 1995) for details). One can observe the eigenvalues of A_{22}, cannot be chosen as A_{22} is the partitioned matrix from the plant. Equation (5.46) must be modified if A_{22} has eigenvalues outside the unit circle,

and it may also be desirable to modify Equation (5.46) if the eigenvalues are inside, but close to the unit circle. We first rename the variables in Equation (5.46) and rewrite them in a more general form as,

$$\begin{aligned} x_{NMG}(k+1) &= A_{ro}x_{NMG}(k) + B_{ro1}u(k) + B_{ro2}y(k) \\ \hat{x}_{NM}(k) &= x_{NMG}(k) + L_{ro}y(k) \\ u(k) &= -K_{NM}\hat{x}_{NM}(k) - K_M C_1^{-1} y(k) \end{aligned} \tag{5.47}$$

where $A_{ro} \in \mathbb{R}^{(n-m)\times(n-m)}$, $B_{ro1} \in \mathbb{R}^{(n-m)\times p}$, $B_{ro2} \in \mathbb{R}^{(n-m)\times m}$ and $L_{ro} \in \mathbb{R}^{(n-m)\times m}$.

The second equation in Equation (5.47) is the update equation based on the measurement $y(k)$ and L_{ro} is the reduced order observer gain. Note that, we can get back Equation (5.46) from Equation (5.47) if we set $A_{ro} = A_{22}$, $B_{ro1} = B_2$, $B_{ro2} = A_{21}C_1^{-1}$ and $L_{ro} = 0$.

We are interested in the dynamics of the error between the true states and the estimated states and would like the error dynamics to follow an equation of the form

$$e_{NM}(k+1) = A_{ro}e_{NM}(k) \tag{5.48}$$

where $e_{NM}(k) := x_{NM}(k) - \hat{x}_{NM}(k)$ and A_{ro} has the desired eigenvalues that ensure the error goes to zero asymptotically. We proceed to show how we arrive at Equation (5.48). With

$$e_{NM}(k+1) = x_{NM}(k+1) - \hat{x}_{NM}(k+1) \tag{5.49}$$

and substituting $x_{NM}(k+1)$ from the second equation of Equation (5.45) together with $\hat{x}_{NM}(k+1)$ from the second equation of Equation (5.47) into Equation (5.49), we have

$$e_{NM}(k+1) = [A_{21}x_M(k) + A_{22}x_{NM}(k) + B_2u(k)] - [x_{NMG}(k+1) + L_{ro}y(k+1)] \tag{5.50}$$

From Equation (5.47), the expression $x_{NMG}(k+1)$ can be written as

$$\begin{aligned} x_{NMG}(k+1) &= A_{ro}x_{NMG}(k) + B_{ro1}u(k) + B_{ro2}y(k) \\ &= A_{ro}[\hat{x}_{NM}(k) - L_{ro}y(k)] + B_{ro1}u(k) + B_{ro2}y(k) \\ &= A_{ro}[x_{NM}(k) - e_{NM}(k) - L_{ro}y(k)] + B_{ro1}u(k) + B_{ro2}y(k) \\ &= A_{ro}[x_{NM}(k) - e_{NM}(k)] + B_{ro1}u(k) + [B_{ro2}C_1 - A_{ro}L_{ro}C_1]x_M(k) \end{aligned} \tag{5.51}$$

where we have used $e_{NM}(k) = x_{NM}(k) - \hat{x}_{NM}(k)$ and $y(k) = C_1x_M(k)$ to get the third

and last line of Equation (5.51) respectively. $y(k+1)$, can be written as

$$\begin{aligned} y(k+1) &= C_1 x_M(k+1) \\ &= C_1[A_{11}x_M(k) + A_{12}x_{NM}(k) + B_1 u(k)] \end{aligned} \tag{5.52}$$

where we have used the first line of Equation (5.45) for $x_M(k+1)$. Substituting both Equations (5.51) and (5.52) into Equation (5.50), we arrive at the following equations,

$$\begin{aligned} e_{NM}(k+1) = {} & A_{ro}e_{NM}(k) + (A_{21} + A_{ro}L_{ro}C_1 - B_{ro2}C_1 - L_{ro}C_1A_{11})x_M(k) \\ & + (A_{22} - A_{ro} - L_{ro}C_1A_{12})x_{NMG}(k) \\ & + (B_2 - B_{ro1} - L_{ro}C_1B_1)u(k) \end{aligned} \tag{5.53}$$

To obtain Equations (5.48) from (5.53), we set the terms $(A_{21} + A_{ro}L_{ro}C_1 - B_{ro2}C_1 - L_{ro}C_1A_{11})$, $(A_{22} - A_{ro} - L_{ro}C_1A_{12})$ and $(B_2 - B_{ro1} - L_{ro}C_1B_1)$ to zero. In the process, we obtain the design equations for the reduced order observer itself. The design equations for the reduced order observer are thus given by (see (Vaccaro, 1995), Chapter 7),

$$A_{ro} = A_{22} - L_{ro}C_1A_{12} \tag{5.54}$$

$$B_{ro1} = B_2 - L_{ro}C_1B_1 \tag{5.55}$$

$$B_{ro2} = (A_{21} - L_{ro}C_1A_{11})C_1^{-1} + A_{ro}L_{ro} \tag{5.56}$$

From Equation (5.54), we observe that if the designer places the desired poles in A_{ro} to achieve a certain performance, the reduced order observer gain matrix L_{ro} can be found provide C_1A_{12} is invertible. Then, B_{ro1} and B_{ro2} can subsequently be found by solving Equations (5.55) and (5.56).

The use of those design equations and how L_{ro} can be computed depends on the relationship between n and m. In the case where $m \geq \frac{n}{2}$ and $\text{rank}(A_{12}) = (n-m)$, the designer can place the desired eigenvalues into $A_{ro} = \text{diag}(\lambda_1, \lambda_2, \ldots)$ and solve for L_{ro}, B_{ro1} and B_{ro2}. L_{ro} is computed using minimum norm solution, which is given by

$$L_{ro} = (A_{22} - A_{ro})(A_{12}^T C_1^T C_1 A_{12})^{-1} A_{12}^T C_1^T \tag{5.57}$$

As we have $\text{rank}(A_{12}) = (n-m)$ (i.e. full rank) and C_1 is nonsingular, $(A_{12}^T C_1^T C_1 A_{12})^{-1}$ is nonsingular.

For the case where $m = 1$, we are no longer able to place the poles as the diagonal entries in A_{ro} since by doing so, we would end up with an overdetermined system of equations. Moreover, when $m = 1$, $A_{12}^T C_1^T C_1 A_{12}$ in Equation (5.57) is not invertible as $A_{12} \in \mathbb{R}^{1\times(n-m)}$. Thus, we need to use a pole placement formula (e.g. Ackermann's formula) instead, which is given by

$$L_{ro} = \begin{bmatrix} C_1A_{12} \\ C_1A_{12}A_{22} \\ \vdots \\ C_1A_{12}A_{22}^{n-2} \end{bmatrix}^{-1} \begin{bmatrix} B_2 \\ A_{22}B_2 \\ \vdots \\ A_{22}^{n-2}B_2 \end{bmatrix} \begin{bmatrix} \lambda_{D,1} - \lambda_{A,1} \\ \lambda_{D,2} - \lambda_{A,2} \\ \vdots \\ \lambda_{D,n-1} - \lambda_{A,n-1} \end{bmatrix} \tag{5.58}$$

where λ_D and λ_A are our desired poles and the poles of A_{22} respectively. Note that Equation (5.58) is only valid for the case $m = 1$.

For the case where neither the two conditions above fits (e.g. $n = 5$ and $m = 2$ or $\text{rank}(A_{21}) \neq (n - m)$), the method of multivariable pole placement need to be used (see (Vaccaro, 1995), Chapter 9 for details).

Having introduced the design method for reduced order observer, next, we show how the reduced order observer is used for reverse engineering. The idea is similar to the use full order observer (see Figure 5.5 and compare it with Figure 5.3). The idea is to make use of the gain K_M and K_{NM} (these terms are introduced later in the next paragraph) to assign the relevant eigenvalues to the state feedback controller and then use the design equations for reduced order observer to assign the remaining eigenvalues to the reduced order observer.

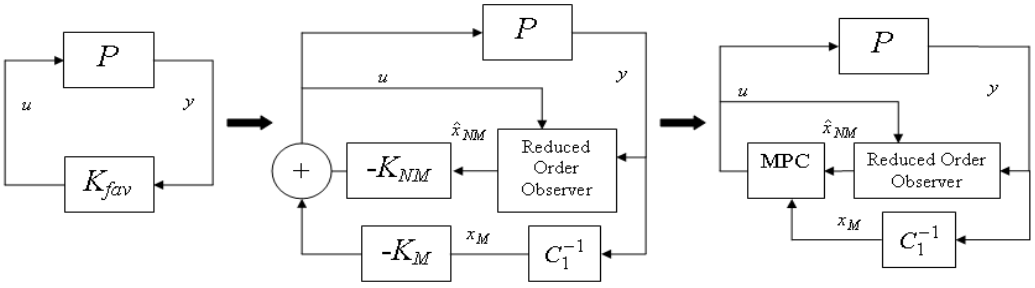

Figure 5.5: Reverse engineering using reduced order observer.

In the method of using the full order observer, we have computed $K = -C_K T$ and with

this K, some eigenvalues of A_{CL} have been assigned to the dynamics of the state feedback controller. We can make us of this K to ensure that when we combine the state feedback controller with the reduced order observer, we have also assigned some eigenvalues of A_{CL} to the dynamics of the state feedback controller. This can be done in the following manner. As the states of the plant have been partitioned, we can also partition the state feedback vector $K = [K_M|K_{NM}]$, where K_M acts on the measured states and K_{NM} acts on the estimated states from the reduced order observer.

The control law can then be written as

$$u(k) = -K_M x_M(k) - K_{NM}\hat{x}_{NM}(k) \tag{5.59}$$

Substituting Equation (5.59) into Equation (5.18), we get

$$x(k+1) = Ax(k) - BK_M x_M(k) - BK_{NM}\hat{x}_{NM}(k) \tag{5.60}$$

From $e_{NM}(k) = x_{NM}(k) - \hat{x}_{NM}(k)$, we have $\hat{x}_{NM}(k) = x_{NM}(k) - e_{NM}(k)$ and substituting it into Equation (5.60), we get,

$$\begin{aligned} x(k+1) &= Ax(k) - BK_M x_M(k) - BK_{NM}x_{NM}(k) + BK_{NM}e_{NM}(k) \\ &= Ax(k) - BKx(k) + BK_{NM}e_{NM}(k) \\ &= (A - BK)x(k) + BK_{NM}e_{NM}(k) \end{aligned} \tag{5.61}$$

where $BK_M x_M(k) + BK_{NM}x_{NM}(k) = BKx(k)$ as x_M and x_{NM} are the true states of the plant (see Equation (5.43)). We now need an equation in terms of $e_{NM}(k)$ such that we can formulate the closed loop system between the plant and the reduced order observer using the states $[x(k), e_{NM}(k)]^T$. In fact we already have the equation for $e_{NM}(k)$ i.e. Equation (5.48). With that the closed loop between the plant and the reduced order observer using the state vector $[x(k), e_{NM}(k)]^T$ is given by

$$\begin{bmatrix} x(k+1) \\ e_{NM}(k+1) \end{bmatrix} = \begin{bmatrix} A - BK & BK_{NM} \\ 0 & A_{ro} \end{bmatrix} \begin{bmatrix} x(k) \\ e_{NM}(k) \end{bmatrix} \tag{5.62}$$

Equation (5.62) tells us that the eigenvalues of this closed loop system is given by $\text{eig}(A - BK) \cup \text{eig}(A_{ro})$. Here, in order for the closed loop system using the reduced order observer to reproduce K_{fav}, the eigenvalues of $A - BK$ and A_{ro} must include the

eigenvalues of A_{CL}. As we have used the same $K = -C_K T$, from the full order observer, we have already assigned the eigenvalues to the dynamics of the state feedback controller and what is left is to assign the remaining eigenvalues of A_{CL} to the dynamics of the reduced order observer, i.e. to A_{ro} using the design equations presented above (i.e. Equations (5.54) to (5.56)) subject to the relationship between n and m. In the case where there are an extra of $(n - n_K - m)$ eigenvalues, these can be chosen arbitrarily by the designer and be assigned to A_{ro}. The above procedure guarantees that the eigenvalues of Equation (5.62) are the same as that of A_{CL} in the absence of constraint. The eigenvectors may be different, however no adverse effect of this has been observed so far in the reverse engineering.

For MPC to reproduce K_{fav}, the MPC implementation must be based on the feedback of the $n - m$ states by the reduced order observer and m measured states as illustrated in Figure 5.5.

5.5.3 Using state augmentation

We now present the third method of reverse engineering via state augmentation. A standard way to achieve integral action with a state feedback controller is to augment the plant with an integrator (Franklin *et al.*, 2006). This can be taken one step further. For an arbitrary controller in the form of Equation (5.19), we augment the plant with the controller such that,

$$\begin{aligned} A_{aug} &= \begin{bmatrix} A & 0 \\ B_K C & A_K \end{bmatrix} \quad B_{aug} = \begin{bmatrix} B \\ 0 \end{bmatrix} \\ C_{aug} &= \begin{bmatrix} C & 0 \end{bmatrix} \end{aligned} \tag{5.63}$$

with the new state $x_{aug}(k) = [x^T(k), x_K^T(k)]^T$. As $u(k) = C_K x_K(k)$, we have

$$K = [0, -C_K] \tag{5.64}$$

Note that if we choose $A_{ro} = A_K$, $B_{ro2} = B_K$, $K_{nm} = -C_K$, $B_{ro1} = 0$, $K_m = 0$ and $L_{ro} = 0$ in Equation (5.47), then the reduced order observer approach is the same as the state augmentation approach.

Remark: One thing worth mentioning here is that for the method of state augmentation,

we actually do not require that $D_K \neq 0$. With $y(k) = Cx(k)$ and the augmented states are $[x^T(k), x_K^T(k)]$, we can write $u(k) = C_K x_K(k) + D_K y(k) = C_K x_K(k) + D_K C x(k)$. Equation (5.64) then becomes

$$K = [-D_K C, -C_K] \tag{5.65}$$

5.6 Illustrative examples

We apply the three methods for reverse engineering to two examples. In the first example, we apply the method to a reach of the Broken River between Casey's and Gowangardie Weirs, i.e. Reach CG. This reach is controlled by a simple I-controller. The second example is a third order system controlled by a PI-controller, where we illustrate the use of loop shifting method to ensure a strictly proper controller prior to reverse engineering. For both the examples, the formulation of the quadratic programming problem is done in MATLAB® using YALMIP (Löfberg, 2004). The commercial package CPLEX 12.2 (IBM, 2009) is used to solve the optimisation problem.

5.6.1 Reach between Casey's and Gowangardie Weir

Figure 5.6 shows the control configuration.

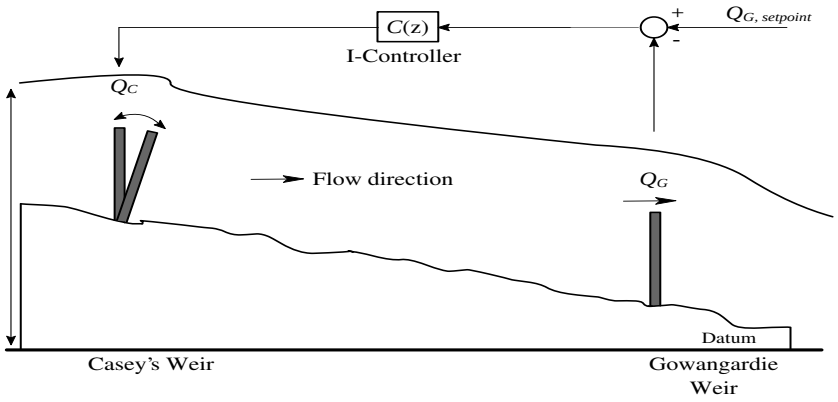

Figure 5.6: Control configuration of Reach Casey's Weir to Gowangardie Weir.

Farmers will pump water from the river and these offtakes act as disturbances. The I-

controller is used to reject these disturbances. We treat these disturbances as unmeasured disturbances. Hence, the control objective is for the I-controller to maintain the flow at Gowangardie Weir at setpoint in the presence of these offtakes.

In Section 5.1.5, we have presented ways to deal with disturbances whether they are either measured or unmeasured. As MPC is to reproduce the I-controller, and with the integral action reproduced by MPC, there is no necessity to augment the plant with the disturbance model, as the integral action reproduced by MPC will reject these unmeasured disturbances.

The reach between Casey's and Gowangardie Weir can be modelled as a simple time delay system (see Chapter 4),

$$Q_G(k) = Q_C(k - \tau) \tag{5.66}$$

where Q_C and Q_G are the flows over Casey's and Gowangardie Weirs respectively. The time delay for this reach is 1800 minutes. With a sampling interval of $T_s = 360$ minutes, $\tau = 5$.

Rewriting Equation (5.66) as a state space model, we obtain,

$$A = \begin{bmatrix} 0 & 1 & 0 & 0 & 0 \\ 0 & 0 & 1 & 0 & 0 \\ 0 & 0 & 0 & 1 & 0 \\ 0 & 0 & 0 & 0 & 1 \\ 0 & 0 & 0 & 0 & 0 \end{bmatrix} \quad B = \begin{bmatrix} 0 \\ 0 \\ 0 \\ 0 \\ 1 \end{bmatrix}$$
$$C = \begin{bmatrix} 1 & 0 & 0 & 0 & 0 \end{bmatrix} \tag{5.67}$$

The I-controller $C(z) = \frac{K_I}{z-1} = \frac{0.0529}{z-1}$ is chosen as K_{fav} where the matrices are given by $A_K = 1$, $B_K = K_I$ and $C_K = 1$.

Using Full Order Observer

For this system, $n = 5$ and $n_K = 1$. The eigenvalues of A_{CL} (Equation (5.20)) are $\lambda_{CL} = 0.9194, 0.7133, 0.1122 \pm j0.5398, -0.4285 \pm j0.2862$. We need to assign five poles to the state feedback controller. As the pairs of complex conjugate poles cannot be split and we prefer the fastest real pole to be placed at the observer dynamics (i.e., $\lambda = 0.7133$), we assigned $\lambda = 0.9194, 0.1122 \pm j0.5398, -0.4285 \pm j0.2862$ to the state feedback dynamics.

The extra $n - n_K$ eigenvalues were also chosen to be "fast", thus we arbitrary choose 0.1, 0.2, -0.3 and -0.4. Solving the Riccati Equation (Equation (5.30)) using an invariant subspace method, we obtained

$$\begin{aligned} T &= [0.0742, 0.1041, 0.1459, 0.2045, 0.2867] \\ T^{\#} &= [5.9179, 6.7116, -0.5276, -0.3418, 0.0323]^T \\ L &= [-0.3133, -0.3553, 0.0279, 0.0181, -0.0017]^T \\ K &= [-0.0742, -0.1041, -0.1459, -0.2045, -0.2867] \end{aligned}$$

Substituting these values together with Equations (5.31) and (5.32) into Equation (5.21) and rewriting in terms of transfer function, we obtained $C_{full}(z) = \frac{0.0529}{z-1}$ which is the I-controller.

Using Reduced Order Observer

The eigenvalues of A_{CL} should be contained in $\text{eig}(A - BK) \cup \text{eig}(A_{ro})$. In the full order observer, we have assigned n eigenvalues of A_{CL} using Equation (5.31). Using the same K, we partitioned it as $K = [K_M | K_{NM}]$ with $K_M = -0.0742$ and $K_{NM} = [-0.1041, -0.1459, -0.2045, -0.2867]$. The final control law is given by Equation (5.59). Thus, we are left with assigning the remaining n_K eigenvalues by placing them into A_{ro}.

With this choice of K, we are left to assign $\lambda = 0.7133$ to the observer dynamic. As $A_{ro} \in \mathbb{R}^{4\times4}$, we have an extra three poles that need to be assigned to the observer dynamic. We can again arbitrary choose any "fast" eigenvalues and we chose $\lambda = 0.4$, 0.5 and 0.6 to the reduced order observer. Placing the poles into A_{ro} using Equation (5.58) and solving for Equations (5.54) to (5.56), we obtain the following values,

$$\begin{aligned} L_{ro} &= [-2.2133, 1.8100, -0.6478, 0.0856]^T \\ A_{ro} &= \begin{bmatrix} 2.2133 & 1 & 0 & 0 & 0 \\ -1.8100 & 0 & 1 & 0 & 0 \\ 0.6478 & 0 & 0 & 1 & 0 \\ -0.0856 & 0 & 0 & 0 & 1 \end{bmatrix} \\ B_{ro1} &= [0, 0, 0, 1]^T \\ B_{ro2} &= [-3.0888, 3.3581, -1.3483, 0.1895]^T \end{aligned} \tag{5.68}$$

Note that the eigenvalues of A_{ro} are exactly the four eigenvalues we assigned to the reduced order observer. Substituting these values into Equation (5.47) and rewriting Equation (5.47) transfer function form, we obtain $C_{red}(z) = \frac{0.0529}{z-1}$, which is again the I-controller.

Using State Augmentation

The derivation is straight forward. From Equations (5.63) and (5.64) we have

$$\begin{aligned} u(k) &= -Kx_{aug}(k) = C_K x_K(k) = x_K(k) \\ &= K_I C x_{aug}(k-1) + x_K(k-1) \\ &= K_I y(k-1) + u(k-1) \end{aligned} \tag{5.69}$$

Rewriting Equation (5.69) in transfer function form, we obtain $C_{sa}(z) = \frac{U(z)}{Y(z)} = \frac{K_I}{z-1} = \frac{0.0529}{z-1}$, which is the I-controller.

Simulation results

In the simulation, a constant offtake occurs at time 7200 minutes. The flow setpoint at Gowangardie Weir is 0.5787 m^3/s (50ML/day). The offtakes will cause the flow at Gowangardie Weir to be less than the desired setpoint and the controller will make appropriate flow adjustment at Casey's Weir to maintain the flow at Gowangardie Weir at setpoint.

Figures 5.7 to 5.9 show the simulation results. The MPC prediction horizon is $N_p = 10T_s$. From Figure 5.7, we can see that the three reverse engineered MPC reproduce the I-controller very well as the plots are on top of each other making them indistinguishable. In addition, we plot the difference between the three methods compared to the I-controller in Figure 5.8 where we can see that the difference between all the three methods are small.

We now explore the potential benefit of using MPC in the presence of constraints. Although we have treated these offtakes as unmeasured disturbance, in practice, these offtakes to farm are usually known in advanced as farmers need to place the water orders with the water authority. In view of that, these offtakes are now treated as measured disturbances and we can include them in MPC as part of "feedforward" control as discussed in Section 5.1.5. In the following simulation, we constrain Q_G to be larger than $0.4m^3/s$ (34.5ML/Day) and we let this flow be a soft constraint. In practice, there are situations where a minimum flow is required in the river for environmental purposes (e.g. habitat

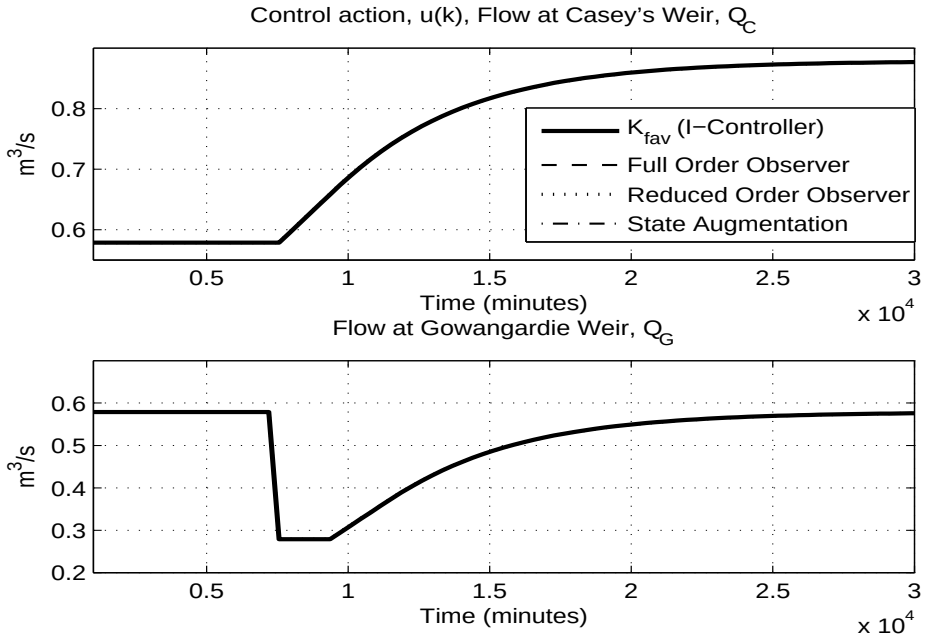

Figure 5.7: Reverse engineering using the three methods.

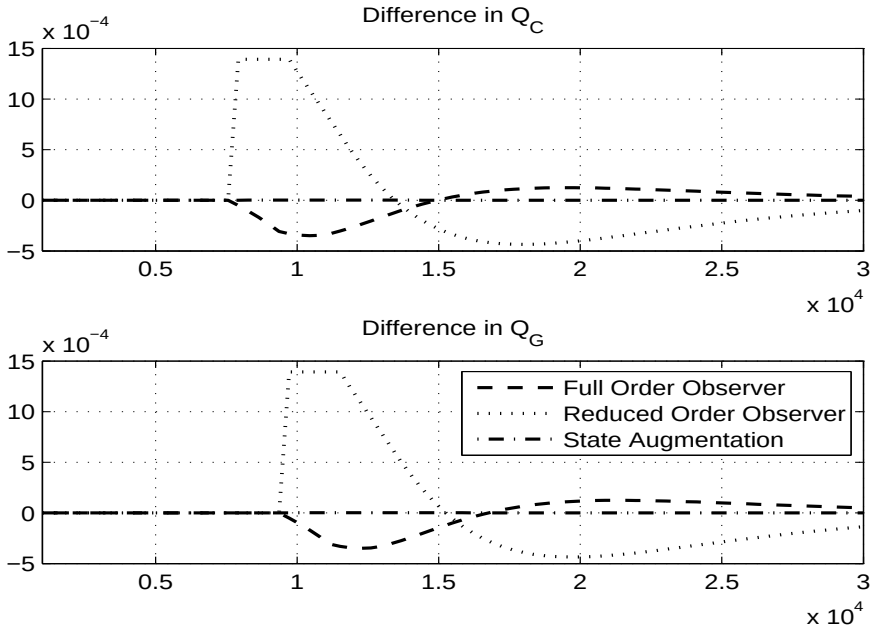

Figure 5.8: Difference between the three methods.

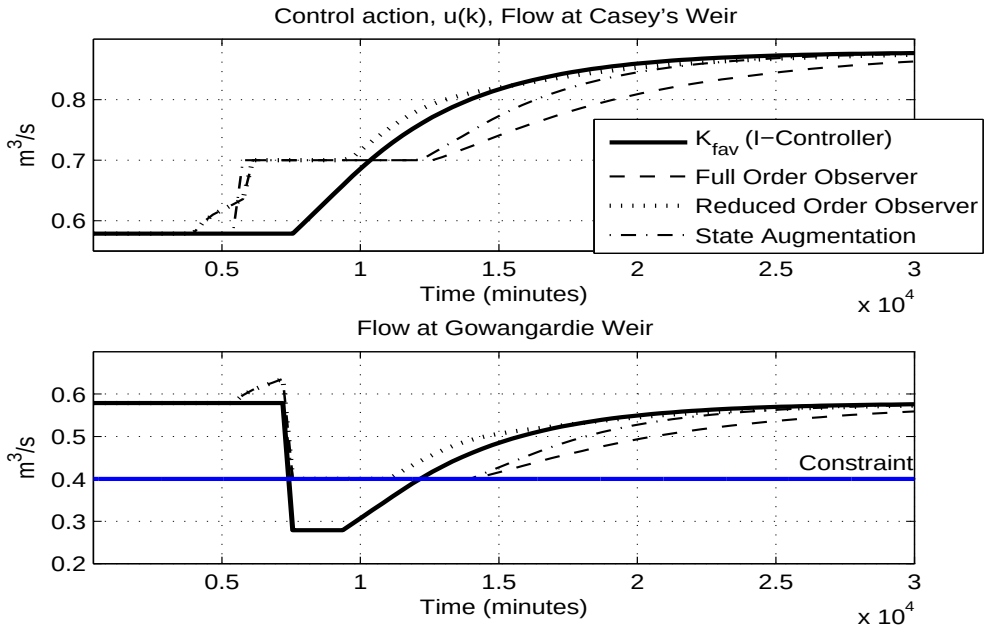

Figure 5.9: Constraints on Q_G.

preservation for aquatic creatures). From Figure 5.9 we can see that due to the prediction of future states, for all three methods, the MPC controller releases the flow earlier in order to avoid violating the constraints.

The simulations shown in Figures 5.7 to 5.9 are simulated on the time delay model, which is used for control design. To illustrate the effect of model mismatch and uncertainties in the system, the simulation is next carried out using the calibrated Saint Venant equations for Reach CG (see Chapter 3). The above simulations are repeated and the results are shown in Figures 5.10 to 5.12. From Figure 5.10, we can see that due to model mismatch the plots are no longer on top of each other. The plots in Figure 5.11 shows that the differences between the three methods are now larger. In terms of constraints handling capability (Figure 5.12), we do notice that there is violation of the constraints. This is due to model mismatch as the model used for control design is different from the model used for simulation. With the flow being a soft constraints, the violation of constraints occurs for a short period of time. Nonetheless, all three methods behave similarly to the case when the simulations are carried out using the time delay model.

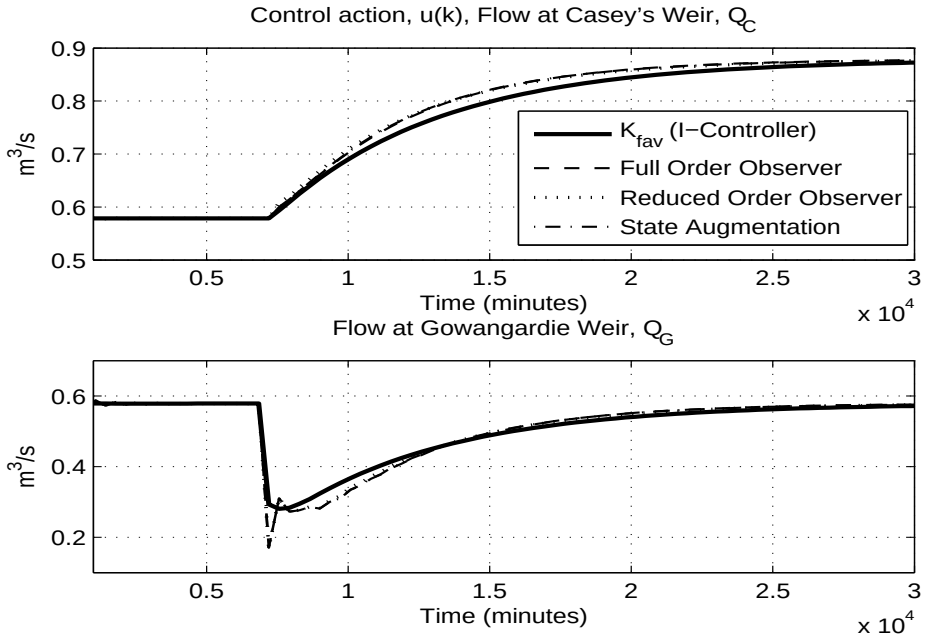

Figure 5.10: Reverse engineered MPC controllers simulated using Saint Venant Equations.

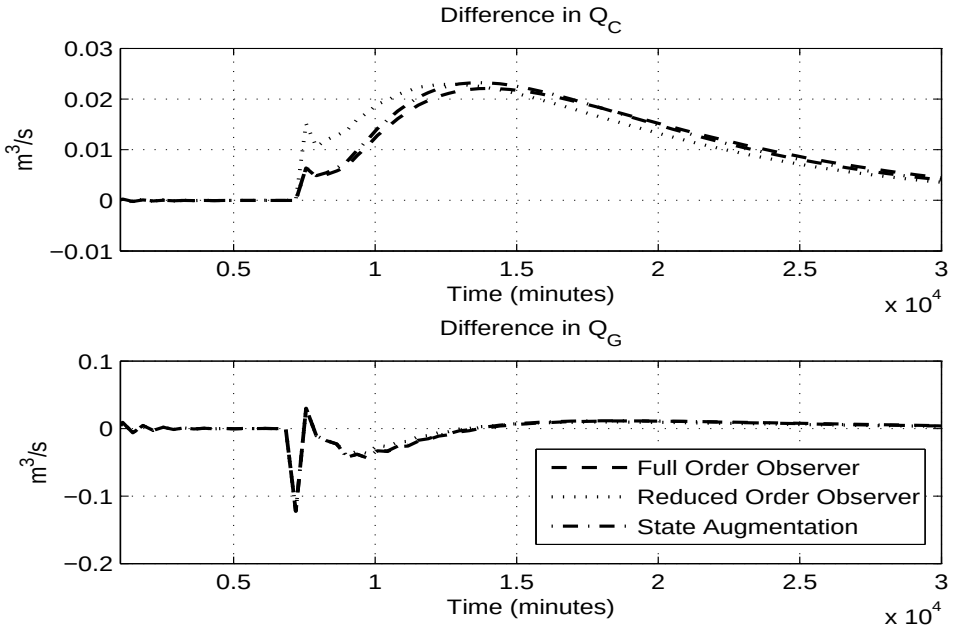

Figure 5.11: Difference between the three methods.

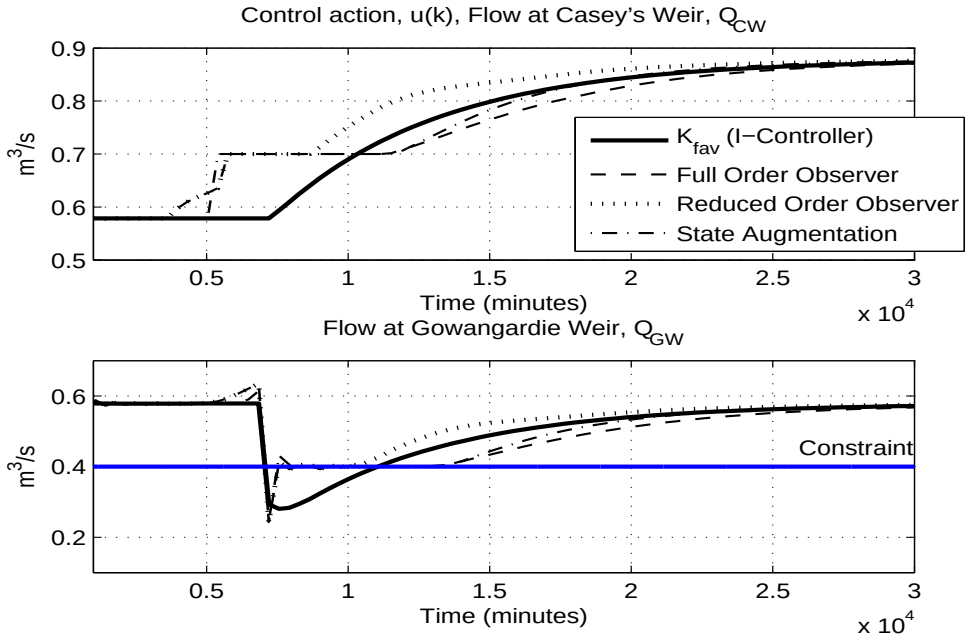

Figure 5.12: Constraints on Q_G.

5.6.2 Third order system

In this section, we illustrate the reverse engineering of K_{fav} when $D_K \neq 0$. The system we want to control is a cascade of three first order system with their transfer function given by $G_1(z) = \frac{1}{z-0.1}$, $G_2(z) = \frac{1}{z-0.3}$ and $G_3(z) = \frac{1}{z-0.5}$. The controller K_{fav} that we want to reproduce is a PI-controller given by $C(z) = K_P + \frac{K_I}{z-1} = 0.01 + \frac{0.02}{z-1}$.

Rewriting the plant in state space representation, we get the following dynamic matrices, i.e.

$$A = \begin{bmatrix} 0.1 & 1 & 0 \\ 0 & 0.3 & 1 \\ 0 & 0 & 0.5 \end{bmatrix} \qquad B = \begin{bmatrix} 0 \\ 0 \\ 1 \end{bmatrix} \qquad C = \begin{bmatrix} 1 & 0 & 0 \end{bmatrix} \tag{5.70}$$

For the PI-controller, the state space representation is given by

$$\begin{aligned} x_K(k+1) &= x_K + K_I y(k) \\ u(k) &= x_K + K_P y(k) \end{aligned} \tag{5.71}$$

with $A_K = 1$, $B_K = K_I = 0.02$, $C = 1$ and $D_K = K_P = 0.01$.

Using Full Order Observer

For this system, $n = 3$ and $n_K = 1$. Using the loop shifting method, the new A matrix for the plant is given by,

$$\bar{A} = A + BD_KC = \begin{bmatrix} 0.1 & 1 & 0 \\ 0 & 0.3 & 1 \\ 0.01 & 0 & 0.5 \end{bmatrix}$$

The eigenvalues of A_{CL} (Equation (5.20) but now with the (1,1) element equal $\bar{A}$) are $\lambda_{CL} = 0.9020, 0.7373, 0.1303 \pm j0.1435$. We need to assign three poles to the state feedback controller. Again, we have a pair of complex conjugate poles that cannot be split, and we prefer the fastest real pole to be placed at the observer dynamics (i.e., $\lambda = 0.7373$), we assigned $\lambda = 0.9020, 0.1303 \pm j0.1435$ to the state feedback dynamics. The extra $n - n_K$ poles were chosen to be 0.03 and 0.04.

Solving the Riccati Equation (Equation (5.30)) using an invariant subspace method, we obtained

$$\begin{aligned} T &= [0.0273, 0.0623, 0.2627] \\ T^{\#} &= [-4.6352, 5.1513, 3.0652]^T \\ L &= [0.0927, -0.1030, -0.0613]^T \\ K &= [-0.0273, -0.0623, -0.2627] \end{aligned}$$

Substituting these values together with Equations (5.31) and (5.32) into Equation (5.21) and rewriting in terms of transfer function, we obtained $C_{full}(z) = 0.01 + \frac{0.02}{z-1}$ which is the PI-controller.

Using Reduced Order Observer

Repeating the same procedure as before, we partitioned the K matrix into $K_M = -0.0273$ and $K_{NM} = [-0.0623, -0.2627]$. We are left with assigning $\lambda = 0.7373$ to the observer dynamic. As $A_{ro} \in \mathbb{R}^{2\times 2}$, we have one pole extra that needs to be assigned to the observer dynamic and we arbitrary chose $\lambda = 0.03$, which is a fast eigenvalue to the reduced order

observer. Placing the poles into A_{ro} using Equation (5.58) and solving for Equations (5.54) to (5.56), we obtain the following values,

$$\begin{aligned} L_{ro} &= [0.0327, -0.1115]^T \\ A_{ro} &= \begin{bmatrix} 0.2673 & 1 \\ 0.1115 & 0.5 \end{bmatrix} \\ B_{ro1} &= [0, 1]^T \\ B_{ro2} &= [-0.1061, -0.0510]^T \end{aligned}$$

Again, note that the eigenvalues of A_{ro} are exactly the two eigenvalues we had assigned to the reduced order observer. Substituting these values into Equation (5.47) and rewriting in terms of transfer function, we obtained $C_{red}(z) = 0.01 + \frac{0.02}{z-1}$, which is again the PI-controller.

Using State Augmentation

From Equation (5.65), we have

$$\begin{aligned} u(k) &= -Kx_{aug}(k) = C_K x_K(k) + D_K Cx(k) = x_K(k) + K_P y(k) \\ &= x_K(k-1) + K_I y(k-1) + K_P y(k) \\ &= u(k-1) - K_P y(k-1) + K_I y(k-1) + K_P y(k) \end{aligned}$$

Here, we used $u(k-1) = x_K(k-1) + K_P y(k-1)$, such that $x_K(k-1) = u(k-1) - K_P y(k-1)$ to get the third line of the equation above. Again, rewriting them in transfer function form, we obtain $C_{sa}(z) = \frac{U(z)}{Y(z)} = 0.01 + \frac{0.02}{z-1}$, which is the PI-controller.

Simulation results

At time $k = 5$, the setpoint is changed to 0.3. At time $k = 100$, the output is corrupted by a constant disturbance of 0.2. Like in the previous example, in the absence of constraints, the disturbance is initially treated as unmeasured disturbances for all the controllers as the goal is for MPC to reproduce K_{fav}. When the constraints are active, we then treat these disturbances as a measured disturbance and use it as part of "feedforward" control in MPC, and at the same time explore the benefit of constraint handling in MPC. The

simulation results using the three reverse engineering methods are shown in Figure 5.13.

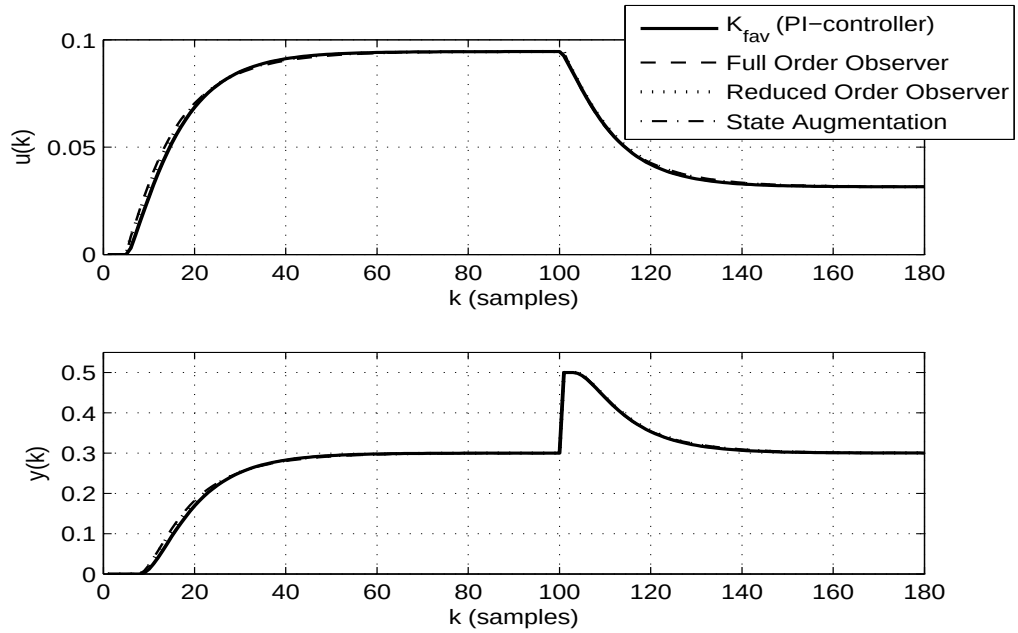

Figure 5.13: Reverse engineering of PI-controller using the three methods.

We plot the difference between each of the methods and the favourite PI-controller and as expected the differences are very small (see Figure 5.14). In addition, we constrained the output to be less than 0.4. From Figure 5.15, as the disturbance of 0.3 enters at time $k = 100$, it causes the output to reach 0.5 before the controller rejects it. As we have constrained the output to be less than 0.4, we can see that due to the prediction horizon, both the reverse engineering methods using the observers do not even reach the constraints and return to the setpoint at time $k = 130$. For the method of state augmentation, the output stays at the constraint for about 20 samples before returning to setpoint.

The simulation results show that the three method reverse engineered the PI-controller well and constraints are also handled well. The results also show that in the event of $D_K \neq 0$, we first do a loop shifting method before proceeding with the methods of reverse engineering.

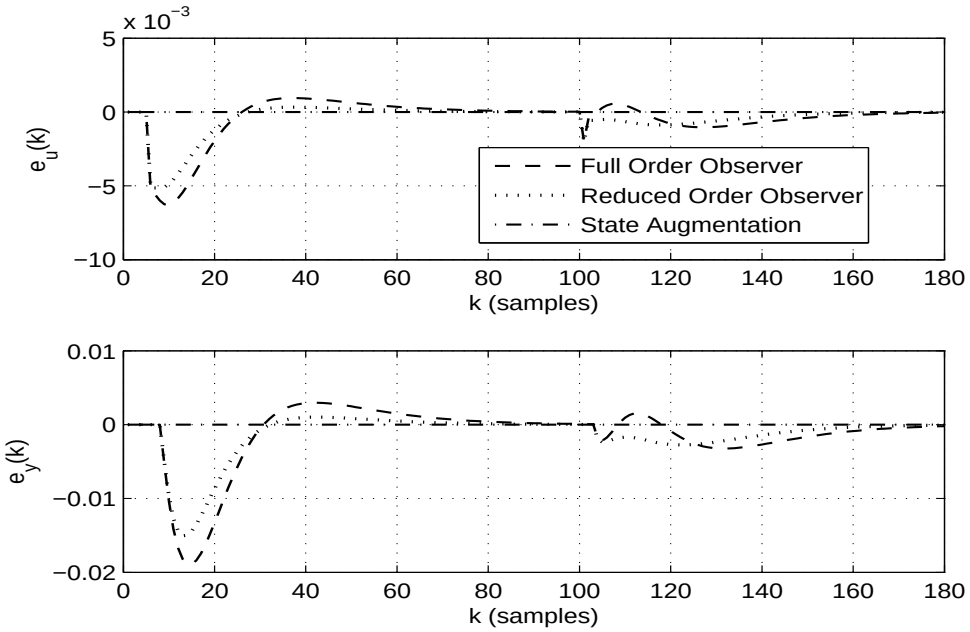

Figure 5.14: Difference between the three methods.

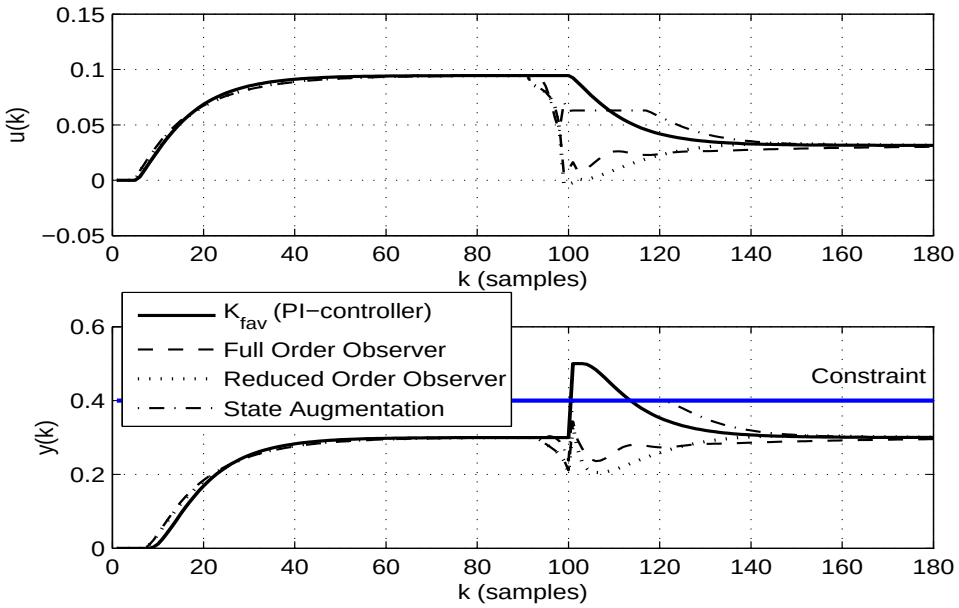

Figure 5.15: Constraints on output, $y(k)$.

5.7 Remarks on reverse engineering

5.7.1 The choice of cost function

The cost function, Equation (5.16) constructed using $u = -Kx$ is required in order for MPC to reproduce K_{fav}. Thus, when solving the optimisation problem, the computed optimal control input could potentially drive the system to satisfy the control law, $u = -Kx$ rather than to a desirable region. The effect of this phenomena is observed when we reverse engineer K_{fav} using the method of state augmentation.

Going back to the simulation of reach Casey's Weir to Gowangardie Weir, where in the simulation scenario, the flow over Gowangardie Weir is constrained $Q_G \geq 0.4\text{m}^3/\text{s}$ with the prediction horizon $N_P = 10T_s$ (see Figure 5.9). As the time delay for this reach is 1800 minutes, and offtakes occurred at time 7200 minutes, we expect the MPC controller to release the flow at Casey's Weir early as we have included the information about the offtakes as part of the "feedforward control". The MPC controller reverse engineered using the method of state augmentation does release the flow early at time 5400 minutes, which is exactly 1800 minutes (the time delay of this reach) early before the commencement of the offtakes. We also observe that the early release at time 5400 minutes resembles a step input.

In the next simulation scenario, we increase the prediction horizon to $N_P = 15T_s$, hoping to obtain a better performance with a larger prediction horizon. With a larger prediction horizon, we expect the MPC controller to release the flow much earlier than 5400 minutes. However, as shown in Figure 5.16, instead of releasing the flow earlier, the MPC controller reduces the flow earlier at time 2100 minutes. At time 5400 minutes, the MPC controller releases the required flow like the case when $N_p = 10T_s$ is used. As we increase the prediction horizon to $N_p = 20T_s$, the flow is reduced much earlier, at time 400 minutes and again the required flow is released at time 5400 minutes (see Figure 5.16). The reason for this phenomena is attributed to the computed optimal control input aims to satisfy the control law $u = -Kx$ than to drive the system to a desirable region. To be more specific, it is the cross term in the criterion function, (i.e. K or K^T term in Equation (5.16)) that create such behaviour. To illustrate the point that the cross term in the criterion function create that behaviour, we repeat the same simulation but this time, the cross term is removed from the criterion. The simulation results are shown in Figure 5.17. With a larger prediction horizon, i.e. $N_p = 15T_s$ and $N_p = 20T_s$, the flows at

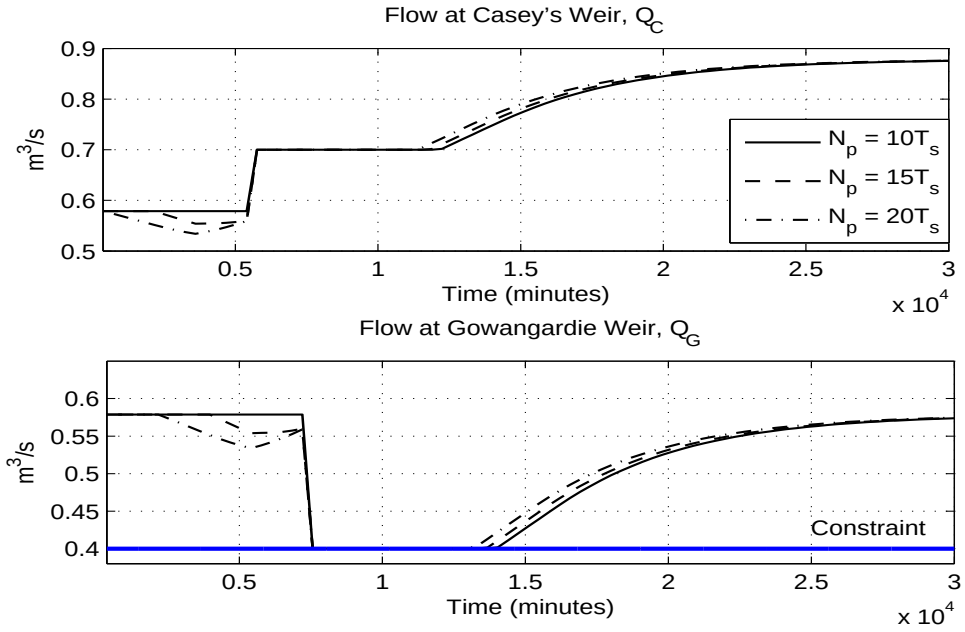

Figure 5.16: Reverse engineering using state augmentation with different N_P in the presence of constrain using the criterion with cross term.

Casey's Weir are released earlier at time 2600 minutes and 800 minutes respectively and no reduction of flow is observed. We note that the performance of the controller without the cross term is poor. Nonetheless, as the point we want to illustrate here is the effect of the cross term and not so much of the performance of the controller (other than the stability).

The reason behind this is the MPC controller, which reproduces the I-controller, upon "seeing" this offtakes earlier due to the larger prediction horizon starts to make the integral of the setpoint error more negative in order for the controller to be able to deliver the flow at time 5400 minutes. As $u = -Kx = K_I x_K$, for the integral of the setpoint error to become more negative means the control input u has to be reduced, leading to the early reduction of flow at Casey's Weir as shown in Figure 5.16. With the cross term becoming more negative, the controller in some sense is "storing" the effort to deliver the large flow at time 5400 minutes.

In the following simulation, we constrain the rate of change of flow at Casey's Weir, i.e. $|\Delta Q_C| < 0.01\text{m}^3/\text{s}$. The reason for constraining ΔQ_C is to ensure that the MPC

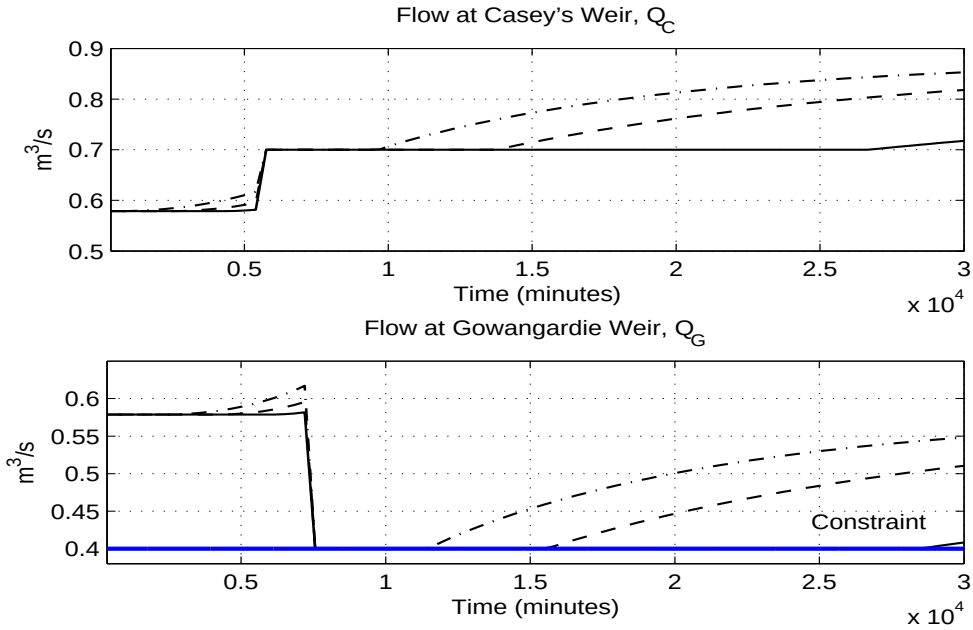

Figure 5.17: Reverse engineering using state augmentation with different N_P in the presence of constraint using the criterion without cross term.

controller will not be able to release the large flow and with that we would expect that the controller has no choice but to release the flow earlier. Furthermore, we also included a terminal cost P. Usually P is obtained as the solution of the Discrete Algebraic Riccati Equation (DARE), but as this value is zero (see Section 5.4), an alternative way of obtaining P is needed. As the controller state, which is also the state of the integrator has been augmented to the plant, we penalise this state with a weight of 20. As for the remaining states are just the delayed version of the control input, they are not penalise. Thus, the terminal cost P only has one weight at the diagonal entry that penalises the integrator state. We repeat the simulation using $N_p = 20T_s$ for both the cases of having constraint on ΔQ_C and using the terminal cost and the results are shown in Figure 5.18. By constraining ΔQ_C, the MPC controller is no longer able to deliver the large flow at time 5400 minutes. Thus, the MPC controller now starts releasing the flow earlier at time 1080 minutes. Similar behaviour is observed for the case where the terminal cost is included. The inclusion of terminal cost means that the system is no longer satisfying $u = -Kx$, thus resulting in the plot in Figure 5.18. With the terminal cost included, we also observe that the output goes back to the setpoint quicker. The findings presented

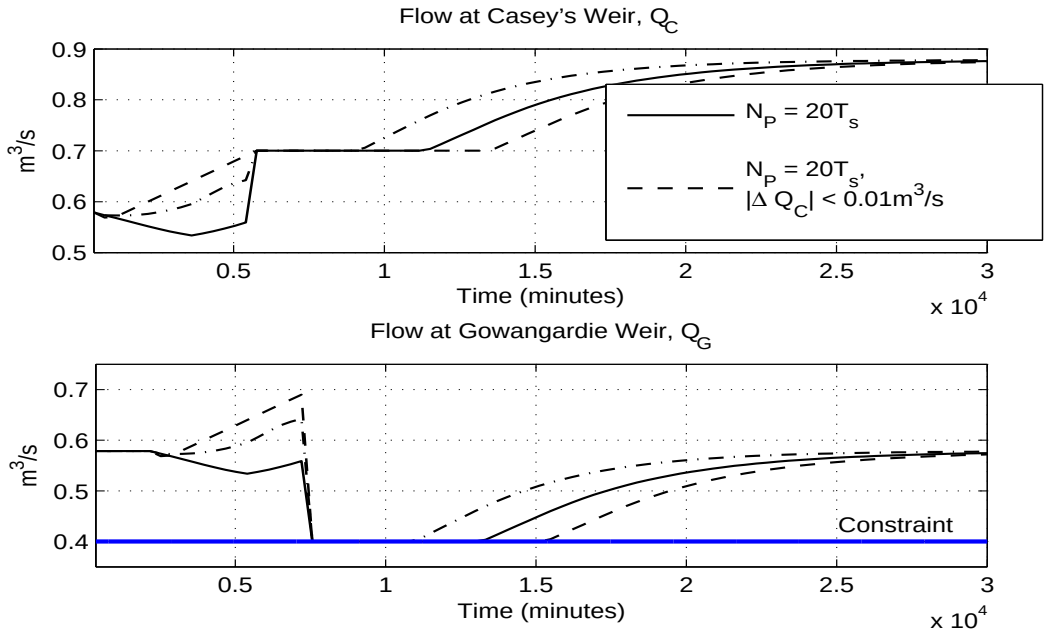

Figure 5.18: Comparison with constraint on rate of change of flow and terminal cost for $N_p = 20T_s$.

here, illustrated well that the computed control input would drive the system to satisfy the control law $u = -Kx$, rather than to the desirable region.

5.7.2 The role of the observer

In the method of reverse engineering that uses the full order and the reduced order observer, the main role of those observers is to reproduce the state of K_{fav} rather than estimating the states of the plant. We shall attempt to illustrate this point using the example of the third order system. The aim here is to show that these observers designed using the standard pole placement method would reproduce the states of the plant while the observers designed for reverse engineering would reproduce the states of K_{fav}. We use the term "conventional" observers to denote the observers designed using the pole placement method. We retain the same simulation settings used in Section 5.6.2, except that we redesign the gain for the state feedback controller and the gain for the conventional observers using the pole placement method.

For this simulation, we give an unmeasured input disturbance to the plant. Because

the gain of the state feedback and the conventional observer are chosen using the pole placement method, the integral action from the PI-controller is no longer reproduced by MPC. Thus, it is necessary for the plant to be augmented with the disturbance model as in Equation (5.7) in order to reject this disturbance. The observers are then designed using this augmented plant (i.e Equation (5.9)).

For the conventional full order observer, with the augmented plant (see Equation (5.9)), we have four poles that need to be assigned to the full order observer and we choose them to be 0.11, 0.13, 0.15 and 0.17. The gain of the full order observer is calculated using the *place* command in MATLAB®, and is given by, $L_{fo,con} = [1.340, 1.399, 1.059, 0.546]^T$. By augmenting the plant with the disturbance model means we have uncontrollable state. Thus the state feedback controller needs to be design using the original plant model and thus we have three poles that need to be assigned to the state feedback controller. We choose them to be 0.35, 0.36 and 0.37. Again, using the *place* command in MATLAB®, the state feedback gain is given by $K_{fo,con} = [-0.018, 0.087, -0.180]$.

For the conventional reduced order observer, with the augmented plant, we have three poles that need to be assigned to the reduced order observer. We choose them to be 0.13, 0.15 and 0.17. The gain of the reduced order observer is calculated using Equation (5.58) and it is given by, $L_{ro,con} = [1.350, 1.142, 0.614]^T$. As for the gain for the state feedback controller, the same poles used in the conventional full order observer are chosen leading to the same state feedback gain, i.e. $K_{ro,con} = K_{fo,con} = [-0.018, 0.087, -0.180]$.

In this simulation, at time $k = 25$, the disturbance of 0.5 enters at the input side of the plant. As K_{fav} is the PI-controller, the MPC is able to reject this disturbance due to the integral action inherited from the PI-controller. For the controller using the "conventional" observers, since we have augmented the plant with the disturbance model, the estimation of the disturbance made by the observers is able to cancel the effect of this disturbance, thus achieving a zero steady state error (see Figure 5.19). What is of more interest to us is the behaviour of the true states of the plant and the estimated states by the observers. The plots of the true states and the estimated states by the full order and reduced order observer are shown respectively in Figures 5.20 and 5.21.

From Figure 5.20 (left), when the conventional full order observer is used, we observe that the estimated states resemble the true states of the plant, which is expected given the role of the conventional observer is to estimate the states of the plant. On the other hand, in Figure 5.20 (right), the estimated states by the full order observer used for reverse

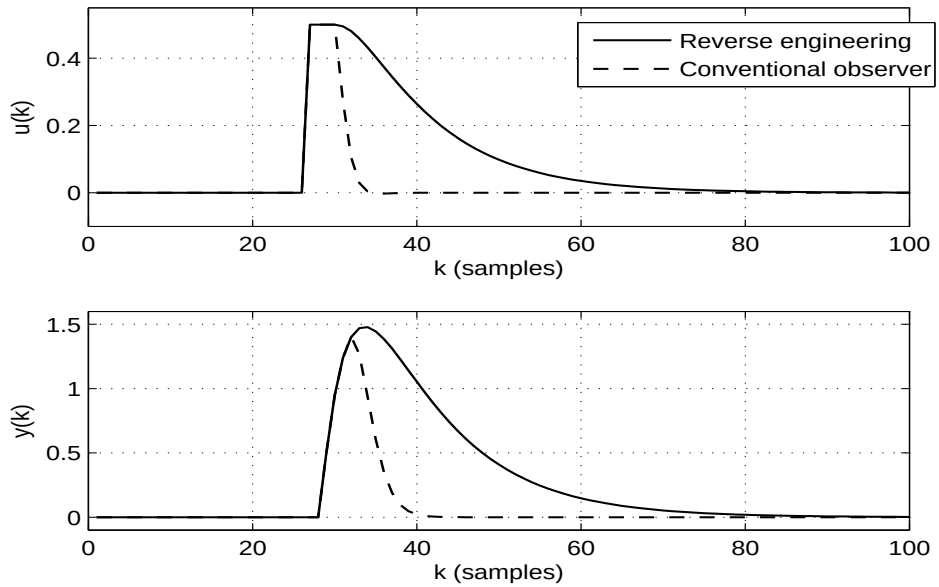

Figure 5.19: Third order system subject to input disturbance.

engineering is behaving very differently compared to the true states of the plant. This is because the role of the full order observer used for reverse engineering now is to reproduce K_{fav} than to estimate the states of the plant.

The true and estimated states when the reduced order observer is used is shown in Figure 5.21. Similar behaviours as when the full order observer is used are observed. The only thing we want to highlight is that for x_1, the true state and the estimated state are the same as this is the measured state, which is not estimated by the reduced order observer.

The illustrations from Figures 5.20 and 5.21 show that the main role of the observers used in reverse engineering is to reproduce K_{fav} and not for estimating the states of the plant. As the states of the observer are used as initial states to predict the future states within the controller, the dual role of the observer could potentially lead to a poor accuracy in the prediction (and hence, a poor control performance or even state constraint violation) due to this incorrect values of the initial states. This point has to be taken into account whenever the observer is used for reverse engineering especially when dealing with constraints.

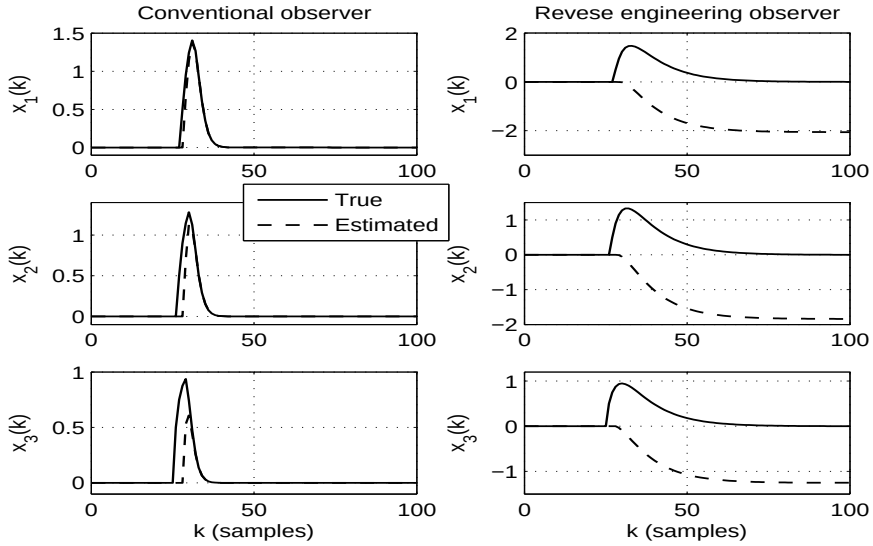

Figure 5.20: Comparison of the true and estimated states using the full order observer. Left: Conventional full order observer. Right: Reverse engineering using full order observer.

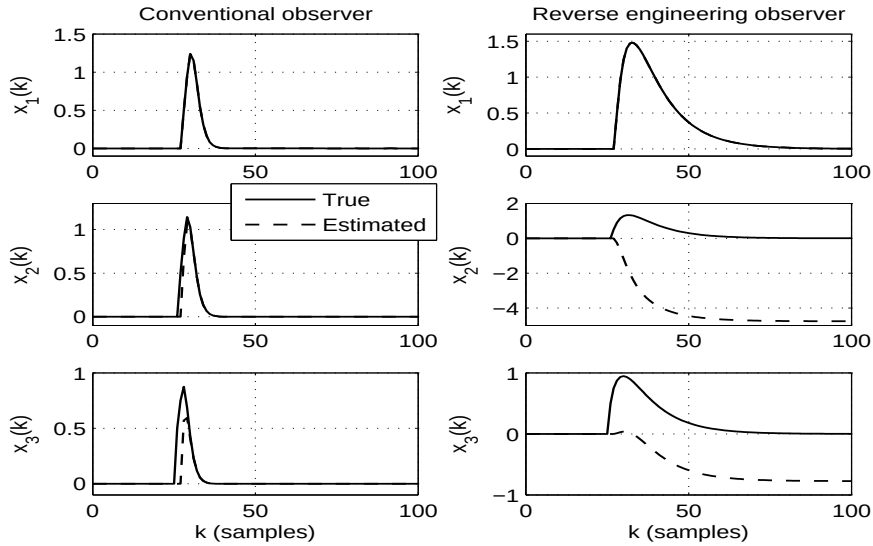

Figure 5.21: Comparison of the true and estimated states using the reduced order observer. Left: Conventional reduced order observer. Right: Reverse engineering using reduced order observer.

5.8 Summary

In this chapter, we have presented methods for reproducing an existing controller as an MPC controller. In the case where an observer is used, either a full order or a reduced order observer formulation can be used for reverse engineering. Alternatively, the method of state augmentation of the plant with the controller can be used. The methods are applied to two examples. From the simulation results, all the methods are able to reproduce the existing controller well and constraints are also handled well. We have illustrated that with the choice of $u = -Kx$ as the MPC criterion, the controller could actually drive the system to satisfy the control law rather than to the desirable region, when the constraints are active. Furthermore, the role of the observers in reverse engineering is mainly to reproduce the favourite controller, and not to estimate the states of the plant.

Chapter 6

Control of Broken River

In the previous chapter, the Model Predictive Controller (MPC) is introduced and methods for designing MPC via reverse engineering are presented. In this chapter, we apply MPC to control the Broken River. The objectives of the control system for the Broken River are to reduce water wastage, improve water delivery service to irrigators and meet the environmental demands. To ensure minimal water wastage, the control system need to ensure the releases from Lake Nillahcootie, which is the water supply for the Broken River are as small as possible. For improving water delivery service, we aim at reducing the advance water order time by the irrigators which can lead to improved farm planning and increased productivity. In order to meet the environmental demands, the control system has to ensure there is a minimum flow in the river and that there are suitable conditions for the creation of slack water pockets at certain times of the year.

Based on the objectives mentioned above, we can view the control problem as a problem where the flows and water levels in the Broken River are subjected to constraints. Thus, the use of MPC is deemed a suitable control strategy due to its capability to handle such constraints explicitly when solving the optimisation problem. Two MPC designs are considered in this chapter. The first design is based on reverse engineering, using the materials introduced in Chapter 5. The second design is the design of MPC from scratch, i.e, we obtain the tuning matrices of MPC based on the control objectives.

A year long realistic simulation of the Broken River with the demand from the irrigators, demand from the environments and in-flows from creeks based on historical data and realistic assumptions is carried out. The performance of the two MPC designs are

evaluated against current manual operation and a decentralised control strategy. The evaluation of the performance is based on the number of days in breach at the flow or water level constraints, and the amount of water released from Lake Nillahcootie.

We first present the control problems and the objectives associated with the Broken River in Section 6.1. The control configurations used for the Broken River are then discussed in Section 6.2. In Section 6.3, the state space representation of the river models of the Broken River used for control design are presented and this is followed by the MPC design in Section 6.4. Discussion of the simulation settings and the performance of the controllers are given in Sections 6.5 and 6.6 respectively and a summary is given at the end of the chapter.

6.1 Control problems, challenges and objectives

6.1.1 Control problems

In a wider perspective, the main control problem is to improve water resource management and operation for the benefit of the irrigators and the environment in the Broken River. To be more specific, we would like to ensure that there are minimal operational water wastage when supplying water to the irrigators and at the same time ensure that enough water is delivered to them. In order to define a quantitative measure for evaluating the performance of the controller, we used the term excess water to gauge the amount of operational water wastage. Excess water is defined as the amount of water leaving the study area that is not needed to satisfy all the required demands from the irrigators and the environments. As a note, the amount excess water leaving our study area is not deemed as wasted water, as it can be used to supply the demands for the irrigators further downstream from our study area. The strategies for how the water should be distributed between our study area and the downstream of our study area is dependent on the decision made by the water authorities.

We would also like to aim at improving water delivery service to the irrigators. Under current practice, the irrigators need to order their water four days in advance. There would be some potential benefits if the irrigators can order water on a shorter notice as this would allow more timely applications of water to pastures, crops, horticultural trees and viticulture vines, which may lead to improved productivity for the irrigators.

Apart from the demands from the irrigators, there are also the environmental demands that need to be satisfied. There is the need to ensure a minimum flow in the river for habitat preservation of aquatic life. There is also the need to maintain slack water pocket in the river for breeding of fish, shrimp, plankton, etc (see e.g. (Bowen *et al.*, 2003) and (Richardson *et al.*, 2004)). Slack water is understood as small, shallow areas of still water, which exhibits little or no discernible current and it is commonly formed by sand bars, boulders, woods, etc. From an ecological point of view, it is desirable that the variation in average daily flow is within certain limits. Furthermore, there is a need to ensure the water level variation in Lake Benalla is kept to a minimum since it is used for recreational activities.

In summary, the control problem in the Broken River is not just merely about delivery of water to the irrigators but there are a number of constraints imposed by the environment, which make the control problem challenging. There are a number of works on control of rivers using MPC but their focus is on optimising the hydroelectric operation, cost of pumping, ensuring a navigable river or satisfying ecological flow constraints (see Chapter 2). As far as the author is aware of, this is the first example of control of a river using MPC with the combined purpose of improving the efficiency, accuracy, and timeliness of water deliveries to the irrigators as well as the environment.

6.1.2 Main challenges

To have a better idea of what the main challenges are in the control of the Broken River, a description of the river is first given. Figure 6.1 shows a map of the Broken River. The area we consider begins from Lake Nillahcootie and ends at Gowangardie Weir. In the Broken River, the release of water from Lake Nillahcooties takes about four to six days to reach downstream locations between Casey's Weir and Gowangardie Weir, where most of the water demands are. This means that there are long time delays between the points of supply to the points of demand. Moreoever, these time delays vary with flow conditions as shown in Section 4.4.

What makes the control problem even more challenging is that there are very few points in the river where the flow can be regulated. At the time of writing, only the flow at Lake Nillahcootie and Broken Weir can be regulated. The benefit of having more regulation points is that the time delays between the points of supply and points of demand can be reduced. For example, if we can regulate flow at Casey's Weir, the demand between

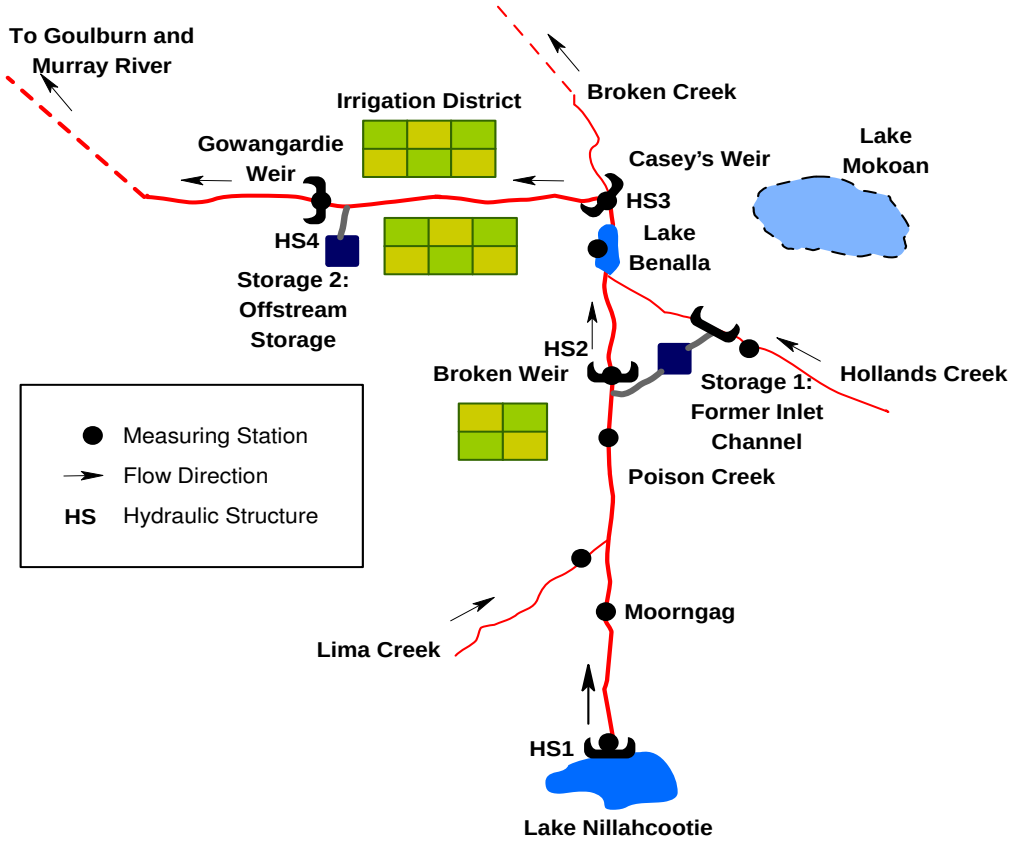

Figure 6.1: Top view of Broken River. Note: Figure is not to scale.

Casey's Weir and Gowangardie Weir can be supplied from Casey's Weir rather than all the way from Lake Nillahcootie. With a shorter time delay, a more accurate delivery of water can be achieved and the uncertainty in the time delays is also smaller. This can also help to reduce water wastage caused by releasing water too early or releasing too much water.

In some sense, the amount of water that need to be released from Lake Nillahcootie is actually still the same. This is because we are "borrowing" water from Casey's Weir while waiting for the water from Lake Nillahcootie to arrive. As we are "borrowing" the water from Casey's Weir, it is therefore essential to have storage near the regulation point and typical example of such storages are weir pools, lakes or an off-stream storage. This poses another challenge in the Broken River as there are also limited opportunities to store

water in-stream along the Broken River. There are identified potential in-stream storages, at the weir pool at Casey's Weir and Lake Benalla.

In order to increase the storage capacity along the river, two off-stream storages are considered. One of the storages is located in the upper part of the river (labelled Storage 1 in Figure 6.1) and one small off-stream storage along the reach between Casey's Weir and Gowangardie Weir (labelled Storage 2 in Figure 6.1). Storage 1 is the former in-let channel from Broken River via Hollands Creek to the now decommissioned Lake Mokoan. The out-flow from this storage is through Hollands Creek. At this point of writing, Storage 1 is currently being built. Billabong located in between Casey's and Gowangardie Weir is used as Storage 2. A billabong is a small pool of water, adjacent to the river. The billabong is the dead end pool of water created by a previous river path as a new river path is formed in the river.

In order to satisfy the water demands from the irrigators and the environment, it would be advantageous to have more regulated points close to the demands in the river. With more regulation points, the time delays from the points of supply to the points of demand can be shortened. Thus, we assume that on top of the available regulation points at Lake Nillahcootie and Broken Weir, the flow at Lake Benalla and Casey's Weir can also be regulated. We also assume that the in- and out-let of Storage 1 and Storage 2 can be regulated. As a note, the capacity for Storages 1 and 2 are 300ML and 6ML respectively. To have the regulation point at Lake Benalla, Casey's Weir and both the storages, an infrastructure upgrade is required.

6.1.3 Control objectives

Having taking into account the control problems, the encountered challenges and the defined constraints in the Broken River, the control objectives for the Broken River are summarised as follows:

- Ensure the timely delivery of water to the irrigators.

- Ensure minimum environmental flow at Lake Benalla, Gowangardie, Casey's and Broken Weirs. The minimum environmental flow requirements are 25ML/day for Gowangardie Weir and 22ML/day for Lake Benalla, Broken and Casey's Weirs.

- Maintain the flow over Gowangardie Weir at flow setpoint such that the demand downstream of Gowangardie Weir and the minimum environmental flow are satisfied.
- The release from Lake Nillahcootie should be as small as possible.
- Maintain the water levels at Broken Weir, Lake Benalla and Casey's Weir at setpoints. The water level setpoints are 2.15m, 2.25m and 2.00m respectively. However, there is an allowable limit of deviation for these water levels from their setpoints (see below).
- Ensure the mean daily flow in the river be between 0.76 and 1.5 of the flow from the previous day.
- Ensure the maximum flow released by the controller is less than 190ML/day to maintain slack water.
- Maintain Storages 1 and 2 at 50% and 80% full respectively.

As the irrigators draw water from the river (using pumps), there is a limit on how far down the water levels in the river can be drawn and the assumed limit in this chapter is 15cm. For Lake Benalla, which is used for recreational purposes, it is important to maintain the water level within a reasonable range, and it is also assumed to be 15cm from setpoint in this thesis.

Under the current practices for water ordering by the irrigators, once the water order is approved by the water authority, the irrigators can draw the water at the agreed time regardless of the flows and water levels condition in the river (assuming the water level in the river is high enough for the pump to operate). Also, with the water order approved, the water will be delivered and failure to release sufficient water will manifest itself through the drop in water levels in the in-stream storages associated with the regulation points, which could lead to violation of the limits on the water levels.

6.2 Control configuration for Broken River

The two most common control configurations for interconnected systems like the Broken River are the centralised and the decentralised control configurations. In the centralised configuration, all the control actions in the river reach are governed by a central controller.

This configuration is preferred when the number of reaches to be controlled are small as this configuration often lead to good performance due to that the interaction between all control actions are taken into account. Nonetheless, the drawback of a centralised controller, is high computational load in the design if the number of reaches is large. In addition, it is also computational heavy if a controller based on online optimisation such as MPC is used. In the implementation, the performance is susceptible to sensors and actuators communication failure.

On the other hand, in the decentralised configuration, each reach is controlled by a local controller. Thus, the implementation and the design of the local controller is simpler. It is more robust to data communication failure as there is minimal transmission of measurements and control actions between the controllers between neighbouring reaches. Nonetheless, because there is minimal transmission of measurements and control actions between the controllers between neighbouring reaches, the performance will not be as good as the centralised configuration.

In this chapter, two centralised MPC designs are considered. The first MPC design is based on reverse engineering of the decentralised controllers from (Ooi *et al.*, 2010). The second MPC design is an MPC design from scratch. Since the first MPC design is reverse engineered from the decentralised controllers in (Ooi *et al.*, 2010), these controllers are introduced in the next section.

6.2.1 Decentralised control configuration

In (Ooi *et al.*, 2010), there are four types of decentralised configurations used in the Broken River. The need for the different configurations arises from the different infrastructures and requirements along the Broken River. The first configuration is the distant downstream configuration. This configuration is used for the reach between Lake Benalla and Casey's Weir, the reach between Storage 1 and Lake Benalla and the reach between Lake Nillahcootie and Storage 1. The second configuration is the distant downstream control with storage, which is the configuration used for the reach between Casey's Weir and Gowangardie Weir. The third configuration is the upstream level control, which is the configuration at the in-let to Storage 1 and lastly, the fourth configuration is the flow mode configuration, which is used at Broken Weir. Due to the large time delays from the points of supply to the points of demand, feedforward of known future water order[1]

[1] As mentioned in Section 6.1.3, farmers need to order water four days in advance.

is included in the control configuration. The feedforward controller releases water earlier based on the time delays in each of the reaches such that the water arrive at the points of demand at the required time. The description of the four control configurations are given next.

Distant downstream configuration

Figure 6.2 shows the distant downstream control configuration. This configuration uses the upstream gate to control the flow or water level at the downstream end. The feedforward controller will release water based on the known future water orders and the required environmental flow $Q_{i,FF}$. The flow is released early such that it arrives when needed by the irrigators.

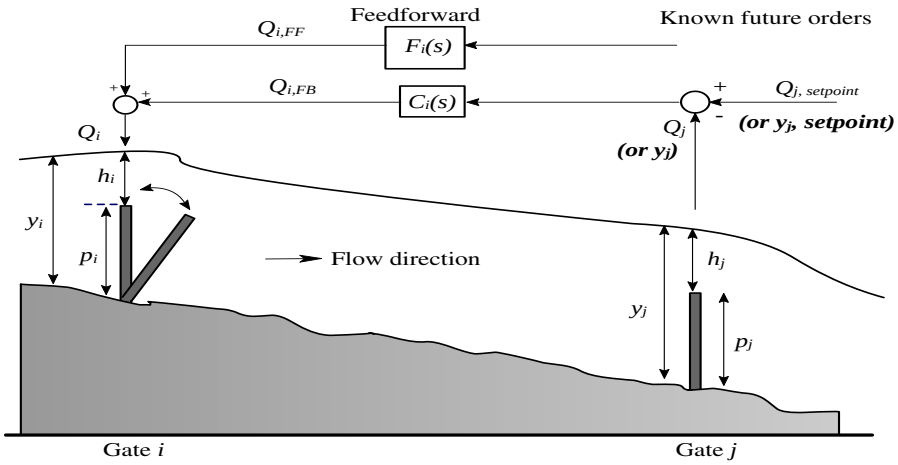

Figure 6.2: Distant downstream control configuration with early release.

In the event of model or time delay mismatch, which would lead to the water level deviating from the setpoint, the controller $C_i(s)$ upon measuring this deviation, will compute the required flow $Q_{i,FB}$ to bring the flow or water level back to the desired setpoint. The sum of these two flows Q_i constitute the flow at the upstream end of the reach.

Distant downstream configuration with storage

A variant of the distant downstream configuration is shown Figure 6.3 where a storage is included. The principle is similar to the case without storage. The controller $C_1(s)$ upon knowing the deviation of flow or water level from the setpoint, computes the required flow Q_{FB} and this flow is added to the feedforward of known future order and required environmental flow Q_{FF}. The sum of these two flows $Q = Q_{FB} + Q_{FF}$ constitutes the required flow at the storage. The flow required at the upstream end is the sum of the flow Q and the flow Q_U computed by the controller $C_2(s)$ when the water level (or volume) of the storage deviates from its setpoint. The in- and out-flow of the storage Q_S is determined based on the difference between the flow in the river Q and the delayed version $Q(t - \tau')$, which is the flow that is expected to arrive at the storage after τ' minutes when the flow Q is required. τ' is the delay time from upstream gate to the storage.

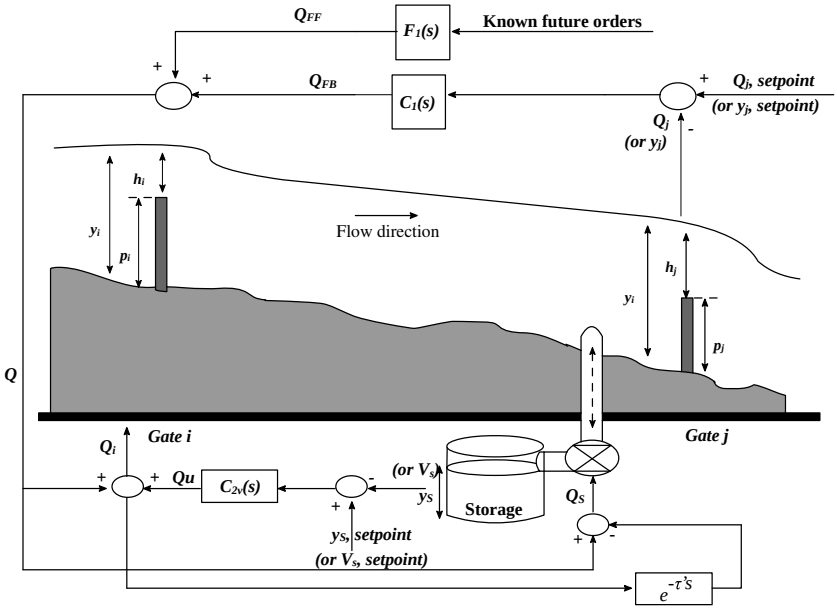

Figure 6.3: Distant downstream control with storage configuration with early release.

Upstream level control configuration

Figure 6.4 shows the upstream level configuration. The gate is regulated to control the water level immediately upstream of the gate. The response of this configuration is faster

as there is no delay involved. This configuration is suitable in scenarios where there is a need to control the water level within a narrow range. The controller $C(s)$ takes the

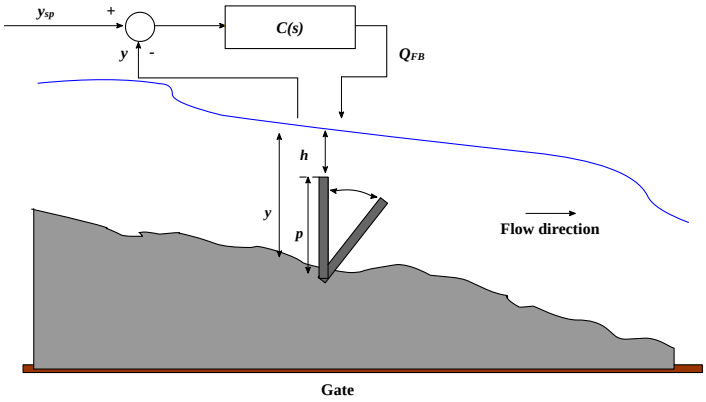

Figure 6.4: Upstream level control configuration.

difference between the controlled variable and its setpoint and adjust the gate accordingly and the effect is almost immediate. As the effect is almost immediate, it essentially just passes through any flow that is coming from the upstream end.

Flow mode configuration

Figure 6.5 shows the flow mode configuration. In this configuration, the flow is kept at

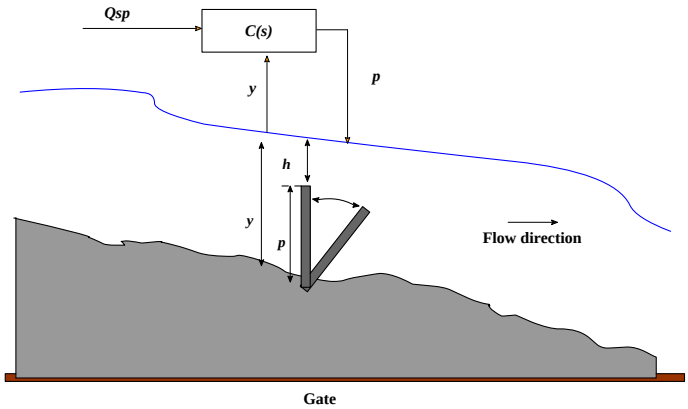

Figure 6.5: Flow mode configuration.

the desired setpoint and any adjustment is made to the gate based on the current water level upstream of the gate.

The decentralised control configuration used in (Ooi *et al.*, 2010) is shown in Figure 6.6. $C_1(s)$ to $C_3(s)$ are the distant downstream PI-controllers. $C_4(s)$ is a distant downstream I-controller, $C_5(s)$ is a P-controller and $C_6(s)$ is an upstream level PI-controller. $F_1(s)$ to $F_4(s)$ are the feedforward controllers. Each of the feedforward controllers releases the required flow according to the known future order and the environment flow of its respectively reaches earlier such that the water arrives at the time the irrigators require the water. $e_{Q,y,V}$ are the differences of the flows, water levels or volumes from their respective setpoints. For reverse engineering, MPC will reproduce this control configuration as shown by the dotted box on top of Figure 6.6. As Broken Weir is in flow mode, it is treated as a known disturbance and thus it is not considered in the reverse engineering. Note that MPC only reproduces all the $C(s)$ blocks and not the $F(s)$ blocks. For the MPC control configuration designed from scratch, the configuration is shown in Figure 6.7.

6.3 Models of Broken River for control design

6.3.1 Models of reaches in the Broken River

In Chapter 4, we have shown that the time delay and the integrator delay models are accurate in describing the dynamics of the reaches in the Broken River. In Section 6.1.3, the regulation points considered in the Broken River are at Lake Nillahcootie, Broken Weir, in- and out-let of Storage 1, Lake Benalla and Casey's Weir. Based on the configuration shown in Figure 6.6, the reaches from Lake Nillahcootie to Broken Weir, from in-let to out-let of Storage 1, from out-let of Storage 1 to Lake Benalla and from Lake Benalla to Casey's Weir are modelled using integrator delay models. The integrator delay models are used here because all the downstream flows of those reaches can be regulated independently of the upstream flows. Moreover, the weir pool at Casey's Weir and Lake Benalla, acts as storages.

The flow at Gowangardie Weir cannot be regulated at present and it is not likely that it will be upgraded with regulation gates due to the costs involved. Thus, it will remain a free overfall weir. Hence, the reach from Casey's Weir to Gowangardie Weir is modelled using a time delay model.

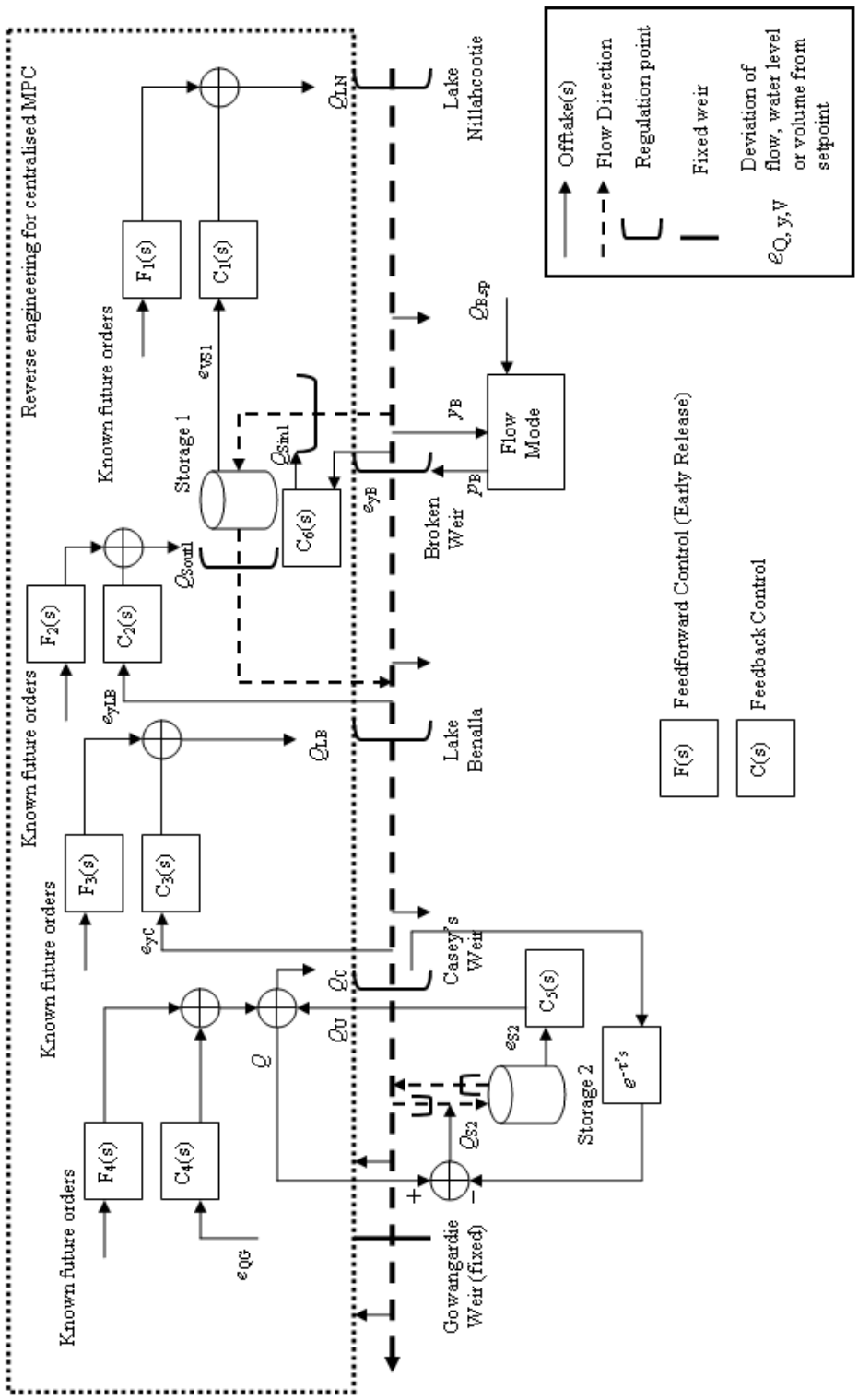

Figure 6.6: Decentralised control configuration for the Broken River in (Ooi *et al.*, 2011) for reverse engineering.

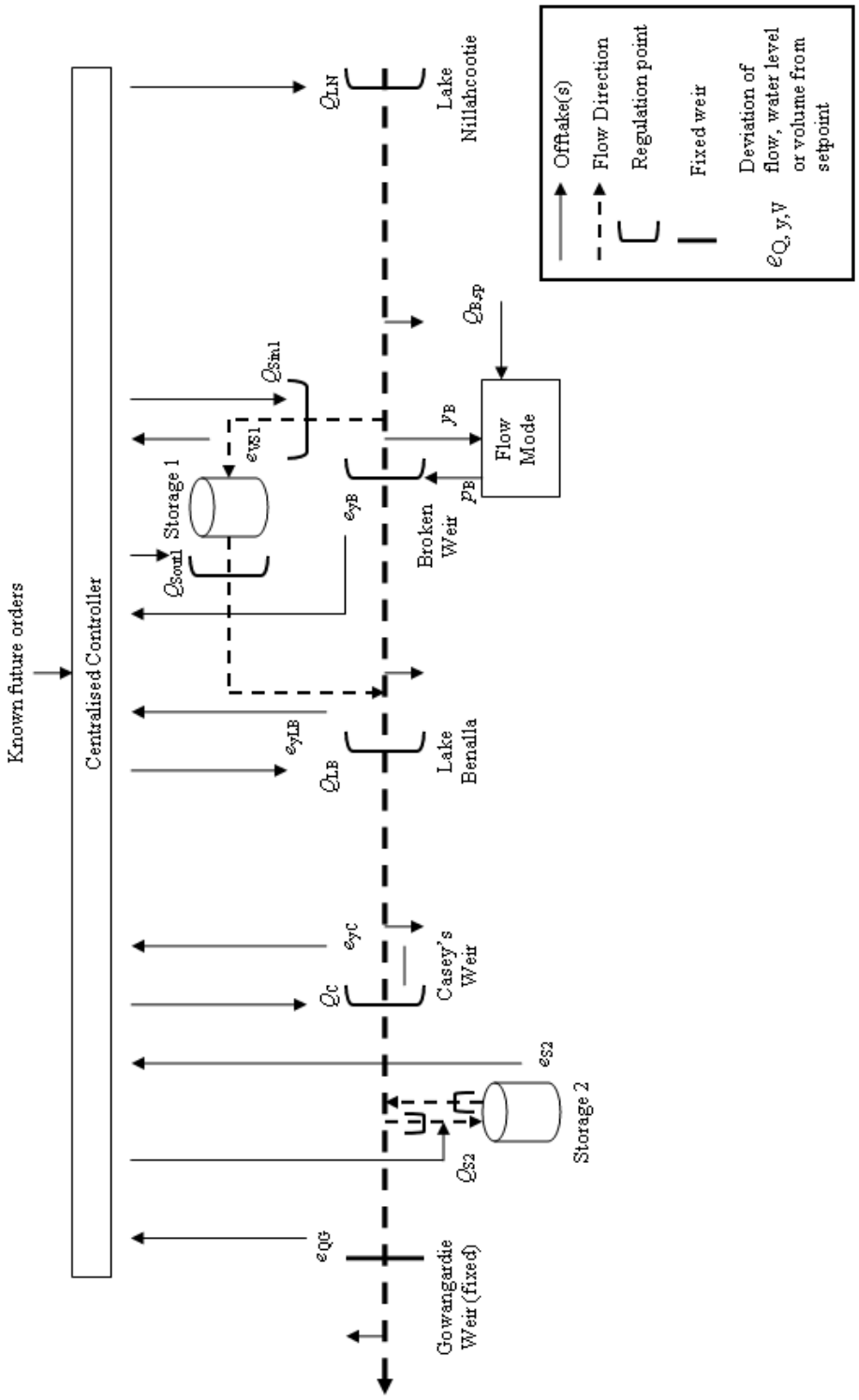

Figure 6.7: Centralised control configuration for the Broken River.

In addition, we will assume that overshot gates are used as regulation gates. The flow over these gates can be approximated by

$$Q(t) = ch^{3/2}(t) = c[y(t) - p(t)]^{3/2} \tag{6.1}$$

where Q is the flow, c is a constant, y is the water level and p is the height of the gate. Note that, although the models for some of the reaches in the Broken River have been discussed in Chapter 4, we shall present a brief discussion on these model here. The reason is because based on the control configuration shown in Figure 6.6, we have additional new reaches.

Reach Lake Nillahcootie to Broken Weir (Reach LNB)

Reach LNB can be modelled as

$$\dot{V}_B(t) = c_{1,B}Q_{LN}(t - \tau_{LNB}) - c_{2,B}[y_B(t) - p_B(t)]^{3/2} - c_{3,B}Q_{Sin1}(t) \tag{6.2}$$

where the subscripts "LN", "B" and "Sin1" represent Lake Nillahcootie, Broken Weir and in-let to Storage 1 respectively. τ_{LNB} is the time delay from Lake Nillahcootie to Broken Weir. Note that the upstream level control configuration is used here where the flow at in-let to Storage 1 Q_{Sin1} is used to control water level at Broken Weir y_B. With the in-let to Storage 1 is located close to Broken Weir, the time delay is negligible. Using an Euler approximation for the derivative and assuming the water level is proportional to the volume, we get

$$\begin{aligned} y_B(k) = y_B(k-1) &+ \left(\frac{T_s c_{1,B}}{A}\right) Q_{LN}(k - \tau_{LNB} - 1) - \left(\frac{T_s c_{2,B}}{A}\right) [y_B(k-1) - p_B(k-1)]^{3/2} \\ &- \left(\frac{T_s c_{3,B}}{A}\right) Q_{Sin1}(k-1) \end{aligned} \tag{6.3}$$

where k is the discrete time index, T_s is the sampling interval and A is the surface area.

Reach Lake Nillahcootie to out-let of Storage 1 (Reach LNSout1)

The change of volume in Storage 1 can be modelled as

$$\dot{V}_{S1}(t) = Q_{Sin1}(t) - Q_{Sout1}(t) \tag{6.4}$$

Instead of using the in-let to Storage 1, the release from Lake Nillahcootie is used to control the volume of Storage 1. As the in-let to Storage 1 is controlled by a fast acting upstream level controller, it will essentially passes the release from Lake Nillahcootie into Storage 1, while maintaining the water level at Broken Weir at setpoint. Therefore, $Q_{Sin1}(t) \approx Q_{LN}(t - \tau_{LNSout1}) - Q_B(t)$ is a reasonable approximation. As the in-let to Storage 1 is located near Broken Weir, the time delay from in-let to Storage 1 to Broken Weir is assumed negligible. With that, Equation (6.4) can be rewritten as,

$$\dot{V}_{S1}(t) = Q_{LN}(t - \tau_{LNSout1}) - Q_{Sout1}(t) - Q_B(t) \tag{6.5}$$

where the subscripts "LN", "Sout1" and "B" represent Lake Nillahcootie, out-let of Storage 1 and Broken Weir respectively. We call this reach, Reach LNSout1. $\tau_{LNSout1}$ is the time delay from Lake Nillahcootie to the out-let of Storage 1. Using an Euler approximation for the derivative, we arrive at

$$\begin{aligned} V_{S1}(k) = V_{S1}(k-1) + T_s Q_{LN}(k - \tau_{LNSout1} - 1) - T_s Q_{Sout1}(k-1) \\ - T_s Q_B(k-1) \end{aligned} \tag{6.6}$$

Reach out-let of Storage 1 to Lake Benalla (Reach Sout1LB)

For Reach Sout1LB, it is modelled as

$$\dot{V}_{LB}(t) = c_{1,LB} Q_{Sout1}(t - \tau_{Sout1LB}) - c_{2,LB}[y_{LB}(t) - p_{LB}(t)]^{3/2} + c_{3,LB} Q_B(t - \tau_B) \tag{6.7}$$

where the subscripts "Sout1", "LB" and "B" represent out-let of Storage 1, Lake Benalla and Broken Weir respectively. $\tau_{Sout1LB}$ is the time delay from out-let of Storage 1 to Lake Benalla and τ_B is the time delay from Broken Weir to Lake Benalla. Again using an Euler approximation for the derivative, we get

$$\begin{aligned} y_{LB}(k) = y_{LB}(k-1) + \left(\frac{T_s c_{1,LB}}{A}\right) Q_{Sout1}(k - \tau_{Sout1LB} - 1) \\ - \left(\frac{T_s c_{2,LB}}{A}\right) [y_{LB}(k-1) - p_{LB}(k-1)]^{3/2} + \left(\frac{T_s c_{3,LB}}{A}\right) Q_B(k - \tau_B - 1) \end{aligned} \tag{6.8}$$

Reach Lake Benalla to Casey's Weir (Reach LBC)

Reach LBC is modelled as

$$\dot{V}_C(t) = c_{1,C}Q_{LB}(t - \tau_{LBC}) - c_{2,C}[y_C(t) - p_C(t)]^{3/2} \tag{6.9}$$

where the subscripts "LB" and "C" represent Lake Benalla and Casey's Weir respectively. τ_{LBC} is the time delay from Lake Benalla to Casey's Weir. Again, using an Euler approximation for the derivative, we get

$$y_C(k) = y_C(k-1) + \left(\frac{T_s c_{1,C}}{A}\right) Q_{LB}(k - \tau_{LBC} - 1) - \left(\frac{T_s c_{2,C}}{A}\right) [y_C(k-1) - p_C(k-1)]^{3/2} \tag{6.10}$$

Reach Casey's Weir to Gowangardie Weir (Reach CG)

Reach CG is modelled with a time delay model (in discrete representation),

$$Q_G(k) = Q_C(k - \tau_{CG}) + Q_{S2}(k - \tau_{S2G}) \tag{6.11}$$

where Q is the flow and τ_{CG} is the time delay from Casey's Weir to Gowangardie Weir while τ_{S2G} is the time delay from Storage 2 to Gowangardie Weir. The subscript, "C", "G" and "S2" denote Casey's Weir, Gowangardie Weir and Storage 2 respectively. Storage 2 is modelled using an integrator, i.e.,

$$\dot{V}_{S2}(t) = -Q_{S2}(t) \tag{6.12}$$

where V is the storage volume and Q_{S2} is the storage flow and using an Euler approximation for the derivative, Equation (6.12) becomes

$$V_{S2}(k) = V_{S2}(k-1) + T_s Q_{S2}(k-1) \tag{6.13}$$

The unknown parameters and time delays in the models need to be estimated. The parameters and the time delays identified in Chapter 4 cannot be used directly because those parameters are identified under different flow conditions. Thus, it would be more representative to re-identified the parameters in particular the time delays under the same flow condition for all the reaches. As the typical flow condition in the Broken River is

around 30ML/day, a step test of flow from 30ML/day to 60ML/day is simulated using the calibrated Saint Venant equation (from Chapters 3 and 4) for all the reaches in the Broken River except for Reach LNSout1 and Reach Sout1LB to obtain the time delays. Another reason the flow of 30ML/day is considered is that this flow is considered "low flow" (see Section 4.4). The time delay under low flow condition is the largest, which leads to large phase shift. Thus, a controller with the largest phase leads is then required to ensure stability.

Reach LNSout1 and Reach Sout1LB, are "new" reaches as a result of the control configuration shown in Figure 6.6. However, the time delays for these two reaches can still be estimated. For Reach LNSout1, given that the in-let to Storage 1 is located close to Broken Weir, the time delay from Lake Nillahcootie to Broken Weir can be used. As for Reach Sout1LB, the physical geometries (bottom width, side slope, bottom slope and Manning friction coefficient) for this reach is obtained based on the best approximate using the on-site survey carried out by Goulburn-Broken Catchment Management Authority (GBCMA) (GBCMA, 2009) and observation using Google Earth. Using these best approximated physical geometries, a Saint Venant equations model is built.

As we do not have any measurements to validate the Saint Venant equations for this reach, we are left to treat the Saint Venant equations for this reach as an accurate representation of the reach. Using this Saint Venant equations, the step test is simulated to obtain the time delay from out-let of Storage 1 to Lake Benalla. The estimated time delay for this reach as shown in Table 6.1 is reasonable based on the comparison with the time delays obtained for other reaches in relative to the length of the reaches. As for the estimation of the unknown parameters for each of the reaches, we repeat the parameter estimation procedures discussed in Chapter 4, where we have used the simulated data from the Saint Venant equations to estimate the unknown parameters. It is worth pointing out that, the use of the Saint Venant equations for each of the reaches in the Broken River for re-estimation of the parameters and the time delays are valid to certain extent. This is because most of the Saint Venant equations have been calibrated against the data and shown to be accurate in capturing the dynamics of the river reaches in Chapters 3 and 4. We do note that the time delays change with flow conditions but as the estimated time delays in Table 6.1 are obtained under low flow condition, which has the largest time delays. By designing the controller based on this time delay, we could ensure the robustness specification of the controller.

Table 6.1: Reach lengths, estimated parameters and time delays.

Reach	**Length**	**Estimated parameters**	**Time delay**
Reach LNB	22000m	$\left(\frac{T_s c_{1,B}}{A}\right) = 0.009$ $\left(\frac{T_s c_{2,B}}{A}\right) = 0.090$ $\left(\frac{T_s c_{3,B}}{A}\right) = 0.009$	$\tau_{LNB} = 2160$ minutes
Reach LNSout1	22000m	-	$\tau_{LNSout1} = 2160$ minutes
Reach Sout1LB	7000m	$\left(\frac{T_s c_{1,LB}}{A}\right) = 0.010$ $\left(\frac{T_s c_{2,LB}}{A}\right) = 0.112$ $\left(\frac{T_s c_{3,LB}}{A}\right) = 0.015$	$\tau_{Sout1LB} = 360$ minutes $\tau_B = 720$ minutes
Reach LBC	12000m	$\left(\frac{T_s c_{1,C}}{A}\right) = 0.006$ $\left(\frac{T_s c_{2,C}}{A}\right) = 0.120$	$\tau_{LBC} = 1080$ minutes
Reach CG	26700m	-	$\tau_{CG} = 1800$ minutes $\tau_{S2G} = 200$ minutes

6.3.2 Remarks on the models

In this section, some discussions on the time delay and the integrator delay models obtained in Chapter 4 and the one presented in Section 6.3.1 are given. As a consequence of the control configuration introduced, three reaches in Chapter 4 are retained, while the remaining reaches are "new" reaches. These three reaches are Reach LNB, Reach LBC and Reach CG. We shall highlight some remarks in regards to these three reaches.

Reach LNB

We compare the estimated parameters associated with Lake Nillahcootie and Broken Weir. The estimated parameters (neglecting the sign) using the data set from April to July 2007 considered in Chapter 4 are $\theta_{e,LNB,1} = 0.048$, $\theta_{e,LNB,2} = 0.108$. This data set is selected for comparison as the flow condition observed from the data is in the range of 30 to 50 ML/day (see Figure 4.14), which is similar to the flow of 30ML/day used in the step test. From Table 6.1, we have $\left(\frac{T_s c_{1,B}}{A}\right) = 0.009$ and $\left(\frac{T_s c_{2,B}}{A}\right) = 0.090$. We observe that the values of $\theta_{e,LNB,2}$ and $\left(\frac{T_s c_{2,B}}{A}\right)$ are similar. As for $\theta_{e,LNB,1}$ and $\left(\frac{T_s c_{1,B}}{A}\right)$, there is a big difference observed. This is primarily due to the fact that a parameterised flow is used at Lake Nilllahcootie in this chapter. As for the time delay, the time delay of 3060 minutes was obtained in Chapter 4 and 2160 minutes from Table 6.1. As the flow

condition is similar we expect the time delay to be similar. However, as the time delay of 3060 minutes obtained using the cross-correlation analysis as shown in Figure 4.15 has large uncertainty, we do not want to draw any further conclusion. In summary, although a direct comparison cannot be made, the estimated parameters and time delays of the models under different flow condition for this reach seems reasonable.

Reach LBC

For this reach, the estimated parameters (neglecting the sign) using the data set from October to December 2010 from Chapter 4 are $\theta_{e,LBC,1} = 2.200$ and $\theta_{e,LBC,2} = 1.394$, while from Table 6.1, we have $\left(\frac{T_s c_{1,C}}{A}\right) = 0.006$ and $\left(\frac{T_s c_{2,C}}{A}\right) = 0.120$. The flow condition at Casey's Weir observed from data is in the range of 400ML/day to 500ML/day with several large flow peaks along the way (see Figure 4.17) . We observe that there is a big difference between $\theta_{e,LBC,2}$ and $\left(\frac{T_s c_{2,C}}{A}\right)$. The larger value of $\theta_{e,LBC,2}$ is due to the presence of the several large flow peaks occurring in the measured data. For the parameters related to Lake Benalla, again a direct comparison cannot be made given that the identification exercise uses the measured data from Lake Benalla obtained in the middle of the lake while in this chapter, the simulated measurements used for identification assumes that the data is measured at the downstream of Lake Benalla. As for the time delay, as expected, the higher flow condition results in a smaller time delay of 540 minutes compared to the lower flow condition where we have time delay of 1080 minutes. In summary, the estimated parameters and the time delays under the different flow conditions for this reach is reasonable.

Reach CG

In this reach, we are interested in the estimated time delay as the flow model used are not parameterised. The flow condition in Casey's Weir observed from data is in the range of 50ML/day to 70ML/day (see Figure 4.6) and the estimated time delay is 1650 minutes. From Table 6.1, the time delay is 1800 minutes obtained using a step test of 30ML/day. The estimated time delays is in agreement with the fact that a larger flow leads to a smaller time delay. In summary, the estimated time delay for this reach is reasonable.

6.4 MPC design for Broken River

The principle operation of MPC has been introduced in Chapter 5. Here, the operation is summarised as a quick review. MPC is an online optimal controller. At each time step, the controller generates a sequence of control inputs (flow releases), based on the predicted behaviour of the river (described using the river models obtained in Chapter 4) over a finite the prediction horizon (several days ahead) by solving an optimisation criterion. Only the first flow releases is applied to the river. At the next time step, the prediction horizon is shifted by one step and the whole process is repeated over the same finite prediction horizon. The control objectives are normally reflected in the criterion. Constraints such as the limits on flows and water levels can be incorporated in the optimisation problem.

6.4.1 Design of MPC via reverse engineering

In Chapter 5, we introduce methods for obtaining the weights in the MPC cost function through reverse engineering. In this section, we use the method of state augmentation to reverse engineer the decentralised controller for MPC. This method is chosen as it is simple, since we augment the plant with the state of the favourite controller and there is no need to design an observer.

As the model used for prediction in MPC is generally in state space form, we need to rewrite Equations (6.3), (6.6), (6.8), (6.10), (6.11) and (6.13) into a linear state space representation. The control variables are flows at Lake Nillahcootie Q_{LN}, in-let to Storage 1 Q_{Sin1}, out-let of Storage 1 Q_{Sout1}, Lake Benalla Q_{LB}, Casey's Weir Q_C and in- and out-let of Storage 2 Q_{S2}. The controlled variables are the water level at Broken Weir y_B, storage level at Storage 1 V_{S1}, water level at Lake Benalla y_{LB}, water level at Casey's Weir y_C, storage level at Storage 2 V_{S2} and flow at Gowangardie Weir Q_G. Introducing the state variable $x_e = a - a_{sp}$, where a are the controlled variables and the subscript "sp" denotes their respective setpoints. The state variable x_e is the deviation of the controlled variable from their respective setpoint. In other words, we reformulate the problem by looking at the deviation of each controlled variables from its setpoint.

Let $u_{LN} = Q_{LN}$, $u_{Sin1} = Q_{Sin1}$, $u_{Sout1} = Q_{Sout1}$, $u_{LB} = Q_{LB}$, $u_C = Q_C$ and $u_{S2} = Q_{S2}$. Due to the time delays, we need a number of states to remember the past flows. We introduce the states $x_{j,i} = u_j(k-i)$, where j = LN, Sin1, Sout1, LB, C and S2. As Broken Weir is in flow mode, and changes of the flow is according to the defined flow setpoint,

we treat the flow at Broken Weir Q_B as a known disturbance. In view of the large time delays (see Table 6.1), it would be impractical to choose a small sampling interval as this will introduce a large number of states, which would lead to a heavy computational burden. Thus, we chose $T_s = 360$ minutes (6 hours). This also allows ample time for online optimisation used in MPC for computation of the optimal control input. The discrete time delays, which we denote by $\delta := \lceil \frac{\tau}{T_s} \rceil$, are $\delta_{LNB} = 6$, $\delta_{LNSout1} = 6$, $\delta_{Sout1LB} = 1$, $\delta_B = 2$, $\delta_{LBC} = 3$, $\delta_{CG} = 5$ and $\delta_{S2G} = 1$. Equipped with all these variables, we arrive with the following state space model.

$$
\begin{aligned}
x_{Sin1,1}(k) &= u_{Sin1}(k-1) \\
x_{e,B}(k) &= x_{e,B}(k-1) + \left(\frac{T_s c_{1,B}}{A}\right) x_{LN,6}(k-1) - \left(\frac{T_s c_{2,B}}{A}\right) Q_B(k-1) \\
&\quad - \left(\frac{T_s c_{3,B}}{A}\right) u_{Sin1}(k-1) + d_{LNB}(k-1) \\
x_{LN,1}(k) &= u_{LN}(k-1) \\
x_{LN,i+1}(k) &= x_{LN,i}(k-1) \quad i = 1, \ldots, 5 \\
x_{e,S1}(k) &= x_{e,S1}(k-1) + T_s x_{LN,6}(k-1) - T_s u_{Sout1}(k-1) - T_s Q_B(k-1) \\
x_{Sout1,1}(k) &= u_{Sout1}(k-1) \\
x_{e,LB}(k) &= x_{e,LB}(k-1) + \left(\frac{T_s c_{1,LB}}{A}\right) x_{Sout1,1}(k-1) - \left(\frac{T_s c_{2,LB}}{c_{LB} A}\right) u_{LB}(k-1) \\
&\quad + \left(\frac{T_s c_{3,LB}}{A}\right) Q_B(k-\delta_B-1) + d_{Sout1LB}(k-1) \\
x_{LB,1}(k) &= u_{LB}(k-1) \\
x_{LB,i+1}(k) &= x_{LB,i}(k-1) \quad i = 1, \ldots, 2 \\
x_{e,C}(k) &= x_{e,C}(k-1) + \left(\frac{T_s c_{1,C}}{A}\right) x_{LB,3}(k-1) - \left(\frac{T_s c_{2,C}}{c_C A}\right) u_C(k-1) + d_{LBC}(k-1) \\
x_{C,1}(k) &= u_C(k-1) \\
x_{C,i+1}(k) &= x_{C,i}(k-1) \quad i = 1, \ldots, 3 \\
x_{e,G}(k) &= x_{C,4}(k-1) + u_{S2}(k-1) + d_{CG}(k-1) \\
x_{S2,1}(k) &= u_{S2}(k-1) \\
x_{e,S2}(k) &= x_{e,S2}(k-1) - T_s u_{S2}(k-1)
\end{aligned}
\tag{6.14}
$$

Here, $c_B = 10.00\text{m}^{3/2}/\text{s}$, $c_{LB} = 10.15\text{m}^{3/2}/\text{s}$ and $c_C = 19.73\text{m}^{3/2}/\text{s}$ are used to con-

vert $h_B^{3/2}$, $h_{LB}^{3/2}$ and $h_C^{3/2}$ in Equations (6.3), (6.8) and (6.10) to flow respectively. d_{LNB}, $d_{Sout1LB}$, d_{LBC} and d_{CG} denote the disturbances at each reach, which comprise of offtakes to farm, flow from creeks and change of flow setpoint at Gowangardie Weir. Notice that from Equation (6.14), we have accessed to all the states. These states are the flow computed by the controller and its propagated delay. In addition, the controlled variables, i.e. the flows, water levels and storage levels are also measured. As we have access to all the states, hence there is no need to design an observer.

Equation (6.14) can be written in the form of

$$\begin{aligned} x(k+1) &= Ax(k) + Bu(k) + B_d d(k) \\ y(k) &= Cx(k) \end{aligned} \tag{6.15}$$

where $d(k)$ represents all the known disturbances and includes the offtakes, change of flow setpoints at Gowangardie Weir, flows from creeks and flow at Broken Weir. The output of the model, which is used for reverse engineering are all the x_e states, which are the errors between the controlled variable and its setpoints

The favourite controller K_{fav} that we would like to reverse engineer are the decentralised controller designed in (Ooi *et al.*, 2010). The decentralised controller is made up of I-controllers, P-controllers and PI-controllers. The PI-controllers are used in all the reaches except Reach CG and Storage 2. The controllers considered in (Ooi *et al.*, 2010) are in continuous form. Thus, these controllers are first discretised. The discrete transfer function of the PI-controller is given by

$$U(z) = \left(K_P + \frac{K_I}{z-1} \right) Y(z) \tag{6.16}$$

where K_P is the proportional gain, K_I is the integral gain, $Y = e_B, e_{S1}, e_{LB}$ and e_C are the deviations of the controlled variables from their respective setpoints. Then, $U = u_{Sin1}, u_{LN}, u_{Sout1}$ and u_{LB}, are the control variables in Equation (6.16).

For Reach CG, the I-controller is used to control the flow at Gowangardie Weir, while the P-controller is used to control the in-let and out-let of Storage 2. Based on the configuration described in Figure 6.3, the discrete transfer function for these controllers

are given by

$$u_C(z) = \left(\frac{K_{I,CG}}{z-1}\right) e_G(z) + K_{PS} e_{S2}(z)$$
$$u_{S2}(z) = \left(\frac{K_{I,CG}}{z-1}\right) e_G(s) - u_C(z) z^{-\delta'} \tag{6.17}$$

where e_G and e_{S2} are the deviations of Q_G and Q_{S2} from setpoints. $\delta' = \delta_{CG} - \delta_{S2G} = 4$.

All the controllers are tuned using frequency response techniques. As time delays vary with flow, the controllers in (Ooi *et al.*, 2010) are tuned conservatively. The proportional gain for Storage 2 is $K_{PS,CG} = 0.0001$. The controller parameters, phase margins, gain margins and extra tolerable time delays are tabulated in Table 6.2.

Table 6.2: Controller parameters.

Reach	K_P	K_I	**Gain Margin**	**Phase Margin**	**Extra delay tolerable**
In-let Storage 1	1	0.0450	17.0 dB	65.8°	1860 minutes
Reach LNSout1	0.002	2.4×10^{-5}	14.5 dB	59.4°	7570 minutes
Reach Sout1LB	0.7	0.0252	19.1 dB	65.6°	2330 minutes
Reach LBC	0.5	0.0180	16.5 dB	40.8°	2860 minutes
Reach CG	-	0.0529	10.9 dB	64.2°	4480 minutes

For reverse engineering, we need to rewrite K_{fav} into state space representation as well. The state space representation for a PI-controller (Equation (6.16)) is given by

$$x_K(k+1) = x_K(k) + K_I e(k)$$
$$u(k) = x_K(k) + K_P e(k) \tag{6.18}$$

where e is the error between the controlled variable and its setpoint. Thus, the PI-controllers used in upstream level control at in-let to Storage 1, Reach LNSout1, Reach Sout1LB and Reach LBC can be respectively written as

$$x_{K,LNB}(k+1) = x_{K,LNB}(k) + K_{I,LNB} e_B(k)$$
$$u_{Sin1}(k) = x_{K,LNB}(k) + K_{P,LNB} e_B(k) \tag{6.19}$$

$$\begin{aligned} x_{K,LNSout1}(k+1) &= x_{K,LNSout1}(k) + K_{I,LNSout1} e_{S1}(k) \\ u_{LNB}(k) &= x_{K,LNSout1}(k) + K_{P,LNSout1} e_{S1}(k) \end{aligned} \tag{6.20}$$

$$\begin{aligned} x_{K,Sout1LB}(k+1) &= x_{K,Sout1LB}(k) + K_{I,Sout1LB} e_{LB}(k) \\ u_{Sout1}(k) &= x_{K,Sout1LB}(k) + K_{P,Sout1LB} e_{LB}(k) \end{aligned} \tag{6.21}$$

$$\begin{aligned} x_{K,LBC}(k+1) &= x_{K,LBC}(k) + K_{I,LBC} e_C(k) \\ u_{LB}(k) &= x_{K,LBC}(k) + K_{P,LBC} e_C(k) \end{aligned} \tag{6.22}$$

For Reach CG, rewriting Equation (6.17) into state space, we get

$$\begin{aligned} x_{K,CG}(k+1) &= x_{K,CG}(k) + K_{I,CG} e_G(k) \\ u_{C,1}(k) &= x_{K,CG}(k) + K_{PS,CG} e_{S2}(k) \\ u_{C,i+1}(k) &= u_{C,i}(k-1) \quad i = 1, \ldots, 4 \\ u_{S2}(k) &= x_{K,CG}(k) - u_{C,4}(k) \end{aligned} \tag{6.23}$$

Equations (6.19), (6.20), (6.21), (6.22) and (6.23) can be written in the form of

$$\begin{aligned} x_K(k+1) &= A_K x_K(k) + B_K e(k) \\ u(k) &= C_K x_K(k) + D_K e(k) \end{aligned} \tag{6.24}$$

With the plant and K_{fav} in the form of Equations (6.15) and (6.24), we are in the position to use the method of state augmentation for reverse engineering. Following the procedures described in Section 5.5.3, the augmented plant with the states of the controllers yield,

$$A_{aug} = \begin{bmatrix} A & 0 \\ B_K C & A_K \end{bmatrix} \qquad B_{aug} = \begin{bmatrix} B \\ 0 \end{bmatrix} \qquad C_{aug} = \begin{bmatrix} C & 0 \end{bmatrix} \tag{6.25}$$

with the new state $x_{aug}(k) = [x^T(k), x_K^T(k)]^T$. The control law is then given by $u(k) = D_K C x(k) + C_K x_K(k)$, where we have

$$K = [-D_K C, -C_K] \tag{6.26}$$

For reverse engineering, the criterion to be minimised by MPC is given by (see Chapter 5)

$$J_{MPC,RE} = \sum_{k=0}^{N_p-1} \begin{bmatrix} x(k) \\ u(k) \end{bmatrix}^T \begin{bmatrix} K^T K & K^T \\ K & I \end{bmatrix} \begin{bmatrix} x(k) \\ u(k) \end{bmatrix} \tag{6.27}$$

where N_P is the prediction horizon. Rewriting it in standard form,

$$\begin{aligned} J_{MPC,RE} = \sum_{t=0}^{N_p-1} & x(k)^T Q_{RE} x(k) + u(k)^T R_{RE} u(k) \\ & + x(k)^T S_{RE} u(k) + u^T(k) S_{RE}^T x(k) \end{aligned} \tag{6.28}$$

where Q_{RE}, R_{RE} and S_{SE} are weight matrices and these weights are given by $Q_{RE} = K^T K$, $R_{RE} = I$ and $S_{RE} = K^T$ with K from Equation (6.26).

6.4.2 Design of MPC from scratch

The same model as in Equation (6.14) is used. In addition, to achieve a zero steady state error in the presence of disturbances, we augment the plant with the integral of the setpoint errors, i.e.

$$x_{int,i}(k) = x_{int,i}(k-1) + T_s x_{e,i}(k-1) \tag{6.29}$$

where i = B, S1, LB, C, and G. There is no integral of setpoint errors for Storage 2 as there is no offtake to farms occurring between the in- and out-let of Storage 2. Equations (6.14) and (6.29) can be written in the form of Equation (6.15) with

$$A_{aug,DS} = \begin{bmatrix} A & 0 \\ C & I \end{bmatrix} \qquad B_{aug,DS} = \begin{bmatrix} B \\ 0 \end{bmatrix} \qquad C_{aug,DS} = \begin{bmatrix} C & 0 \end{bmatrix} \tag{6.30}$$

with the new state $x_{aug,DS}(k) = [x^T(k), x_{int}^T(k)]^T$. Again, since we have access to all states, there is no need to design an observer.

For the design of MPC from scratch, the criterion to be minimised is given by

$$J_{MPC,DS} = x(N_p)^T P_{DS} x(N_p) + \sum_{k=0}^{N_p-1} x(k)^T Q_{DS} x(k) + u(k)^T R_{DS} u(k) \tag{6.31}$$

where Q_{DS} and P_{DS} are positive definite matrices and R_{DS} is a positive semi definite

matrix. The matrix P_{DS}, which is called terminal cost[2] in the literature can be found using the solution of the Discrete Algebraic Riccati Equation (DARE) (Rawlings and Muske, 1993), i.e.

$$A^T P_{DS} A - P_{DS} - A^T P_{DS} B(B^T P_{DS} B + R_{DS})^{-1} B^T P_{DS} A + Q_{DS} = 0 \tag{6.32}$$

where A and B are the plant matrices (see Equation (6.15)). The matrices Q_{DS} and R_{DS} can be derived based on the control objectives outlined in Section 6.1.3 and we will discuss them in the following paragraphs.

As one of the control objectives is to minimise the setpoint errors, thus $(y_B - y_{B,sp})^2$, $(V_{S1} - V_{S1,sp})^2$, $(y_{LB} - y_{LB,sp})^2$, $(y_C - y_{C,sp})^2$, $(Q_G - Q_{G,sp})^2$ and $(V_{S2} - V_{S2,sp})^2$ need to be penalised in the criterion. The associated weights for the setpoint errors are $q_{e,B}$, $q_{e,S1}$, $q_{e,LB}$, $q_{e,C}$, $q_{e,G}$ and $q_{e,S2}$. To ensure zero steady state error in the presence of disturbances, the integral of setpoints errors need to be included in the criterion and the associated weights for the integral of setpoint errors are assigned weights $q_{int,B}$, $q_{int,S1}$, $q_{int,LB}$, $q_{int,C}$ and $q_{int,G}$. With all these weights, we can derive the matrix Q_{DS}.

With the control objective to ensure minimal release from Lake Nillahcootie, the control variable u_{LN} need to be penalised and it is assigned with weight r_{LN}. For the other control variables, they are all assigned the weight 1. With these weights, we can derive the R_{DS} matrix. In regards to the variations in flow, they are not penalised in the criterion but are formulated as part of constraints, which will be discussed in the next section.

We would like to mention that, the choice of weights mentioned above are not trivial and they required a fair amount of effort in selecting these weights such that a satisfactory performance is achieved. These weights are shown in Table 6.3 in page 213 and are reported together with the weights chosen to penalise the soft constraints, which are discussed next.

6.4.3 Dealing with constraints

In general, there are two types of constraints. The first is what we call hard constraints, which cannot be violated. In the Broken River, the hard constraints are the physical limit of the storages. The second type of constraint is what we call soft constraints. This

[2]Usually, the terminal cost is included for stability purposes (see e.g. (Maciejowski, 2002). As the open channel systems are inherently semi-stable system; the inclusion of terminal cost for stability purposes may not be relevant. Nonetheless, the author notices improved performance with the inclusion of the terminal cost, thus retaining it in the cost function.

type of constraints can be violated for a short period of time without causing serious consequences. In the Broken River, the soft constraints are the water levels at Casey's Weir, Lake Benalla and Broken Weir and flow at Gowangardie Weir. The inclusion of soft constraints rather than hard constraints increases the chances of finding a feasible solution when solving the optimisation problem in MPC. By feasible solution, we mean that while solving the optimisation problem, the optimiser can find a solution to satisfy all the defined constraints simultaneously. To include the soft constraints in the criterion, both Equations (6.28) and (6.31) becomes

$$J_{MPC,RE}(x,u,k,N_p) = \sum_{k=0}^{N_p-1} x(k)^T Q_{RE} x(k) + u(k)^T R_{RE} u(k) + x(k)^T S_{RE} u(k) + u^T(k) S_{RE}^T x(k) + s_L^T(k) Q_{s,L} s_L(k) + s_H^T(k) Q_{s,H} s_H(k) \quad (6.33)$$

and

$$J_{MPC,DS}(x,u,k,N_p) = x(N_p)^T P_{DS} x(N_p) + \sum_{k=0}^{N_p-1} x(k)^T Q_{DS} x(k) + u(k)^T R_{DS} u(k) + s_L^T(k) Q_{s,L} s_L(k) + s_H^T(k) Q_{s,H} s_H(k) \quad (6.34)$$

where $Q_{s,L}$ and $Q_{s,H}$ are positive definite matrices of large weights. s_L and s_H are called the slack variables with the subscripts "L" and "H" denote the slack variables for minimum and maximum bound respectively. The slack variables are defined in a way that they are zero when the constraints are not violated and non zero when the constraints are violated. With the slack variables becoming non zero, they are penalised with large weights in the criterion. This large penalty will make the optimiser try to maintain the slack variables at zero if possible.

Referring to the control objectives outlined in Section 6.1.3, some of the control objectives can be formulated in terms of constraints. To include constraints in the MPC optimisation problem, the constraints are normally expressed in the form of linear inequalities. The minimum flow over Gowangardie Weir is 25ML/day. Thus, in terms of linear inequality, we have $25\text{ML/day} - s_{L,QG}(k) \leq Q_G(k)$. This flow is made a soft constraint and the slack variable $s_{L,QG}$ is used to represent the amount of flow going below 25ML/day and it is penalised with the weight $q_{L,QG}$. For Casey's Weir and Lake Benalla, the minimum flow is 22ML/day and expressing it in terms of linear inequality, we have $22\text{ML/day} - s_{L,QC}(k) \leq Q_C(k)$ and $22\text{ML/day} - s_{L,QLB}(k) \leq Q_{LB}(k)$. We make the con-

straints on both these flows, soft constraints and the slack variables $s_{L,QC}$ and $s_{L,QLB}$ are used to represent the amount of these flows go below 22ML/day, and they are penalised with the weights $q_{L,QC}$ and $q_{L,QLB}$ respectively. For the minimum flow at Broken Weir, since it is in flow mode, we set the flow at Broken Weir to be 22ML/day.

For the water levels at Broken Weir y_B, Lake Benalla y_{LB} and Casey's Weir y_C, it is preferred that they are within ±15cm of their setpoints. However, we defined a tighter bound, where ±5cm is considered for the robustness against model mismatch. Expressing them in terms of linear inequalities, we have $2.10\text{m} - s_{L,yB}(k) \leq y_B(k) \leq 2.20\text{m} + s_{H,yB}(k)$, $2.20\text{m} - s_{L,yLB}(k) \leq y_{LB}(k) \leq 2.30\text{m} + s_{H,yLB}(k)$ and $1.95\text{m} - s_{L,yC}(k) \leq y_C(k) \leq 2.05\text{m} + s_{H,yC}(k)$. These water levels constraints are also made soft constraints, where the slack variables $s_{L,yB}$, $s_{L,yLB}$ and $s_{L,yC}$ represent the amount of water level drop below 2.10m, 2.20m and 1.95m respectively. Similarly, the slack variables $s_{H,yB}$, $s_{H,yLB}$ and $s_{H,yC}$ represent the amount of water level rise above 2.20m, 2.30m and 2.05m respectively. These slack variables are penalised with weights $q_{L,yB}$, $q_{L,yLB}$, $q_{L,yC}$, $q_{H,yB}$, $q_{H,yLB}$ and $q_{H,yC}$.

To maintain the slack water in the river, the flow released by the controller at Casey's Weir, Lake Benalla and Lake Nillahcootie should not exceed 190ML/day. Thus, the following linear inequalities are considered $Q_C(k) \leq 190\text{ML/day} + s_{H,QC}(k)$, $Q_{LB}(k) \leq 190\text{ML/day} + s_{H,QLB}(k)$ and $Q_{LN}(k) \leq 190\text{ML/day} + s_{H,QLN}(k)$. Again, all these flows constraints are made soft constraints with the slack variables given by $s_{H,QC}$, $s_{H,QLB}$ and $s_{H,QLN}$ and they are penalised with weights $q_{H,QC}$, $q_{H,QLB}$ and $q_{H,QLN}$.

With all the penalty weights for the slack variables chosen, we can derive matrices $Q_{s,L}$ and $Q_{s,H}$. Note that these weights are normally chosen to be larger than the weights in Q_{DS} as we want the period of violation of the soft constraints to be as short as possible. The weights are shown in Table 6.3.

The capacity for Storages 1 and 2 are 300ML and 6ML respectively. Thus, the constraints expressed in linear inequalities are given by $0\text{ML} \leq V_{S1}(k) \leq 300\text{ML}$ and $0\text{ML} \leq V_{S2}(k) \leq 6\text{ML}$. The volume of the storages are hard constraints as they represent the physical limit of the storage.

Lastly, in order to satisfy the control objective of ensuring the mean daily flow variations at the regulation point to be between 0.76 and 1.5 of the flow from previous day, the following constraints are expressed in terms of linear inequalities, i.e.

$$0.76[Q_j(k) - \Delta Q_j(k)] \leq Q_j(k) \leq 1.5[Q_j(k) - \Delta Q_j(k)]$$

where $\Delta Q_j(k) = Q_j(k) - Q_j(k-1)$ and j = LN, Sin1, Sout1, LB and C.

Putting all the constraints together, the MPC optimisation problem is given by

$$\begin{aligned}
u = & \underset{u(t),u(t+1),\ldots,u(t+N_p-1)}{\operatorname{argmin}} J(x,u,t,N_p) \\
\text{subject to: } x(t+1) &= Ax(t) + Bu(t) + B_d d(t) \\
y(t) &= Cx(t) \\
\Delta u(t) &= u(t) - u(t-1) \\
25\text{ML/day} - s_{L,QG}(t) &\leq Q_G(t) \\
22\text{ML/day} - s_{L,QC}(t) &\leq Q_C(t) \leq 190\text{ML/day} + s_{H,QC}(t) \\
22\text{ML/day} - s_{L,QLB}(t) &\leq Q_{LB}(t) \leq 190\text{ML/day} + s_{H,QLB}(t) \\
Q_{LN}(t) &\leq 190\text{ML/day} + s_{H,QLN}(t) \\
0\text{ML} \leq V_{S1}(t) &\leq 300\text{ML} \\
0\text{ML} \leq V_{S2}(t) &\leq 6\text{ML} \\
2.10\text{m} - s_{L,yB}(t) &\leq y_B(t) \leq 2.20\text{m} + s_{H,yB}(t) \\
2.20\text{m} - s_{L,yLB}(t) &\leq y_{LB}(t) \leq 2.30\text{m} + s_{H,yLB}(t) \\
1.95\text{m} - s_{L,yC}(t) &\leq y_C(t) \leq 2.05\text{m} + s_{H,yC}(t) \\
0.76[Q_{LN}(t) - \Delta Q_{LN}(t)] &\leq Q_{LN}(t) \leq 1.5[Q_{LN}(t) - \Delta Q_{LN}(t)] \\
0.76[Q_{Sin1}(t) - \Delta Q_{Sin1}(t)] &\leq Q_{Sin1}(t) \leq 1.5[Q_{Sin1}(t) - \Delta Q_{Sin1}(t)] \\
0.76[Q_{Sout1}(t) - \Delta Q_{Sout1}(t)] &\leq Q_{Sout1}(t) \leq 1.5[Q_{Sout1}(t) - \Delta Q_{Sout1}(t)] \\
0.76[Q_{LB}(t) - \Delta Q_{LB}(t)] &\leq Q_{LB}(t) \leq 1.5[Q_{LB}(t) - \Delta Q_{LB}(t)] \\
0.76[Q_C(t) - \Delta Q_C(t)] &\leq Q_C(t) \leq 1.5[Q_C(t) - \Delta Q_C(t)] \\
s_{L,i}(t), s_{H,i}(t) &\geq 0
\end{aligned} \tag{6.35}$$

where $i = QG$, QC, QLB, yB, yLB or yC. $J(x,u,k,N_p)$ is either Equations (6.33) (reverse engineering) or (6.34) (design from scratch). Note that instead of expressing all the linear inequalities in x and u, which could lead to confusion, we use Q, y and V to denote the variables explicitly. The prediction horizon, N_p used in MPC is chosen to be 4 days (5760 minutes) based on the advance order time by the irrigators is 4 days.

The control problem is a quadratic programming[3] problem in which we formulate using YALMIP (Löfberg, 2004) in MATLAB® and solved using the commercial package CPLEX 12.2 (IBM, 2009). The sampling interval used for the controller is 360 minutes.

Table 6.3: Weights used for MPC designed from scratch.

Setpoint errors		Integral of setpoint errors		Control actions		Soft constraints	
Parameter	**Value**	**Parameter**	**Value**	**Parameter**	**Value**	**Parameter**	**Value**
$q_{e,B}$	1×10^{-7}	$q_{int,B}$	1×10^{-6}	r_{LN}	2.5	$q_{H,QLN}$	10
$q_{e,S1}$	1×10^{-7}	$q_{int,S1}$	5×10^{-7}	r_{Sin1}	1	$q_{L,yB}$	10
						$q_{H,yB}$	10
$q_{e,LB}$	1×10^{-7}	$q_{int,LB}$	5×10^{-6}	r_{Sout1}	1	$q_{L,QLB}$	10
						$q_{H,QLB}$	10
						$q_{L,yLB}$	10
						$q_{H,yLB}$	10
$q_{e,C}$	1×10^{-7}	$q_{int,C}$	5×10^{-6}	r_{LB}	1	$q_{L,QC}$	10
						$q_{H,QC}$	10
						$q_{L,yC}$	10
						$q_{H,yC}$	10
$q_{e,G}$	1×10^{-7}	$q_{int,G}$	2×10^{-6}	r_C	1	$q_{L,QG}$	10
$q_{e,S2}$	3×10^{-6}			r_{S2}	1		

6.4.4 Measured and known disturbances

Under the current practice, the irrigators need to order water four days in advance when they require water for their farms. As we have access to the known future orders from the irrigators, we can include them as part of the "feedforward control". In MPC, this "feedforward control" is easily handled by including this information directly in the prediction model over the horizon (see (Maciejowski, 2002)).

In addition, the flow setpoints at Gowangardie and Broken Weirs are also known in advance. Thus, they can also be included in the prediction model over the horizon. For the flows from creeks, they can also be included directly in the prediction model over the horizon. However, unlike the case of known future orders and the flow setpoints, we do not know the flows in the creeks in advance. Thus, once we obtain the measurement, we assume that the measurement is constant over the entire prediction horizon and use this in the prediction model.

[3]A quadratic programming solves the problem that is formulated in the form of $\min_x \frac{1}{2}x^T Qx + p^T x$ subject to $Ax \leq b$ (inequality constraint) and/or $Cx = d$ (equality constraint).

6.5 Simulation settings

In this section, the simulation settings to assess the performance of the control system is explained. The simulations are a realistic year long simulations using the historical data of offtakes to farm and flow contribution from creeks, which are adjusted according to a drier future. As the geographical area we consider ends in Gowangardie Weir, all the demands of water from both the irrigators and the environment downstream of Gowangardie Weir are aggregated in the required flow over Gowangardie Weir. For flow contribution from creeks, only the contribution from the two major creeks are considered and we assume that all the unmeasured creeks can be aggregated into those two creeks. We also assume that Lake Nillahcootie is always able to supply the required flow.

6.5.1 External input to the simulation

The external input to the simulation are the water orders from the irrigators, the environmental flow requirements and the flow from creeks. We will discuss each of these external inputs.

Water order from the irrigators

From the historical data of water orders from the irrigators obtained from the Goulburn Murray Water, Victoria, Australia, we have identified that the water orders from July 2006 to June 2007 is most representative as the usage from this year is evenly distributed across the months with the exception of the water orders from the Broken Creek and the downstream of Gowangardie Weir, where the water orders from July 2007 to June 2008 are used for those two locations as they are considered more representative with the anticipated drier future trends and the buyback of water in the Broken System (Water Entitlements, 2010) taken into account. In addition, these water orders also create a bimodal demand patterns with large demand in spring and autumn instead would appear (Langford, 2010).

The proposed monthly order volume for each of the reaches in the Broken River from July 2006 to June 2007 is shown in Figure 6.8, while Figure 6.9 shows the water orders by the irrigators used in the simulation. In both the figures, we have included the water orders from the irrigators along the Broken Creek. Note that, we are not controlling the

flow along the Broken Creek but we treat the flow (which include the water orders) into Broken Creek as an out-flow.

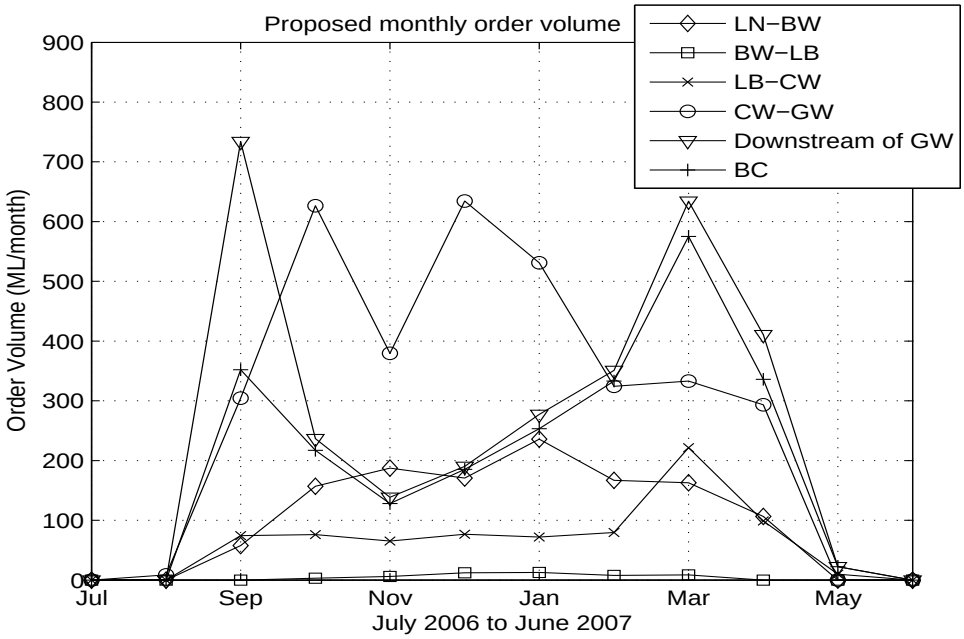

Figure 6.8: Proposed monthly order volume between the reaches in the Broken River. LN - Lake Nillahcootie, BW - Broken Weir, LB - Lake Benalla, CW - Casey's Weir, GW - Gowangardie Weir, BC - Broken Creek.

In the Broken River, these offtakes occur physically at several different locations along the river. However, in the simulation, a maximum of six offtakes are considered per reach. In other words, the different offtake locations are aggregated into one offtake to make up to a total of six offtakes per reach. All the demands for water (including minimum environmental flow requirement) downstream of Gowangardie Weir is aggregated into a desired flow over Gowangardie Weir. Similarly, for Broken Creek, the water orders at Broken Creek are aggregated into a desired flow diverted to Broken Creek. Although the demand patterns shown in Figure 6.9 is for the whole year, the controller only have the information regarding these water orders four days in advance. We also assume that the offtakes take place as ordered and hence, assume perfect prediction.

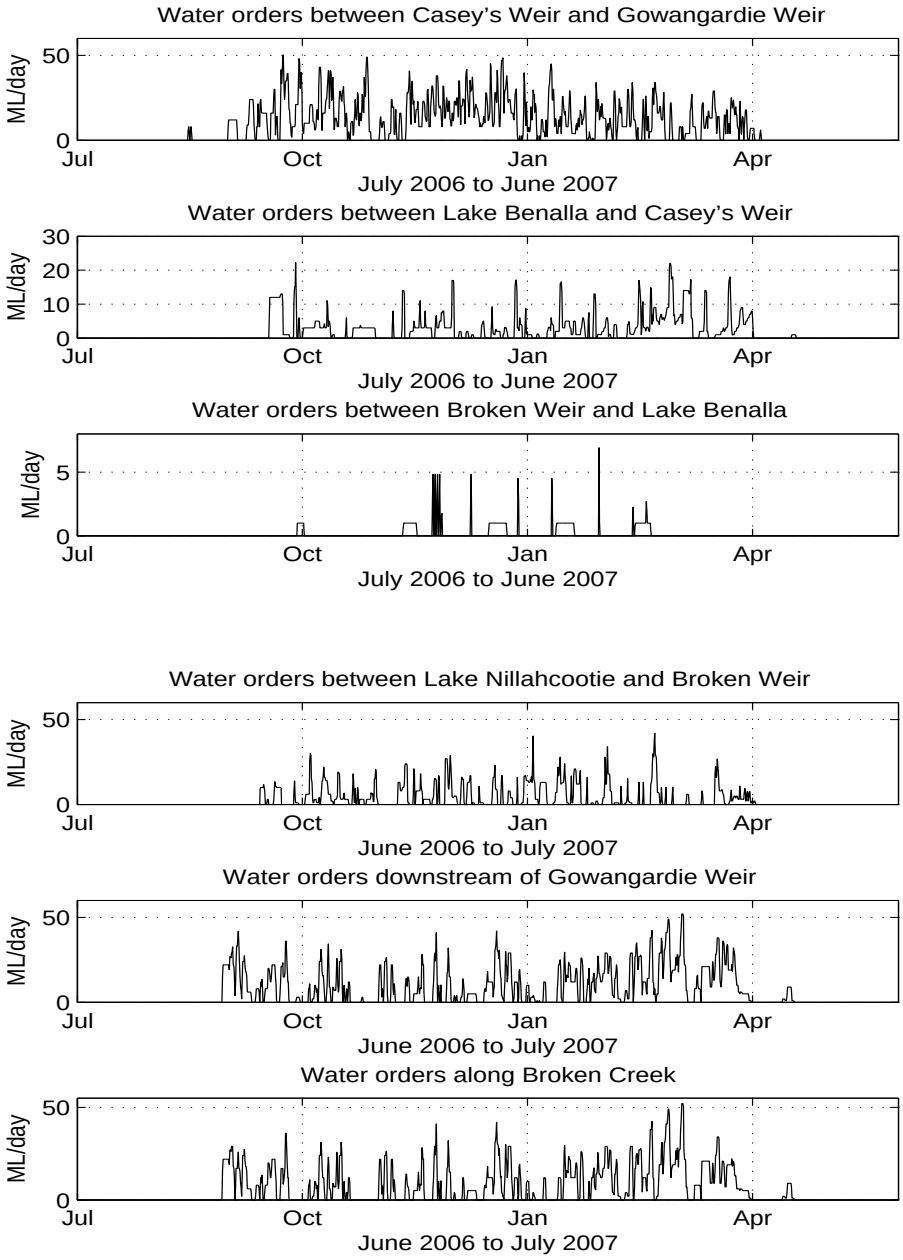

Figure 6.9: Water orders between different reaches along the Broken River.

Environmental flow requirement

The minimum flow values defined in the Bulk Entitlement (Bulk Entitlements, 2010) are used. The minimum environmental flow at Gowangardie Weir is 25ML/day, while at Lake

Benalla, Broken and Casey's Weirs, they are 22ML/day.

In-flows from creeks

Two creeks are considered. This first one is Lima Creek, which is located between Lake Nillahcootie and Broken Weir. The second one is Hollands Creek, which is located between Broken Weir and Lake Benalla. We assume that the contribution from other unmeasured creeks can be aggregated into these two creeks. The data used are the historical measurement data from June 2006 to July 2007 scaled down to represent a drier future. The flow contribution from both creeks used in the simulation are shown in Figure 6.10

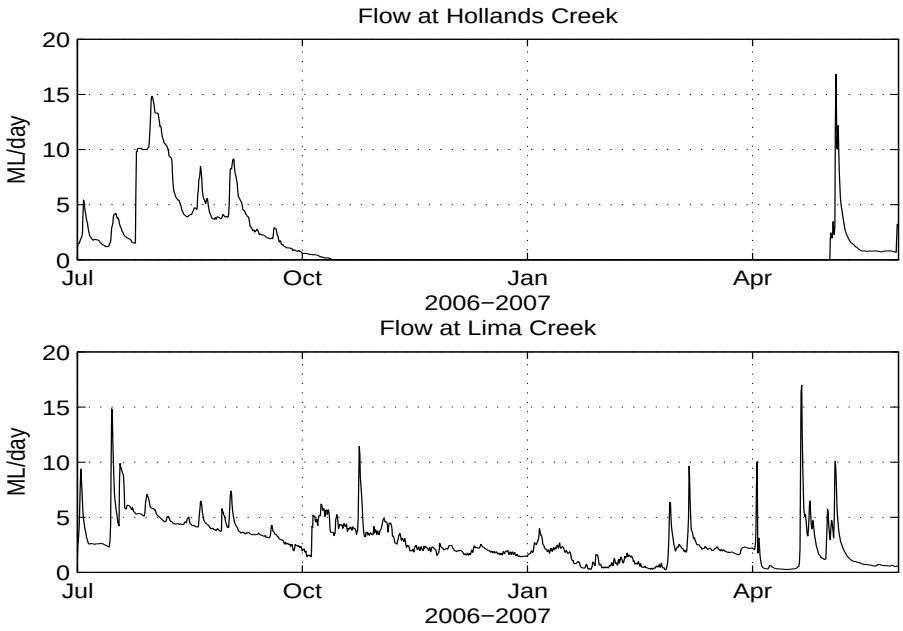

Figure 6.10: Flow contribution from creeks.

6.5.2 Output of the simulation

The output of the simulations are all the control actions and the controlled variables. The control actions are flows at Lake Nillahcootie Q_{LN}, in-let to Storage 1 Q_{Sin1}, out-let of Storage 1 Q_{Sout1}, Lake Benalla Q_{LB}, and Casey's Weir Q_C. The controlled variables are water levels at Broken Weir y_B, Lake Benalla y_{LB} and Casey's Weir y_C, flow at

Gowangardie Weir Q_G and volumes of Storages 1 and 2, V_{S1} and V_{S2}. Although the MPC controllers are designed using the models obtained through system identification (i.e., the time delay and integrator delay models obtained in Chapter 4), the controllers in the Broken River are simulated using the calibrated Saint Venant equations with the sampling interval of 360 minutes.

6.6 Evaluation of the control system

To evaluate the performance of the control system, three different management objectives are considered. A brief description of each of the management objectives is described below.

Minimal release from Lake Nillahcootie

The emphasis of the control system is to ensure the release from Lake Nillahcootie to be as small as possible and at the same, the demands from the irrigators and the environment need to be satisfied. The excess water is calculated to measure the amount of wasted water. Excess water is defined as the amount of water flowing out of our study area (i.e. Gowangardie Weir), which is not needed to satisfy demands from the irrigators and the environment. The number of days in breach over a year is used to measure the severity of the controlled variables breaching their defined constraints.

Benefit of having more regulation points

In Section 6.1.3, we have assumed that the flow at Lake Nillahcootie, Broken Weir, Lake Benalla, Casey's Weir and the in-let and out-let of Storages 1 and 2 can be regulated. The aim here is to evaluate the performance of the controllers in the case where we have fewer regulation points in the Broken River. Two cases are considered; (i) No regulation at Lake Benalla, (ii) No regulation at Casey's Weir and Lake Benalla. For the assessment of the controller, more emphasis is placed on the number of days in breach over a year of the controlled variables breaching their defined constraints.

Improve water delivery service to the irrigators

As of the current practice, the irrigators need to order water four days in advance. The aim here is to investigate the possibility for the irrigators to order water on a shorter notice. With a shorter notice of the water order, the irrigators can plan the application of water to their crops, which may lead to increase in farming productivity. In this management objectives, all the location of flows mentioned in Section 6.1.3 can be regulated.

6.6.1 Minimal release from Lake Nillahcootie

As one of the control objectives mentioned in Section 6.1.3 is to have the release from Lake Nillahcootie to be as small as possible, the amount of excess water is evaluated. The excess water is defined as the amount of water flowing out of Gowangardie Weir, which is not needed to satisfy the demands from the irrigators and the environment. Excess water is calculated by taking the sum of releases from Lake Nillahcootie and the flow contribution from creeks minus the total water orders from the irrigators and the environment along the Broken River both upstream and downstream of Gowangardie Weir.

It is desirable to have the flow at Lake Benalla, Gowangardie, Casey's and Broken Weirs to be above the minimum environmental flow. Thus, the number of days in breach of the minimum flow requirements are calculated to measure the performance. Similarly, the number of days in breach of the limits on the water levels at Broken Weir, Lake Benalla and Casey's Weir are also calculated.

Control options

To evaluate the performance of the MPCs, a comparison between the current manual operation and the two different options of the decentralised control configurations design used in (Ooi *et al.*, 2010) is made. We denote the two different options for the decentralised controllers as DCC-A and DCC-B. We would like to note that all the results of the manual operation and the decentralised controllers used throughout this thesis are obtained from (Ooi *et al.*, 2010) (with permission) for the purpose of comparison the performance of the different control options.

For the manual operation, the release from Lake Nillahcootie is made early according to the known future orders and the time delays for the water to reach the points of demand

such that the water would arrive at the time the water is required. On top of that, an additional 20ML/day is added to account for any uncertainties in the actual released flow and losses along the river. The manual operation is similar to the current control operation at the Broken River (Bailey, 2010).

For both DCC-A and DCC-B, the configuration shown in Figure 6.6 is used. The difference between these two options is that for DCC-B, an additional 10% is added to flow setpoints at Gowangardie Weir and Broken Weir to improve satisfaction of demands.

For MPC, the MPC designed via reverse engineering and the MPC designed from scratch are used. We denote the designs of the two MPCs as MPC RE and MPC DS. The MPC RE reproduces the decentralised controller shown in Figure 6.6. The configuration in Figure 6.7 is used for MPC DS.

Simulation results

A yearly long realistic simulations using both MPCs are carried out. For the clarity of presentation, only the simulation results over the month of July to November 2006, (i.e., the end of winter to the start of irrigation period) will be presented here and we only present plots of flow at Casey's Weir Q_C, Gowangardie Weir Q_G, water level at Casey's Weir y_C and Lake Benalla y_{LB}. For the complete simulation plots, see Appendix B.

In Figure 6.11, the minimum flows and the $\pm$5cm water levels bound, which we set as the constraints are represented by the bold solid line. We see that, despite the constraints are imposed in the MPC optimisation problem, constraint violations still occur due to the model and the time delay mismatch as the model used to design MPC are the time delay and integrator delay models, while the simulation model is the calibrated Saint Venant equations. In addition, as we have imposed constraints on both input and output, the optimisation can fail to produce meaningful results in the event when all these constraints cannot be satisfied simultaneously. In fact, these constraint violations actually lead to infeasible solution when solving the optimisation problem. As we have made the flow over Gowangardie Weir, water levels at Casey's Weir and Lake Benalla soft constraints, the constraints are allowed to be violated for short period of time and this also ensure no issue of infeasible solution in the optimisation.

Figure 6.12 shows water released from Lake Nillahcootie and the calculation of the excess water for each of the control options, while Table 6.4 shows the yearly volume of

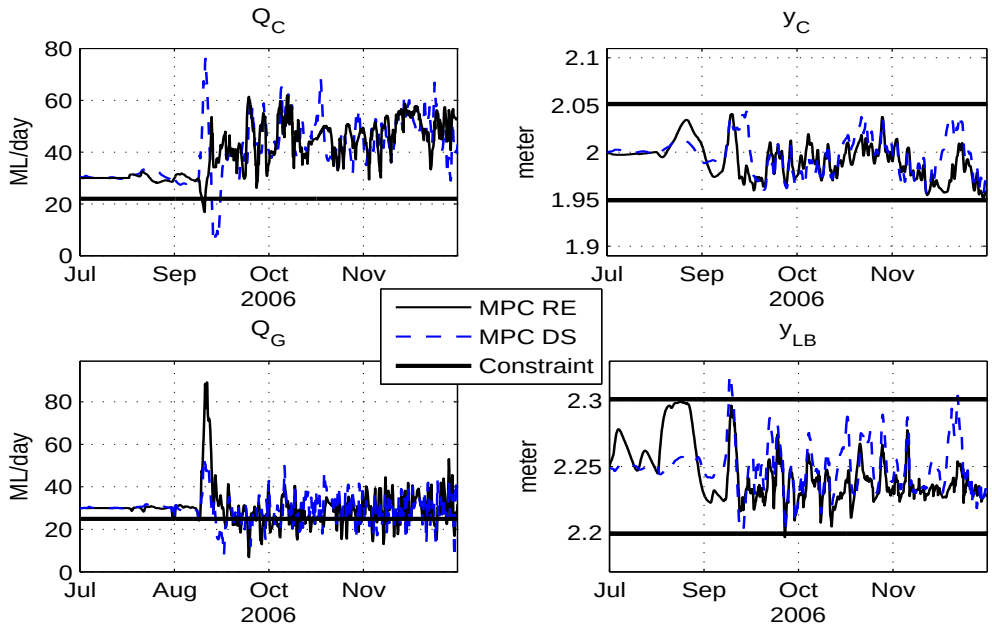

Figure 6.11: Simulation results from July to November 2006.

water needed for irrigations and the flow contribution from the creeks. Table 6.5 tabulates the number of days in breach (over a year) of the average daily flows and water levels from the defined constraints. In Table 6.5, the inclusion of the measure of the amount of

Table 6.4: Yearly volumes of water.

Total volume of water required downstream of Gowangardie Weir (irrigation and environment)	9600ML
Total volume diverted for irrigation (from Lake Nillahcootie to Gowangardie Weir)	11000ML
Total flow from Lima and Hollands Creeks	1550ML

percentages the flow are 20%, 40% and 60% below the minimum flow requirements is to illustrate the severity of the breach.

As for the water levels, we want to highlight that when y_B, y_{LB} and y_C are below their setpoints, this does not mean that the water demands are not satisfied. This basically means the water has not yet been supplied from Lake Nillahcootie while the water has been drawn by the irrigators to satisfy the water demand.

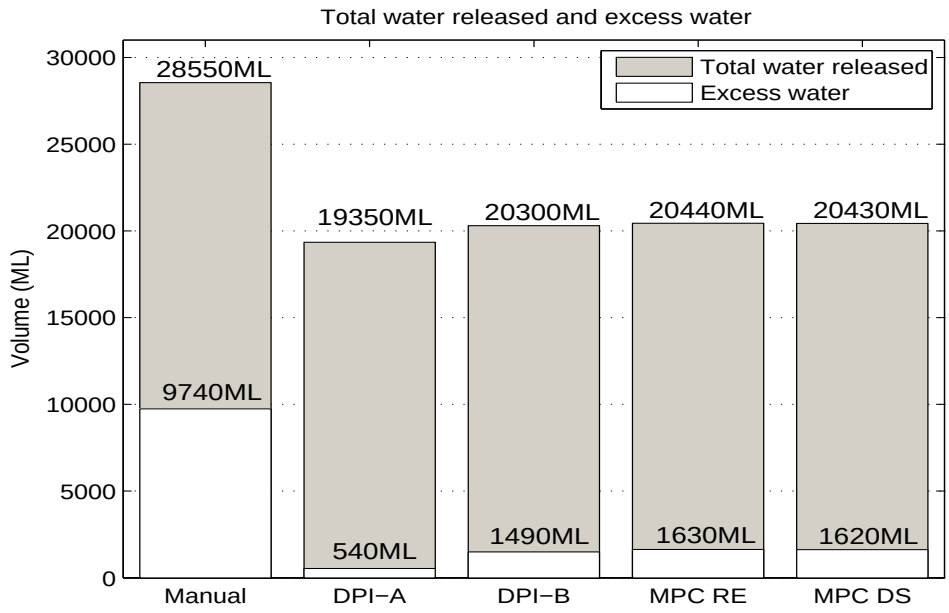

Figure 6.12: Total water released from Lake Nillahcootie and excess water for all control options.

Comparison between different control options

Under all the control options, 100% of satisfaction of water orders from the irrigators is achieved. All the control options have smaller release at Lake Nillahcootie and also a smaller amount of excess water compared to the manual operation. The various control options release between 28% to 32% less water compared to the manual operation. The excess water is reduced by between 83% to 94%. The results shown in Table 6.5 shows that under the manual operation, the number of days in breach of $Q_G < Q_{G,min}$ is smaller compared to all the other control options. This is due to the extra 20ML/day that has been added to the release at Lake Nillahcootie. These extra releases also lead to larger number of days in breach of the limit of the water levels at Lake Benalla and Broken Weir.

Between all the control options, DCC-A achieves the smallest amount of excess water, while the amount of excess water for DCC-B and the two MPCs are similar. If the control objective is only to have minimal release from Lake Nillahcootie, then DCC-A has the best performance. However, with all the control objectives mentioned in Section 6.1.3 are taken in account, DCC-A is not the preferred option. This is because the number of days in

Table 6.5: Performance measure.

Criteria	Number of days in breach (over a year) in season 2006/2007				
	Manual	DCC-A	DCC-B	MPC RE	MPC DS
Gowangardie Weir					
$Q_{\mathrm{G}} < Q_{\mathrm{G,min}}$	6	185	42	55	45
Q_{G} 20% $< Q_{\mathrm{G,min}}$	0	26	12	7	14
Q_{G} 40% $< Q_{\mathrm{G,min}}$	0	4	1	2	1
Q_{G} 60% $< Q_{\mathrm{G,min}}$	0	0	0	0	0
Daily flow change ratios <0.76, >1.5	59	52	42	0	0
Casey's Weir					
$y_{\mathrm{C}} \geq$ 5cm above setpoint	11	0	0	0	0
$y_{\mathrm{C}} \geq$ 5cm below setpoint	0	0	2	0	0
$y_{\mathrm{C}} \geq$ 15cm above setpoint	0	0	0	0	0
$y_{\mathrm{C}} \geq$ 15cm below setpoint	0	0	0	0	0
$Q_{\mathrm{C}} < Q_{\mathrm{C,min}}$	0	4	0	0	0
Q_{C} 20% $< Q_{\mathrm{C,min}}$	0	0	0	0	0
Q_{C} 40% $< Q_{\mathrm{C,min}}$	0	0	0	0	0
Q_{C} 60% $< Q_{\mathrm{C,min}}$	0	0	0	0	0
Daily flow change ratios <0.76, >1.5	16	47	42	0	0
Lake Benalla					
$y_{\mathrm{LB}} \geq$ 5cm above setpoint	147	82	56	2	0
$y_{\mathrm{LB}} \geq$ 5cm below setpoint	0	52	54	0	0
$y_{\mathrm{LB}} \geq$ 15cm above setpoint	2	2	3	0	0
$y_{\mathrm{LB}} \geq$ 15cm below setpoint	0	3	0	0	0
$Q_{\mathrm{LB}} < \mathrm{Q}_{\mathrm{LB,min}}$	0	0	0	0	0
Daily flow change ratios <0.76, >1.5	2	24	21	0	0
Broken Weir					
$y_{\mathrm{B}} \geq$ 5cm above setpoint	162	0	0	26	0
$y_{\mathrm{B}} \geq$ 5cm below setpoint	0	0	0	0	0
$y_{\mathrm{B}} \geq$ 15cm above setpoint	2	0	0	0	0
$y_{\mathrm{B}} \geq$ 15cm below setpoint	0	0	0	0	0
$Q_{\mathrm{B}} < Q_{\mathrm{B,min}}$	0	175	0	0	0
Daily flow change ratios <0.76, >1.5	9	0	0	0	0

breach of $Q_G < Q_{G,min}$ is the largest among all the control options. Similarly, the number of days in breach of the limit of the water levels at Lake Benalla and Broken Weir is also large. For all the control options, there is the occurrence of flow at Gowangardie Weir below up to 40% the required minimum flow. However, such scenarios are rare and may be tolerable depending on the purpose of the minimum flow. If the purpose of the minimum flow is for habitat preservation, these violations may not be impacting. However, if the purpose is to avoid stratification in the river, then the duration of the violation would be of concern especially in summer, (Gawne, 2010). In comparing the performance between the two MPCs and DCC-B, we observe that in general the performance of the two MPCs is very good. Although the number of days in breach of $Q_G < Q_{G,min}$ are similar compared to DCC-B, for other locations, MPC have almost all zero number of days in breach. The small number of breaches for MPC is due to the incorporation of constraint handling capability into the optimisation problem.

As MPC RE reproduces the decentralised controller, it is of interest to compare the performance between these two control options. We make a comparison between MPC RE and DCC-B. In terms of releases from Lake Nillahcootie, the excess water and the number of days in breach of $Q_G < Q_{G,min}$, both control options have similar performance. However, for other locations (except the water levels at Broken Weir and Lake Benalla), MPC RE outperforms DCC-B, with zero number of days in breach for the remaining criterias. For both the MPCs, similar performance between them is observed.

Summary

From the simulation results, we can see that the performance of MPC in general is better compared to the decentralised controllers in terms of similar or smaller number of days in breach in particular the for environmental daily flow change ratio. This is largely attributed to the ability of MPC to incorporate constraints handling in the optimisation problem. As for the head-to-head comparison between the two MPCs, their performance are very similar.

Contribution of Storage 2

The volume capacity for Storage 2 is about 6ML, which is very small relative to the volume capacity of Storage 1, which is about 300ML. At the moment, there is no infrastructure available to control the in- and out-flow at Storage 2. In this section, we investigate the performance of both the MPCs without the contribution from Storage 2. The analysis from this investigation would be useful for the water authority in deciding whether the contribution from Storage 2 is sufficient to warrant the infrastructure upgrade. We repeat the year long realistic simulations but without Storage 2. The plots of the simulations are presented in Appendix B. The release from Lake Nillahcootie and the excess water are shown in Figure 6.13 and the same performance measures used in previous section are tabulated in Table 6.6.

Without Storage 2, the water demand is still satisfied. For the MPCs, as expected, the number of days in breach of $Q_G < Q_{G,min}$ is now higher as the flow now need to be supplied from Casey's Weir instead of Storage 2. For other reaches, no significant difference in terms of number of days in breach is observed. On whether the improvement in the number of days in breach of $Q_G < Q_{G,min}$ is deemed significant to warrant the

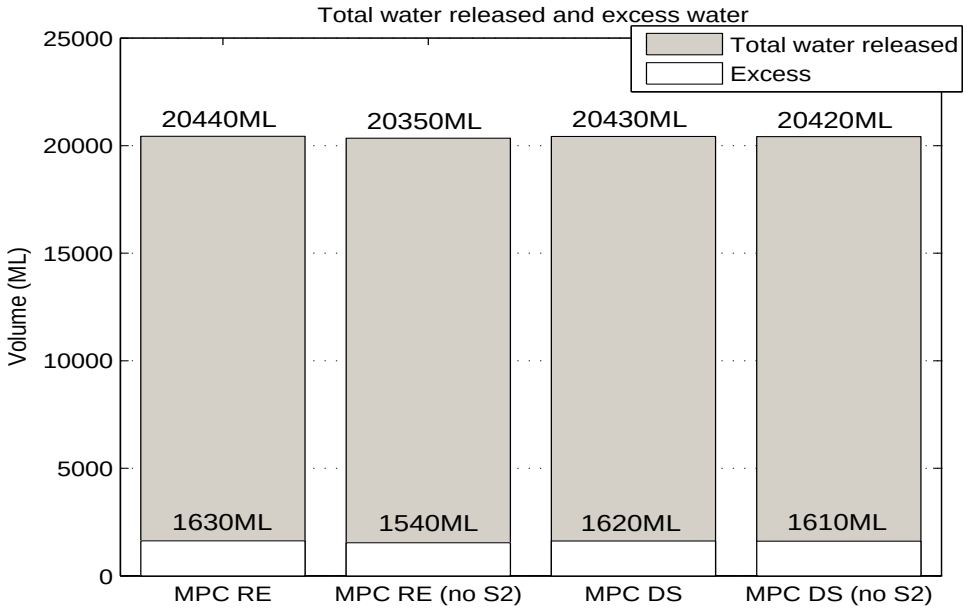

Figure 6.13: Total water released from Lake Nillahcootie and excess water with and without Storage 2.

need for infrastructure upgrade remains an open question. For instance, one can reduce the number of days in breach by increasing the flow setpoint at Gowangardie Weir by say additional 10%. This of course would lead to more release from Lake Nillahcootie but the release would still be much less compared to current manual operation, which means we would still have water savings albeit smaller. Moreover, with the size of Storage 2 being small, it would be difficult to get a good justification for infrastructure upgrade if the suggested solution of increasing the flow setpoint at Gowangardie Weir can get the job done. With that, it is reasonable for us to say that the contribution of Storage 2 may not be significant enough to warrant an infrastructure upgrade. Therefore, the analyses from this point onward will be carried out without the contribution from Storage 2.

6.6.2 Benefit of having more regulation points

To continue our analyses on the matter of infrastructure upgrade in the Broken River, in this section, we study the effect of having fewer regulation points in the Broken River. In all our simulations so far, we have assumed that the flow can be regulated at Lake

Table 6.6: Performance measure with and without Storage 2.

Criteria	Number of days in breach (over a year) in season 2006/2007			
	MPC RE (With S2)	MPC RE (No S2)	MPC DS (With S2)	MPC DS (No S2)
Gowangardie Weir				
$Q_{\mathrm{G}} < Q_{\mathrm{G,min}}$	55	67	45	50
Q_{G} 20% $< Q_{\mathrm{G,min}}$	7	25	14	31
Q_{G} 40% $< Q_{\mathrm{G,min}}$	2	5	1	9
Q_{G} 60% $< Q_{\mathrm{G,min}}$	0	1	0	4
Daily flow change ratios <0.76, >1.5	0	0	0	0
Casey's Weir				
$y_{\mathrm{C}} \geq$ 5cm above setpoint	0	0	0	0
$y_{\mathrm{C}} \geq$ 5cm below setpoint	0	0	0	0
$y_{\mathrm{C}} \geq$ 15cm above setpoint	0	0	0	0
$y_{\mathrm{C}} \geq$ 15cm below setpoint	0	0	0	0
$Q_{\mathrm{C}} < Q_{\mathrm{C,min}}$	0	0	0	0
Q_{C} 20% $< Q_{\mathrm{C,min}}$	0	0	0	0
Q_{C} 40% $< Q_{\mathrm{C,min}}$	0	0	0	0
Q_{C} 60% $< Q_{\mathrm{C,min}}$	0	0	0	0
Daily flow change ratios <0.76, >1.5	0	0	0	0
Lake Benalla				
$y_{\mathrm{LB}} \geq$ 5cm above setpoint	2	2	0	2
$y_{\mathrm{LB}} \geq$ 5cm below setpoint	0	0	0	0
$y_{\mathrm{LB}} \geq$ 15cm above setpoint	0	0	0	0
$y_{\mathrm{LB}} \geq$ 15cm below setpoint	0	0	0	0
$Q_{\mathrm{LB}} < Q_{\mathrm{LB,min}}$	0	0	0	0
Daily flow change ratios <0.76, >1.5	0	0	0	0
Broken Weir				
$y_{\mathrm{B}} \geq$ 5cm above setpoint	26	33	0	0
$y_{\mathrm{B}} \geq$ 5cm below setpoint	0	0	0	0
$y_{\mathrm{B}} \geq$ 15cm above setpoint	0	0	0	0
$y_{\mathrm{B}} \geq$ 15cm below setpoint	0	0	0	0
$Q_{\mathrm{B}} < Q_{\mathrm{B,min}}$	0	0	0	0
Daily flow change ratios <0.76, >1.5	0	0	0	0

Nillahcootie, Broken Weir, Lake Benalla, Casey's Weir and in-let and out-let of Storage 1. Two scenarios are analysed here, where in the first scenario, we no longer have regulation at Lake Benalla and in the second scenario, we have no regulation at Casey's Weir and Lake Benalla.

No regulation at Lake Benalla

We investigate the performance of both MPCs with no regulation at Lake Benalla. This means that the water level at Casey's Weir is now controlled by the out-let of Storage 1. This also lead to changes in the model. We note that as there is no regulation at Lake Benalla, the lake could damp the flow released from the out-let of Storage 1, which may

result in the integrator delay model may no longer be a suitable model structure. As we carried out the step test of flow from 30ML/day to 60ML/day using the calibrated Saint Venant equations to obtain the time delay for this new reach, the step response shows that the time delay is larger than the time constant. This finding suggests to us that the effect of the lake does not damp the flow as much as we have expected. Based on this, the integrator delay model is still used to model this reach.

The model for the reach from out-let of Storage 1 to Casey's Weir (Reach Sout1C) is given by

$$\dot{V}_C(t) = c_{1,C'}Q_{Sout1}(t - \tau_{Sout1C}) - c_{2,C'}[y_C(t) - p_C(t)]^{3/2} + c_{3,C'}Q_B(t - \tau_{BC}) \qquad (6.36)$$

where the subscripts "Sout1", "C" and "B" represent out-let of Storage 1, Casey's Weir and Broken Weir respectively. $\tau_{Sout1C} = 1440$ minutes and $\tau_{BC} = 1800$ minutes are the time delays from out-let of Storage 1 and Broken Weir to Casey's Weir respectively. Using an Euler approximation for the derivative, Equation (6.36) can be written as

$$y_C(k) = y_C(k-1)\left(\frac{T_s c_{1,C'}}{A}\right)Q_{Sout1}(k - \tau_{Sout1C} - 1) - \left(\frac{T_s c_{2,C'}}{A}\right)[y_C(k-1) - p_C(k-1)]^{3/2} + \left(\frac{T_s c_{3,C'}}{A}\right)Q_B(k - \tau_{BC} - 1) \qquad (6.37)$$

The identified parameters using the simulated data from the calibrated Saint Venant equations are $\left(\frac{T_s c_{1,C'}}{A}\right) = 0.001$, $\left(\frac{T_s c_{2,C'}}{A}\right) = 0.076$ and $\left(\frac{T_s c_{3,C'}}{A}\right) = 0.005$. The MPC RE and MPC DS are redesigned using this new model. For MPC RE, the tuned parameters for the PI-controller is given by $K_P = 2.5$, $K_I = 0.1125$ with a gain margin of 19.1dB and a phase margin of 37.3°, which means that an additional time delay of 4490 minutes can be tolerated.

For MPC DS, the following weights $q_{e,B}$, $q_{e,S1}$, $q_{e,C}$ and $q_{e,G}$ are all assigned with weight 2×10^{-7} to penalise $(y_B - y_{B,sp})^2$, $(V_{S1} - V_{S1,sp})^2$, $(y_C - y_{C,sp})^2$ and $(Q_G - Q_{G,sp})^2$. For the penalty on the integral of setpoint errors, $q_{int,B} = 9 \times 10^{-6}$, $q_{int,S1} = 1 \times 10^{-6}$, $q_{int,C} = 1 \times 10^{-5}$ and $q_{int,G} = 2 \times 10^{-6}$ are used. For the control actions and the soft constraints, the same weights (except r_{LB}, r_{S2}, $q_{L,QLB}$, $q_{H,QLB}$, $q_{L,yLB}$ and $q_{H,yLB}$) shown in Table 6.3 are used.

We repeat the yearly realistic simulation without Storage 2. The results are shown in Figure 6.14 and Table 6.7.

No regulation at Casey's Weir and Lake Benalla

In this scenario, there is no regulation available at Casey's Weir and Lake Benalla. This configuration is equivalent to using the available existing infrastructures (except the use of Storage 1, where the construction is on-going at the time of writing). With this configuration, the flow at Gowangardie Weir Q_G is now controlled by the out-let of Storage 1. We again note that with no regulation at Casey's Weir and Lake Benalla, the presence of the weir pool and the lake would potentially damp the released flow from the out-let of Storage 1. We apply the step test of flow from 30ML/day to 60ML/day to obtain the time delay for this reach using the calibrated Saint Venant equations. We again notice from the step response that the time delay is still larger than the time constant. This suggests that the presence of the weir pool and the lake do not change the flow dynamics as much as we have expected. With the flow at Gowangardie Weir cannot be regulated, we can use a time delay model to model this reach.

Thus, the model for this reach (in discrete representation), i.e. from the out-let of Storage 1 to Gowangardie Weir (Reach Sout1G) is given by

$$Q_G(k) = Q_{Sout1}(k - \tau_{Sout1G}) + Q_B(k - \tau_{BG}) \tag{6.38}$$

where the subscript, "Sout1", "G" and "B" denote out-let of Storage 1, Gowangardie Weir and Broken Weir respectively. $\tau_{Sout1G} = 3240$ minutes and $\tau_{BG} = 3600$ minutes.

The I-controller parameter is $K_I = 0.045$ with a gain margin of 11.8dB and a phase margin of 66.8°, which means additional tolerable time delay of 9330 minutes. Again, the MPC RE and MPC DS are redesigned using this new model.

For MPC DS, the following weights $q_{e,B}$, $q_{e,S1}$ and $q_{e,G}$ are all now assigned with weight 2×10^{-7} to penalise $(y_B - y_{B,sp})^2$, $(V_{S1} - V_{S1,sp})^2$ and $(Q_G - Q_{G,sp})^2$. For the penalty on the integral of setpoint errors, the following weights $q_{int,B} = 1 \times 10^{-7}$, $q_{int,S1} = 1 \times 10^{-7}$, and $q_{int,G} = 5 \times 10^{-7}$ are used. The same weights to penalise the control actions and the soft constraints used in Table 6.3 (except r_C, r_{LB}, r_{S2}, $q_{L,QLB}$, $q_{H,QLB}$, $q_{L,yLB}$, $q_{H,yLB}$ $q_{L,QC}$, $q_{H,QC}$, $q_{L,yC}$ and $q_{H,yC}$) are used.

We repeat again the yearly realistic simulations without Storage 2. The results are shown in Figure 6.14 and Table 6.7. We included the results without Storage 2 from Figure 6.13 and Table 6.6 such that we can have a comparison of the scenarios between all regulation points available and fewer regulation points.

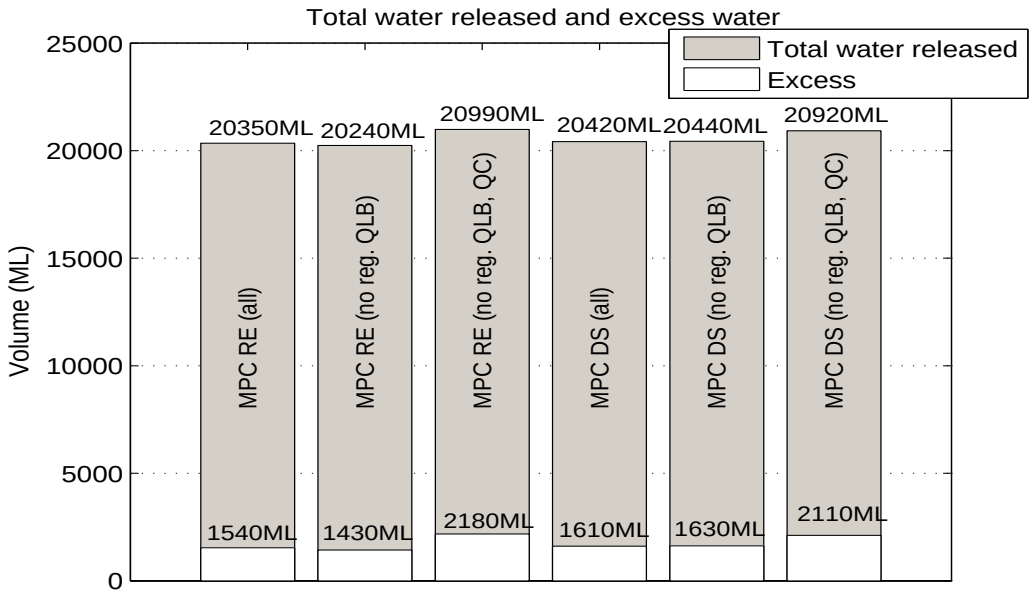

Figure 6.14: Total water released from Lake Nillahcootie and excess water with fewer regulation points.

Discussions of the results

From Figure 6.14, we can see that the release from Lake Nillahcootie and the amount of excess water are similar between all considered scenarios. With fewer regulation, we still achieve 100% demand satisfaction to the irrigators. From Table 6.7, we can see that the performance of the controllers in terms of the number of days in breach becomes worse as the number of regulation points decreases. This is mainly due to the increase in the time delay from the points of supply to the points demand. With a larger time delay, the time of delivery of water is now less accurate as the uncertainties in the time delays are now larger.

With no regulation at Casey's Weir and Lake Benalla, we see that the number of days in breach (except the water level at Casey's Weir) are generally higher compared to the case where we do not have regulation at Lake Benalla. The smaller number of days in breach of the water level at Casey's Weir is due to no adjustment of gate to maintain the water level at Casey's Weir at setpoint and essentially the flow just pass through Casey's Weir.

We also note that the numbers of day in breach for the water level 5 cm above setpoint at Lake Benalla is larger. As there is no regulation to control the water level at Lake Benalla at setpoint, the flow released from Broken Weir and the out-let from Storage 1 would naturally increased the water level at Lake Benalla, leading to a larger number of days in breach. More importantly, the results obtained here indicate that the performance of the control system can be improved significantly with more regulation points along the Broken River, thus making a good case for infrastructure upgrade.

Table 6.7: Performance measure with lesser regulation points.

Criteria	Number of days in breach (over a year) in season 2006/2007					
	MPC RE (all)	MPC RE (No reg. Q_{LB})	MPC RE (No reg. Q_C, (Q_{LB})	MPC DS (all)	MPC DS (No reg. Q_{LB})	MPC DS (No reg .Q_C,Q_{LB})
Gowangardie Weir						
$Q_G < Q_{G,min}$	67	87	89	50	75	80
Q_G 20% $< Q_{G,min}$	25	37	47	31	36	46
Q_G 40% $< Q_{G,min}$	5	14	28	9	16	24
Q_G 60% $< Q_{G,min}$	1	2	13	4	9	9
Daily flow change ratios <0.76, >1.5	0	0	0	0	0	0
Casey's Weir						
$y_C \geq$ 5cm above setpoint	0	29	10	0	11	9
$y_C \geq$ 5cm below setpoint	0	30	0	0	15	0
$y_C \geq$ 15cm above setpoint	0	0	0	0	0	0
$y_C \geq$ 15cm below setpoint	0	0	0	0	0	0
$Q_C < Q_{C,min}$	0	0	0	0	0	0
Q_C 20% $< Q_{C,min}$	0	0	0	0	0	0
Q_C 40% $< Q_{C,min}$	0	0	0	0	0	0
Q_C 60% $< Q_{C,min}$	0	0	0	0	0	0
Daily flow change ratios <0.76, >1.5	0	0	0	0	0	0
Lake Benalla						
$y_{LB} \geq$ 5cm above setpoint	2	76	90	2	108	128
$y_{LB} \geq$ 5cm below setpoint	0	2	0	0	0	0
$y_{LB} \geq$ 15cm above setpoint	0	0	1	0	0	2
$y_{LB} \geq$ 15cm below setpoint	0	0	0	0	0	0
$Q_{LB} < Q_{LB,min}$	0	2	0	0	0	0
Daily flow change ratios <0.76, >1.5	0	0	0	0	0	0
Broken Weir						
$y_B \geq$ 5cm above setpoint	33	41	38	0	0	4
$y_B \geq$ 5cm below setpoint	0	20	27	0	1	8
$y_B \geq$ 15cm above setpoint	0	0	0	0	0	0
$y_B \geq$ 15cm below setpoint	0	0	0	0	0	0
$Q_B < Q_{B,min}$	0	0	0	0	0	0
Daily flow change ratios <0.76, >1.5	0	0	0	0	0	0

Comparison between MPC RE and decentralised controller

In (Ooi *et al.*, 2010), the decentralised controller (DCC) has also been tested for the two cases with fewer regulation points mentioned above. For a better visual comparison, we tabulate the number of days in breach between MPC RE and DCC, which the MPC RE reproduces in Table 6.8. Again, we note that the results of DCC are obtained from (Ooi *et al.*, 2010) (with permission) for the purpose of comparison of the different control options.

The comparison shows that DCC has smaller number of days in breach for all the criterias for Gowangardie Weir and Broken Weir, while MPC RE has smaller number of days in breach for all the criterias for Casey's Weir and Lake Benalla. As for the criteria on daily flow change ratios, the MPC RE has zero number of days in breach in all locations compared to the DCC. Nonetheless, the results for both the control options are in agreement that with fewer regulation points, the number of days in breach of the considered criterias are higher.

6.6.3 Improve water delivery service to the irrigators

In this section, we shift our attention to improve water delivery service to the irrigators. As of the current practice, the irrigators need to order water four days in advance. We would like to investigate the possibilities to improve the service to the irrigators by reducing the advanced order time for the irrigators from four days down to possibly one day and yet still able to satisfy the water demand. From Table 6.1, one could notice that the maximum time delay of the reaches in the Broken River is 1.5 day (2160 minutes). Thus, any demand satisfaction resulting from the shorter notice would be regarded as an improve water delivery service to the irrigators.

We repeat the yearly realistic simulation using both the MPCs with the order time reduced from four days in advance down to one day in advance. The results on the release from Lake Nillahcootie and the amount of excess water for both MPCs are shown in Figure 6.15. For this management objective, the decentralised controller is not compared due to the decentralised controller is unable to satisfy the water demand when the order time is less than 2 days (see (Ooi *et al.*, 2010)). The performance measure in terms of number of days in breach for both MPCs are shown in Tables 6.9 and 6.10.

Table 6.8: Performance measure between MPC RE and DCC.

Criteria	Number of days in breach (over a year) in season 2006/2007			
	MPC RE	DCC	MPC RE	DCC
	(No reg. Q_{LB})	(No reg. Q_{LB})	(No reg. Q_C, Q_{LB})	(No reg. Q_C, Q_{LB})
Gowangardie Weir				
$Q_{\mathrm{G}} < Q_{\mathrm{G,min}}$	87	30	89	62
Q_{G} 20% $< Q_{\mathrm{G,min}}$	37	2	47	30
Q_{G} 40% $< Q_{\mathrm{G,min}}$	14	1	28	17
Q_{G} 60% $< Q_{\mathrm{G,min}}$	2	0	13	8
Daily flow change ratios <0.76, >1.5	0	8	0	65
Casey's Weir				
$y_{\mathrm{C}} \geq$ 5cm above setpoint	29	65	10	32
$y_{\mathrm{C}} \geq$ 5cm below setpoint	30	51	0	0
$y_{\mathrm{C}} \geq$ 15cm above setpoint	0	3	0	0
$y_{\mathrm{C}} \geq$ 15cm below setpoint	0	0	0	0
$Q_{\mathrm{C}} < Q_{\mathrm{C,min}}$	0	0	0	4
Q_{C} 20% $< Q_{\mathrm{C,min}}$	0	0	0	0
Q_{C} 40% $< Q_{\mathrm{C,min}}$	0	0	0	0
Q_{C} 60% $< Q_{\mathrm{C,min}}$	0	0	0	0
Daily flow change ratios <0.76, >1.5	0	32	0	23
Lake Benalla				
$y_{\mathrm{LB}} \geq$ 5cm above setpoint	76	139	90	170
$y_{\mathrm{LB}} \geq$ 5cm below setpoint	2	0	0	0
$y_{\mathrm{LB}} \geq$ 15cm above setpoint	0	3	1	4
$y_{\mathrm{LB}} \geq$ 15cm below setpoint	0	0	0	0
$Q_{\mathrm{LB}} < Q_{\mathrm{LB,min}}$	0	0	0	0
Daily flow change ratios <0.76, >1.5	0	12	0	9
Broken Weir				
$y_{\mathrm{B}} \geq$ 5cm above setpoint	41	0	38	0
$y_{\mathrm{B}} \geq$ 5cm below setpoint	20	0	27	0
$y_{\mathrm{B}} \geq$ 15cm above setpoint	0	0	0	0
$y_{\mathrm{B}} \geq$ 15cm below setpoint	0	0	0	0
$Q_{\mathrm{B}} < Q_{\mathrm{B,min}}$	0	0	0	0
Daily flow change ratios <0.76, >1.5	0	0	0	0

Discussion on the results

The results show that with both MPCs, the irrigators can order water on a shorter notice and all the water demands are still satisfied. The fact that both MPCs are able to satisfy the demands from the irrigators with one day advance order has shown its advantage over the decentralised controller. Here, we would like to highlight an important point. The one day advance order only applies to our study area, which ends in Gowangardie Weir. This does not apply for the water orders downstream of Gowangardie Weir as their orders have been aggregated into the desired flow at Gowangardie Weir, where this desired flow is known to the controller in advance. Thus, the demand from the irrigators further downstream needs to be known earlier, which is reflected in the desired flow at Gowangardie Weir.

Looking at the results in Tables 6.9 and 6.10, with the irrigators order the water on a

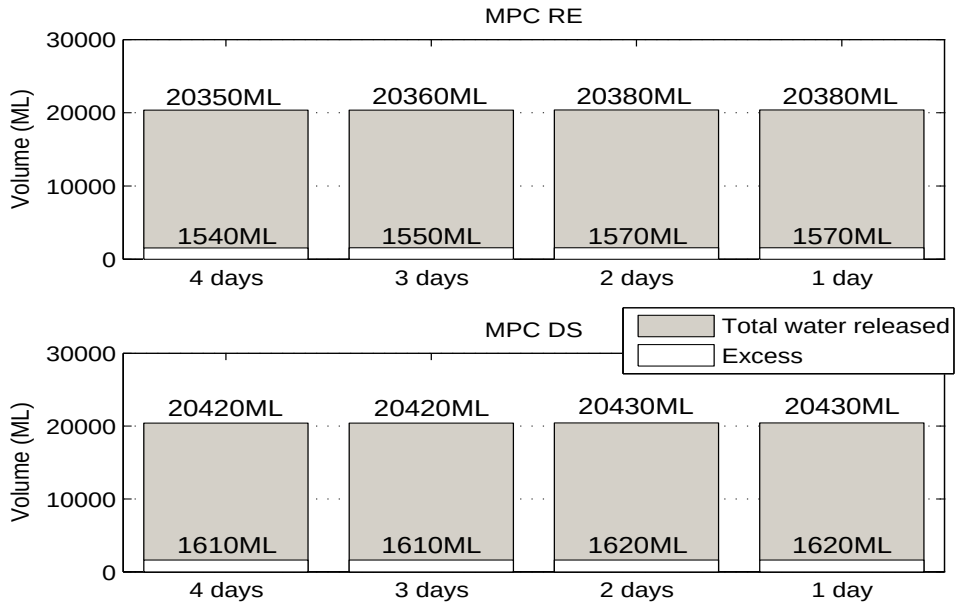

Figure 6.15: Total water released from Q_{LN} and excess for different order time. Top: MPC RE. Bottom: MPC DS.

shorter notice, we observe that the general trend is that the number of days in breach at Gowangardie Weir and Casey's Weir is larger as the water has been drawn by the irrigators but the released water has yet to arrive. However, at Lake Benalla and in particularly Broken Weir, we see that the number of days in breach of the water level above the setpoint are smaller. The reason for this is illustrated in Figure 6.16, where we show the simulation results using MPC RE.

Figure 6.16 (top) shows the offtake at Reach LNB, (middle) the flow released by the controller at Lake Nillahcootie and (bottom) the water level at Broken Weir from 1 October 2006 to 8 October 2006. We can see that, with the water order made four days in advance, due to the prediction horizon, MPC RE can "see" the order of about 3ML/day made on 4 October 2006 and the controller releases the flow early on the middle of 2 October 2006. At the bottom of the figure shown by the solid line, we see that as this early release arrives at Broken Weir, it causes y_B to exceed the 5cm bound. As the irrigators draw that required amount of water in the middle of 4 October 2006, this causes y_B to drop below the 5cm bound.

Table 6.9: Performance measure for different order time using MPC RE.

Criteria	Number of days in breach in season 2006/2007			
	4 days	3 days	2 days	1 day
Gowangardie Weir				
$Q_{\mathrm{G}} < Q_{\mathrm{G,min}}$	67	64	65	64
Q_{G} 20% $< Q_{\mathrm{G,min}}$	25	26	23	31
Q_{G} 40% $< Q_{\mathrm{G,min}}$	5	7	7	15
Q_{G} 60% $< Q_{\mathrm{G,min}}$	1	1	1	6
Daily flow change ratios <0.76, >1.5	0	0	0	0
Casey's Weir				
$y_{\mathrm{C}} \geq$ 5cm above setpoint	0	0	0	0
$y_{\mathrm{C}} \geq$ 5cm below setpoint	0	0	10	21
$y_{\mathrm{C}} \geq$ 15cm above setpoint	0	0	0	0
$y_{\mathrm{C}} \geq$ 15cm below setpoint	0	0	0	0
$Q_{\mathrm{C}} < Q_{\mathrm{C,min}}$	0	0	0	0
Q_{C} 20% $< Q_{\mathrm{C,min}}$	0	0	0	0
Q_{C} 40% $< Q_{\mathrm{C,min}}$	0	0	0	0
Q_{C} 60% $< Q_{\mathrm{C,min}}$	0	0	0	0
Daily flow change ratios <0.76, >1.5	0	0	0	0
Lake Benalla				
$y_{\mathrm{LB}} \geq$ 5cm above setpoint	2	2	2	1
$y_{\mathrm{LB}} \geq$ 5cm below setpoint	0	0	0	0
$y_{\mathrm{LB}} \geq$ 15cm above setpoint	0	0	0	0
$y_{\mathrm{LB}} \geq$ 15cm below setpoint	0	0	0	0
$Q_{\mathrm{LB}} < Q_{\mathrm{LB,min}}$	0	0	0	0
Daily flow change ratios <0.76, >1.5	0	0	0	0
Broken Weir				
$y_{\mathrm{B}} \geq$ 5cm above setpoint	33	32	33	22
$y_{\mathrm{B}} \geq$ 5cm below setpoint	0	0	0	0
$y_{\mathrm{B}} \geq$ 15cm above setpoint	0	0	0	0
$y_{\mathrm{B}} \geq$ 15cm below setpoint	0	0	0	0
$Q_{\mathrm{B}} < Q_{\mathrm{B,min}}$	0	0	0	0
Daily flow change ratios <0.76, >1.5	0	0	0	0

In the case where the water order is made one day in advance, the release at Lake Nillahcootie made by MPC RE is now later, i.e. at around mid day of 3 October 2006 (notice the small peak shown by the dotted line in the middle plot of Figure 6.16). As this small peak of flow arrives at Broken Weir, it causes y_B to exceed the 5cm bound but only for a very short period of time (shown by the dashed line) before the occurrence of the offtake cause y_B to go below the 5cm bound. It is clear that between the two plots shown in the bottom of Figure 6.16, the duration of y_B exceeding the 5cm bound is longer with four days advanced order compared to the one day advanced order.

Another point we want to highlight is that we observe that with a shorter notice of water order, the number of days in breach of $Q_G < Q_{G,min}$ are now larger. However, as mentioned before, this large number may be tolerable depending on the purpose of this minimum flow.

Table 6.10: Performance measure for different order time using MPC DS.

Criteria	Number of days in breach in season 2006/2007			
	4 days	3 days	2 days	1 day
Gowangardie Weir				
$Q_{\mathrm{G}} < Q_{\mathrm{G,min}}$	50	51	54	64
Q_{G} 20% $< Q_{\mathrm{G,min}}$	31	31	33	34
Q_{G} 40% $< Q_{\mathrm{G,min}}$	9	9	10	16
Q_{G} 60% $< Q_{\mathrm{G,min}}$	4	4	4	7
Daily flow change ratios <0.76, >1.5	0	0	1	0
Casey's Weir				
$y_{\mathrm{C}} \geq$ 5cm above setpoint	0	0	0	0
$y_{\mathrm{C}} \geq$ 5cm below setpoint	0	0	0	2
$y_{\mathrm{C}} \geq$ 15cm above setpoint	0	0	0	0
$y_{\mathrm{C}} \geq$ 15cm below setpoint	0	0	0	0
$Q_{\mathrm{C}} < \mathrm{Q_{C,min}}$	0	0	0	0
Q_{C} 20% $< \mathrm{Q_{C,min}}$	0	0	0	0
Q_{C} 40% $< \mathrm{Q_{C,min}}$	0	0	0	0
Q_{C} 60% $< \mathrm{Q_{C,min}}$	0	0	0	0
Daily flow change ratios <0.76, >1.5	0	0	0	0
Lake Benalla				
$y_{\mathrm{LB}} \geq$ 5cm above setpoint	2	2	2	0
$y_{\mathrm{LB}} \geq$ 5cm below setpoint	0	0	0	0
$y_{\mathrm{LB}} \geq$ 15cm above setpoint	0	0	0	0
$y_{\mathrm{LB}} \geq$ 15cm below setpoint	0	0	0	0
$Q_{\mathrm{LB}} < Q_{\mathrm{LB,min}}$	0	0	0	0
Daily flow change ratios <0.76, >1.5	0	0	0	0
Broken Weir				
$y_{\mathrm{B}} \geq$ 5cm above setpoint	0	0	0	0
$y_{\mathrm{B}} \geq$ 5cm below setpoint	0	0	0	0
$y_{\mathrm{B}} \geq$ 15cm above setpoint	0	0	0	0
$y_{\mathrm{B}} \geq$ 15cm below setpoint	0	0	0	0
$Q_{\mathrm{B}} < \mathrm{Q_{B,min}}$	0	0	0	0
Daily flow change ratios <0.76, >1.5	0	0	0	0

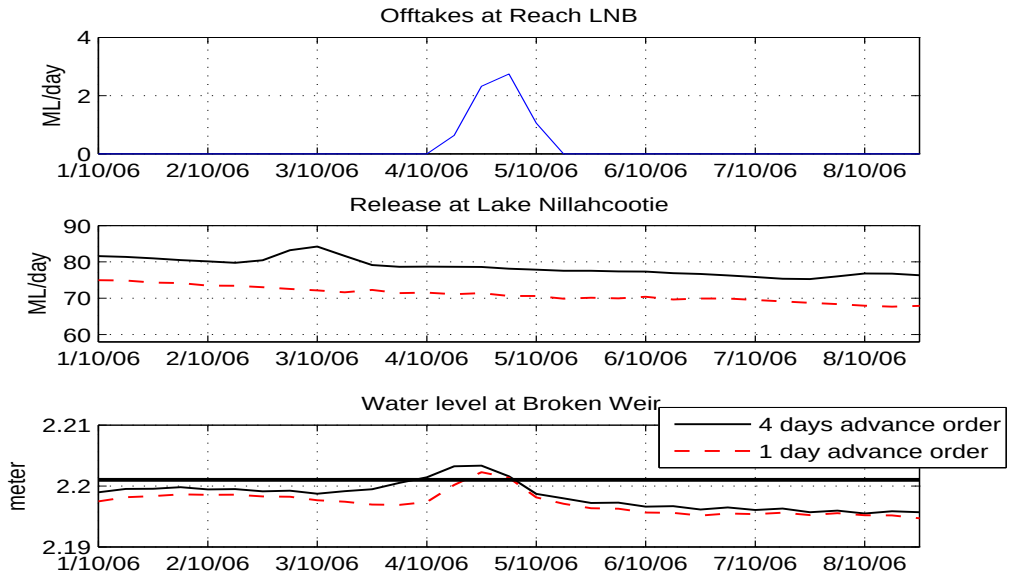

Figure 6.16: Illustration of effect of order time.

6.7 Summary

In this chapter, we have assessed the performance of MPC on the Broken River subject to all the defined control objectives. From the results of the yearly realistic simulations for different management objectives considered, we have shown that with the control system in place, we save substantial amount of water compared to the current manual operation with all the water demands are satisfied. This is evident from the amount of excess water for all the different management objectives considered, are lesser than the excess water when manual operation is used. The performance of the two MPCs seems to be better compared to the use of the decentralised controllers in particular satisfying the environmental demand. This is due to the constraint handling capability of MPC in the optimisation problem.

We have also shown that better performance can be achieved with the control system if we have more regulation points. Moreover, the improvement is significant to make a case of infrastructures upgrade in the Broken River.

In terms of improving water delivery service to the irrigators, we have shown that with the control system, the order time from the irrigators within our study area can be reduced

to one day. With the order time reduced, the irrigators would benefit from a more timely application of water to pastures, crops, etc that would lead to an increase of productivity.

Between MPC RE and the decentralised controller, we have illustrated the benefit of constraint handling of using MPC. With constraint handling, the performance of MPC RE in terms of number of days in breach for all the different management objectives considered are similar if not smaller compared to the decentralised controller.

Between the two designs of MPC, the performance between them are similar. However, the tuning of MPC DS is not trivial and requires a lot of effort in selecting the weights such that a satisfactory performance is achieved. Further improved performance for MPC DS can be expected if more extensive tuning attempts are made. Whether the improvement in using MPC DS outweighs the tuning effort as compared to MPC RE is an open question and this requires further investigation.

Chapter 7

Conclusions and future works

7.1 Conclusions

There are two main objectives considered in this thesis; modelling of river systems and control of river systems. The aims of the modelling part are to develop models of river systems useful for control design and to develop models of river system useful for simulation. On the other hand, the aims of the control part are to design controller using the developed model and assess the performance of the controllers through simulation.

In Chapter 3, the main objective is to develop models of river systems useful for simulations. We investigated how the Saint Venant equations should be segmented using the Preissmann scheme to represent a river. In addition, we also investigated how sensitive the simulation results are to the variation of the parameters in the Saint Venant equations. Through experimental validation, we had shown that a few segments are often sufficient to obtain an accurate representation of a river and furthermore, the accuracy of the Saint Venant equations have been validated against the measured data of a river.

The Saint Venant equations are not easy to use for control design as they are nonlinear partial differential equations. In Chapter 4, the main objective is to develop river models useful for control design. We built river models through system identification and had shown that a simple time delay and integrator delay models were accurate in capturing the relevant dynamics of a river useful for control design. We had validated the accuracy of these models against measured data and moreover, they were as accurate as the Saint Venant equations around the operating region.

In Chapter 5, we presented three systematic methods of obtaining weights in the MPC criterion through reverse engineering of our "favourite" controller for MPC. Building on the reverse engineering work from (Hartley and Maciejowski, 2009), which uses a full order observer, two reverse engineering methods were developed in this chapter. These two methods used a reduced order observer and augmenting the plant with the state of the our "favourite" controller. In addition, we had illustrated that the choice of $u = -Kx$ as the MPC criterion function would drive the system to satisfy the control law than to the desirable region. The role of the observer used in reverse engineering had also been illustrated to mainly reproduce the "favourite" controller rather than to estimate the states of the plant.

In Chapter 6, the main objectives are to design MPC controller using the time delay and integrator delay models and to assess the performance of MPC through simulation. Two MPC designs were considered; MPC design via reverse engineering and MPC design from scratch. Through a realistic year long simulation, we had shown that with MPC, we achieved significant water savings, improved water service delivery to the irrigators and improved environmental benefits compared to current operation in the river.

7.2 Future works

There are several directions of further research following the above works.

- The effects of rainfall, evapotranspiration and ground water/surface water interaction are not taken into account in the empirical modelling exercise. It would be of interest to see how much improvement from a control point of view can be made by incorporating all these factors into the model.
- In addition, modelling of rivers with intermediate measurements or with extra measurements along the river is another interesting aspect to look at. This model can be useful for control design that involves control of intermediate points along the river. In a related problem, the optimal number and placement of sensors for control is a research of interest. This can facilitate the appropriate number of sensors to be installed, which is vital from economical reason point of view.
- For the reverse engineering of MPC from existing controller, it would be of interest to provide a guideline on fine tuning the obtained weights when reproducing MPC

from the existing controller. In addition, a robust MPC need to be considered, in particularly when there is a model mismatch.

- One of the MPC designed to control the Broken River was reverse engineered from a decentralised PI controller. As distributed control configuration with H-infinity loop shaping controller achieves better performance compared to the decentralised control configuration, it would be of interest to reverse engineer MPC from this controller and explore the potential constraint handling benefits.

- The redesigning of MPC with the use of additional measurement sensors for the control of Broken River is another aspect that can be investigated to evaluate any potential benefit of having additional measurements in the control system.

Appendix A

Derivation Of The Navier-Stoke Equations

Here, the simplified derivation of the Navier-Stoke equations will be derived from the conservation of mass and the conservation of momentum under the assumption that the fluid particle is continuum (i.e. the fluid is treated as a continuous substance). For a more detailed derivation can be found in standard computational fluid dynamics textbook (e.g. (Vreugdenhil, 1994), (Wu, 2008), (Zienkiewicz *et al.*, 2006)).

A.1 Mass equation

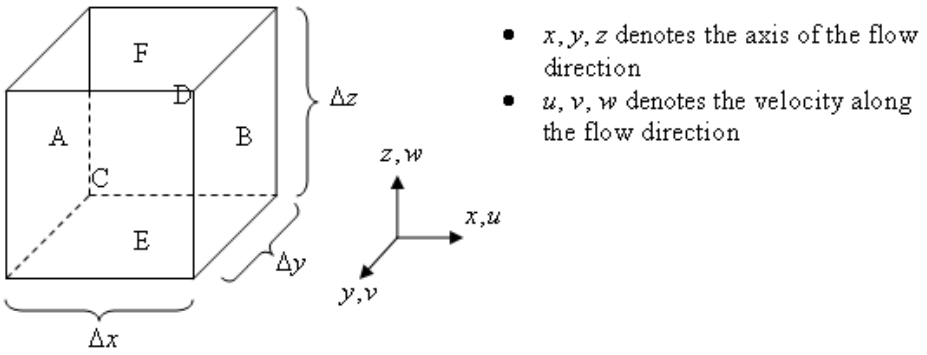

Figure A.1: Sketch of the control volume.

Consider a small volume of the fluid in the middle of the flow, called the control volume (CV) as shown in Figure A.1. We shall first derive the continuity equation for Navier-Stoke from the conservation of mass i.e.

$$\begin{array}{l}\text{Net rate of mass entering/leaving the volume element}\\ = \\ \text{Rate of change of mass in the volume element}\end{array} \tag{A.1}$$

Let us consider the left hand side of Equation (3.1). Looking at Figure A.1, the CV has six sides indicating six possible ways the mass could enter or leave the CV. Consider the sides along the x-axis. The mass flux entering and leaving through this side is given by

$$\begin{aligned}\text{Mass flux in along } x\text{-axis} &= \rho u \Delta y \Delta z \\ \text{Mass flux out along } x\text{-axis} &= -(\rho + \Delta\rho)(u + \Delta u)\Delta y \Delta z\end{aligned}$$

Similarly, considering the sides along y- and z-axis,

$$\begin{aligned}\text{Mass flux in along } y\text{-axis} &= \rho v \Delta x \Delta z \\ \text{Mass flux out along } y\text{-axis} &= -(\rho + \Delta\rho)(v + \Delta v)\Delta x \Delta z \\ \text{Mass flux in along } z\text{-axis} &= \rho w \Delta x \Delta y \\ \text{Mass flux out along } z\text{-axis} &= -(\rho + \Delta\rho)(w + \Delta w)\Delta x \Delta y\end{aligned}$$

On the right hand side of Equation (3.1), the rate of change of mass within the CV is given by

$$\left(\frac{\Delta\rho}{\Delta t}\right)\Delta x \Delta y \Delta z$$

Putting all the equations for the conservation of mass together gives us

$$\begin{aligned}\left(\frac{\Delta\rho}{\Delta t}\right)\Delta x \Delta y \Delta z = \rho u \Delta y \Delta z + \rho v \Delta x \Delta z + \rho w \Delta x \Delta y \\ -(\rho + \Delta\rho)(u + \Delta u)\Delta y \Delta z - (\rho + \Delta\rho)(v + \Delta v)\Delta x \Delta z - (\rho + \Delta\rho)(w + \Delta w)\Delta x \Delta y\end{aligned} \tag{A.2}$$

Simplifying Equation (A.2) and neglecting higher order terms of $\Delta\rho\Delta x\Delta y\Delta z$ leads to

$$\begin{aligned}\left(\frac{\Delta\rho}{\Delta t}\right)\Delta x\Delta y\Delta z &= -(\rho\Delta u + u\Delta\rho)\Delta y\Delta z - (\rho\Delta v + v\Delta\rho)\Delta x\Delta z - (\rho\Delta w + w\Delta\rho)\Delta x\Delta y \\ &= -\Delta(\rho u)\Delta y\Delta z - \Delta(\rho v)\Delta x\Delta z - \Delta(\rho w)\Delta x\Delta y \end{aligned} \tag{A.3}$$

Dividing the left hand side by $\Delta x\Delta y\Delta z$,

$$\left(\frac{\Delta\rho}{\Delta t}\right) + \frac{\Delta(\rho u)}{\Delta x} + \frac{\Delta(\rho v)}{\Delta y} + \frac{\Delta(\rho w)}{\Delta z} = 0 \tag{A.4}$$

As Δx, Δy, Δz and Δt approach zero, we arrive at

$$\left(\frac{\partial\rho}{\partial t}\right) + \frac{\partial(\rho u)}{\partial x} + \frac{\partial(\rho v)}{\partial y} + \frac{\partial(\rho w)}{\partial z} = 0 \tag{A.5}$$

Equation (A.5) is the *continuity equation*. In the case of incompressible fluid, (e.g. water in our case), the value of ρ is constant. This means $\partial\rho/\partial t = 0$. We can then rewrite Equation (A.5) as

$$\begin{aligned}\rho\frac{\partial(u)}{\partial x} + \rho\frac{\partial(v)}{\partial y} + \rho\frac{\partial(w)}{\partial z} &= 0 \\ \frac{\partial u}{\partial x} + \frac{\partial v}{\partial y} + \frac{\partial w}{\partial z} &= 0 \end{aligned} \tag{A.6}$$

A.2 Momentum equation

Let us now derive the momentum equation. Consider again the same CV as shown in Figure A.1. From the conservation of momentum, i.e.

Rate of change of the momentum within the volume element
=
Net rate of momentum transfer into the volume element (A.7)
+
Sum of all forces that acts on the volume element

$$\frac{\partial(\rho u)}{\partial t}\Delta x\Delta y\Delta z$$

For the right hand side of Equation (A.7), there are six momentum fluxes along x-axis to be considered. Momentum flux is the product of mass flux direction of momentum and the surface area.

$$\begin{aligned}
&\text{Momentum flux for surface A} = \rho uu\Delta y\Delta z \\
&\text{Momentum flux for surface B} = -\left(\rho uu + \frac{\partial}{\partial x}\rho uu\Delta x\right)\Delta y\Delta z \\
&\text{Momentum flux for surface C} = \rho uv\Delta x\Delta z \\
&\text{Momentum flux for surface D} = -\left(\rho uv + \frac{\partial}{\partial y}\rho uv\Delta y\right)\Delta x\Delta z \\
&\text{Momentum flux for surface E} = \rho uw\Delta x\Delta y \\
&\text{Momentum flux for surface F} = -\left(\rho uw + \frac{\partial}{\partial z}\rho uw\Delta z\right)\Delta x\Delta y
\end{aligned}$$

Denote $\sum F_x$ be the sum of all forces acting on the CV along x-axis. The conservation of momentum along x-axis becomes

$$\begin{aligned}
\frac{\partial(\rho u)}{\partial t}\Delta x\Delta y\Delta z = \rho uu\Delta y\Delta z + \rho uv\Delta x\Delta z + \rho uw\Delta x\Delta y \\
-\left(\rho uu + \frac{\partial}{\partial x}\rho uu\Delta x\right)\Delta y\Delta z - \left(\rho uv + \frac{\partial}{\partial y}\rho uv\Delta y\right)\Delta x\Delta z - \left(\rho uw + \frac{\partial}{\partial z}\rho uw\Delta z\right)\Delta x\Delta y \\
+\sum F_x
\end{aligned} \tag{A.8}$$

Simplifying Equation (A.8)

$$\left[\frac{\partial(\rho u)}{\partial t} + \frac{\partial(\rho uu)}{\partial x} + \frac{\partial(\rho uv)}{\partial y} + \frac{\partial(\rho uw)}{\partial z}\right]\Delta x\Delta y\Delta z = \sum F_x \tag{A.9}$$

Using the product rule, Equation (A.9) can be rewritten as

$$\begin{aligned}
\Bigg[\rho\frac{\partial u}{\partial t} + \rho u\frac{\partial u}{\partial x} + \rho v\frac{\partial u}{\partial y} + \rho w\frac{\partial u}{\partial z} \\
+u\frac{\partial \rho}{\partial t} + u\frac{\partial \rho u}{\partial x} + u\frac{\partial \rho v}{\partial y} + u\frac{\partial \rho w}{\partial z}\Bigg]\Delta x\Delta y\Delta z = \sum F_x
\end{aligned} \tag{A.10}$$

Notice that the last four terms of Equation (A.10) is actually the continuity equation (Equation (A.6)) multiply with u. Since the continuity equation is zero for incompressible

fluids, the last four terms of Equation (A.10) becomes zero. This lead to

$$\left[\rho\frac{\partial(u)}{\partial t}+\rho u\frac{\partial(u)}{\partial x}+\rho v\frac{\partial(u)}{\partial y}+\rho w\frac{\partial(u)}{\partial z}\right]\Delta x\Delta y\Delta z=\sum F_x \tag{A.11}$$

Doing the similar derivation along the $y-$ and $z-$ axis yield,

$$\left[\rho\frac{\partial(v)}{\partial t}+\rho u\frac{\partial(v)}{\partial x}+\rho v\frac{\partial(v)}{\partial y}+\rho w\frac{\partial(v)}{\partial z}\right]\Delta x\Delta y\Delta z=\sum F_y \tag{A.12}$$

$$\left[\rho\frac{\partial(w)}{\partial t}+\rho u\frac{\partial(w)}{\partial x}+\rho v\frac{\partial(w)}{\partial y}+\rho w\frac{\partial(w)}{\partial z}\right]\Delta x\Delta y\Delta z=\sum F_z \tag{A.13}$$

From Equations (A.11), (A.15) and (A.16), the only thing left to be derived are the term $\sum F_{x,y,z}$. Now, let us derive the external force. Here, we will consider the derivation along the x-axis, $\sum F_x$. Similar derivation can be carried out along y- and z-axis to obtain $\sum F_y$ and $\sum F_z$.

There are two types of force that act on the CV. There are the body force and the surface force. The body force, is the force due to the gravity acceleration. For the considered CV, the body force is the product of the gravity acceleration along x-axis and the mass. This is given by

$$\text{Body force} = g_x(\rho\Delta x\Delta y\Delta z) \tag{A.14}$$

The surface force on the other hand is the force that acts on a particular surface, which is also known as stress. The stress on the CV acts in the outward direction. Let us denoted the stress term by $S_{i,j}$. The first subscript, i represents the normal direction of the surface on which the stress acts. The second subscript, j represents the direction of the stress. For example, $S_{y,x}$ means the stress acts upon the side normal to y-axis and in the direction of the x-axis. The force due to stress is the product of the stress with the area of the surface where the force acts on.

Consider again the CV shown in Figure A.1. Stating the force due to stress on all six

surfaces, we get

$$\begin{aligned}
&\text{Force due to stress on surface A, } F_{x,x} = -S_{x,x}\Delta y\Delta z \\
&\text{Force due to stress on surface B, } F_{x,x} = \left(S_{x,x} + \frac{\partial S_{x,x}}{\partial x}\Delta x\right)\Delta y\Delta z \\
&\text{Force due to stress on surface C, } F_{y,x} = -S_{y,x}\Delta x\Delta z \\
&\text{Force due to stress on surface D, } F_{y,x} = \left(S_{y,x} + \frac{\partial S_{y,x}}{\partial y}\Delta y\right)\Delta x\Delta z \\
&\text{Force due to stress on surface E, } F_{z,x} = -S_{z,x}\Delta x\Delta y \\
&\text{Force due to stress on surface F, } F_{z,x} = \left(S_{z,x} + \frac{\partial S_{z,x}}{\partial z}\Delta z\right)\Delta x\Delta y
\end{aligned}$$

Summing all the forces due to stress and doing some manipulation, yield

$$\left(\frac{\partial S_{x,x}}{\partial x} + \frac{\partial S_{y,x}}{\partial y} + \frac{\partial S_{z,x}}{\partial z}\right)\Delta x\Delta y\Delta z \tag{A.15}$$

The stress, $S_{i,j}$ comprises of pressure, p and normal viscous stress, τ. Since the derivation is along x-axis, only the pressure along the x-axis will be contributing and the contribution is in the opposite direction. Therefore we have,

$$\begin{aligned}
S_{x,x} &= -p + \tau_{x,x} \\
S_{y,x} &= \tau_{y,x} \\
S_{z,x} &= \tau_{z,x}
\end{aligned} \tag{A.16}$$

Substituting Equation (A.16) into Equation (A.15), we get

$$\left(-\frac{\partial p}{\partial x} + \frac{\partial \tau_{x,x}}{\partial x} + \frac{\partial \tau_{y,x}}{\partial y} + \frac{\partial \tau_{z,x}}{\partial z}\right)\Delta x\Delta y\Delta z \tag{A.17}$$

Let us analyse further the normal viscous stress. The normal viscous stress depends on whether the fluid is Newtonian or not. The majority of the fluids (including water) are Newtonian. A Newtonian fluid is fluid for which the normal viscous stress is linearly proportional to the rate of deformation of the fluid. μ is generally used to denote the proportionality constant. For an incompressible fluid, the normal viscous stress are given

by

$$\begin{aligned}\tau_{x,x} &= \mu\left(\frac{\partial u}{\partial x}+\frac{\partial u}{\partial x}\right) = 2\mu\frac{\partial u}{\partial x}\\ \tau_{y,x} &= \mu\left(\frac{\partial v}{\partial x}+\frac{\partial u}{\partial y}\right)\\ \tau_{z,x} &= \mu\left(\frac{\partial w}{\partial x}+\frac{\partial u}{\partial z}\right)\end{aligned} \tag{A.18}$$

Substituting Equation (A.18) into Equation (A.17),

$$\left[-\frac{\partial p}{\partial x}+\frac{\partial}{\partial x}\left(\mu\frac{\partial u}{\partial x}+\mu\frac{\partial u}{\partial x}\right)+\frac{\partial}{\partial y}\left(\mu\frac{\partial v}{\partial x}+\mu\frac{\partial u}{\partial y}\right)+\frac{\partial}{\partial z}\left(\mu\frac{\partial w}{\partial x}+\mu\frac{\partial u}{\partial z}\right)\right]\Delta x\Delta y\Delta z \tag{A.19}$$

Simplifying Equation (A.19), we get

$$\left[-\frac{\partial p}{\partial x}+\mu\left(\frac{\partial^2 u}{\partial x^2}+\frac{\partial^2 u}{\partial y^2}+\frac{\partial^2 u}{\partial z^2}\right)+\mu\frac{\partial}{\partial x}\left(\frac{\partial u}{\partial x}+\frac{\partial v}{\partial y}+\frac{\partial w}{\partial z}\right)\right]\Delta x\Delta y\Delta z \tag{A.20}$$

The last term of Equation (A.20) becomes zero from the continuity equation. Rewriting Equation (A.20), we get

$$\left[-\frac{\partial p}{\partial x}+\mu\left(\frac{\partial^2 u}{\partial x^2}+\frac{\partial^2 u}{\partial y^2}+\frac{\partial^2 u}{\partial z^2}\right)\right]\Delta x\Delta y\Delta z \tag{A.21}$$

Now, we can write the complete equation for the term $\sum F_x$. From Equations (A.14) and (A.21), we get

$$\sum F_x = \left[g_x\rho-\frac{\partial p}{\partial x}+\mu\left(\frac{\partial^2 u}{\partial x^2}+\frac{\partial^2 u}{\partial y^2}+\frac{\partial^2 u}{\partial z^2}\right)\right]\Delta x\Delta y\Delta z \tag{A.22}$$

Rewriting the conservation of momentum along x-axis gives

$$\rho\left[\frac{\partial(u)}{\partial t}+u\frac{\partial(u)}{\partial x}+v\frac{\partial(u)}{\partial y}+w\frac{\partial(u)}{\partial z}\right]-g_x\rho+\frac{\partial p}{\partial x}-\mu\left(\frac{\partial^2 u}{\partial x^2}+\frac{\partial^2 u}{\partial y^2}+\frac{\partial^2 u}{\partial z^2}\right)=0 \tag{A.23}$$

Replacing the last terms with the Laplace operator, $\nabla^2=\dfrac{\partial^2}{\partial x^2}+\dfrac{\partial^2}{\partial y^2}+\dfrac{\partial^2}{\partial z^2}$ in Equa-

tion (A.23), we get

$$\rho\left[\frac{\partial(u)}{\partial t}+u\frac{\partial(u)}{\partial x}+v\frac{\partial(u)}{\partial y}+w\frac{\partial(u)}{\partial z}\right]-g_x\rho+\frac{\partial p}{\partial x}-\mu\nabla^2 u=0 \tag{A.24}$$

Similar derivations along the y- and z- axis give

$$\rho\left[\frac{\partial(v)}{\partial t}+u\frac{\partial(v)}{\partial x}+v\frac{\partial(u)}{\partial y}+w\frac{\partial(v)}{\partial z}\right]-g_y\rho+\frac{\partial p}{\partial y}-\mu\nabla^2 v=0 \tag{A.25}$$

$$\rho\left[\frac{\partial(w)}{\partial t}+u\frac{\partial(w)}{\partial x}+v\frac{\partial(w)}{\partial y}+w\frac{\partial(w)}{\partial z}\right]-g_z\rho+\frac{\partial p}{\partial z}-\mu\nabla^2 w=0 \tag{A.26}$$

Equations (A.24), (A.25) and (A.26) are the *dynamic equations* for Navier-Stoke equations.

A.3 The two-dimensional flow equations

The Navier-Stokes equations describe three-dimensional flow. To describe two-dimensional flow, we need to integrate the continuity and the dynamic equations over flow depth. Here we are interested in the two-dimensional flow along the x- and $y-$ axis (see Figure A.1). The derivation presented here is the simplified form. See (Chaudhry, 1993) or (Wu, 2008) for the detailed version.

Integrating Equation (A.6) over the flow depth, we obtain

$$\int_{Z_b}^{Z}\frac{\partial u}{\partial x}dz+\int_{Z_b}^{Z}\frac{\partial v}{\partial y}dz+\int_{Z_b}^{Z}\frac{\partial w}{\partial z}dz=0 \tag{A.27}$$

where Z is the z-coordinate of the water surface and Z_b is the z-coordinate at the channel bottom. Using Leibnitz Rule, we rewrite Equation (A.27) as

$$\begin{aligned}\frac{\partial}{\partial x}\int_{Z_b}^{Z}udz-u(Z)\frac{\partial Z}{\partial x}+u(Z_b)\frac{\partial Z_b}{\partial x}+\frac{\partial}{\partial y}\int_{Z_b}^{Z}vdz\\ -v(Z)\frac{\partial Z}{\partial y}+v(Z_b)\frac{\partial Z_b}{\partial y}+w(Z)-w(Z_b)=0\end{aligned} \tag{A.28}$$

Note that the channel bottom is rigid, hence we have

$$u(Z_b) = v(Z_b) = w(Z_b) = 0 \tag{A.29}$$

The surface however, moves freely. Therefore, $w(Z)$ is expressed as the total derivative with respect to t given by

$$w(Z) = \frac{DZ}{Dt} = \frac{\partial Z}{\partial t} + u(Z)\frac{\partial Z}{\partial x} + v(Z)\frac{\partial Z}{\partial y} \tag{A.30}$$

Substituting Equations (A.29) and (A.30) into Equation (A.28) and let $h = Z - Z_b$, after some algebraic manipulation we get

$$\frac{\partial h}{\partial t} + \frac{\partial (uh)}{\partial x} + \frac{\partial (vh)}{\partial y} = 0 \tag{A.31}$$

Let us now integrate the dynamic equations over the flow depth. Assuming that the pressure is hydrostatic, we get

$$\rho g + \frac{\partial p}{\partial z} = 0 \tag{A.32}$$

Integrating Equation (A.32) over the flow depth and assuming atmospheric pressure to be zero, we get

$$p = \rho g(Z - Z_b) \tag{A.33}$$

Substituting Equation (A.33) into Equations (A.24) and (A.25) with some algebraic manipulation, we get

$$\frac{\partial u}{\partial t} + \frac{\partial u^2}{\partial x} + \frac{\partial (uv)}{\partial y} + \frac{\partial (uw)}{\partial z} = g_x + g_z\frac{\partial Z}{\partial x} + \frac{\mu}{\rho}\nabla^2 u \tag{A.34}$$

$$\frac{\partial v}{\partial t} + \frac{\partial (uv)}{\partial x} + \frac{\partial v^2}{\partial y} + \frac{\partial (vw)}{\partial z} = g_y + g_z\frac{\partial Z}{\partial x} + \frac{\mu}{\rho}\nabla^2 v \tag{A.35}$$

Integrating Equations (A.34) and (A.35) over flow depth and let $h = Z - Z_b$, we arrive with

$$\frac{\partial uh}{\partial t} + \frac{\partial u^2 h}{\partial x} + \frac{\partial (uvh)}{\partial y} = \left(g_x + g_z\frac{\partial h}{\partial x}\right)h - \tau_{bx} \tag{A.36}$$

$$\frac{\partial vh}{\partial t} + \frac{\partial (uvh)}{\partial x} + \frac{\partial v^2 h}{\partial y} = \left(g_y + g_z \frac{\partial h}{\partial x} \right) h - \tau_{by} \tag{A.37}$$

where the term τ_{bx} and τ_{by} are the shear stress term coming from integrating $\int_{Z_b}^{Z} \frac{\mu}{\rho} \nabla^2 u dz$ and $\int_{Z_b}^{Z} \frac{\mu}{\rho} \nabla^2 v dz$ respectively.

Note that the term g_x, g_y and g_z are vector components of $\mathbf{g}$. For small channel bottom slope and after some manipulation (see (Chaudhry, 1993) and (Wu, 2008)), we can express Equations (A.36) and (A.37) as

$$\frac{\partial uh}{\partial t} + \frac{\partial}{\partial x} \left(u^2 h + \frac{1}{2} g h^2 \right) + \frac{\partial (uvh)}{\partial y} = gh(S_{0x} - S_{fx}) \tag{A.38}$$

$$\frac{\partial vh}{\partial t} + \frac{\partial (uvh)}{\partial x} + \frac{\partial}{\partial y} \left(v^2 h + \frac{1}{2} g h^2 \right) = gh(S_{0y} - S_{fy}) \tag{A.39}$$

where S_0 is the channel bottom slope, S_f is the friction slope and subscripts x and y denote the direction of the slope.

Equations (A.31), (A.38) and (A.39) are the depth averaged equation for two-dimensional flow.

Appendix B

Performance of the MPC controllers

B.1 Yearly realistic simulation results

B.1.1 Simulation with Storage 2

The yearly realistic simulation results described in Section 6.6 using MPC RE and MPC DS are shown in Figures B.1 to B.3. The simulation results look like "noise" and this is due to the many offtakes happening along the reaches in the Broken River. Nonetheless, there is one thing we would like to highlight. Using MPC RE, we can see that there are times when the Storage 2 is completely empty and also completely filled. On the other hand, when using MPC DS, Storage 2 is not utilised as much. This is due to the difficulty in obtaining the appropriate weight in penalising the deviation of Storage 2 from setpoint.

B.1.2 Simulation without Storage 2

The yearly realistic simulation results without the contribution from Storage 2, described in Section 6.6.1 using MPC RE and MPC DS are shown in Figures B.4 to B.5. Comparing this simulation results with the one with Storage 2, we can see that the only significant difference in the flow at Casey's and Gowangardie Weir is that the flow peak around September 2006 is released from Casey's Weir instead of Storage 2. Other than that, the

rest of the plots are similar thus leading us to make the case that the contribution of Storage 2 may not be significant to warrant the infrastructure upgrades.

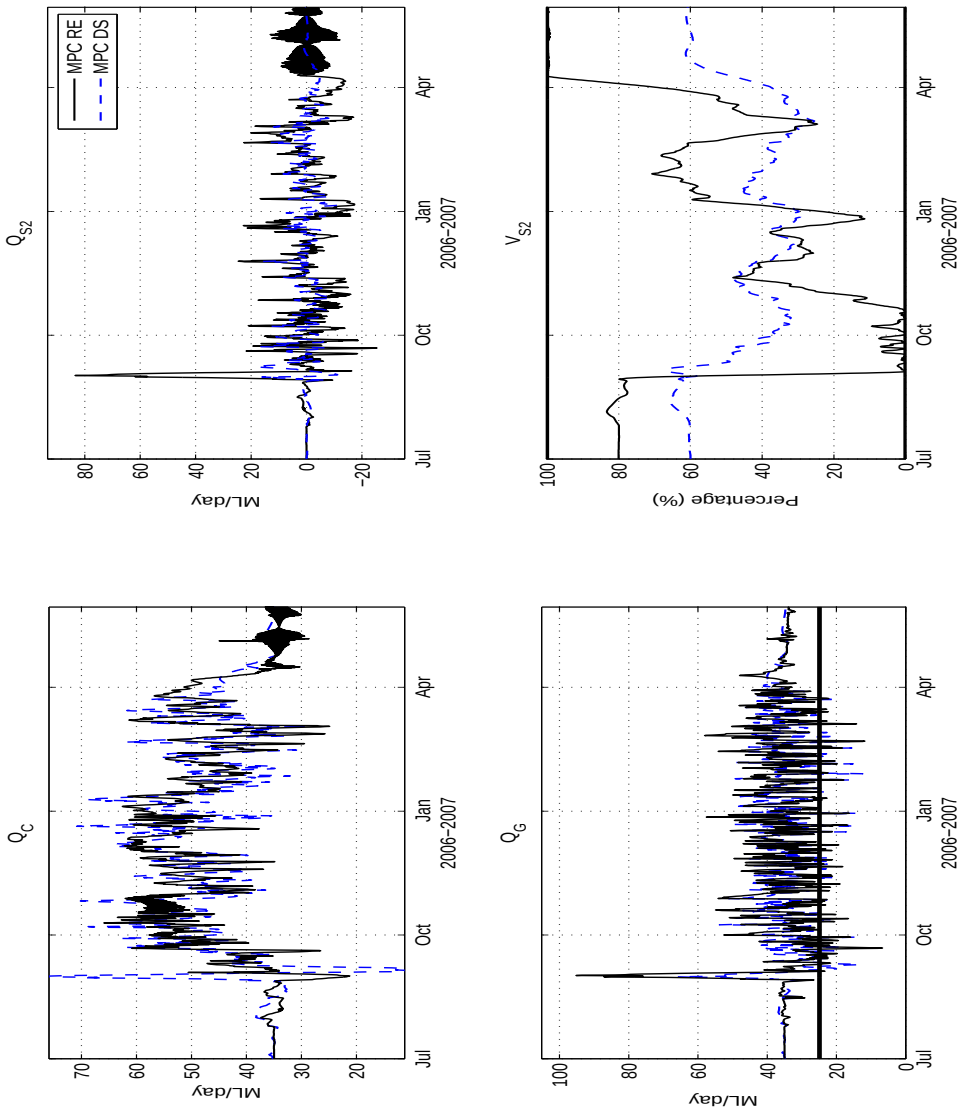

Figure B.1: Year long realistic simulation I.

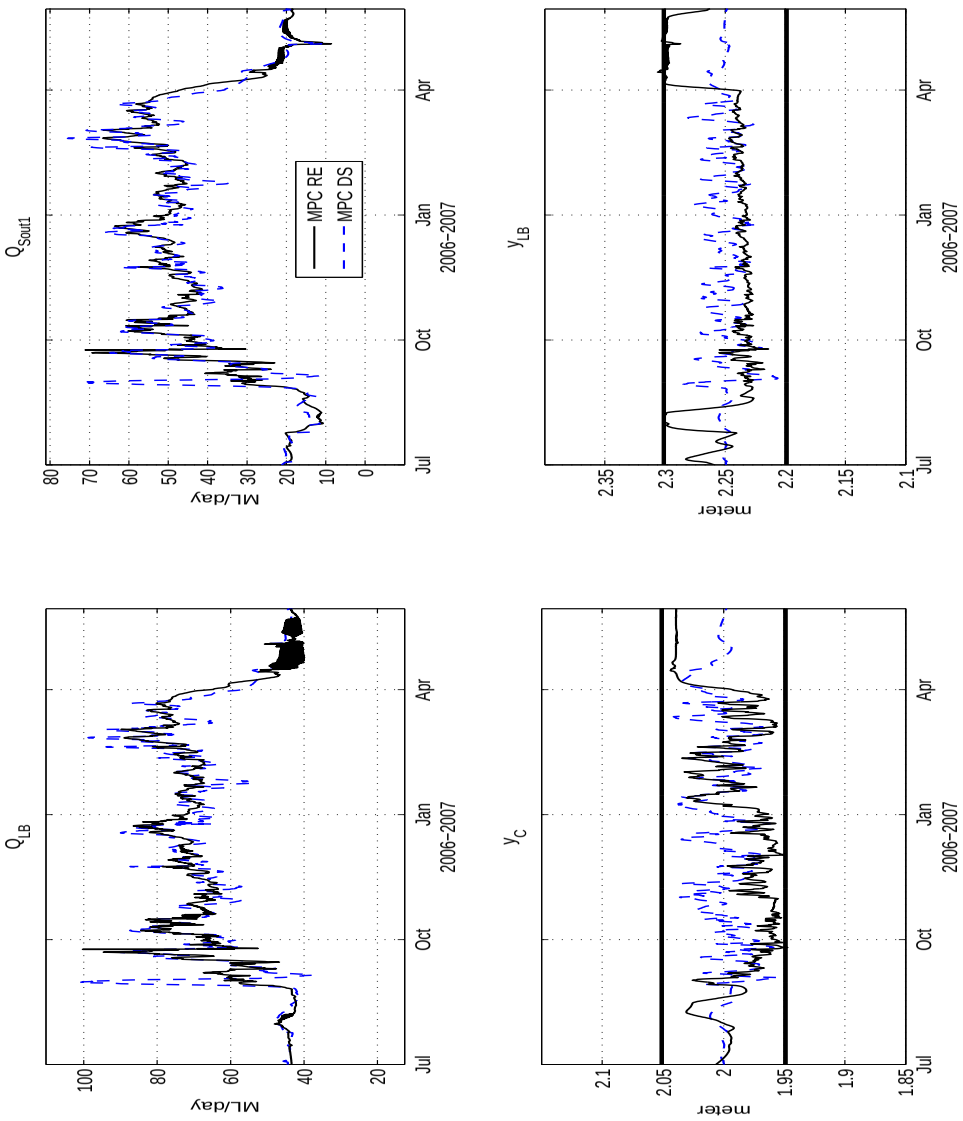

Figure B.2: Year long realistic simulation II.

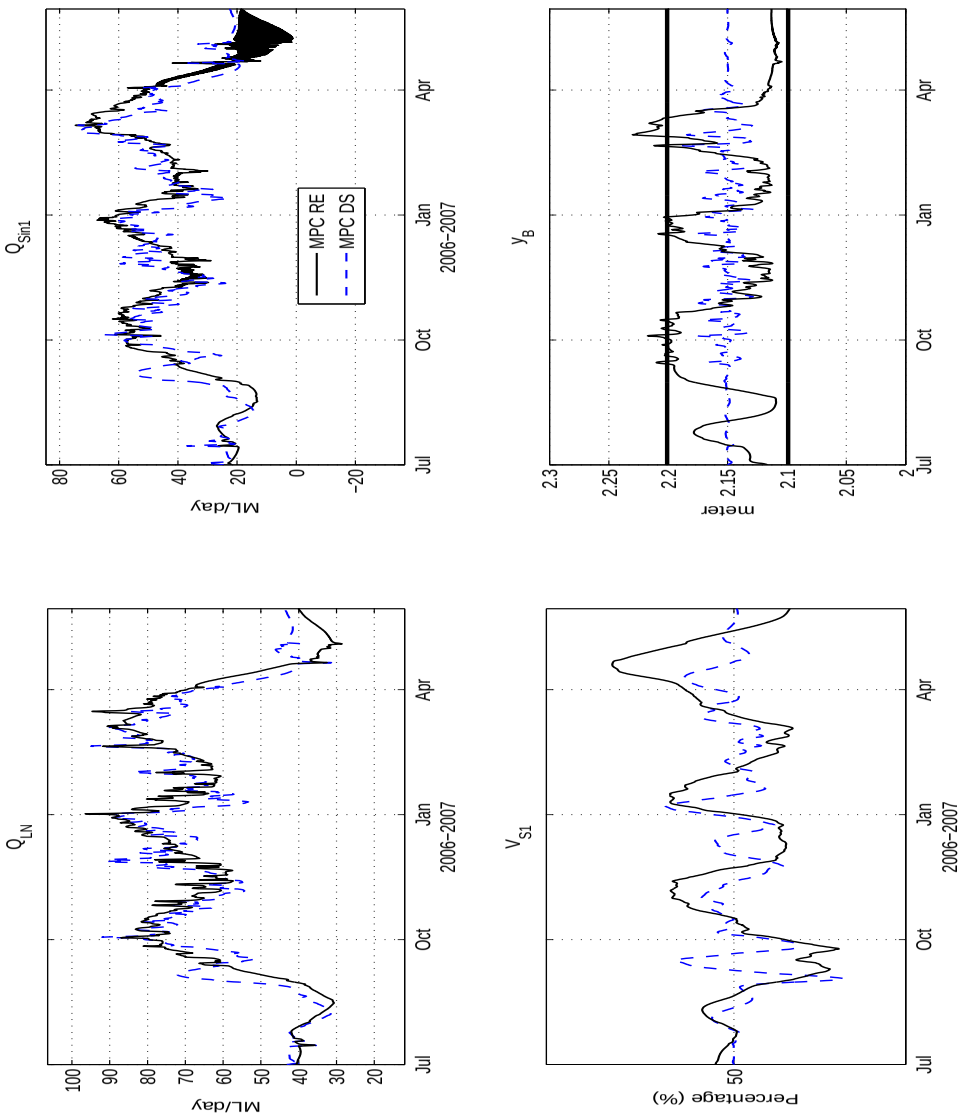

Figure B.3: Year long realistic simulation III.

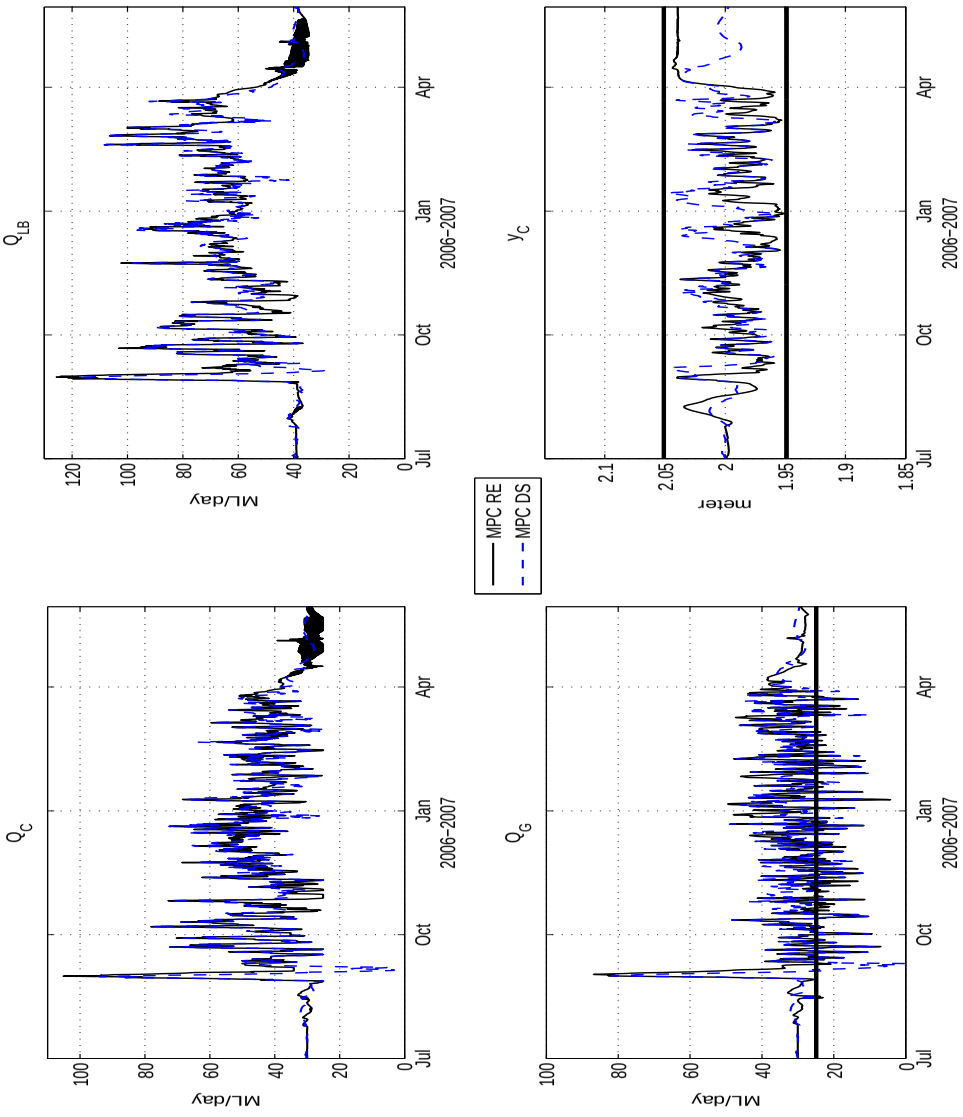

Figure B.4: Year long realistic simulation without Storage 2 I.

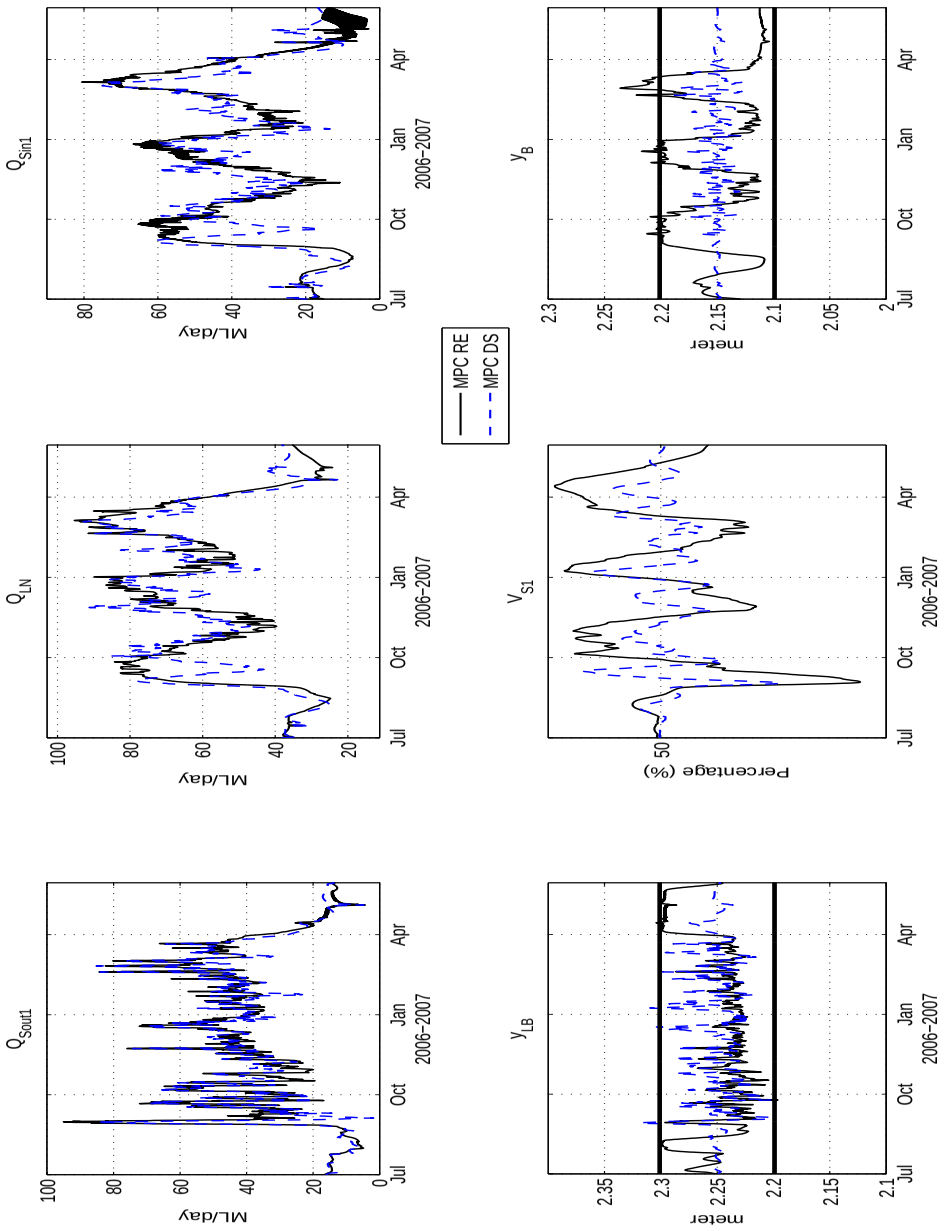

Figure B.5: Year long realistic simulation without Storage 2 II.

Bibliography

Adams, R. and A.W. Western (2010). Using uncertainty analysis to improve estimates of water availability for a regulated catchment in Southern Australia. *Proceedings of BHS International Symposium Role of Hydrology in Managing Consequences of a Changing Global Environment, Newcastle, UK.*

Aguilar, J.V., P. Langarita, L. Linares and J.A. Rodellar (2009). Automatic control of flows and water levels in an irrigation canal. *IEEE Transactions on Industrry Applications* **45**(6), 2198–2208.

Akan, A. O. (2006). *Open channel hydraulics*. Butterworth-Heinemann Elsevier, Oxford.

Alazard, D. and P. Apkarian (1999). Exact observer-based structures for arbitrary compensators. *International Journal of Robust and Nonlinear Control* **9**(2), 101–118.

Arcement, G.J. and V.R. Schneider (1989). Guide for selecting Manning's roughness coefficient for natural channels and floodplains. Technical report. US Geological Service, Water Supply Paper 2339, Washington DC.

Bailey, M. (2010). Private communication with Mark Bailey of Goulburn-Murray Water.

Barjas Blanco, T., P. Willems, B. De Moor and J. Berlamont (2008). Flooding prevention of the Demer River using model predictive control. *Proceedings of IFAC World Congress, Seoul, South Korea.*

Barjas Blanco, T., P. Willems, P-K. Chiang, N. Haverbeke, J. Berlamont and B. De Moor (2010). Flood regulation using nonlinear model predictive control. *Control Engineering Practice* **18**, 1147–1157.

Bastin, G., J-M. Coron and B. D'André-Novel (2009*a*). On Lyapunov stability of linearised Saint-Venant equations for a sloping channel. *Networks and Heterogeneous Media* **4**(2), 177–187.

Bastin, G., L. Moens and P. Dierickx (2009*b*). On-line river flow forecasting with 'Hydromax': Success and challenges after twelve years of experience. *Proceedings of IFAC Symposium on System Identification, Saint-Malo, France.*

Baume, J-P., J. Sau and P.O. Malaterre (1998). Modelling of irrigation channel dynamics for controller design. *Proceedings of IEEE Conference on Systems, Man and Cybernetics, San Diego, USA.*

Baume, J-P., P-O. Malaterre, G. Belaud and B. Le Guennec (2005). SIC: A 1D Hydrodynamic model for river and irrigation canal modeling and regulation. Technical report. CEMAGREF Montpellier.

Baume, J-P., P.O. Malaterre and J. Sau (1999). Tuning of PI controllers for an irrigation canal using optimization tools. *Workshop on Modernization of Irrigation Water Delivery Systems, Phoenix, USA* pp. 483–500.

Beam, R. M. and R. F. Warming (1976). An implicit finite-difference algorithm for hyperbolic systems in conservation-law form. *Journal of Computational Physics* **22**, 87–110.

Begovich, O., V.M. Ruiz, G. Besançon, C.I. Aldana and D. Georges (2007). Predictive control with constraints of a multi-pool irrigation canal prototype. *Latin American Applied Research* **37**, 177–185.

Bender, D.J. (1985). Some considerations for estimator-based compesator design. *International Journal of Control* **41**(6), 1133–1138.

Bender, D.J. and R.A. Fowell (1985). Computing the estimator-controller form of a compensator. *International Journal of Control* **41**(6), 1565–1575.

Billings, S. A. and W. S. F. Voon (1983). Structure detection and model validity tests in the identification of nonlinear systems. *IEE Proceedings* **130, Part D**(4), 193–199.

Bleninger, T., J. D. Fenton and R. Zentgraf (2006). One-dimensional flow modelling and a case study of the River Rhine. *Proceedings of International Conference of Fluvial Hydraulics, Lisbon, Portugal.*

Boiten, W. (2002). Flow measurement structures. *Flow Measurement and Instrumentation* **13**, 203–207.

Bolea, Y., A. Martinez-Gonzalez, R. Grau and H. Martinez-Garcia (2010). An LPV fractional Hayami model for canal control. *Proceedings of Conference on Methods and Models in Automation and Robotics, Miedzyzdroje, Poland*.

Bolea, Y., R. Martinez-Gonzalez, A. Grau and H. Martinez-Garcia (2009). An LPV fractional model for canal control. *Proceedings of IFAC Symposium on System Identification, Saint-Malo, France*.

Booij, M. J. (2002). Appropriate hydrological modelling of climate change impacts on river flooding. *Proceedings of International Environmental Modelling and Software Society, Lugano, Switzerland*.

Bos, M. G. (1978). Discharge measurement structures. Technical report. International Institute for Land Reclamation and Improvement (IIRI), The Netherlands.

Bowen, Z.H., K.D. Bovee and T.J. Waddle (2003). Effects of flow regulation on shallow-water habitat dynamics and floodplain connectivity. *Transactions of the American Fisheries Society* **132**(4), 809–823.

Brookes, M. (2005). The matrix reference manual. *http://www.ee.ic.ac.uk/hp/staff/dmb/matrix/intro.html*.

Brunner, G. W. (2008). HEC-RAS river analysis system: User's manual. Technical report. US Army Corp of Engineers, Hydraulic Engineering Center.

Brutsaert, W. (1971). De Saint-Venant equations experimentally verified. *Journal of Hydraulic Division* **97**(9), 1387–1401.

Bulk Entitlements (2010). Bulk entitlements and environment entitlements, Department of Sustainability and Environment, Victorian Water Register. Available via http://www.waterregister.vic.gov.au/public/reports/bulkentitlements.aspx, Cited 27 Aug 2010. Technical report.

Cantoni, M., E. Weyer, Y. Li, S. K. Ooi, I. Mareels and M. Ryan (2007). Control of large-scale irrigation networks. *Proceedings of IEEE Special Issue on the Technology of Networked Control Systems* **95**, 75–91.

Castelletti, A., F. Pianosi, R. Soncini-Sessa and P. Young (2009). A DBM model for snowmelt simulation. *Proceedings of IFAC Symposium on System Identification, Saint-Malo, France.*

Chaudhry, M. (1993). *Open-channel flow.* Englewood Cliffs, NJ, Prentice Hall.

Chentouf, B., C-Z. Xu and M. Boulbrachene (2001). Robust regulation of a river reach governed by Hayami model. *Proceedings of IEEE Conference on Decision and Control, Orlando, USA.*

Chow, V. T., R. M. Maidment and L. W. Mays (1988). *Applied Hydrology.* McGraw-Hill Book, Co., New York NY.

Coron, J.M., B. D'Andréa-Novel and G. Bastin (1999). A Lyapunov approach to control irrigation canals modeled by Saint-Venant equations. *Proceedings of European Control Conference, Karlsruhe, Germany.*

Costelloe, J. (2010). Broken River data collection by Justin Costelloe, Department of Infrastructure Engineering, The University of Melbourne.

Cottingham, P., M. Stewardson, J. Roberts, L. Metzeling, P. Humphries, T. Hillman and G. Hannan (2001). Report of the Broken River scientific panel on the environmental condition and flow in the Broken River and Broken Creek. Technical report. Cooperative Research Centre for Freshwater Ecology, University of Canberra.

Courant, R., K. Friedrichs and H. Levy (1967). On the partial difference equations of mathematical physics. *IBM Journal* pp. 215–234.

Craig, I., V. Aravinthan, C. Baillie, A. Beswick, G. Barnes, R. Bradbury, L. Connell, P. Coop, C. Fellows, L. Fitzmaurice, J. Foley, N. Hancock, D. Lamb, P. Marrison, R. Misra, R. Mossad, P. Pittway, E. Prime, S. Rees, E. Schmidt, D. Solomon, T. Symes and D. Turnbull (2007). Evaporation, seepage and water quality management in storage dams: A review of research methods.. *Environmental Health* **7**(3), 84–97.

Cunge, J. A., F. M. Holly and A. Verwey (1980). *Practical aspects of computational river hydraulics.* Boston Pitman Advanced Publication Program.

Cunge, J.A. (1969). On the subject of flood propagation computation method (Muskingum method). *Journal of Hydraulic Research* **7**(2), 205–230.

Delmond, F., D. Alazard and C. Cumer (2006). Cross standard form: A solution to improve a given controller with H_2 or H_∞ specifications. *International Journal of Control* **79**(4), 279–287.

Deodhar, M.J. (2009). *Elementary Engineering Hydrology*. Pearson Education.

Department of Primary Industries (2009). http://www.dpi.vic.gov.au/, The Department of Primary Industries (DPI), Victoria, Australia. Technical report.

Di Cairano, S. and A. Bemporad (2010). Model predictive control tuning by controller matching. *IEEE Transactions of Automatic Control* **55**(1), 185–190.

Elfawal-Mansour, H., D. Georges and N. Ohnishi (2000). Optimal control of an open irrigation system based on nonlinear models. *Proceedings of IEEE TENCON 2000 , Kuala Lumpur, Malaysia*.

Eurén, K. and E. Weyer (2007). System identification of open water channels with undershot and overshot gates. *Control Engineering Practice* **15**, 813–824.

Evans, D. C., D. Rees and D. L. Jones (1994). Identifying linear models of systems suffering nonlinear distortions. *Proceedings of IEE Control 94, Coventry, UK*.

Evans, R., L. Li, I. Mareels, N. Okello, M. Pham, W. Qiu and S.K. Saleem (2011). Real-time optimal control of river basin networks. *Proceedings of IFAC World Congress, Milan, Italy*.

Feliu-Batlle, V., R. Rivas Pérez and L. Sánchez Rodríguez (2007). Fractional robust control of main irrgation canals with dynamic parameter. *Control Engineering Practice* **15**, 673–686.

Franklin, G.F., J.D. Powell and A. Emami-Naeini (2006). *Feedback Control of Dynamic Systems*. 5th ed.. Prentice Hall.

Franklin, G.F., J.D. Powell and M.L. Workman (1998). *Digital control of dynamic systems*. 3rd ed.. Addison-Wesley.

Fread, D. L. (1991). Flood routhing models and Manning, n. *Channel Flow Resistance: Centennial of Manning's Formula, Water Resources Publications* pp. 421–435.

FRM (2009). http://www.frm.unimelb.edu.au/default.htm, Farms, Rivers and Market Project.. Technical report.

Fujii, T. (1987). A new approach to the LQ design from the viewpoint of the inverse regulatator problem. *IEEE Transactions of Automatic Control* **32**(11), 995–1004.

Gawne, B. (2010). Private communication with Ben Gawne of The Murray-Darling Freshwater Research Centre, Latrobe University.

GBCMA (2009). http://www.gbcma.vic.gov.au/, Goulburn-Broken Catchment Management Authority, Australia.. Technical report.

Glanzmann, G., M. von Siebenthal, T. Geyer, G. Papafotiou and M. Morari (2005). Supervisory water level control for cascaded river power plants. *Proceedings of International Conference on Hydropower, Stavanger, Norway.*

Gómez, M., J. Rodellar and J.A. Mantecón (2002). Predictive control method for decentralized operation of irrigation canals. *Applied Mathematical Modelling* **26**, 1039–1056.

Goodwin, G.C., S.F. Graebe and M.E. Salgado (2001). *Control System Design.* Prentice Hall.

Haber, R. (1979). Parametric identification of nonlinear dynamic systems based on correlation functions. *Proceedings of IFAC Symposium on Identification and Parameter Estimation, Darmstadt, Germany.*

Haber, R. (1985). Nonlinearity tests for dynamic processes. *Proceedings of IFAC/IFORS Symposium on Identification and Parameter Estimation, York, UK.*

Haber, R. and L. Keviczky (1999). *Nonlinear System Identification - Input-Output Modeling Approach, Volume 2: Nonlinear System Structure Idenfitication.* Kluwer Academic Publishers.

Hartley, E. and J. Maciejowski (2009). Initial tuning of predictive controllers by reverse engineering. *Proceedings of European Control Conference, Budapest, Hungary.*

Hayami, S. (1951). On the propagation of flood waves. Technical report. Disaster Prevention Research Institute, Kyoto University.

Holland, R. (1984). Implicit three-dimensional finite differencing of Maxwell's Equations. *IEEE Transactions on Nuclear Science* **31**(6), 1322–1326.

Holly, F. M. and A. Preismann (1977). Accurate calculation of transport in two dimensions. *Journal of the Hydraulics Division* **103**(HY11), 1259–1277.

IBM (2009). *CPLEX User's Guide 12.1.*

IRIN (2006). Running dry: the humanitarian impact of the global water crisis. Technical report. IRIN In-depth Edition.

Jacobsen, J.L, H. Madsen and P. Harremoës (1997). A stochastic model for two-statioin hydraulics exhibiting transient impact. *Journal of Water Science and Technology* **36**(5), 19–26.

Jónsdóttir, H., J.L. Jacobsen and H. Madsen (2001). A grey-box model describing the hydraulics in a creek. *Environmetrics* **12**, 347–356.

Julien, P. Y. (2002). *River mechanics*. Cambridge University Press.

Kalman, R.E. (1964). When is a linear control system optimal?. *Transactions of ASME, Journal of Basic Engineering* **86**, 51–60.

Kearney, M., M. Cantoni and P.M. Dower (2011*a*). Non-iterative distributed mpc for large-scale irrigation channels. *Proceedings of Australian Control Conference, Melbourne, Australia*.

Kearney, M., P.M. Dower and M. Cantoni (2011*b*). Model predictive control for flood mitigation: A Wivenhoe Dam case study. *Proceedings of Australian Control Conference, Melbourne, Australia*.

Korenberg, M. J. and I. W. Hunter (1990). The identification of nonlinear biological systems Wiener kernel approaches. *Annals of Biomedical Engineering* **18**, 629–654.

Kreindler, E. and A. Jameson (1972). Optimality of linear control systems. *IEEE Transactions of Automatic Control* **17**(3), 349–351.

Kreyzig, E. (1988). *Advanced Engineering Mathematics*. 6th ed.. John Wiley & Sons, Inc.

Krutzen, M. P. M. (2000). Estimation of parameters in the St. Venant equations from observed data: Developing a full simulation model for an irrigation channel. Internal report. Department of Electrical and Electronic Engineering, The University of Melbourne, Australia.

Langendoen, E. J. (2000). Concepts: Conservational channel evolution and pollutant transport system. Research Report 16. United States Department of Agriculture - Agricultural Research Service National Sedimentation Laboratory.

Langford, J. (2010). Private communication with John Langford of Uniwater, The University of Melbourne, Farms, Rivers and Market Project Leader.

Laub, A.J. (1979). A Schur method for solving Riccati equations. *IEEE Transactions of Automatic Control* **24**(6), 913–921.

Lebosse, A. (1989). Estimation of the Manning-Strickler roughness. *Proceedings of International Conference on Channel Flow and Catchment Runoff, Charlottesville, USA.*

Li, Y. and M. Cantoni (2008). Distributed controller designs for open water channels. *Proceedings of IFAC World Congress, Seoul, South Korea.*

Li, Y., M. Cantoni and E. Weyer (2004). Design of a centralized controller for an irrigation channel using loop-shaping. *Proceedings of UKACC Control Conference, Bath, UK.*

Li, Y., M. Cantoni and E. Weyer (2005). On water-level error propagation in controlled irrigation channels. *Proceedings of IEEE Conference on Decision and Control, Seville, Spain.*

Linke, H. (2010). A model-predictive controller for optimal hydro-power utilization of river reservoirs. *Proceedings of IEEE International Conference on Control Applications, Yokohama, Japan.*

Litrico, X. (2001). Nonlinear diffusive wave modeling and identification of open channels. *Journal of Hydraulic Engineering* **127**(4), 313–320.

Litrico, X. and D. Georges (1997). Nonlinear identification of an irrigation system. *Proceedings of IEEE Conference on Decision and Control, San Diego, USA.*

Litrico, X. and D. Georges (1999). Robust continuous-time and discrete-time flow control of a dam-river system (I) Modelling. *Applied Mathematical Modelling* **23**, 809–827.

Litrico, X. and D. Georges (2001). Robust LQG control of single input multiple outputs dam-river systems. *International Journal of Systems Science* **32**(6), 795–805.

Litrico, X. and J-B. Pomet (2003). Nonlinear modelling and control of a long river stretch. *Proceedings of European Control Conference, Cambridge, UK.*

Litrico, X. and V. Fromion (2002). Real-time management of multi-reservoir hydraulic systems using H_∞ optimization. *Proceedings of IFAC World Congress, Barcelona, Spain.*

Litrico, X. and V. Fromion (2004*a*). Analytical approximation of open-channel flow for controller design. *Applied Mathematical Modelling* **28**, 677–695.

Litrico, X. and V. Fromion (2004*b*). Simplified modeling of irrigation canals for controller design. *Journal of Irrigation and Drainage Engineering* **130**(5), 373–383.

Litrico, X. and V. Fromion (2009). *Modeling and Control of Hydrosystems*. Springer.

Litrico, X., J-B. Pomet and V. Guinot (2010). Simplified nonlinear modeling of river flow routing. *Advances in Water Resources* **33**, 1015–1026.

Litrico, X., V. Fromion, J-P. Baume and M. Rijo (2003). Modelling and PI control of an irrigation channel. *Proceedings of European Control Conference, Cambridge, UK*.

Liu, F., J. Feyen and J. Berlamont (1994). Downstream control algorithm for irrigation canals. *Journal of Irrigation and Drainage Engineering* **120**(3), 468–483.

Ljung, L. (1999). *System Identification: Theory for the user, 2nd edition*. Englewood Cliffs, NJ: Prentice-Hall.

Ljung, L. and T. Glad (1994). *Modeling of Dynamic Systems*. Upper Saddle River, NJ: Prentice-Hall.

Löfberg, J. (2004). Yalmip : A toolbox for modeling and optimization in MATLAB®. *Proceedings of CACSD Conference, Taipei, Taiwan*.

Lyn, D. A. and P. Goodwin (1987). Stability of a general preissmann scheme. *Journal of Hydraulic Engineering* **113**(1), 16–28.

Maciejowski, J. (2007). Reverse engineering existing controllers for MPC design. *Proceedings of IFAC Symposium of System Structure and Control, Iguassu Falls, Brazil*.

Maciejowski, J.M. (2002). *Predictive control with constraints*. Pearson Education.

Malaterre, P.O. (1995). Regulation of irrigation canals. *Journal of Irrigation and Drainage Engineering* **9**(4), 297–327.

Malaterre, P.O. (1998). PILOTE: Linear quadratic optimal controllers for irrigation canals. *Journal of Irrigation and Drainage Engineering* **124**(4), 187–194.

Malaterre, P.O. and J-P. Baume (1998). Modeling and regulation of irrigation canals: existing applications and ongoing researches. *Proceedings of IEEE Conference on Systems, Man and Cybernetics, San Diego, USA*.

Malaterre, P.O., D.C. Rogers and J. Schuurmans (1998). Classification of canal control algorithms. *Journal of Irrigation and Drainage Engineering* **124**(1), 3–10.

Mandeville, A.N., P.E. O'Connell, J.V. Sutcliffe and J.E. Nash (1970). River flow forecasting through conceptual models. Part III - The Ray catchment at Grendon Underwood. *Journal of Hydrology* **11**, 109–128.

Mareels, I., E. Weyer, S. K. Ooi, M. Cantoni, Y. Li and G. Nair (2005). System engineering for irrigation systems: Success and challenges. *Annual Reviews in Control* **29**, 191–204.

Maxwell, M. and S. Warnick (2006). Modeling and identification of the Sevier River system. *Proceedings of IEEE American Control Conference, Minneapolis, USA*.

McCormack, A. S., K. R. Godfrey and J. O. Flower (1994). The detection of and compensation for nonlinear effects for frequency domain identification. *Proceedings of IEE Control 94, Coventry, UK*.

Mokoan Wetlands (2006). http://www.lakemokoan.com/project.htm, Mokoan: Return to wetland.. Technical report.

Molinari, B.P. (1973). The stable regulatator problem and its inverse. *IEEE Transactions of Automatic Control* **18**(5), 454–459.

Nash, J. E. (1957). The form of the instantaneous unit hydrograph. *International Association of Science Hydrology* **3**(45), 114–121.

Nash, J.E. (1959). Systematic determination of unit hydrograph parameters. *Journal of Geophysical Research* **64**(1), 111–115.

Nash, J.E. and J.V. Sutcliffe (1970). River flow forecasting through conceptual models. Part I - A discussion of principles. *Journal of Hydrology* **10**, 282–290.

Natke, H. G., Juang J-N. and W. Gawronski (1988). A brief review on the identification of nonlinear mechanical systems. *Proceedings of International Modal Analysis Conference, Kissimee, USA*.

Negenborn, R.R., A. Şahin, Z. Lukszo, B. De Schutter and M. Morari (2009*a*). A non-iterative cascaded predictive control approach for control of irrigation canals. *Proceedings of IEEE International Conference on Systems, Man and Cybernetics, San Antonio, USA*.

Negenborn, R.R., P-J. van Overloop, T. Keviczky and B. De Schutter (2009*b*). Distributed model predictive control of irrigation canals. *Networks and Heterogeneous Media* **4**(2), 359–380.

NRW (2001). Asset management: water loss management implementation guide. Technical report. Department of Natural Resources and Water of Queensland Total Management Planning Guidelines.

O'Connell, P.E., J.E. Nash and J.P. Farrell (1970). River flow forecasting through conceptual model. Part II - The Brosna catchment at Ferbane. *Journal of Hydrology* **10**, 317–329.

Ooi, S. K. (2003). Modelling and Control Design of Irrigation Channels. PhD thesis. The University of Melbourne.

Ooi, S. K. and E. Weyer (2001). Closed loop identification of irrigation channel. *Proceedings of IEEE Conference on Decision and Control, Orlando, USA*.

Ooi, S. K. and E. Weyer (2008). Control design for an irrigation channel from physical data. *Control Engineering Practice* **16**, 1132–1150.

Ooi, S. K., M. P. M. Krutzen and E. Weyer (2005). On physical and data driven modelling of irrigation channels. *Control Engineering Practice* **13**, 461–471.

Ooi, S.K., M. Foo and E. Weyer (2010). Farms, rivers and markets project: Real time information and control - Control options and initial design and evaluation of a control system for the Broken River. Technical report. The University of Melbourne.

Ooi, S.K., M. Foo and E. Weyer (2011). Control of the Broken River. *Proceedings of IFAC World Congress, Milan, Italy.*

Papageorgiou, M. and A. Messmer (1985). Continous-time and discrete-time design of water flow and water level regulators. *Automatica* **21**(6), 649–661.

Papageorgiou, M and A. Messmer (1989). Flow control of a long river stretch. *Automatica* **25**(2), 177–183.

Pintelon, R. and J. Schoukens (2001). *System Identification - A Frequency Domain Approach*. IEEE Press.

Puig, V., J. Romera, J. Quevedo, C.M. Cardona, A. Salterain, E. Ayesa, I. Irizar, A. Castro, M. Lujan, P. Charbonnaud, P. Chiron and J.-L. Trouvat (2009). Optimal predictive control of water transport systems: Arrê-Darré/Arros case study. *Water Science and Technology* **60**(8), 2125–2133.

Rabbani, T.S., F. Di Meglio, X. Litrico and A.M. Bayen (2010). Feed-forward control of open channel flow using differential flatness. *IEEE Transactions on Control Systems Technology* **18**(1), 213–221.

Rawlings, J. and K. Muske (1993). The stability of constrained receding horizon control. *IEEE Transactions of Automatic Control* **38**(10), 1512–1516.

Rawlings, J.B. and D.Q. Mayne (2009). *Model Predictive Control: Theory and Design*. Nob Hill Publishing.

Richardson, A.J., J.E. Growns and R.A. Cook (2004). Distribution and life history of caridean shrimps in regulated lowland rivers in Southern Australia. *Marine and Freshwater Research* **55**(3), 295–308.

Rivas-Pérez, R., V. Feliu-Batlle and L. Sanchez-Rodriguez (2007). Robust system identification of an irrigation main canal. *Advances in Water Resources* **30**, 1785–1796.

Rivas-Pérez, R., V. Feliu-Batlle, F. Castillo-Garcia and A. Linarez-Saez (2008). System identification for control of a main irrigation canal pool. *Proceedings of IFAC World Congress, Seoul, South Korea*.

Rodgers, J. L. and W. A. Nicewander (1988). Thirteen ways to look at the correlation coefficient. *American Statistical Association* **42**(1), 59–66.

Romera, J., C. Ocampo-Martinez, V. Puig, J. Quevedo, P. Garcia and G. Perez (2011). Flooding management using hybrid model predictive control at the Ebro River in Spain. *Proceedings of IWA Symposium on Systems Analysis and Integrated Assessment, San Sebastian, Spain*.

Rossiter, J.A. (2005). *Model-based Predictive Control. A Practical Approach*. CRC Press.

Ruiz, V.M. and L. Ramirez (1998). Predictive control in irrigation canal operation. *Proceedings of IEEE International Conference on Systems, Man and Cybernetics, San Diego, USA*.

Sahin, A. and M. Morari (2010). Decentralized model predictive control for a cascade of river power plants. In: *Intelligent Infrastructure* (R. R. Negenborn, Z. Lukszo and H. Hellendoorn, Eds.). Vol. 42. pp. 463–486. Springer. Dordrecht, The Netherlands.

Sawadogo, S., R.M. Faye, P.O. Malaterre and F. Mora-Camino (1998). Decentralized predictive controller for delivery canals. *Proceedings of IEEE International Conference on Systems, Man and Cybernetics, San Diego, USA*.

Schroeder, M.R. (1970). Synthesis of low-peak-factor signals and binary sequences with low autocorrelation. *IEEE Transactions of Information Theory* **16**, 85–89.

Schuurmans, J. (1997). Control of water levels in open-channels. PhD thesis. Technical University of Delft.

Schuurmans, J., A. Hof, S. Dijkstra, O.H. Bosgra and R. Brouwer (1999*a*). Simple water level controller for irrigation and drainage canals. *Journal of Irrigation and Drainage Engineering* **125**(4), 189–195.

Schuurmans, J., A.J. Clemmens, S. Dijkstra, Hof. A. and R. Brouwer (1999*b*). Modeling of irrigation and drainage canals for controller design. *Journal of Irrigation and Drainage Engineering* **125**(6), 338–344.

Schuurmans, J., O. Bosgra and R. Brouwer (1995). Open-channel flow model approximation for controller design. *Applied Mathematical Modelling* **19**, 525–530.

Sepúlveda, C. and J. Rodellar (2005). Irrigation canal system identification for control purposes. Technical report. Polytechnic University of Catalunya.

Setz, C., A. Heinrich, P. Rostalski, G. Papafotiou and M. Morari (2008). Application of model predictive control to a cascade of river power plants. *Proceedings of IFAC World Congress, Seoul, South Korea*.

Shrestha, R. R. and F. Nestmann (2005). River water level prediction using physically based and data driven models. *In Zerger A. and Argent R.M. (Eds) MODSIM 2005 International Congress on Modelling and Simulation: Modelling and Simulation Society of Australia and New Zealand* pp. 1894–1900.

Silvis, L.G., A. Hof, P.M.J van den Hof and A.J. Clemmens (1998). System identification on open-channels. *Proceedings of International Conference on Hydroinformatics, Copenhagen, Denmark*.

Singh, V. P. and R. N. Yadava (2003). *Water resources system operation*. Allied Publisher Ptd. Ltd.

Söderström, T. and P. Stoica (1988). *System Identification*. Englewood Cliffs, NJ: Prentice-Hall.

Sohlberg, B. and M. Sernfält (2002). Grey box modelling for river control. *Journal of Hydroinformatics* **4**, 265–280.

Sumner, G. (1988). *Precipitation: Process and Analysis*. John Wiley & Sons, Inc.

Thomassin, M., T. Bastogne and A. Richard (2009). Identification of a managed river reach by a Bayesian approach. *IEEE Transactions on Control Systems Technology* **17**(2), 353–365.

UNESCO (2006). World water assessment program: water - a shared responsibility. Technical report. The United Nations World Water Development Report.

Vaccaro, R.J. (1995). *Digital control. A State-Space Approach*. McGraw-Hill Series in Electrical and Computer Engineering.

van Ekeren, H., R.R. Negenborn, P.J. van Overloop and B. De Schutter (2011). Hybrid model predictive control using time-instant optimization for the Rhine-Meuse Delta. *Proceedings of IEEE International Conference on Networking, Sensing and Control, Delft, The Netherlands*.

van Overloop, P.-J (2006). Model predictive control on open water system. PhD thesis. Technical University of Delft.

van Overloop, P.-J., R.R. Negenborn, B. De Schutter and N.C. van de Giesen (2010). Predictive control for national water flow optimization in the netherlands. In: *Intelligent Infrastructures* (R. R. Negenborn, Z. Lukszo and H. Hellendoorn, Eds.). pp. 439–461. Springer. Dordrecht, The Netherlands.

van Overloop, P.J., J. Schuurmans, R. Brouwer and C.M. Burt (2005). Multiple-model optimization of Proportional Integral controllers on canals. *Journal of Irrigation and Drainage Engineering* **131**(2), 190–196.

Várlaki, P., G. Terdik and V. A. Lototsky (1985). Tests for linearity and bilinearity of dynamic systems. *Proceedings of IFAC/IFORS Symposium on Identification and Parameter Estimation, York, UK*.

Venutelli, M. (2002). Stability and accuracy of weighted four-point implicite finite difference schemes for open channel flow. *Journal of Hydralic Engineering* **128**(3), 281–288.

Venutelli, M. (2007). Extension of Preissmann scheme to two-dimensional flows. *Journal of Hydraulic Engineering* **133**(10), 1171–1176.

Victorian Water Resources (2009). http://www.vicwaterdata.net/vicwaterdata/home.aspx, victorian Water Resources Data Warehouse. Technical report.

Vreugdenhil, C. D. (1994). *Numerical methods for shallow-water flow*. Kluwer Academic Publisher.

Wagenpfeil, J., E. Arnold and O. Sawodny (2010). Modleing and optimized water management of inland waterway systems. *Proceedings of IEEE International Conference on Control Applications, Yokohama, Japan*.

Wahlin, B.T. (2007). Performance of Model Predictive Control on ASCE Test Canal 1. *Journal of Irrigation and Drainage Engineering* **130**(3), 227–238.

Wang, L. (2009). *Model Predictive Control System Design and Implementation using MATLAB®*. Springer.

Water Entitlements (2010). Restoring the balance in the Murray-Darling Basin. Water entitlement purchasing in the Murray-Darling Basin (water buyback). Available via http://www.environment.gov.au/water/policyprograms/entitlement-purchasing/, September 2010. Technical report.

Water In Our Environment (2010). Water in our environment. Available via http://www.environment.gov.au/water/policy-programs/environment/index.html, August, 2010.. Technical report.

Weyer, E. (2001). System identification of an open water channel. *Control Engineering Practice* **9**, 1289–1299.

Weyer, E. (2002). Decentralised PI control of an open water channel. *Proceedings of IFAC, World Congress, Barcelona, Spain*.

Weyer, E. (2003). LQ control of an irrigation channel.. *Proceedings of IEEE Conference on Decision and Control, Hawaii, USA*.

Weyer, E. (2008). Control of irrigation channels. *IEEE Transactions on Control Systems Technology* **16**(4), 664–675.

Wu, Q., Sa. Amin, S. Munier, A.M. Bayen, X. Litrico and G. Belaud (2007). Parameter identification for the shallow water equations using modal decomposition. *Proceedings of IEEE Conference on Decision and Control, New Orleans, USA*.

Wu, W. (2008). *Computational River Dynamics*. Taylor and Francis.

Young, P. (2002). Advances in real-time flood forecasting. *Philosophical Transaction: Mathematical, Physical and Engineering Sciences* **360**(1793), 1433–1450.

Young, P. (2003). Top-down and data based mechanistic modelling of rainfall-flow dynamic at the catchment scale.. *Hydrological Process* **17**, 2195–2217.

Young, P. and A. Chotai (2001). Data-based mechanistic modeling, forecasting and control.. *IEEE Control Systems Magazine* **21**(5), 14–27.

Young, P., D. Leedal, K. J. Beven and C. Szczypta (2009). Reduced order emulation of distributed hydraulic simulation models. *Proceedings of IFAC Symposium on System Identification, Saint-Malo, France*.

Young, P.C. (1998). Data-based mechanistic modelling of environmental, ecological, economic and engineering systems.. *Environmental Modelling and Software* **13**, 105–122.

Zhou, K., J. C. Doyle and K. Glover (1996). *Robust and Optimal Control*. Prentice Hall.

Zhuan, X., G. Zheng and X. Xia (2009). A modelling methodology for natural dam-river network systems. *Control Engineering Practice* **17**, 534–540.

Zienkiewicz, O. C., R. L. Taylor and P. Nithiarasu (2006). *The Finite Element Method for Fluid Dynamics, 6th Edition*. Elsevier Butterworth-Heinemann.